2

PHYSICS THROUGH EXPRIMENT

MECHANICAL SYSTEMS

Study of Some Fundamental Processes in Physics

437

PHYSICS THROUGH EXPERIMENT

2

MECHANICAL SYSTEMS

Study of Some Fundamental Processes in Physics

PHYSICS THROUGH EXPERIMENT

2

MECHANICAL SYSTEMS

Study of Some Fundamental Processes in Physics

Contributors

B. Saraf (Retired)
D.P. Khandelwal (Retired)

B.C. Mazumdar (Retired)
Y.S. Shishodia (USIC)
R.S. Tailor (USA)

University of Rajasthan,
Jaipur (India)

UBSPD

UBS Publishers' Distributors Ltd
8/1-B, Chowringhee Lane, Calcutta-700 016
Ph:212451, 249473

VIKAS PUBLISHING HOUSE PVT LTD

VIKAS PUBLISHING HOUSE PVT LTD
576 Masjid Road, Jangpura, New Delhi 110 014

COPYRIGHT © 1979, Authors

Reprint 1989

Acc No - 15448

All rights reserved. The contents of this book, or parts thereof, may not be reproduced without written permission from Babulal Saraf, Physics Education Centre, Badnawar, Distt. Dhar, M.P. Pin: 454660, India.

Printed at Bharat Offset, Delhi-110 006

STATEMENT

It was in January 1975 when the first volume of *Physics Through Experiment—EMF—Constant and Varying*—was published. The second volume was promised early. In the event, it has turned out to be nearly four years. Part of the reason, in fact, has been our effort to make the design of the equipment conform to requirements of a fair degree of accuracy and sturdiness and this has created more problems in mechanics experiments than were anticipated. We also wanted the benefit of criticism from the wider academic community. Accordingly, in this period we published a booklet in the year 1977, describing the equipment and possible experiments with them, and also presented the equipment at a large number of academic gatherings both in India and abroad. In July 1978 some of the equipment was displayed at the Oxford Conference on the "Role of the Laboratory in Physics Teaching" and we were encouraged by the response. We have also fabricated and supplied the equipment to more than thirty institutions of repute, including the IITs in India and the International Centre for Theoretical Physics, Trieste.

The importance of experimentation in the learning process of the student is emphasised all the world over and we do not wish to restate this case, except to say that in the developing countries there is all the more reason for emphasizing the role of experiment as the major part of scientific culture.

This volume centres on the use of three units of equipment—(*i*) The linear air track, (*ii*) Pendulum oscillator, and (*iii*) Mechanical transmission line. The phenomena of oscillations in systems of different kinds, interaction among oscillators and the process of wave propagation cover more than half of the entire physics. If this claim sounds extravagant, we would seek to justify it on our belief that even the particle physicists look to mechanics for the source of their ideas.

The academic spectrum of experiments designed with any one unit is indeed very wide and the level at which experiments may be performed depends on the desire and capacity of the student and the teacher. By no means would we claim that the book explores the full range of these ideas.

The work reported in this book has received help and advice from several workers. The group of authors have made their contribution in a number of ways.

The development of equipment has been spread over several years. B.C. Mazumdar, Y.S. Shishodia* and R.C. Tailor** have been the major contributors in the design of equipment and experimentation.

---

*Now at North-Eastern Hill University, Shillong, Meghalaya.

**Now at Ohio State University, Athens, USA (on study leave).

Professor D.P. Khandelwal of HBTI, Kanpur is exclusively responsible for the preparation of the script. While writing this book, many ideas on experimentation and analysis have come from him. I appreciate the kind assistance of the authorities of HBTI, Kanpur, in allowing him to work with us.

R.S. Chhabra, A.K. Arora and N.L. Sharma have participated in a critical reading of the manuscript. Their observations and suggestions have very significantly contributed to improvement in the final version.

K.B. Garg, B.K. Sharma and D.T. Chandwani have contributed in the early stages of the preparation of the book. In fact, they have entirely looked after the editing and publication of the booklet published in 1977.

The academic contribution of several workers who have helped in performing the experiments is indeed difficult to record. But I must specifically mention the names of Usha Bhatia and V.K. Gupta whose critical view of the measurement and data processing has been of high quality.

Since this book is a report of actual measurement of quantities in a possible experiment performed with equipment fabricated in our workshop, it is my pleasure to record that the quality of mechanical systems has been the exclusive achievement of George Thomas and Kailash Sharma.

The list of associates, critics, helpers and workers is indeed very long and it is impossible to name them all. However, I must mention my colleague Prof. S. Lokanathan. For the entire programme of this project (University Leadership Project), through thick and thin, his assistance has been invaluable—in the ideas, critical analysis of experiments, putting us to work, its format and what not. Without him, I hardly think any of this work would have been possible.

One wonders if academic recognition and fruitful response needs a personal association to render active support to such a project. But this indeed has been our story. Ajoy Ghatak and C.L. Mehta at IIT, Delhi, M.R. Bhiday at the University of Poona, Girijesh Mehta and H.S. Mani of the IIT, Kanpur; C. Mande of the University of Nagpur, and A.R. Patel of the University of Vallabh Vidyanagar, among others, not only encouraged us in work but also placed the equipment before their students.

The University Grants Commission has a very positive attitude towards improvement of Physics Education. Professor B. Ramchandra Rao and Professor B.M. Udgaonkar have kept their keen and sustained interest in our work and we hope to enjoy their confidence and encouragement in the coming years. The administrative help and understanding shown to us by Dr Shankarnarayan and prompt help from A.G. Deshmukh at the UGC end deserve specific mention. At the Rajasthan University, L.P. Vaish has been unique as an administrator, rendering us all possible assistance as and when needed and taking pride in our work. We share our achievement with all of them.

I hope we have lost years, but not face. We have struggled, sometimes against heavy odds, and we have tried to present our ideas and contribution to the big task of recasting Physics Education. A critical review from the academic community will indeed help us in our future work on the project.

B. SARAF

PREFACE

This book is the second of the series we are bringing on laboratory work in Physics and deals with experiments on mechanics carried out with the equipment especially designed and developed by us for the purpose. It covers a comprehensive family of experiments involving motion in different kinds of potential fields, starting from simple one dimensional motion and collisions, going through oscillations and leading upto wave transmission.

Classical mechanics remains the most fundamental of all branches of Physics. Although the framework of Newton's laws is now realised to be inadequate and insufficient when atomic and nuclear interactions are to be studied, these laws are exact for all practical purposes for an engineer and a technologist, including the space scientist. An even more compelling reason for a thorough study of this discipline is that mechanics offers a large variety of models and is a rich source of ideas in all areas of physics. The concepts here are easily visualised. Even the most sophisticated modern theoretician carries the models of mechanics in his mind.

In the modern method of teaching physics, mechanics is not treated as an isolated branch but as the backbone of physics. The experiments which we have designed take special care of this aspect; potentials of forms similar to those one comes across in atomic and nuclear interactions are produced and motions under them are studied. That the studies deal with potential energy variation and not force makes it easier to compare the experiments with parallel situations in atomic physics. One may then see to what extent quantum mechanics would give results appreciably different from Newtonian mechanics.

Unfortunately, the undergraduate laboratories are at present inadequately equipped with experiments on mechanics. There are two reasons for this. Firstly, damping is a formidable enemy of moving systems, so that it is not really easy to design mechanical experiments whose behaviour would sufficiently approach the ideal. Secondly, measurement of velocities using small enough sampling distance involves time-intervals much smaller than what the best of stop-watches can measure.

We have constructed a linear air-track, where the bodies under study glide on a cushion of air so that friction becomes negligibly small. This limits our study to one-dimensional motion, but this incidentally gives us a simplification to start with. We have also developed an electronic timer counter with photo-transistor sensing to measure time intervals with least count upto 10 microsecond without direct mechanical contact with the moving gliders.

The experiments on the air-track designed by us use magnetic interaction, instead of the usual elastic interaction through springs. This extends the range of experiments, insofar as a large variety of potentials can be generated. Also one can do experiments on the passage of a projectile through a potential field, when the field magnets are placed sideways from the track. Use of magnetic interaction made it necessary to avoid a metallic air-track, which causes electromagnetic damping. We, therefore designed and fabricated the air-track from perspex sheets.

While the perspex air-track and the electronic timer opened the gates for a wide range of experiments on one-dimensional motion, the timer also helped us to develop another series of experiments centred on the rigid pendulum. Apart from quantitative experiments on damping, we developed a maintained oscillator for the study of forced oscillations (including phase relations), and a simple quantitative coupling device for the study of frequency splitting in normal modes in coupled oscillations.

Finally, a torsional transmission line (vertical) has been designed for the study of wave propagation under variable termination.

The range of equipment described in this book is now being used at a large number of institutions all over India.* Under a programme of the UGC we are supplying the equipment at bare cost basis to educational institutions. However, for those who have the facilities and a desire to make their own equipment we have given complete details of the equipment (including those for the fabrication of the perspex air-track) and of the circuits for the electronic digital timer counter and the phototransistor sensor.

Unlike the electrical experiments described in Vol. 1 of this series, the experiments in mechanics have a much wider range and variety. Therefore, they permit the teacher a larger degree of freedom as regards both the sequence and the content of experiments. We have chosen a sequence based on the use of the air-track, the oscillators and the transmission line. But one could, for example, start with the harmonic oscillator, go on to oscillations in potential wells of different shapes (using the air-track), then to forced and coupled oscillators, and then to inelastic collisions, time-delay, etc. We hope that what is described in this book will not limit the teachers' choice, but will enable him to design a programme best suited to his line of thought and environment.

B. SARAF

---

*One set has gone to UNESCO through the International Centre for Theoretical Physics, Trieste, Italy.

BRIEF DESCRIPTION OF BASIC EQUIPMENT AND GENERAL SUGGESTIONS FOR THE STUDENTS

Physics is primarily an experimental science. While concepts are important in interpreting experimental results and in proposing new experiments, the ultimate basis of all physics is experiment. It is therefore important that you learn physics through experiment.

What you learn out of an experiment depends partly on the equipment available and partly on how you apply your mind to collect the data, to understand the underlying concepts and to extend those concepts to other parallel situations. The discussion below will be of help to you in these directions.

1. The Linear Air-Track

For meaningful experiments on mechanics you need to keep bodies practically free from friction. This is achieved by making the bodies float on a cushion of air. The linear air-track is one such device. Full details of this are given in Appendix I-A and it will be useful for you to go through it. Figure 0.1 gives a photograph of the air-track with its accessories.

Briefly speaking, the linear air-track is a two-metre long hollow horizontal tube of triangular cross-section fabricated out of perspex (acrylic plastic) sheets. Holes are drilled at regular intervals along the length of the tube, through which air may be blown with a blower. Aluminium gliders literally float on this cushion of air and can move along the track freely with little friction.

To avoid the effect of gravitation on the motion under study the air-track must be set accurately horizontal. Levelling screws are provided at the ends of the track for this purpose. The best check of horizontality is that the glider (when floating) should not move either way on its own.*

Some of the questions which could arise in your mind are: could you use gliders of smaller or larger length? Would the glider float with equal ease if the load is increased? Could the air passage at the end farther from the blower be closed or made much wider? To these questions the best answer is given by experiment.

---

*You will notice that there will be some small disturbances even with the best setting. This is either because the track is not perfectly straight or because of small drafts of air (Bernoulli effect). You should be satisfied if the effects of such disturbance are negligible compared with the effect of the interactions under study.

2. Use of Magnetic Interactions

The riders employed for experiments on the air-track carry a bar magnet each to provide magnetic interactions.* Direct hits between two bodies do not provide margin for studying what happens *during* a collision. They also involve loss of energy into forms other than mechanical, *e.g.*, heat. Springs may be used, but it is difficult to keep them horizontal and obtain reproducibility. Electrical and magnetic bodies provide *interaction at a distance* and one can also arrange several of them to make their interactions superpose. But static electrical charges are difficult to maintain. For these reasons we have chosen to use magnetic interactions. Incidentally the interaction range of the magnets used is of sufficient span (25 to 40 cm) to permit use of sampling distance 0.3 to 1.0 cm for velocity measurement.

The magnets provided for the experiments have to be short, of high magnetic moment, and capacity to retain their magnetism for long time. You will be well advised to use them with some respect—handle them without jerks and pack them with keepers when they are not in use.

In mounting the magnets on the riders, care must be taken that they remain either parallel to the track or perpendicular to it and symmetrical as desired. Also the interacting magnets must be kept at the same height from the track, otherwise wobbling may occur, resulting in some energy loss. When extra mass is added on the gliders, care may be taken that the centre of mass of the system may not go far from the line of the magnetic axis, otherwise wobbling occurs.

The reason for our using a perspex (non-metallic) air-track is that magnets moving near a conductor experience electromagnetic damping. Obviously, you should not place other metallic bodies too close to the track.**

3. The Measurement of Time Intervals: The Digital Timer Counter and Sensors

Two things are necessary for measuring time intervals: (*i*) a time measuring device (clock), and (*ii*) a 'sensor' which is to tell the clock when to start and when to stop. The least count of a stop-watch is seldom better than 0.1 second. The sensing action is done by your eye and hand, and that too is not good enough when you go down to fraction of a second, since the eye response is not sufficiently fast†

For the measurement of time intervals in the experiments we have

---

*A rider carrying a magnet is hereafter called a *glider* or a projectile.

**The riders, which are of aluminium, would cause some loss when another glider moves in the neighbourhood.

† One of us was acting as a time-keeper in a college 100 metre dash and his poor experience and slow response with the stop-watch resulted in the first four students setting world records!

designed a *sensor* and a *timer*, full details of which are given in Appendix I-B. The sensor uses a narrow* pencil of light falling on a phototransistor. A strip mounted on the moving glider interrupts this pencil of light (Fig. 0.2) and this provides a signal to the timer to start or stop counting time. The time interval measurement is carried out with the digital timer counter. Figure 0.3 gives a photograph showing the front panel of the double channel digital timer counter.

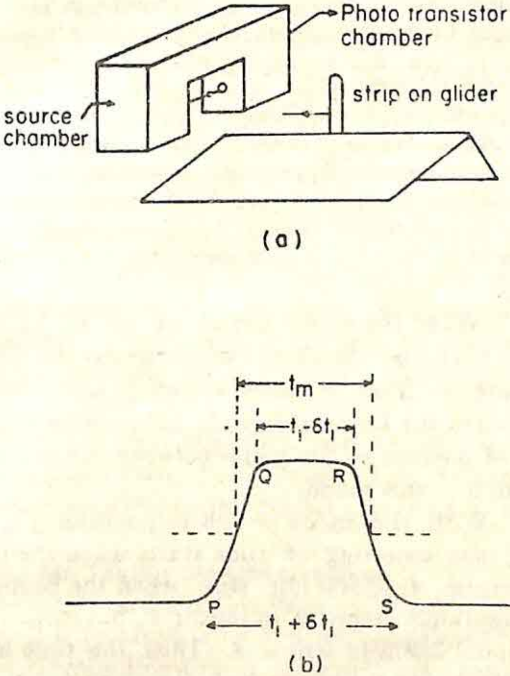

FIGURE 0.2.(*a*) Photosensor and the glider with an intercepting strip, (*b*) the signal produced by the photosensor.

The timer has a quartz crystal-controlled oscillator of frequency 100 KHz and the number of oscillations completed in a given time is displayed on a 4-digit electronic counter. Thus each count means 10 micro-second time-interval. A provision for scaling in steps of ten can make each count equal to 100 micro-second, 1 ms, 10 ms, 100 ms or 1 s. Signals from the sensors control the 'gate' of the counter and provision has been made for three distinct modes in which the signals may instruct the gates.

Mode $\rfloor\overline{A}\lfloor$. When the mode switch is set at $\rfloor\overline{A}\lfloor$, the logic circuit so works that the counter starts counting when the beam of light is interrupted in sensor A and stops counting as soon as the interruption in A ceases. If the count is t and the obstructing strip on the glider has width w, the velocity of the glider is given by w/t. You will appreciate that if w is ~ 5 mm and velocity is ~ 0.5 m/sec, the timer count is ~ 10 ms. Thus a measurement of time with least count 10 μs gives an accuracy of 1 part in 1000.

---

* 'Narrow' is a relative term. A 1 mm wide pencil is quite narrow for a 10 mm wide sampling strip. But with a 3 mm wide sampling strip the 1 mm width ceases to be really narrow (*see* Fig. 0.2).

Increasing the sampling distance w ten-fold would increase the accuracy of measurement of both w and t. But you will then be measuring an 'average' velocity over engtn 50 mm, not over 5 mm. The theoretician would define 'instantaneous velocity' as w/t when w *tends to zero*. But an experimentalist knows that the accuracy of measurement (of both w and t) decreases as w decreases. (In any case it will be absurd to measure time interval for zero travel). A compromise has, therefore, to be made, depending on the total range of interaction and the least count of the measuring devices. With the two-magnet interaction the total range of meaningful interaction is about 25 to 40 cm; it will be obvious that a sampling distance (w) of 10 cm or 5 cm will not give enough details, possibly 1 cm is the uppermost desirable limit, and about 3 mm would be better still if good micrometer and a timer are available.*

Mode $\rfloor\overline{A}\ \rfloor\overline{B}$. When the mode switch is set at $\rfloor\overline{A}\ \rfloor\overline{B}$, the logic circuit so works that the counting starts when the beam of light is interrupted in sensor A, *does not stop counting when this interruption ceases*, but stops when the beam of light is interrupted in another sensor B. Thus the time of passage of the glider between the positions of sensors A and B is measured in this mode.

Mode $\rfloor\overline{A}\ \rfloor\overline{A}$. With the mode switch in position $\rfloor\overline{A}\ \rfloor\overline{A}$, the logic system so works that counting of time starts when the beam of light is interrupted in sensor A, does not stop when the beam in sensor A is cleared or when anything happens in sensor B, but stops when the beam of light is interrupted again in sensor A. Thus, the time interval between two successive passages of the glider from the same position is measured in this mode.

An additional mode is provided in some timers. A switch makes the timer skip the alternate interruptions in the $\rfloor\overline{A}\ \rfloor\overline{A}$ mode. For measurement of period T of an oscillator this is needed. In the absence of this provision you have to measure time T_1 for passage one way and T_2 for the passage the other way and add them. As an analysis would show this will really be a little short of T (why?). Of course, this switch must be kept at 'off' when modes $\rfloor\overline{A}\lfloor$ or $\rfloor\overline{A}\ \rfloor\overline{B}$ are in use.

The Double Channel Timer. For many experiments we need to measure two time intervals in one run. For this purpose a double channel digital timer counter is used. Modes $\rfloor\overline{C}\lfloor$, $\rfloor\overline{C}\ \rfloor\overline{D}$ and $\rfloor\overline{C}\ \rfloor\overline{C}$ of the second counter have the same functions as modes $\rfloor\overline{A}\lfloor$, $\rfloor\overline{A}\ \rfloor\overline{B}$ and $\rfloor\overline{A}\ \rfloor\overline{A}$ respectively of the first counter.

---

[*] In contrast, for a car journey of (say) 100 km, a sampling distance of half a kilometre should be good enough to describe the velocity changes.

Accuracy of Time Measurements. Since the crystal oscillator in the timer is not thermally controlled, a small variation in absolute time measurement may occur. But this is insignificant in the context of the mechanical experiments to be done. In our design of the double timer the same crystal controls both the counters. Therefore, relative error due to the clock itself is excluded.

The major limitation to accuracy really comes from the use of small sampling widths and the finite width of the beam, of light in the sensor. The pin-hole determining the beam has a diameter ~ 1 mm. Therefore, if a 10 mm strip interrupts the beam, the full obstruction lasts for $10-1=9$ mm travel, with slopes on each side corresponding to 1 mm travel (Fig. 0.2b). The timer 'gate' would thus remain open for time corresponding to anything between 9 and 11 mm travel, depending on where the trigger level is set by you in the timer. However, in the practical range of trigger levels the range of error is much less (<5 per cent). In a series of measurements with the same timer, set at a constant trigger level, the effect will be much below 1 per cent. It is advised that you note the two extremes for the trigger knob and set it in the middle for working. This ensures that the time measurement is quite close to that corresponding to the sampling width. It also ensures that stray mains voltage fluctuations do not result in skipping of some counts by the timer.

In a double timer you may adjust the two trigger levels to make the readings match within (say) 1 per cent. This is especially important when smaller sampling widths (like 3 mm) are used.

4. The Technique for Taking the Observations

Suppose you want to measure the velocity V of a glider at different positions x after it is released from a given position. If you had (say) 20 sensors and corresponding timers you could just spread the sensors in the range of x of interest to you and get the corresponding V data in one sweep on the 20 timers. With a single timer the technique will be to repeat the experiment 20 times with the same initial condition, placing the sensor at different positions x in each trial. This method assumes that the initial condition is reproducible to the extent of the accuracy desired. The spacers are particularly useful for this purpose.

Suppose you desire to determine V at different *times* t after release of the glider from some position. For this the double timer is useful. Set one sensor A near the release position of the glider and another sensor B at a variable distance x. Plug-in A and B to the first timer and connect input of B to input C of the other timer.* Set the first timer mode to

---

*There will be many situations in which one of the inputs in two timers needs to be connected to an input of the other. Which one is connected to which will depend upon what corresponding measurements you need from the timers.

$\rfloor\overline{A}\,\rfloor\overline{B}$ and the second timer mode to $\rfloor\overline{C}\lfloor$. The time reading in the first gives travel time t from sensor A to sensor B (this varies with x); the time reading in the second leads to the determination of glider velocity V at sensor position B.

With a single timer you will have to use a different technique. In one series set the timer to mode $\rfloor\overline{A}\,\rfloor\overline{B}$ to get x vs t data; in another series plug-in sensor B to the A socket of the timer and set the latter to mode $\rfloor\overline{A}\lfloor$ to get x vs v data. These then lead to v vs t data.

5. The Scatter of Experimental Data

In repeated measurement of the same experimental quantity there will always be some differences. These may arise from variations of initial conditions in different trials, variations in the unaccounted interactions (like wobbling, air-currents in the room, or even your breathing), or uncertainty in the setting of your measuring device. Such variations are called 'scatter' or 'spread' of the experimental data.

In fact there are experiments in which nature itself provides a scatter in the value of the quantity under measurement. The scatter is then not due to the limitations of the equipment or the experimentalist. As one example, consider an experiment on counting (say) the α particles from a given radioactive sample in a given geometry. Let the experiment be repeated with identical samples and identical geometry. It is found that the count rate shows a scatter far beyond the experimental limitations. Nature obviously plays statistics when it comes to individual events at atomic levels. But in your experiments the scatter is due primarily to the experimental limitations of reproducibility or of measurements.

Reducing the scatter of data to the minimum is the business of a good experimentalist. But even the best performed experiments will have some scatter. What is important is to have an understanding and information about the scatter.

Consider the following set of readings of a timer counter in repeated measurement of velocity under identical situations:

12.54, 12.68, 12.47, 12.59, 12.72, 12.49 ms.

The total spread is 12.72—12.47=0.25 ms, which is about 2 per cent. If the uncertainties elsewhere are likely to be more than 2 per cent, then this scatter is not to be considered as significant. All the same, your conclusions, if drawn from a single set for each situation, should not be stated to an extent better than 2 per cent.

The graphical method of interpreting the data is useful to take a fair degree of care about the scatter; you draw a smooth curve passing in close proximity with the observation points. Figure 0.4 (a) shows how a smooth curve is the best representation of the experimental data, although it does not pass through most of the observation points.

You may have a lingering doubt: should not the curve be drawn to touch each observed point? Well, repeat the same experiment taking (say) four observations of Y for each X. Figure 0.4 (b) shows this. Obviously, now you cannot think of having a curve passing through all the observation points. All you can do is to draw the curve in such a way that it does not go outside the range of scatter in Y.

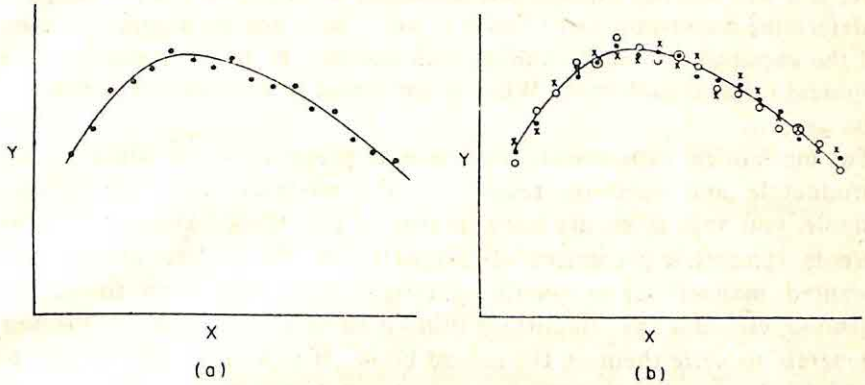

FIGURE 0.4. The graphical treatment of data—(*a*) a smooth curve fitting the experimental data, (*b*) the scatter of data.

6. Attention to Mechanical Designs

Apart from the air-track and the timer, you will be using several other equipment whose mechanical design can best be understood by seeing them critically. As one example, you may take the bar pendulum mounted on two sharp pivots supported on a plate. You may examine why a knife-edge support is not chosen and why the pivot pins as well as the plates must be of hard metal. As another example, the design of the coupled oscillator (one pendulum mounted on another) needs special attention how the relative vertical positions of the axes of oscillation of the two can be changed, and why a counter-weight is to be used for one of the pendulums. If you wish to be a good experimentalist you would do well to pay attention to all these details.

7. Your Laboratory Work

We have provided no particular format for recording the laboratory work. This is because we want you to develop your own method, depending on the relative emphasis in the experiment.

It is a common advice that you may prepare yourself for the experiment *before* doing it. Well, it is true that such preparation will enable you to organise the experiment better. But in mechanical experiments the design details govern the performance of the experiment and hence the most important advance preparation is to have a look at the equipment and to understand the functions of each component. Now, if you are aware of what information you desire to get out of the experiment you can intelligently plan to adjust your parameters as you proceed with the experiment.

As you will see, the experiments described in this book are not designed to determine a constant or to verify a law. They are open-ended studies and the variation of one parameter with another is to be presented in a graphical form in each case. What is important is your interpretation of these graphs.

The mechanical experiments need several precautions in order to get reproducible and accurate results. In the air-track experiments, for example, you have to ensure horizontality of the track, absence of air-currents, symmetric placement of magnets on the rider, absence of unwanted magnets or magnetic materials or metals from the neighbourhood, etc. But the important thing is to *take* these precautions and not merely to *write* them on the record book. If you are able to appreciate how the given equipment may give the best results, you are certainly on the path of becoming a good experimentalist.

CONTENTS

Statement v
Preface ix
Brief Description of Basic Equipment and General Suggestions for the Students xi

Chapter 1 **STUDY OF COLLISIONS** 1
Collision. Isolated Systems. The Conservation Laws. Collision of Two Bodies when one is Initially at Rest. Collision with a Body of 'Infinite' Mass. Preliminary Experiments about Quality of the Air-Track

EXPERIMENTS
1-A. *Energy transfer between two gliders in Collision* 7
1-B. *Dependence of energy transfer on the mass ratio of the colliding gliders* 8
1-C. *Conservation of momentum with initial momentum zero* 9
1-D. *Conservation of momentum with initial momentum non-zero* 10

Appendix I-A **The Perspex Air-Track** 13

Appendix I-B **The Digital Timer Counter** 16

Chapter 2 **THE STUDY OF POTENTIAL ENERGY DIAGRAMS** 28
Mechanics and Newton's Laws of Motion. The Measurement of Potential Energy

EXPERIMENTS
2-A. *Potential energy curve due to magnet-magnet interaction* 31
2-B. *The gravitational potential energy* 35
2-C *Superposition of gravitational and magnetic potential energy curves* 36
2-D. *Potential energy of a magnet bounded by two fixed magnets* 37

Chapter 3 **STUDY OF OSCILLATIONS IN POTENTIAL WELLS OF DIFFERENT SHAPES** 42
Potential Wells. Oscillations in a Potential Well.

EXPERIMENTS

3-A. *Frequency versus energy curves for oscillations in a potential well* 46
3-B. *Effect of oscillator mass on the frequency* 49
3-C. *Frequency versus energy curve when two bodies oscillate against one another* 51
3-D. *Oscillations in a rectangular potential well* 52

Appendix III-A **Graphical Method for Deducing the Details of Motion in a Potential Well** **55**

Appendix III-B **The Concept of Reduced Mass** **61**

Chapter 4 **STUDY OF SOME SPECIAL POTENTIALS** **62**
Introduction. Generating Regions of Different Forms of Potential. Time-Delay in Passing Through a Field.

EXPERIMENTS

4-A. *A potential hill with side wells* 67
4-B. *A potential well with shoulders* 69
4-C. *A simple potential hill or well* 69
4-D. *Oscillations in a potential well with shoulder hills* 70
4-E. *Oscillations in a simple potential well* 70
4-F. *Some other potential shapes and study oscillations in them* 71
4-G. *Time-delay in passing through a potential hill* 75
4-H. *Time-delay in passing through a simple potential well* 78

Appendix IV-A **Deduction of Potential Parameters from Time-Delay** **80**

Chapter 5 **INELASTIC COLLISIONS** **85**
Introduction. Internal Modes of a System. General Description of the Arrangements. Determination of the Energy Transfer. Preliminary Experiments: (a) Constants of the Internal Mode, (b) Torque versus Projectile position.

EXPERIMENTS

5-A. *Energy transfer as a function of projectile energy or velocity* 90
5-B. *Dependence of the absorption curve on the projectile mass* 91

5-C. *Dependence of the energy absorption on the restoring factor C of the internal mode 93*
5-D. *Dependence of the absorption curve on the inertia factor I of the internal mode 94*
5-E. *Effect of phase relation on the energy transfer 98*
5-F. *Energy transfer to a different mode of the target oscillator 101*

Appendix V-A **Analysis of Energy Transfer in Inelastic Collisions of Dipoles** **103**

Chapter 6 **STUDY OF DAMPING IN A HARMONIC OSCILLATOR** **112**
Introduction. The Damped Harmonic Oscillator.

EXPERIMENTS
6-A. *Variation of period with amplitude in large angle oscillations 114*
6-B. *Damping of an oscillator 115*
6-C. *Dependence of damping coefficient* α *on I and C of the oscillator 117*
6-D. *Effect of the total mass on the damping factor* r *119*
6-E. *Air-damping contribution in the oscillations 120*
6-F. *Damping due to a vane in water 122*
6-G. *Electromagnetic damping using a coil 123*
6-H. *Electromagnetic damping using a metal sheet 126*

Appendix VI-A **Proof that Small Oscillations are Harmonic** **128**

Appendix VI-B **Theory of the Rigid Pendulum** **129**

Appendix VI-C **Theory of Damped Oscillations** **130**

Chapter 7 **STUDY OF FORCED OSCILLATIONS** **133**
General. Forced Oscillations. Description of the Apparatus: (a) Maintained Oscillator, (b) The Coupling, (c) Measurement of Relative Amplitudes and Phases, (d) Measurement of Velocity Amplitude.

EXPERIMENTS
7-A. *Amplitude response in force oscillations 138*
7-B. *Velocity response in force oscillations 142*
7-C. *Driven oscillator lags behind the driver in phase 143*

Appendix VII-A **Theory of Forced Oscillations** **148**

Appendix VII-B **Effect of Coupling by Means of a Loaded Thread Tied between Two Rigid Pendulums** 151

Chapter 8 **COUPLED OSCILLATIONS** 154

Free Oscillations of a Coupled System. Normal Modes. The Experimental Set-up

EXPERIMENTS

- 8-A. *Measurement of the coupling factor C_{ab} and its Dependence on different parameters 157*
- 8-B. *Frequency of normal modes in a coupled oscillator 158*
- 8 C. *Frequency of energy transfer between the components in coupled oscillations 161*
- 8-D. *Details of energy transfer between the components in coupled oscillations 162*
- 8-E. *Coupling of simple pendulums through a bar support 164*
- 8-F. *Coupling of rigid pendulums when one rides over the top of the other 166*

Appendix VIII-A **Theory of Coupled Oscillations** 167

Chapter 9 **STUDIES WITH THE TORSIONAL TRANSMISSION LINE** 171

Introduction. Description of the Torsional Transmission Line. Constants of the Line. Exciting the Torsional Transmission Line.

EXPERIMENTS

- 9-A. *Determination of the constant C′ of the transmission line 175*
- 9-B. *Dispersion relation in the transmission line taking the configurations as given 176*
- 9-C. *Normal mode configurations and dispersion relation in the transmission line using the resonance method 179*
- 9-D. *Propagation velocity along the line 181*
- 9-E. *Dependence of propagation velocity on the line parameters 182*
- 9-F. *Variation of reflection coefficient with termination 183*
- 9-G. *Partial reflection and partial transmission at the boundary of two media 186*

Appendix IX-A **Theory of the Mechanical Transmission Line** 189

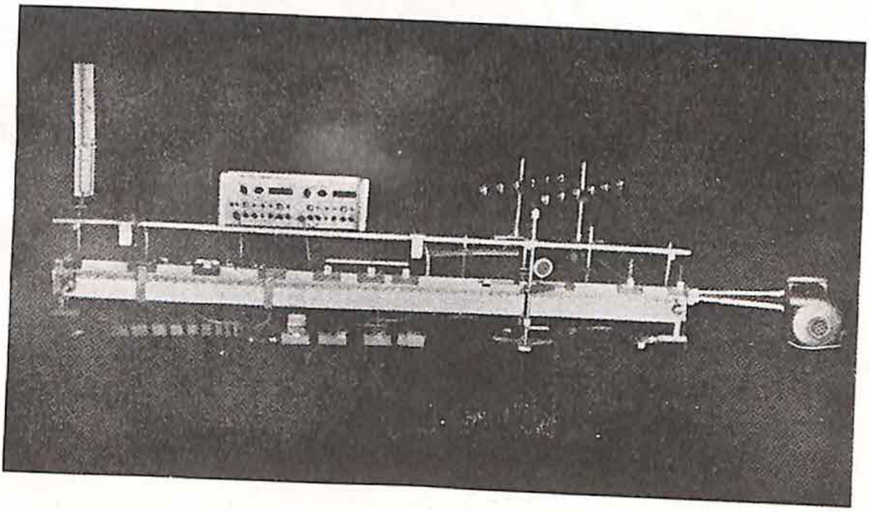

FIGURE 0.1. Photograph of the linear air-track.

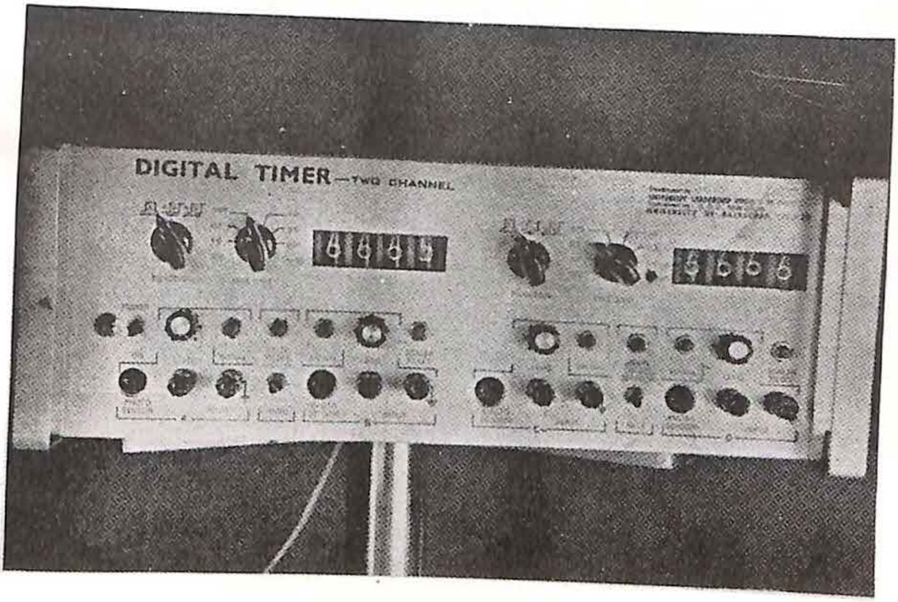

FIGURE 0.3. Photograph of the front panel of the digital double timer counter.

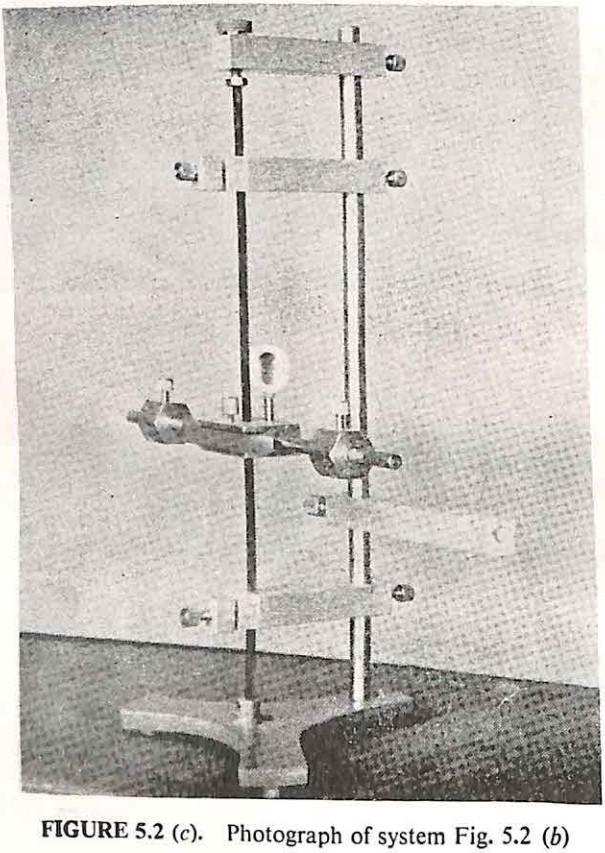

FIGURE 5.2 (*c*). Photograph of system Fig. 5.2 (*b*)

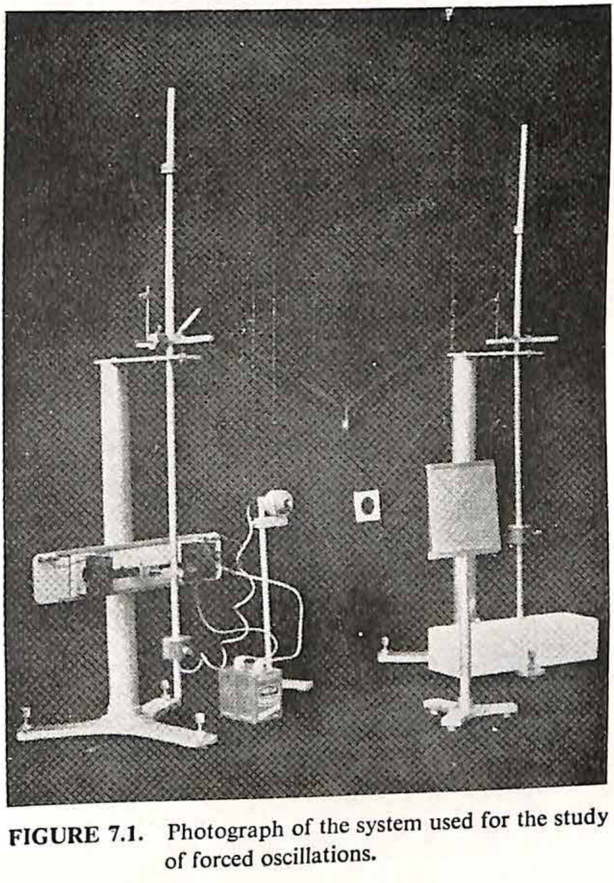

FIGURE 7.1. Photograph of the system used for the study of forced oscillations.

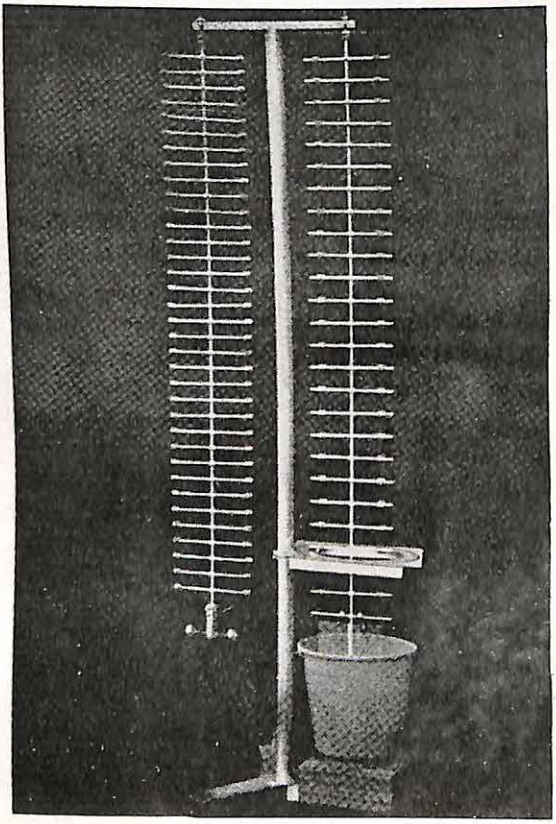

FIGURE 9.1. Photograph of the torsional transmission line.

1

STUDY OF COLLISIONS

1.1. COLLISION

In common language 'collision' is an event in which one body 'hits' another; it involves the interplay of forces between two (or more) bodies and consequent changes in their momentum and kinetic energy. Quite often a collision is taken as a short-time or short-range process so that we may speak of momentum and kinetic energy of a body *before* its collision with another body and *after* the collision, but may ignore the details of what happens *during* the collision. A collision between two steel balls is typical in this category. However, in science any mutual application of force between two bodies is called an 'interaction' and this is not always of short duration in time or distance.* The event from the start to the end of an interaction may be called a 'collision' and we may be interested not only in what happens as a net result of a collision, but also in the details during the collision. The collision of a volley-ball with the net is a typical example in which we can *see* what happens to the net and the ball at different stages *during* the collision. Of course, the duration of the collision becomes shorter if the net is made tighter; we may further reduce the duration if the ball is made to hit a wall; still further if the ball is filled to higher and higher pressure; and finally we may pass on to consider a steel ball hitting a steel wall. The interaction time now becomes very small, yet it is not zero and you could be interested in the details during this collision too.

1.2. ISOLATED SYSTEMS

Your interest in studying collisions is in finding how the energy and momentum exchange occurs. You will realise that for this purpose you will have to clearly identify the interacting bodies, *i.e.*, to isolate the members participating in the collision. If you study the collision of bodies *A* and *B* you must make sure that no other body interacts with either *A* or *B*. In the case of two steel balls, friction is one parasitic interaction and, if the floor is not horizontal, earth's interaction (gravity) is another. In the case of the volley-ball and the net example, you will have to remember that the net is tied to the poles, which in turn are pegged on the earth, so that participants in the collision (the net and the ball) are not well isolated.

---

* Thus the moon is continuously in collision with the earth, the interaction force being gravitational. When we talk of a collision in common language we are merely saying that the elastic force between the two bodies is very much stronger than the gravitational, magnetic or electrical force (in fact, the elastic force is itself understood in terms of electromagnetic force between bodies which are neutral on the whole).

One neat case of collision between two isolated bodies is when a stone falls on ground. While the stone is held by some agency, the earth's pull is balanced by the force from that agency. So that collision may be taken to start only from the moment the body is released.[*] Thereafter the two bodies colliding are the stone and the earth (neglecting air friction). You will notice that if the changes in momentum and energy of the earth are ignored the analysis will be incomplete; the earth *is* a party in the game.

In the experiments which you are to perform two magnets mounted on separate gliders, floating on the horizontal air-track, form the isolated system under study. Because the track is horizontal earth's gravitation does not contribute to the change in motion. And because of the air-cushion, friction with the track does not play appreciable role. Thus the exchange of energy and momentum arises primarily from the interaction between the two magnets, which form an isolated system.

1.3. THE CONSERVATION LAWS

Consider a collision between two bodies A and B, which are isolated from the rest of the universe. If $K_A=\frac{1}{2}\,mv_A^2$ is the kinetic energy and $p_A=mv_A$ is the momentum of A at any stage of the interaction and K_B, p_B are the corresponding quantities for the body B then the conservation of momentum says that

$$\mathbf{p}_A+\mathbf{p}_B=\text{constant} \qquad \ldots(1.1)$$

during all stages of the interaction. If the values *before* the interaction starts are $\mathbf{p}_A^\circ$, $\mathbf{p}_B^\circ$ and those *after* the interaction ends are $\mathbf{p}_A'$, $\mathbf{p}_B'$ then

$$\mathbf{p}_A'+\mathbf{p}_B'=\mathbf{p}_A^\circ+\mathbf{p}_B^\circ \qquad \ldots(1.2)$$

which is a special — and limited — case of relation (1.1). You will certainly like to check the validity of Equation (1.1), which holds at all the stages during an interaction and for this you will need to measure the momenta at various instants *during* the collision.[**]

Let us now have a look at energy conservation. Unlike momentum, energy has several forms—kinetic, thermal, potential, etc. If you include *all* kinds of energy of the given isolated system, then their sum remains constant during all stages of the interaction. This is the law of conservation of energy.

---

[*] In accurate terms before release the interacting system was the stone + earth + the agency. Removal of the agency holding the stone gives us the isolated system of stone+earth. (Of course, ignoring the rest of the Universe !)

[**] To be precise, momentum is a vector quantity and, therefore, Equation (1.1) would really mean three equations for the three dimensional space. Experiments on the linear air-track, being one-dimensional, do not however permit you to verify this wider character of Equation (1.1).

If the collision is such that at the end of the collision no energy is transferred into forms other than kinetic energy of translation, the collision is called an *elastic* collision. For such collisions the total kinetic energy *after* the collision is equal to the total kinetic energy *before* the collision. In the case of two colliding bodies we may then write:

$$K_A' + K_B' = K_A^\circ + K_B^\circ \qquad \ldots (1.3)$$

However, during the collision the sum $K_A + K_B$ is not constant. In view of Equation (1.3) it will be reasonable to assume that the difference of $K_A^\circ + K_B^\circ$ and $K_A + K_B$ during the collision is stored in some other form of energy, to be returned to the kinetic form later. You are familiar that this stored form of energy is called potential energy of the system, denoted by U_{AB}. As parallel to Equation (1.1) you can then write:

$$K_A + K_B + U_{AB} = \text{constant} \qquad \ldots (1.4)$$

during all stages of an elastic collision. But this relation will not hold if the collision results in part of the energy going into forms other than potential (*e.g.*, heat or light). The collision is then called '*inelastic*.' Potential energy will be the subject of your study in the next chapter. For the present your interest is in Equation (1.3).

The conservation laws have a crucial role in all physics because without going into the details of any interaction they set the general rules which must be followed without exception. Thus neither Equation (1.2)* nor Equation (1.4) makes any reference to the details of the interaction. Whether the collision is between two planets or two magnets or two protons, these laws will hold true, although the interactions are so different in character.

Universality is the essence of the conservation laws. What is not allowed by the conservation laws can never be realised in practice.** That is a negative aspect. But the positive aspect is equally significant. What is not forbidden by the conservation laws should be possible. As one example, consider a body moving from left to right with energy E, facing a potential hill of height U. If U is greater than E, then classical mechanics would say that the body can never be found on the right hand side of the hill, because in the region where $U > E$ the kinetic energy $(E - U)$ would become negative, *i.e.*, velocity v of the body would become imaginary. But the law of conservation of energy makes no reference to these details of the motion. So it does not forbid the arrival of the body across the hill; in other words it should, in principle, be possible for the body of energy E to cross over the potential barrier of height U even if U is greater than E. The quantum theory, which uses the conservation laws (rather than the detailed mechanism of the laws of classical mechanics—like Newton's Laws), does predict such occurrences and explains many nuclear phenomena on that basis.

---

* It has three components in the general three dimensional case.

** An industrialist once visited one of us with a retired engineer who claimed that he could design an electrically driven car which would use its own dynamo as a source of electrical power. We did not have to open his files and study the design sheets to tell him that the proposal was not feasible.

Thus the conservation laws are not just deductions from other laws. They are more powerful generalisations, which hold true even if the starting laws are later on modified or given up.

1.4. COLLISION OF TWO BODIES WHEN ONE IS INITIALLY AT REST

Let one of the two colliding bodies, say B, be initially at rest ($K^0{}_B=0$) For that case Equation (1.3) becomes

$$K_A'+K_B' = K_A{}^0 \qquad \ldots(1\ 5)$$

Thus, out of the total energy $K^\circ{}_A$ (which was initially with body (A), an amount K_B' is transferred to body B in the collision. The fraction of energy transfer is thus

$$f=K_B'/K_A^\circ \qquad \ldots(1.6)$$

Since energy transfer through collisions is of considerable practical importance it will be of interest to see what parameters govern f. Let us check by experiment whether f depends on the initial kinetic energy K_A°, or onthe colliding masses m_A and m_B.

1.5. COLLISION WITH A BODY OF 'INFINITE' MASS

This is of special importance, because there are many cases in which one of the interacting bodies is much heavier than the other. Consider a magnet M_1 on a glider released from a specified distance from another magnet M_0 which is clamped on the linear track. Because of 'clamping' the mass of M_0 effectively becomes the earth's mass, thus very much larger than that of M_1. It will be wrong, however, to think that when the system gives a momentum p_1 to M_1, there is a violation of the conservation of momentum. M_0, which is fixed to the track and through it to the earth, gains momentum p_0 exactly equal to $-p_1$. But the corresponding velocity of M_0, given by $v_0=p_0/m_0$, is too small to be noticeable because m_0 is almost 'infinite' compared with m_1. The same happens in the stone-and-earth example of §1.2; as the stone gains downward momentum, the earth gains an equal upward momentum all the time during the fall, though you just cannot see the earth rising because of its large mass.

The kinetic energy is related with momentum through the relation $K=p^2/2m$. Therefore in the aforesaid example the kinetic energies of M_0 and M_1 are $p_0{}^2/2m_0$ and $p_1{}^2/2m_1$ respectively. Thus although $p_0{}^2$ is equal to $p_1{}^2$, we find that K_0 is negligibly small due to large m_0. It is a bad broker's game! Equal momenta, quite honestly; but the consequent kinetic energies are not at all equal if one of the two bodies is much greater in mass than the other.

1.6. PRELIMINARY EXPERIMENTS ABOUT QUALITY OF THE AIR-TRACK

To be able to appreciate the validity of the conclusions from the experiments it will be good to have a preliminary experiment on the quality of the air-track.

Clamp one magnet M_0 at one end and release the glider magnet M_1 from a distance a from M_0. Put one sensor at $\sim$ 40 cm distance (the interaction from M_0 may be taken as negligible there) and another at distance of (say) 100 cm from the first. Measure the velocity of M_1 at the positions of the two sensors. From these values of velocity, using the mass of the glider, deduce the loss of kinetic energy per centimetre travel.

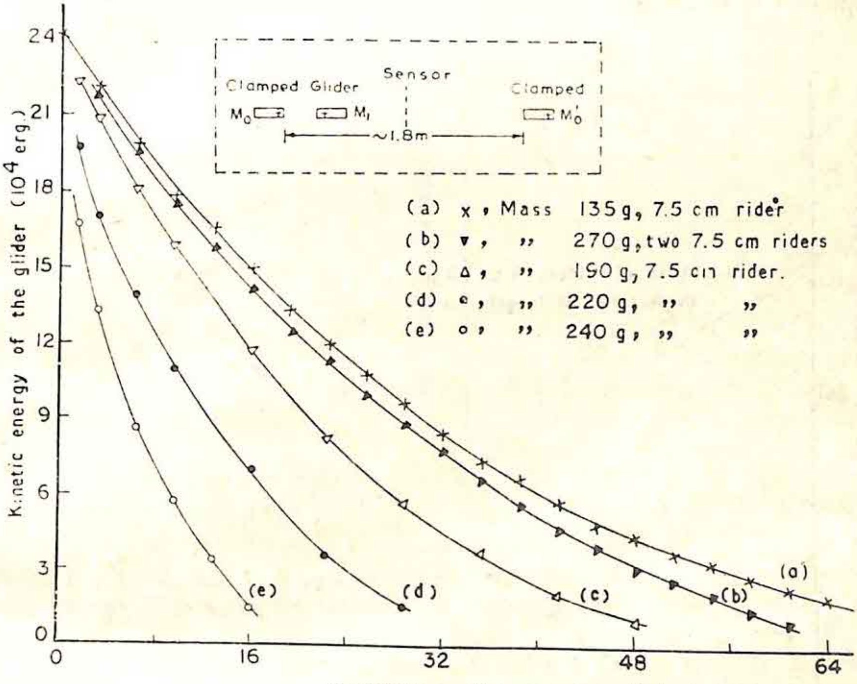

FIGURE. 1-1. Variation of kinetic energy of the glider with distance travelled on an air-track for different masses.

However, you will find that the energy loss over $\sim$1 metre travel is so small that the meaningful results will be swamped by the scatter of data. For this reasons the arrangement shown in the inset of Fig. 1.1 is better where another magnet M_0' is clamped at the other end in repulsive mode with M_1. Release the glider from a position close to one of the end magnets; it will make several transists forward and backward (each amounting to about 4 metre travel) and you may measure the velocity (and hence KE) of the glider at the centre after (say) every 2 transists. A graph of KE against the cumulative travel distance gives you an idea of the damping rate. Figure 1.1 shows the results of one such experiment for different masses of the glider.

It may be noted that the damping increases as the glider mass increases. With a rider of ~ 8 cm length the upper load limit is ~ 200 gm. But hooking up two riders* of 8 cm each permits the glider mass to go up to ~ 400 gm.

For a single rider with a magnet (mass 135 gm) the kinetic energy loss per cm distance is deduced from curve (a) of Fig. 1.1 for different velocities v. This, in effect, gives the frictional force F vs v data, which leads to coefficient of friction μ vs v data ($\mu = F/mg$); Fig. 1.2 shows these results.** It will be seen that increases F with v, although one cannot speak of direct proportionality. The order of μ in the middle range of v is $\sim 2 \times 10^{-4}$.

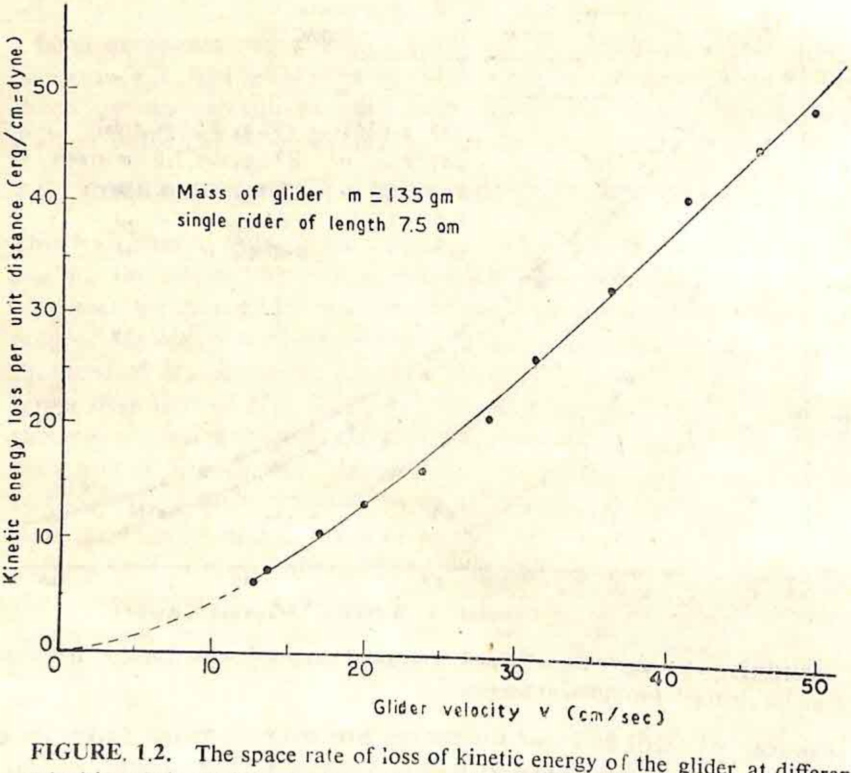

FIGURE. 1.2. The space rate of loss of kinetic energy of the glider at different velocities (deduced from the data of curve (a) in Fig. 1-1.)

---

* See Appendix I-A. 5

** With an aluminium air-track the kinetic energy loss for unit distance, under equivalent conditions, comes out to be appreciably larger and increases in direct proportion to velocity v. This obviously is because of electromagnetic damping due to eddy currents.

EXPERIMENT 1-A *To study the energy transfer between two gliders in collision.*

The inset in Fig. 1.3 shows a magnet M_0 clamped at one end of the air-track and two magnets M_1 and M_2 mounted on gliders. S_1 and S_2 are two sensors for measuring the velocities of the gliders M_1 and M_2 respectively. Sensor S_1 is to be kept far from both M_0 and the initial position of M_2, similarly S_2 is to be kept far from the initial rest position of M_2. The purpose is that velocity of M_1 is to be measured *before* the start of the collision and that of M_2 *after* the end of the collision.

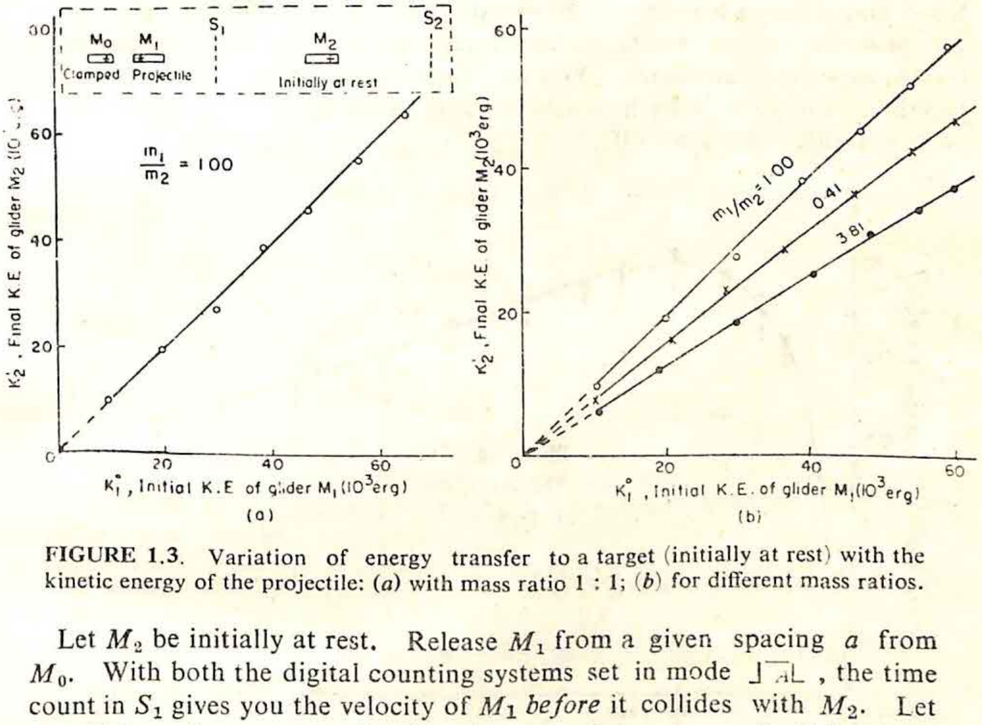

FIGURE 1.3. Variation of energy transfer to a target (initially at rest) with the kinetic energy of the projectile: (*a*) with mass ratio 1 : 1; (*b*) for different mass ratios.

Let M_2 be initially at rest. Release M_1 from a given spacing *a* from M_0. With both the digital counting systems set in mode ⌋‾⌉⌊ , the time count in S_1 gives you the velocity of M_1 *before* it collides with M_2. Let us call it v_1, the corresponding kinetic energy being $\frac{1}{2}\ m_1 v_1^2 = K_1^0$, where m_1 is mass of the glider with magnet M_1. Similarly the time count from S_2 gives the corresponding kinetic energy of M_2 (K_2') after its collision with M_1.

Repeat the measurements with same two gliders but using different release distance *a*, *i.e.*, different initial kinetic energy K_1^0.

Figure 1.3 (a) shows the results of an experiment, plotting K_2' against K_1^0 for a given pair of gliders. Within the range of scatter the graph is a straight line, showing that energy transfer ratio $K_2'/K_1^0 = f$ does not change with initial kinetic energy of glider M_1.

On what factors does f depend? This you will see in the next experiment.

value becomes unity. Figure 1.4 shows this theoretical curve also. It may be noted that the experimental points show good agreement with it.*

Problem 1. From the above expression for f prove that the energy transfer is maximum when $m_1/m_2=1$.

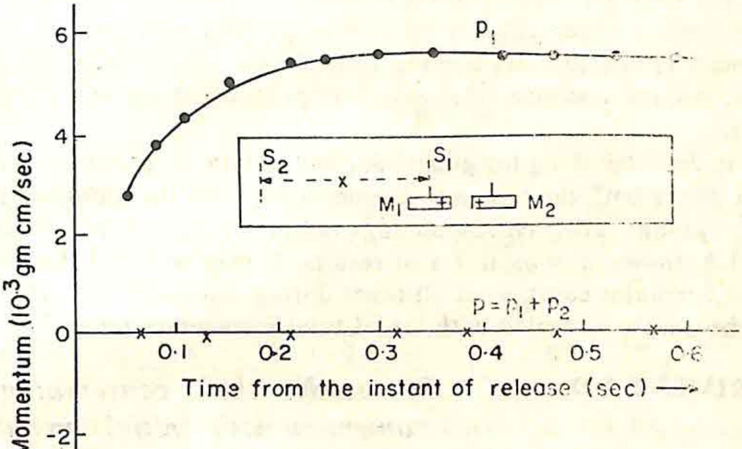

FIGURE 1.5. Plot of momenta of two colliding gliders at different stages of the collision, with zero initial momentum of the system.

Problem 2. A neutron may collide with a nucleus of (*i*) H^1, (*ii*) D^2, (*iii*) C^{12}, (*iv*) U^{238}. Assume the latter to be initially at rest, and deduce the fraction of energy lost in one collision by the neutron in each case.**

EXPERIMENT 1·C *To study conservation of momentum with initial momentum zero.*

On the linear air-track set two gliders M_1 and M_2 in repulsive mode with a separation *a* (Fig. 1.5, inset). If the gliders are *simultaneously*

---

*That the mean experimental values are a little below the theoretical values is due to residual frictional losses.

** This is a case of practical importance. In a nuclear reactor using U^{235} the fission produces *fast* neutrons, whereas for continuing the chain of fissions *slow* neutrons are more effective. The slowing process is called moderation, and as moderators uranium nuclei are no good, C (graphite) is quite good, D (deuterium) in the form of heavy water (D_2O) is still better. (Ordinary water is not used because H atoms capture the neutrons; we want slowing, not capture).

EXPERIMENT 1-B

To study the dependence of energy transfer on the mass ratio of the colliding gliders.

Repeat Experiment 1-A changing the mass ratio m_1/m_2 by increasing the mass of either the glider M_1 or M_2.*

Now with each mass ratio m_1/m_2 you may measure the energy transfer K_2' for various K_1^0 values and plot a graph like Fig. 1.3 (a). Figure 1.3 (b) shows the graph for three mass ratios. You find that in each case you get a straight line, whose slope gives the fraction $f=K_2'/K_1^0$. Now, plot a graph between the mass-ratio and this fraction f. Figure 1.4 shows the typical results, without using Fig. 1.3 for smoothening the typical experimental scatter. You may note that as m_1/m_2 increases the fractional energy transfer increases at first, reaching a maximum value $\sim$ 1, and thereafter falls off.

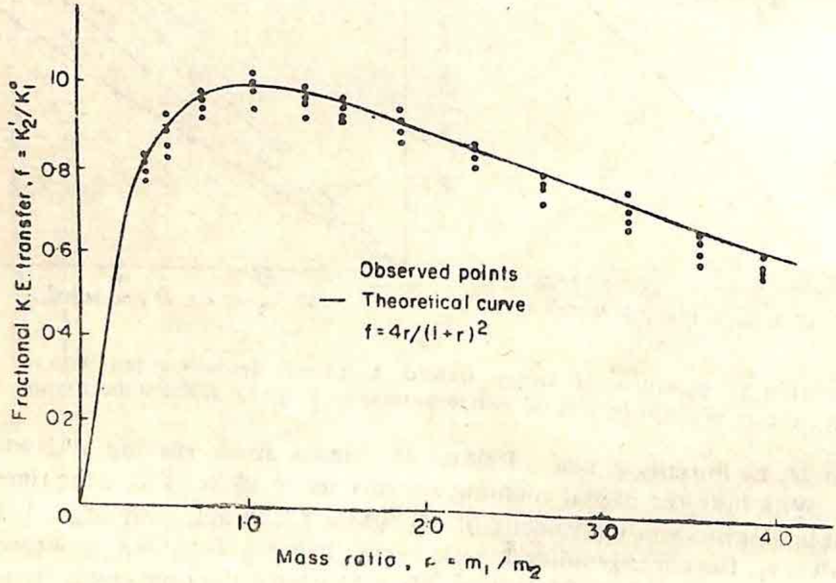

FIGURE 1.4. Energy transfer fraction f versus the mass ratio r for elastic collisions. Five data were taken for each r, some of which coincided.

Theory of *elastic* collisions shows that the energy transfer ratio is given by

$$f = \frac{4r}{(1+r)^2}$$

where r is the mass ratio m_1/m_2. Thus f is maximum when $r=1$ and its released, you would note that one goes to the left, the other to the right. This experiment is aimed at measuring the momenta of M_1 and M_2 at different times after release.

---

* When an additional brass-loaded glider is hooked-up to M_1, the initial motion to M_1 may be given by just pushing it. (Release with the help of M_0 will not work for a larger energy range, Why?).

For this purpose set one sensor S_1 fraction of a mm to the left of the sensing pin over M_1 and another sensor S_2 at a variable distance x from M_1. Thus with a double counter set in appropriate modes you may measure the velocity v_1 of glider M_1 and the time t from the instant of release, From v_1 values compute the momenta p_1 and plot a graph showing p_1 versus t.

Repeat the same thing for glider M_2 and obtain a graph showing p_2 versus t. Since both the time measurements are from the instant of release the two graphs give corresponding values of p_1 and p_2 at time t. Figure 1.5 shows a typical set of results. It may be noted that the sum $p_1+p_2=p$ remains constant at all times during the collision. (Its value is zero because you started with initial total momentum zero.)

EXPERIMENT 1-D *To study the conservation of momentum with initial momentum non-zero.*

You may now take up the case when initial total momentum p is not zero. A simple method is to release the glider M_1 with a given momentum p_1° towards another glider M_2 which is initially at rest and then to measure the momenta of both M_1 and M_2 at different times.

Figure 1.6 (a) (inset) shows the arrangement. M_1 may be repeatedly released with a given momentum by using a constant spacer of width a between it and M_0. Place one sensor S_A at any fixed separation x_0 relative to M_2 and the other sensor S_B at a variable distance x from M_2 in repeated trials. With the double timer counter set in appropriate modes, you now measure two quantities:

(*i*) The travel time t for M_1 from S_A to S_B.

(*ii*) The velocity v_1 (and hence momentum p_1) for M_1 at S_B (*i.e.*, at time t).

Thus you get p_1 vs t data.

Now place S_B at different distances to the other side of M_2, *keeping the position of S_A unchanged*. The timer measurements now give

(*i*) the time from the moment M_1 passes S_A to the moment M_2 passes S_B.

(*ii*) the velocity v_2 (and the momentum p_2) of M_2 at S_B (*i.e.*, at time t).

Since the zero for measurement of time in both cases is the same, the data for p_1 vs t and p_2 vs t have correspondence.

Figure 1.6 (a) shows a typical set of results. You find p_1 falling and p_2 rising, the sum remaining constant throughout the collision. It implies that rate of change of p_1 is equal and opposite to that of p_2. This is just Newton's third law of motion.

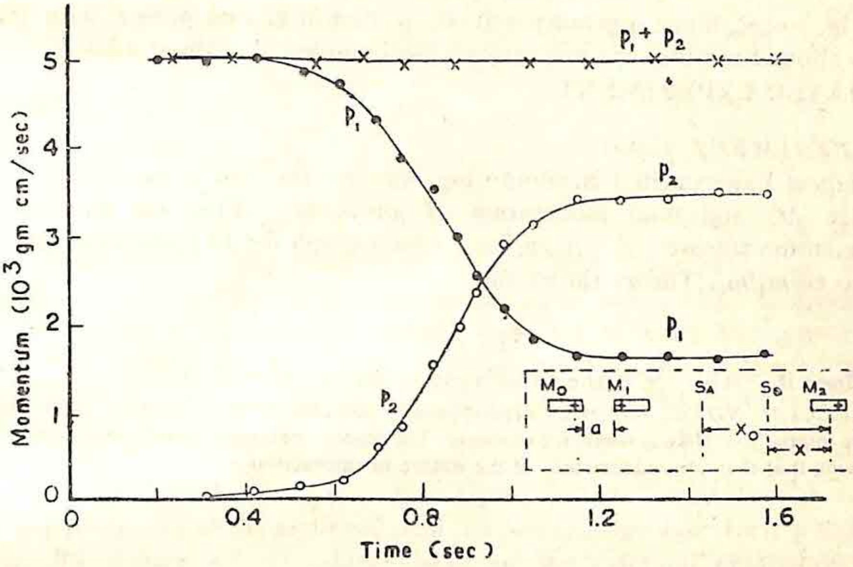

FIGURE 1.6(a). Plot of momenta of two colliding gliders at different stages of a collision, with non-zero initial momentum: when $m_1 > m_2$;

In the experiment of Fig. 1.6(a) mass of M_1 was larger than that of M_2. It is interesting to study the collision when M_2 has larger mass than M_1. Then M_1 rebounds after collision with M_2. Typical results are shown

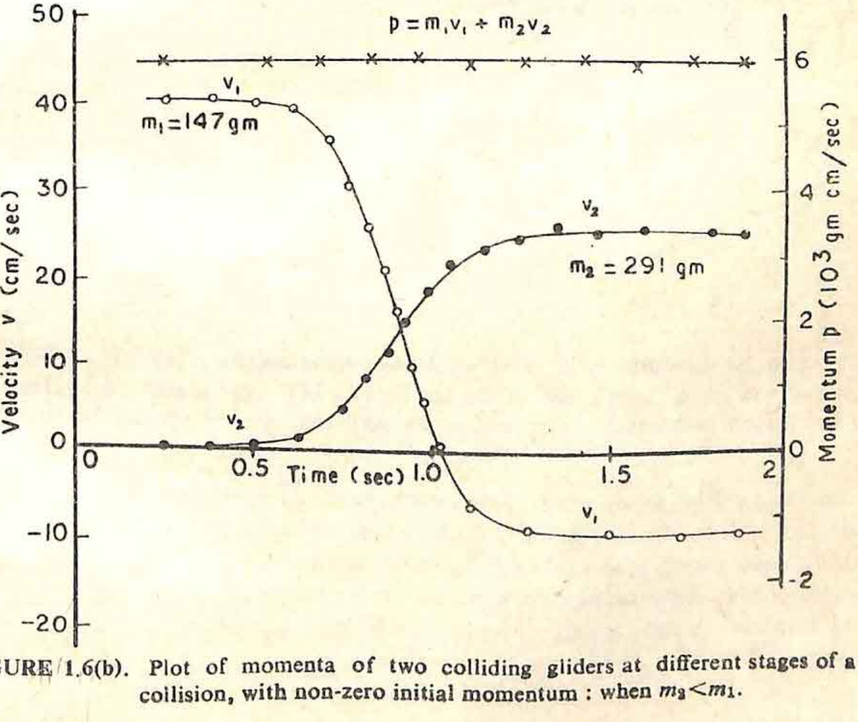

FIGURE 1.6(b). Plot of momenta of two colliding gliders at different stages of a collision, with non-zero initial momentum : when $m_2 < m_1$.

in Fig. 1.6(b). Some ingenuity will be needed in getting p_1 vs t data for the rebound motion. We are sure you will manage it without advice.

RELATED EXPERIMENT

EXPERIMENT 1-D(i)

Repeat Experiment 1-B, computing this time the initial momentum of glider M_1 and final momentum of glider M_2. Find the fractional momentum transfer $f_p = p_2'/p_1^0$ and plot a graph for f_p against the mass ratio $r = m_1/m_2$. Theory shows that

$$f_p = \frac{2}{1+r}$$

Deduce it. Also see if the experimental data agree with it.

SPECIAL NOTE. Any of the experiments in this chapter may be done with any other interaction—like springs, for example. The results obtained would be identical showing that they are independent of the nature of interaction.

APPENDIX I-A

THE PERSPEX AIR-TRACK

An air-track made from aluminium tubes has been in use for about two decades. But we soon found that for magnetic interactions a metallic track showed a considerable energy loss due to eddy currents (*i.e.*, electromagnetic damping). Hence a perpex air-track was designed and made. In what follows we describe the details of this track and the accessories used with it.

1. The Air-track

A photograph of the air-track and its accessories has been given in Fig. 0.1. Figure I-A (1) shows some of the essential details of its construction. From 3 mm thick perspex sheet, two strips ~ 2m × 40 mm are cut to make the slanting faces and a third sheet ~ 2 m × 57 mm to make the base of the tube. Both edges of the slant face sheets are cut to 45° angle and then the three sheets are sealed together with chloroform. Both the end faces are also sealed with perspex sheets, but at one end an air-inlet hole is provided for the blower hose to fit in, and at the other end a 4 mm diameter tube is fitted in for air-outlet.

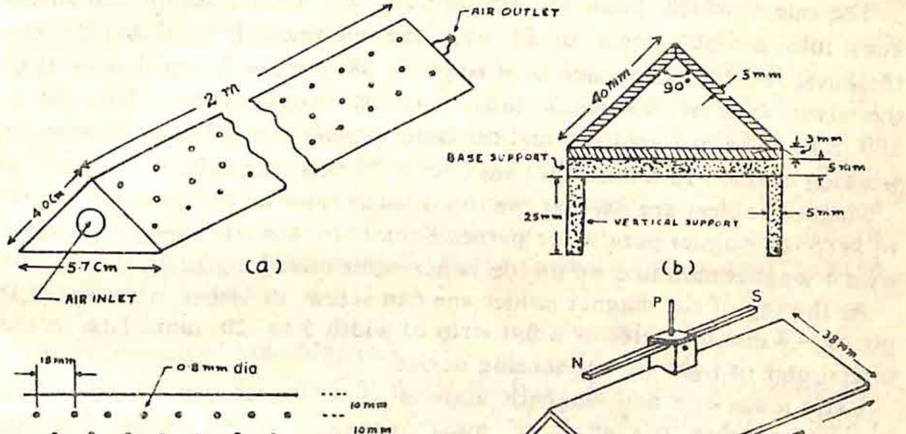

FIGURE I-A (1). (*a*) A schematic view of the air-track. (*b*) A cross-section perpendicular to the track length. (*c*) The spacing and size of the drilled holes on the two slant faces of the track tube. (*d*) The aluminium rider carrying a magnet and a sensing pin.

Three rows of holes are drilled in each of the slant faces all along the length with spacing 15 mm and diameter 0.8 mm each. That gives a hole density of 0.5 per cm^2.

To prevent sagging of the track, the hypotenuse face, kept horizontal, is given extra support with a horizontal base 5 mm thick and two vertical beams, each 25 mm high and 5 mm thick. The whole system is then supported at the two ends on stands, with levelling screws.

A scale affixed on one of the vertical support strips measures the positions of the gliders.

2. Air Blower

An electrical air-blower (350 watt) is used to blow air into the track tube. It is linked with the tube with a rubber hose to avoid rigid mechanical coupling. The blower develops 20 mm mercury pressure inside the track tube. This may be measured with a simple manometer connected at the outlet end.

3. The Gliders

The riders, which float on air-cushion, are simply aluminium sheets bent into a right angle to fit over the air-track [Fig. I-A(1d)]. The thickness is 2 to 3 mm, each bent edge is 38 mm (~ 2 mm shorter than the slant face of the track tube) and the length varies from 50 to 100 mm. The air pressure and the hole density are sufficient to provide working cushion to a mass 200 gm over a 75 mm long rider.

Magnet holders are fixed at the top of each rider in two possible ways: to keep the magnet parallel or perpendicular to the track length. A rider with a magnet mounted on its top is hereafter called a *glider*.

At the top of the magnet holder one can screw in either a cylindrical pin of ~3 mm diameter or a flat strip of width 5 to 10 mm. This is the interrupter of light for the sensing device.

Extra loads of a non-magnetic material (like brass) can be added to the glider when the effect of mass change is to be studied. For this purpose one either uses flat discs with holes so that they fit in the pin at the top, or brass pieces slotted to fit over the magnet itself. A notable point in this design is that such load addition should not lift or lower the centre of mass relative to the magnet axis.

4. The Spacers

In order to set two gliders at a reproducible fixed separation, a set of spacers of various lengths is provided. They are just like the riders without the mounts. The two ends of each spacer (as also of the riders) are ground accurately perpendicular to their lengths to make them function reproducibly.

5. Clamping the Gliders and Hooking-up of Two Gliders

If desired, a glider may be clamped in position on the track by means of a bracket and screws as shown in Fig. I-A(2a). Only light pressure should be used on the screws to avoid damage to the air-track.

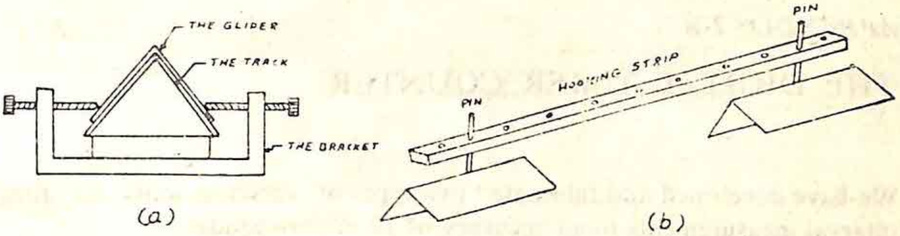

FIGURE I-A (2). (*a*) Clamping a glider at a given position on the air-track. (*b*) Hooking-up of two gliders.

For some experiments two gliders have to be hooked up so as to move as one unit. This is done by using a thin strip with several holes 4 mm diameter [Fig I-A(2b)]. An important point is that pins at the top of the gliders ($\sim$3 mm dia.) should fit *loosely* in the holes to leave freedom to each rider to adjust on the air-cushion.

6. The Mounting for Sensors

For mounting the sensors, a 2 metre long rod is provided parallel to the track. When the sensor is mounted the chambers containing the light source and the photo-transistor (*see* Fig. 0.2) are on two sides of the track line and the narrow beam of light is interrupted when a glider with a mounted pin passes between the chambers. The mounting permits the rod to be raised or lowered; also the sensors can be adjusted in position perpendicular to the track to ensure clear passage for the pin on the glider.

7. The Mounting of Side Magnets

For some experiments two magnets are to be mounted symmetrically on two horizontal sides of the air-track. A U-shaped mount is provided for this purpose with flexibility to adjust the heights and the spacing between the two arms. Care must be taken that the two magnets used are as nearly identical as possible and are mounted symmetrically and at the same height as the glider magnet. This is to avoid wobbling of the glider and consequent loss of energy. The magnets may be mounted parallel or perpendicular to the track.

In a related arrangement one of the two side magnets is not fixed on the mount but is held on a taught vertical metal strip, whose clamp length can be altered. This magnet can therefore make angular oscillations with a variable frequency (*see* Chapter 5 for details).

APPENDIX I-B

THE DIGITAL TIMER COUNTER

We have developed and fabricated two types of versatile units for time interval measurements to an accuracy of 10 microseconds.

(*a*) **The Digital Timer Counter**. This is capable of time interval measurements in three modes $\rfloor\overline{A}\llcorner$, $\rfloor\overline{A}\ \rfloor\overline{A}$ and $\rfloor\overline{A}\ \rfloor\overline{B}$ to measure the pulse-width, pulse period and interval between pulses from different sensors respectively.

(*b*) **The Digital Timer—Two Channel**. This has two independent channels for time interval measurement in the three modes mentioned above. A common oscillator is used for both the channels to minimise relative errors.

The first of these instruments has also a provision for being operated as a 4-digit decade counter for both positive and negative pulses and also as a frequency counter.

The instruments utilise indigenously available transistor-transistor logic (TTL) integrated circuits to achieve the desired operations. A photograph of the front panel of the two channel timer is shown in Fig. 0.3.

1. Principle of an Electronic Digital Timer

A block diagram illustrating the basic principles of the electronic digital timer is given in Fig. I-B(1). The essential features are the following.

(*i*) *A crystal controlled oscillator.* It gives pulses at a precise frequency 100 000± 20 per second.

(*ii*) *A frequency divider.* It reduces the frequency of the counted pulses by steps of 10 at each scaling stage, but maintains the precision of the basic oscillator.

(*iii*) *The gate.* It decides when the counting is to start and when it is to stop. It is controlled by the logic circuits (*see* below).

(*iv*) *The counter.* It displays the number of counts for the time decided by the gate and in time-units decided by the frequency divider.

(*v*) *The sensing device.* It converts a mechanical event into an electrical pulse to be fed to the logic circuit. We use a pencil of light and a phototransistor as the transducer.

(*vi*) *The logic system.* It receives the electrical pulses from various sensing devices and decides which of these signals are to open or close the gate for counting of the oscillator pulses. In our counters the gate responds to signals from the transducer (the sensing device) in three distinct ways: $\rfloor\overline{A}\lfloor$, $\rfloor\overline{A}\rfloor\overline{A}$ and $\rfloor\overline{A}\rfloor\overline{B}$. The significance of these symbols is shown at the bottom of Fig. I-B (1).

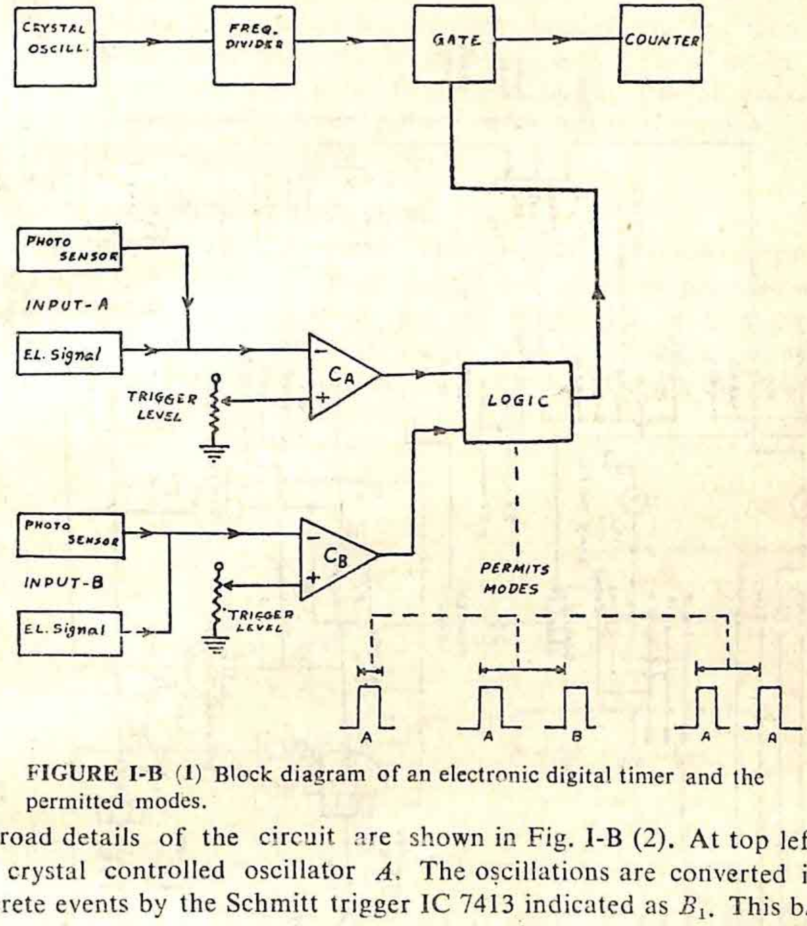

FIGURE I-B (1) Block diagram of an electronic digital timer and the permitted modes.

Broad details of the circuit are shown in Fig. I-B (2). At top left is the crystal controlled oscillator A. The oscillations are converted into discrete events by the Schmitt trigger IC 7413 indicated as B_1. This basic count in time (10 μ sec) is then converted by decade counting units IC 7490 in steps of 10. This is called scaling. The units of the scaler are shown as P, Q, R, S and T and output pulses at these occur at frequency 10 KHz, 1 KHz, 100 Hz and 10 Hz and 1 Hz respectively. The time unit band-switch selects the desired frequency of the pulses to be fed to the counter through the 'gate'.

The mechanical events between which time is to be measured are converted into electrical pulses. In Fig. I-B (2) the input pulses from channels $\rfloor\overline{A}$ and $\rfloor\overline{B}$ are shown at the bottom left. After passing through an over-voltage protection circuit these pulses of about 5 volt height pass through comparators 741 (marked as C_A and C_B) and the trigger level of the comparators can be adjusted between 0 and +5 volt The Schmitt triggers 7413 then gives the appropriate discrete shapes to the pulses compatible with the logic system and capable of driving the succeeding circuitry.

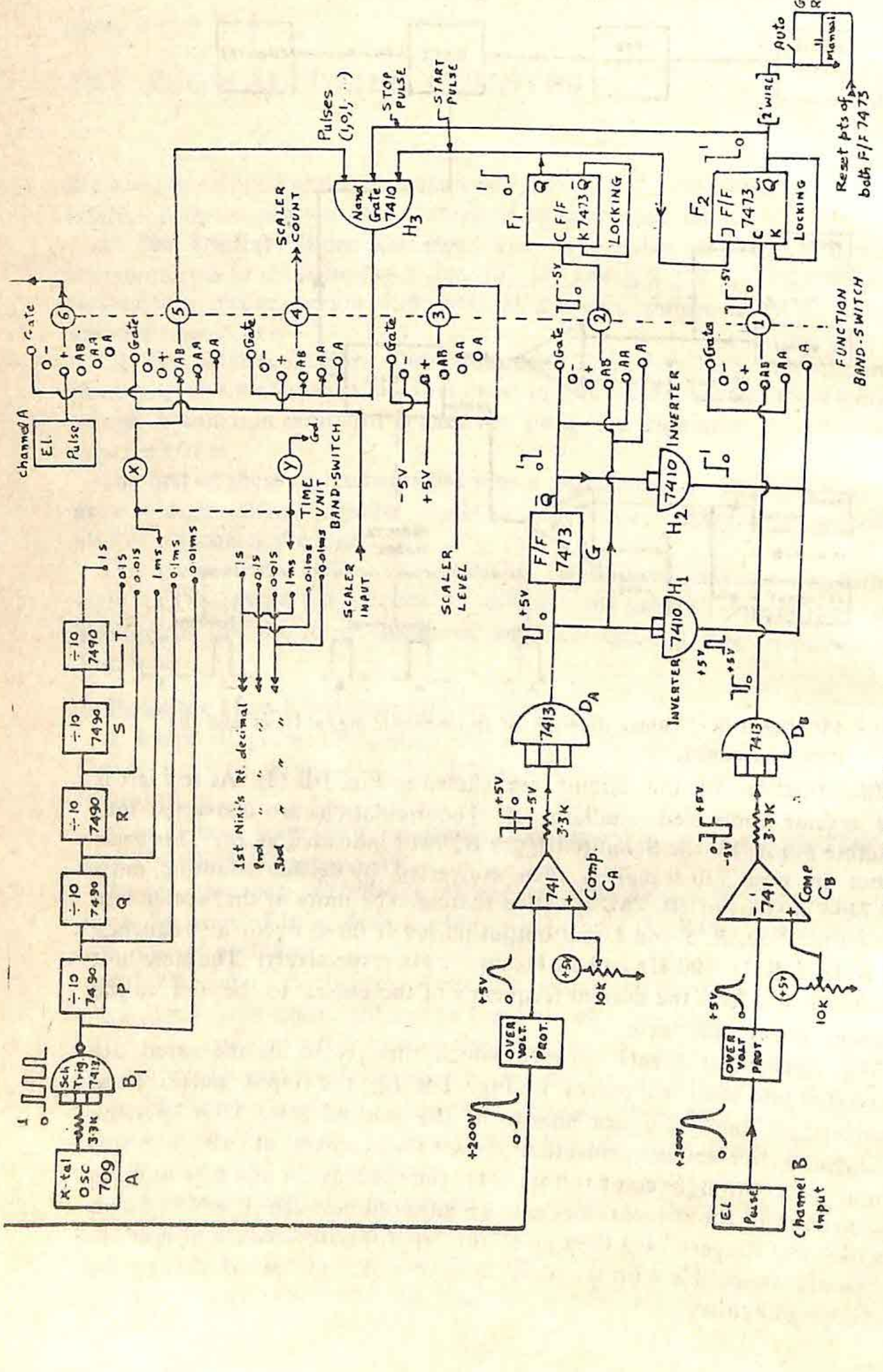

FIGURE I-B (2) Circuit diagram of the digital timer counter.

The logic system now comprises the three Nand gates 7410 (shown as H_1, H_2, H_3) and three flip-flops 7473 (shown as G, F_1, F_2). The working of the logic system needs an understanding of their 'Truth tables' (*see* later). The function band switch decides whether the logic will operate the final gate H_3 in mode $\lrcorner\overline{A}\llcorner$ or $\lrcorner\overline{A}\ \lrcorner\overline{A}$ or $\lrcorner\overline{A}\ \lrcorner\overline{B}$. The start pulse and stop puise [right end of Fig. I-B (2)] ultimately govern the scaler count. A 'reset' pulse can be sent to the counter by a manual press-button to get 0000 reading.

2. Details of the Different Components

(*i*) *Crystal controlled oscillator.* The 100 KHz crystal controlled oscillator is designed by using an operational amplifier μA 709C as an active device. A fixed threshold Schmitt trigger IC 7413 is used to convert the oscillation into discrete events. Thus the basic least count in time is 10μ sec. The circuit diagram is given in Fig. I-B (3); the A and B_1 here correspond to those in Fig. I-B (2).

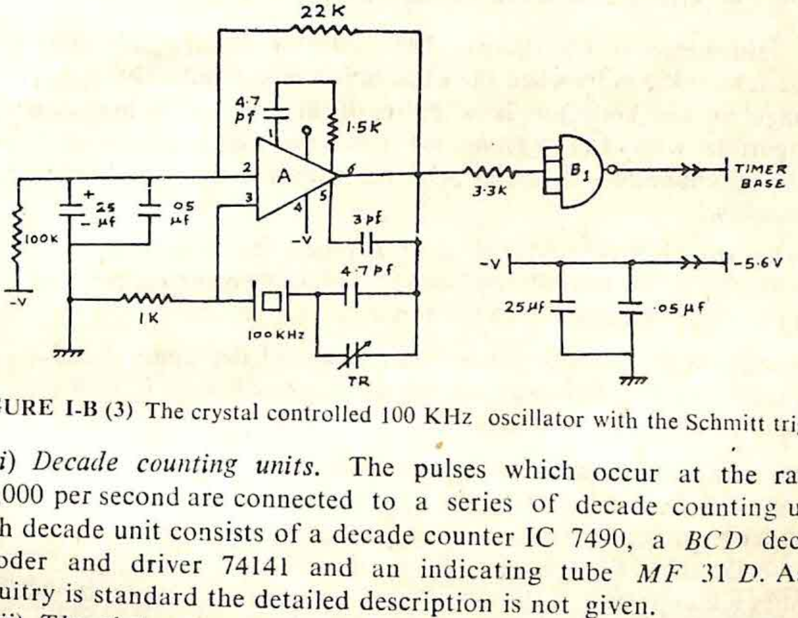

FIGURE I-B (3) The crystal controlled 100 KHz oscillator with the Schmitt trigger.

(*ii*) *Decade counting units.* The pulses which occur at the rate of 100,000 per second are connected to a series of decade counting units. Each decade unit consists of a decade counter IC 7490, a *BCD* decimal decoder and driver 74141 and an indicating tube *MF* 31 *D*. As the circuitry is standard the detailed description is not given.

(*iii*) *The photo-sensor and transducer.* A narrow beam of light from a low power 6V 150 mA bulb is made to fall on a phototransistor MT2 placed at a distance of about 5 cm. The bulb and the transistor are enclosed in two light-tight cases and one hole in each decides the path of the beam of light. Figure 0.4 shows the geometry and Fig. I-B (4) the basic circuit of the transducer. The base emitter junction of MT2 is illuminated by the lamp. The resulting photocurrent is injected into the base of *BC 148A* and takes the transistor into saturation and the **collector voltage to 0.2 approximately.**

An obstruction in the light beam falling on the phototransistor reduces

the photocurrent to less than a microampere, which is insufficient to maintain the transistor *BC 148A* in conduction, so that the collector voltage increases to almost 5 volt. Thus a positive pulse occurs when

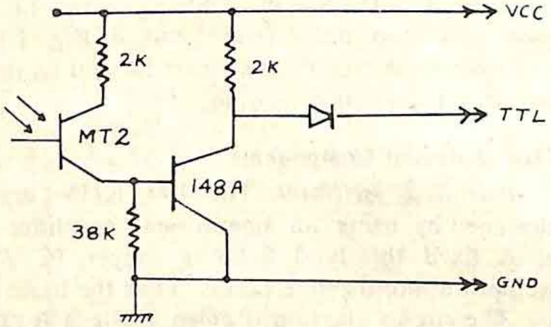

FIGURE I-B (4). Basic circuit for the phototransistor. The diode decouples the outputs of the sensors.

the light beam is obstructed. The collector voltage falls again to low value (about 0.2 volt) when the obstruction is cleared. Thus the output voltage at the collector is a pulse of about 5 volt height, which is compatible with TTL (Transistor-transistor logic) as we shall see. A diode is connected in series with the output to decouple the output of the sensor.

A five pin DIN connector is used between the timer and the sensor to provide the power to both the lamp and photo-transistors, as well as to carry the transducer pulse to the timer.

A separate phototransistor is used for each of the inputs *A* and *B* of the Digital Timer Counter and for each of the inputs *A*, *B*, *C*, and *D* of the Digital Timer-Double Channel.

(*iv*) *The input circuit.* The signals at inputs *A* and *B* (from the transducers) may be coming at widely different voltage levels and impedances. In order to minimise the loading of the signal by the input circuit as well as to make them TTL compatible, an operational amplifier μA 741C is used as a comparator with each of the inputs. The trigger level of the comparator [*see* Fig. I-B (2)] can be adjusted between 50 mV and 5V so as to make the circuit insensitive to noise and other spurious signals.

An overvoltage protection circuit, formed by connecting two 3.9 volt Zener diodes back to back, is also included at each input to protect the circuit from damage by signals as high as 300 V amplitude.

The input impedance at each of the inputs is higher than 500 KΩ.

(*v*) *The Transistor-transistor logic* (*TTL*) *systems.* The logic circuit is what decides when the electronic gate is open or closed for counting. This is achieved by a combination of two digital integrated circuits called 'gate' and 'flip flop,' which we proceed to explain.

3. The Nand Gate and JK Flip Flop

In a digital system there are only two levels and they are indicated variously as HIGH and LOW, 1 and 0, ON and OFF etc. Also the transition from one level to the other is written as 1-0, HIGH-LOW, ON-OFF, indicating the transition from the first mentioned level to the second mentioned level. We will use the 1 and 0 notation.

The output level of the gate, or for that matter of any circuit, for various inputs is usually specified in a tabular form and given the name 'Truth Table.'

Nand Gate. An electronic gate when OPEN allows electrical signals to pass through it; when CLOSED, it stops signals from passing through it. A three input triple NAND gate 7410 is used in our timer circuit [Fig. I-B (2) right]. The 'Truth Table' for it is as given below:

TRUTH TABLE FOR NAND GATE 7410

Input				*Output*
A	*B*	*C*		
One or more inputs			0	1
All inputs			1	0

Thus if one or more inputs are at 0 the output is at 1; only when all the three inputs become 1 does the output become 0. In a TTL system an unconnected input is always at 1.

JK flip flop. A flip flop is a bistable switch, having two distinguishable stable states and can be switched from one state to the other. The two outputs are denoted usually by Q and $\overline{Q}$.

At any time $\overline{Q}$ is always the opposite of Q. That is, if Q is at 1, $\overline{Q}$ will be at 0 and *vice versa*. The state depends on the input signals the unit has received.

A 'reset' pulse takes the flip flop to a definite pre-determined state, which in our case is Q at 0 and $\overline{Q}$ at 1. Now an input pulse to the flip flop will take Q to 1 and $\overline{Q}$ to 0; the next pulse will take Q to 0 and $\overline{Q}$ to 1, and so on. Thus the Q or $\overline{Q}$ points will be alternately at 1 and 0.

Now, to control the switching two inputs J and K are provided in this flip flop besides the signal input. The truth table for the JK flip flop is given below, where t_n and t_{n+1} represent the stages at n^{th} and $n+1^{th}$ input pulse respectively.

15448

TRUTH TABLE FOR JK FLIP FLOP

Input, t_n		*Output, t_{n+1}*
J	K	Q
0	0	Same as Q at t_n
0	1	0
1	0	1
1	1	Same as $\overline{Q}$ at t_n

Thus when both J and K inputs are at 0 the state of Q at t_{n+1} stage is the same as at t_n stage, meaning thereby that the Q and $\overline{Q}$ inputs do not change their state when an input signal is received if both J and K are at 0. On the other hand if both J and K are at 1 (or unconnected) then Q at t_{n+1} is the same as $\overline{Q}$ at t_n, that is the levels of Q and $\overline{Q}$ will change at each input pulse. This performance is like that of an ordinary flip flop.

If $J=0$ and $K=1$ then the transition 0—1 at Q is prevented but transition 1—0 at Q is allowed. The reverse holds if $J=1$ and $K=0$. A reset pulse, as stated earlier, over-rides all other information and take Q at 0 and $\overline{Q}$ at 1. The important thing to remember is that J at 0 prevents 1-0 at $\overline{Q}$. The flip flop is reset by a 0 level signal at reset input.

4. The TTL Logic System and Timing Functions

With this background information we can now proceed with the circuit description and performance of the TTL system for the different timing functions $\lrcorner\overline{A}\llcorner$, $\lrcorner\overline{A}\ \lrcorner\overline{A}$ and $\lrcorner\overline{A}\ \lrcorner\overline{B}$.

In Fig. I-B(2) the non-inverting inputs of both comparators C_A and C_B are shown connected to a positive reference voltage source; the outputs of both of them are therefore HIGH or 1 in the absence of any signal. Whenever a signal more than the reference voltage is received at the inverting input of the comparator, the output makes a transition from HIGH to LOW: it goes back to HIGH when the signal amplitude drops below the reference voltage. The comparator output current is marginally sufficient to drive the subsequent logic circuits.

The triple input NAND gate integrated circuit 7410 is used as an electronic gate and indicated by H_3 in Fig. I-B(2) (right middle). The gate opening and closing is controlled by two flip flops (F/F 7473)—— one to start the count and the other to stop it. They are indicated by F_1 and F_2 with Q_{F1} (Q output of flip flop F_1) and $\overline{Q}_{F2}$ ($\overline{Q}$ output of flip flop F_2) connected to two of the inputs of Nand gate H_3. The remaining input of H_3 is connected to the output of the time unit. When the flip flops are reset $\overline{Q}_{F1}$ is 0 and $\overline{Q}_{F2}$ is 1 and the gate is closed. The $\overline{Q}$ of each of the flip flops F_1 and F_2 is connected to the respective K input to lock the flip flops. Also Q_{F1} is connected to J input of F_2 to disable F_2 until F_1 is triggered.

The timer units are capable of operation in three modes, which we now proceed to explain.

(*i*) *Mode* $\rfloor\overline{A}\lfloor$. In this mode the timer gate is opened by the signal at input A (when the voltage exceeds a predetermined level) and will remain open until the input voltage drops below the set level. Thus the width of the pulse is measured.

When the Time Function band switch is set to mode $\rfloor\overline{A}\lfloor$, the output of Schmitt trigger D [Fig. I-B (2)] is connected to the C input of F_1, while the C input of F_2 receives the pulse from D_1 through an inverter H_1. A positive going pulse to input A (if it exceeds the trigger level of comparator C_A) will make 1-0 transition at output of D_1. At this transition the flip flop F_1 is triggered making $\overline{Q}_{F_1}$ at 1, thus opening the gate. The clock pulses are now counted by the decade scaler. The inverting gate H_1 at the C input of F_2 causes F_2 to trigger on the 0-1 transition of the D output. The resulting 0 at $\overline{Q}_{F_2}$ closes the gate H_3 and the counting stops. The counting interval in this case is precisely the time in which D_1 output is at 0. This interval is also precisely the time for which the input signal at A is above the trigger level of the comparator C_A. Thereafter as the Q outputs of both F_1 and F_2 are at 0 and are also connected to the respective K inputs, a 1-0 transition at Q is prevented for both F_1 and F_2 and any signal received later at input A will be unable to open the gate H_3.

It may also be noted that the start and stop flip flops cannot be triggered in the wrong order because of the connection Q_{F1} to J_{F2}. The flip flop have to be reset for making further measurements.

(*ii*) *Mode* $\rfloor\overline{A}\ \rfloor\overline{A}$. In this mode the gate is opened by a positive signal at the input A when it exceeds the predetermined level. The gate remains open until another positive going voltage signal crossing the same level appears again. In this mode the pulse period is measured.

When the Time Function band switch is set on mode $\rfloor\overline{A}\ \rfloor\overline{A}$ the output of D_1 is fed to C input of flip flop G. The $\overline{Q}$ output is connected to C input of F_1 and through an inverter H_2 to the C input of F_2. The J and K inputs of flip flop G are unconnected and are thus at 1. Thus the *IC* G acts like a normal flip flop and $\overline{Q}$ output changes state at every input pulse. The flip flops are reset and $\bar{Q}_G$ is at 1. A 1—0 transition at the D_1 output triggers flip flop G, inducing at 1-0 transition at $\bar{Q}_G$. The Q_{F1} becomes 1 and the gate H_3 is opened. A 0-1 transition at D_1 output does not change the state of Q_G as the flip flops are triggered only by the 1-0 transition; thus the gate is still open. Another input pulse which induces 1-0 transition at the D_1 output will trigger the flip flop G, inducing a 0-1 transition at $\bar{Q}_G$. This appears as 1-0 transition at C input of F_2 taking $\overline{Q}_{F2}$ at 0 and the gate H_3 is closed. Thus the gate H_3 is open for time equal to the pulse period. The flip flops have to be reset for further measurements.

For the measurement of period T for an oscillating system one needs to measure the time interval from one passage in a particular direction to the next passage in the same direction, thus skipping the reverse passage. A switch changes the $\rfloor\overline{A}\ \rfloor\overline{A}$ mode to this mode. Of course, in using the timer in $\rfloor\overline{A}\llcorner$ or $\rfloor\overline{A}\ \rfloor\overline{B}$ mode this switch should be kept at 'off' position.

(iii) Mode $\rfloor\overline{A}\ \rfloor\overline{B}$. In this mode the gate is opened by an input signal at A, but is then totally inhibited for responding to further signals at input A. The gate is now closed only by a signal at another input B. Thus the time interval between signals at inputs A and B is measured.

When the Time Function band switch is set for this mode the function becomes the following. An input pulse at A which induces 1-0 transition at D_1 output triggers the flip flop F_1, opening the gate at H_3. The gate H_3 is now closed only by a 1-0 transition at the output of D_2 which triggers the flip flop F_2. Of course the pulse at both inputs A and B must be positive going and of amplitude higher than the trigger levels of respective comparators.

(iv) The reset. A '0' level signal is needed at reset input of the flip flops to reset them. In the timer two methods are used to reset the flip flops. In the manual mode a push button will have to be pressed for resetting. This may be an inconvenient operation in some circumstances. A provision is therefore made for automatic resetting of the flip flops. In this case the $\bar{Q}_{F2}$ is connected to the reset input of flip flops. The connecting wire is approximately 50 cm in length, thus providing a delay of a few nano-seconds. This is needed to insure that the reset signal is received after the gate has been closed. In this case the manual resetting is not needed. However, if the events are occurring at a rapid rate (frequency of, say, more than 1 Hz.), when time margin for reading the counter is insufficient, it is best to operate in the manual mode.

5. The Digital Timer—Two Channel

In this device another set of inputs marked C and D is provided in addition to the A and B described above. Thus one can operate this timer for the measurement of two time intervals simultaneously. As an example if $\rfloor\overline{A}\llcorner$ and $\rfloor\overline{A}\ \rfloor\overline{B}$ measurements are simultaneously needed, one may use the A input for $\rfloor\overline{A}\llcorner$ measurements and connecting A and B to C and D respectively one may use the $\rfloor\overline{C}\ \rfloor\overline{D}$ mode of the second counter to get $\rfloor\overline{A}\ \rfloor\overline{B}$. Of course the C and D inputs could be used quite independently of A and B also. Signals of the same crystal controlled oscillator are used for both the systems, so that relative errors may not arise.

6. Additional Features of the Digital Timer Counter

The digital timer counter (with inputs A and B alone) has been provided with the following other features (to increase its versatility) which are not provided with the Two Channel Device, (*i*) *Scaler input: . Decade counting.* The unit is capable of taking a scaler input and operate as a 4-digit decade counter. In this mode it can take both positive and negative signals. This signal input is DC coupled. The frequency range is DC to 10 MHz.

The main features are shown in Fig. I-B (5), which is to be seen with Fig. I-B (2). The input signal is fed to a source follower made by using field effect transistors (FET) providing an input impedance higher than 1 Megohm. The signal is then fed to a fast comparator realised by using IC μA 710C. The comparator reference level is adjustable from 0 to +5 volt, depending on the input signal polarity which is selected by a band switch. The comparator output is connected to Schmitt trigger B_2 and then to the decade counter through a switch.

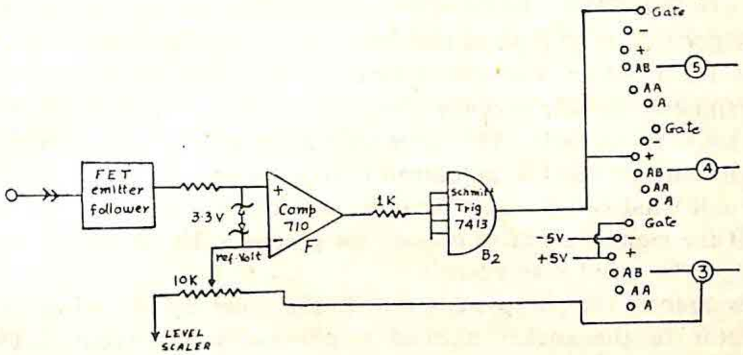

FIGURE I-B (5) Circuit for scaler input decade counting.

(*ii*) *Gate input: Frequency counter.* In this mode the Digital-timer Counter may be used as a frequency counter. The function selector switch is set to the position marked 'Gate' and the signal is fed at the scaler input point. Thus one of the inputs of gate H_3 receives the input signal. The gate opening and closing is again controlled by flip flops F_1 and F_2.

The circuit inter-connections are as a in mode $\rfloor\overline{A}\ \rfloor\overline{A}$ and the pulse is received from the 100 KHz oscillator or other decade divisions of it. Thus if the time unit switch is set at 1 second, the gate H is open precisely for 1 second and the counter reading is the frequency of the input signal. For signals having higher frequencies the gate time may be chosen appropriately.

7. The Power Supplies

The +5 volt supply needed for the digital integrated circuits, lamps and reference voltage for the comparators is obtained from a three terminal 5V 1 amp integrated circuit voltage regulator μA 7805. The other power supplies are Zener regulated. The +200 volt supply for the indicator tubes MF 31 D is unregulated.

8. Operating the Timer

Figure 0.2 shows a photograph of the front panel of a Digital Timer-Two Channel. We will first explain how one of the channels may be used.

Switch on the unit. The decade counter will show some number. Press the push button marked 'scaler reset.' The decade counter will now read 0000.

Set the function band switch to mode $\rfloor\overline{A}\lfloor$ and the time unit band switch to 1 sec. Then the decade counter will receive signals at the rate of one per second as long as the gate is open. Set the timer reset switch to AUTO position and the TRIG LEVEL potentiometer for *A* input approximately at its mid range. Press the button marked MANUAL *A* for about 10 seconds. The decade counter will start registering counts and will indicate 0010 if the button is kept pressed for 10 seconds. If the timer unit band switch is set at 0.01 second, the counter will indicate 1000 if the manual signal is pressed for precisely 10 seconds. (An error of ±1 in the count may occur.)

Now connect the photosensor unit to the timer by inserting the DIN connector to the socket marked as photosensor for input *A*. The lamp in the photosensor would light up. Reset the scaler to make the counter read 0000. Now obstruct the light falling on the phototransistor for a known duration, say 5 seconds. The scaler will indicate 0005 or 0500 according as the time unit band switch is at 1 sec or 0.01 sec.

If on obstructing the light signal the scaler does not respond, it means that the gate is not opened, *i.e.*,the photosensor signal is not able to change the state of the input comparator. This may be either because of the misalignment of the lamp and phototransistor or because the reference level of the comparator is very low (almost 0 volt) or very high (almost 5 volt). Thus it is advisable to keep the trigger level nearly at the mid position. The output of the photosensor can be monitored by connecting a voltmeter of 5 volt or higher range to the terminals marked *El* signal. When the phototransistor is illuminated the voltmeter should read less than 1 volt and when the light beam is obstructed it should read more than 4 volt. The photosensor outputs at the other input *B* (or at *B*, *C*, *D* in a double timer) can also be checked in a similar way.

It must be remembered that the scalar must be reset before the start of any measurement.

The timer operation in mode $\rfloor\overline{A}\ \rfloor\overline{A}$ and mode $\rfloor\overline{A}\ \rfloor\overline{B}$ may also be checked in a similar way by either using manual signals or photosensor signals.

If the timer reset switch is in MANUAL position, after one event counting the timer is insensitive to any more signals. The push button above the MANUAL position has to be pressed to reset the timer and then it is ready to accept the input pulses.

REFERENCES

An excellent discussion of the general principles of digital measuring instruments and digital logic systems is given in the book *Digital Electronics for Scientists* by H.V. Malmstadt and C.E. Enke; W.A. Benjamin Inc., USA, 1969. Figure 6.34 on page 275 of the book contains an error. Q output of T flip flop is shown connected to C input of start flip flop F. In fact the Q output of T, which is at 1 when flip flops are reset, should be connected to C of start flip flop. A similar correction is needed in Fig. 6.36 on page 277.

Another very useful book is *Digital Principles and Applications* by Malvino and Leach, McGraw-Hill (Asian Edition), 1975.

2

THE STUDY OF POTENTIAL ENERGY DIAGRAMS

2.1. MECHANICS AND NEWTON'S LAWS OF MOTION

According to Newtonian mechanics if we know the present positions and velocities of all particles and their interactions (*i.e.*, mutual forces), we can deduce (or predict) the positions and velocities of all these particles at any later time. In the twentieth century, however, we have discovered that at atomic and sub-atomic levels we cannot apply Newton's Laws for telling us the course of events. A new mechanics—called *quantam mechanics*—has grown. But when applied to macroscopic bodies quantum mechanics gives results in such close approximation to Newtonian mechanics that for most purposes we use Newton's Laws to determine the motion of bodies.

Two different procedures are generally used in applying Newton's Laws to study the motion of a body. The choice depends on whether the force F is function of time t or of the position x of the body.* In the first procedure, Newton's second law is directly used in the form

$$m\frac{dv}{dt}=F \qquad \text{.. .(2.1)}$$

where m is mass of the body and v its velocity at time t. Two stages of integration lead to

$$v = v_0+\int_0^t \frac{F}{m}\,dt$$

and

$$x = x_0+v_0 t + \int_0^t\left[\int_0^t \frac{F}{m}dt\right]dt$$

where v_0 and x_0 are the initial velocity and position of the body (at $t=0$).

The second procedure is useful when the force F acting on a body is entirely position-dependent. Use of the identity

$$\frac{dv}{dt}=\frac{dv}{dx}\,\frac{dx}{dt}=v\frac{dv}{dx}$$

gives Equation (2.1) the form

$$mv\,dv=F\,dx$$

---

* For convenience we limit discussion to one-dimensional motion.

If F is a function of space coordinate x alone, we can integrate this to get

$$\tfrac{1}{2}\,mv^2-\tfrac{1}{2}\,mv_0^2=\int_0^x F\,dx \qquad \ldots(2.2)$$

The left-hand side represents the increase in kinetic energy of the body under study ($\triangle K$) and the right-hand side the work done on the body (W) by other interacting bodies. So we may put

$$\triangle K=W=\int_0^x F\,dx \qquad \ldots(2.3)$$

Now, the body under study and the interacting bodies may be taken together to form what is called an *'isolated system.'* We may then say that one part of the system (the body under study) is gaining kinetic energy $\triangle K$ through work $\int_0^x Fdx$ done *by* the rest of the system *on* this body. An alternative view, to satisfy conservation of energy, is to define a quantity—called *potential energy* U of the system—such that

$$\triangle K+\triangle U=0 \qquad \ldots(2.4)$$

Comparison of Equations (2.3) and (2.4) leads to

$$\triangle U=-\triangle K=-\int_0^x F\,dx \qquad \ldots(2.5)$$

The first part $\triangle U=-\triangle K$ provides the experimental approach for measuring $\triangle U$; the second part $\triangle U=-\int_0^x Fdx$ provides the relation of U with force.

You may note that if more than one component of the isolated system is free to move, $\triangle K$ in these equations must be replaced by $\Sigma\triangle K_i$, where the summation covers all the components whose K is changing. Equation (1.4) in Chapter 1 does refer to two bodies A and B of an isolated system, both being free to move.

You may also see that describing the interaction of the body with the rest of the system in terms of $F(x)$ or $U(x)$ are equivalent, because one can be deduced from the other. In the general three-dimensional case it is more convenient to deal with U, because it is a scalar quantity. If systems A, B; B, C and C, A separately have potential energies U_{AB}, U_{BC} and U_{CA} respectively (for the specified configuration), then the potential energy of the system A, B, C will just be equal to the algebraic sum $U_{AB}+U_{BC}+U_{CA}$. Now, if you desire to know the force on (say) A, its three components are given by

$$F_x=-\frac{\partial U}{\partial x}\,;\;F_y=-\frac{\partial U}{\partial y}\,;\;F_z=-\frac{\partial U}{\partial z} \qquad \ldots(2.6)$$

where x, y, z are the coordinates of A.

Equation (2.4) leads to

$$K+U=\text{constant}=E$$

where E is called '*total energy*' of the system. Writing $K=\frac{1}{2}mv^2$ then gives us

$$\frac{1}{2}mv^2=E-U \qquad \ldots(2.7)$$

This is the basic equation in the second procedure to study the motion of a body, just as Equation (2.1) is in the first procedure. Rearranging Equation (2.7) gives

$$v=\left[\frac{2(E-U)}{m}\right]^{\frac{1}{2}}$$

Since $v=dx/dt$, this leads to

$$dx=\left[\frac{2(E-U)}{m}\right]^{\frac{1}{2}}dt$$

Since U is a function of x, we need a transposition; and then integration gives

$$t=\int_0^x\left[\frac{m}{2(E-U)}\right]^{\frac{1}{2}}dx \qquad \ldots(2.8)$$

This equation describes the motion of the body.

In elementary mechanics the first procedure is more popular because it uses Newton's Law, *i.e.*, Equation (2.4), directly and deals with an individual body. In contrast, the second procedure uses the energy conservation law—a deduction from Newton's law—and deals with an isolated system of bodies as a whole. In most situations in advanced mechanics we deal with position-dependent forces and it is more convenient to deal with the system as a whole rather than with individual members of the system. For a general situation Equation (2.7) takes the form

$$\Sigma K_i=E-U \qquad \ldots(2.9)$$

where i refers to the individual members of the isolated system, but E and U still pertain to the system as a whole. In quantum mechanics an equation corresponding to Equation (2.9) is the basis from which all the analysis proceeds.

For these reasons the study of potential energy diagram—*i.e.*, U vs x diagram in the one-dimensional case—is of great significance. It describes the interaction adequately and enables us to analyse the motion of bodies fully.

2.2. THE MEASUREMENT OF POTENTIAL ENERGY

As stated earlier, the first part of Equation (2.5), *i.e.*,

$$\Delta U=-\Delta K$$

is the basis of measurement of potential energy. You *measure* the kinetic energy of the moving member of the isolated system (the glider in your experiments) at two positions 1 and 2 and hence *deduce* the differences of potential energy:

$$U_2-U_1=-(K_2-K_1) \qquad \ldots(2.10)$$

Since only *differences* of U are measurable (and differences alone have meaning), the reference state for $U=0$ may be chosen anywhere according to convenience. We will take up this matter with the related experiments later.

With the reference state chosen, U comes out as a function of position coordinate x of the glider. A graphical plot of U vs x is called the potential energy diagram of the system.

In a typical experiment you will determine the U values for various positions x of a glider magnet M_1 relative to another magnet M_0, which is clamped. The clamped magnet is often called the *field magnet*. The idea is that M_0 creates a 'field' (here magnetic field) around itself, and M_1 experiences a force in that field. In view of this, one often calls U the "PE of magnet M_1 in the field of magnet M_0." But, as you will see by experiment, U comes out to be the same for a given separation x of the two magnets, irrespective of whether M_1 alone is free, or M_0 alone is free or both M_1 and M_0 are free. Therefore, it is more appropriate to call U the "PE of the system M_0+M_1."

For elastic PE a special situation needs mention. Consider a steel ball P of KE K striking a normal spring. As the spring is compressed from state 0 to state 1 the KE of the ball falls to K_1. We now write as usual:

$$\triangle U=U_1-U_0=-(K_1-K_0)$$

The PE value U will be said to belong to the system "spring + ball P." But with the spring in state 1, you may replace the ball P by any other ball Q; when the spring reverts to state 0, it will give Q the same energy as it would have given to P. You will therefore be justified in calling U the PE of the spring without reference to the ball.*

No anomaly is really involved. In a spring case the 'system' really means different parts of the spring itself, the relative separation of which changes in compression or stretching. The ball, if made of steel, suffers negligible compression and hence does not share elastic PE.

EXPERIMENT 2-A *To study the potential energy curve due to magnet-magnet inter-action.*

On the air-track two gliders may be mounted in either (*i*) repulsive mode, or (*ii*) attractive mode. We shall describe the experiment for the repulsive mode only.

Clamp one glider M_0 at one end of the track (inset Fig. 2.1) and mount another glider M_1 in repulsive mode with respect to M_0. Using spacers, release M_1 from different distances x from M_0 (see inset Fig. 2.1) and measure its kinetic energy K at a fixed position S. For this purpose, mount a sensor at S and connect it to the timer counter set in mode ⌋$\overline{A}$⌊ so that the time interval in it measures the velocity v of M_1 as it crosses S. If m is the mass of glider M_1, you get kinetic energy as $1/2\ mv^2 = K_s$. Then

---

* The logic holds true if the ball is incompressible. If the ball is compressible, the potential energy cannot be exclusively attributed to the spring.

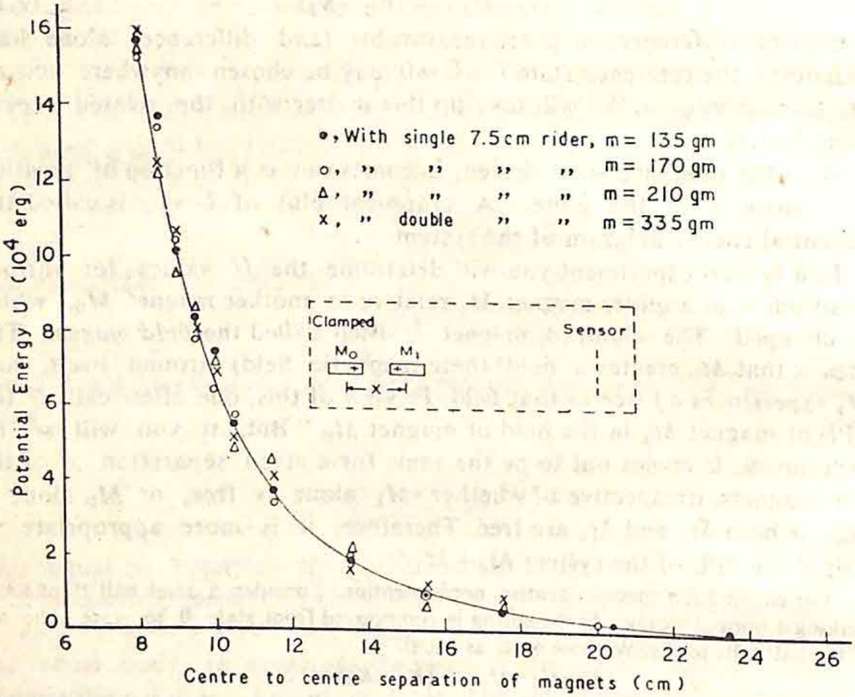

FIGURE 2.1 Variation of potential energy with separation for a system of two coaxial bar magnets.

$$U_s - U_x = -(K_s - 0) = -K_s$$

or

$$U_x = U_s + K_s$$

If S is far from the region of interaction of M_0 and M_1 it is a convenient point for the zero (reference) level for U. You may therefore take $U_s = 0$ to get

$$U_x = K_s \qquad \ldots(2.16)$$

Thus you get U_x versus x data, from which a graph may be plotted. Figure 2.1 shows the typical results.

RELATED EXPERIMENTS

EXPERIMENT 2-A(i)

Interchange the magnets M_0 and M_1 and repeat the Experiment 2-A. Check if U_x vs x curve comes out the same. The identity goes to emphasise that what you measure is the potential energy of the system. It does not matter which magnet is clamped and which is on the glider.

EXPERIMENT 2-A(ii)

Load the glider M_1 with an extra brass load (you may mount the brass load on another glider and hook it up with the glider M_1). Repeat the Experiment 2-A. Due to larger glider mass now the velocity values will be smaller than before. Check if U_x vs x curve comes out the same as before.

Figure 2.1 shows that the observation points for four different glider masses fall on a single curve. This would go to show that the measured U is essentially due to magnetic interaction of the magnets loaded on the gliders. One may, in fact, call it *magnetic potential energy.*

EXPERIMENT 2-A (iii)

Hold the two gliders with magnets M_0 and M_1 in repulsive mode at separation x and release them simultaneously. Measure their kinetic energies K_0 and K_1 by using two sensors placed far from their release positions. K_0+K_1 gives the potential energy U of the M_0+M_1 system corresponding to separation x.

Figure 2.2 shows the results of two such experiments, in one of which

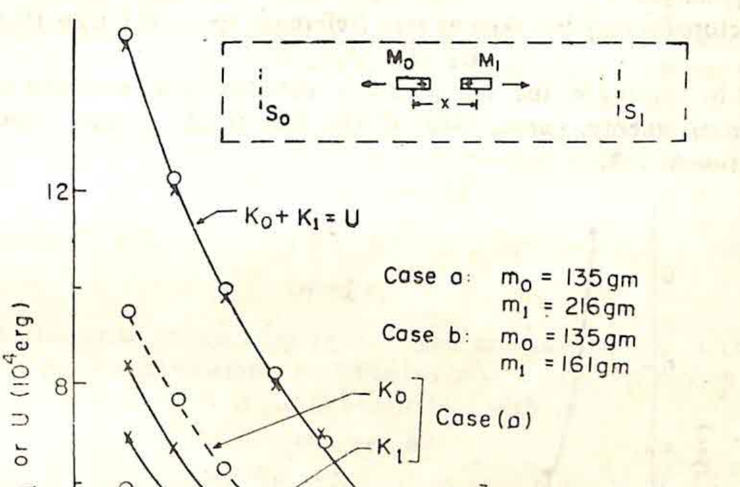

FIGURE 2.2. The potential energy curve for the system of Fig. 2.1 deduced by an alternative procedure.

an extra brass load was added on one of the gliders. Notice that although K_0 vs x and K_1 vs x curves are different, the U vs x points fall on a common curve. Check, if the latter is the same as the curve of Experiment 2-A.

EXPERIMENT 2-A(iv)

Clamp a third magnet M_0' at the other end of the track (Fig. 2.3) to fire M_1 towards M_0. Measure the velocity (hence kinetic energy) of M_1 at a position S_0 in interaction-free region (*i.e.*, far from both M_0 and M_0') and at a near distance x from M_0. If these values are K_0 and K_x respectively, we get

$$U_x - U_0 = -(K_x - K_0) = K_0 - K_x$$

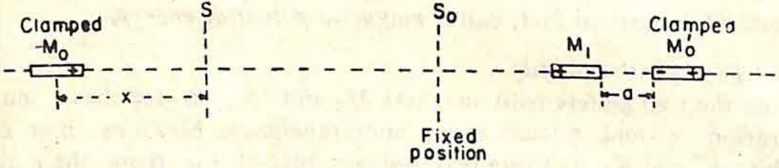

FIGURE 2.3. An alternative arrangement for obtaining the PE diagram.

As before U_0 may be taken as zero (reference level for U), so that

$$U_x = K_0 - K_x$$

Thus by varying x, the U_x versus x data are again obtained to get the potential energy curve. *See* if the PE graph is the same as in Experiment 2-A.

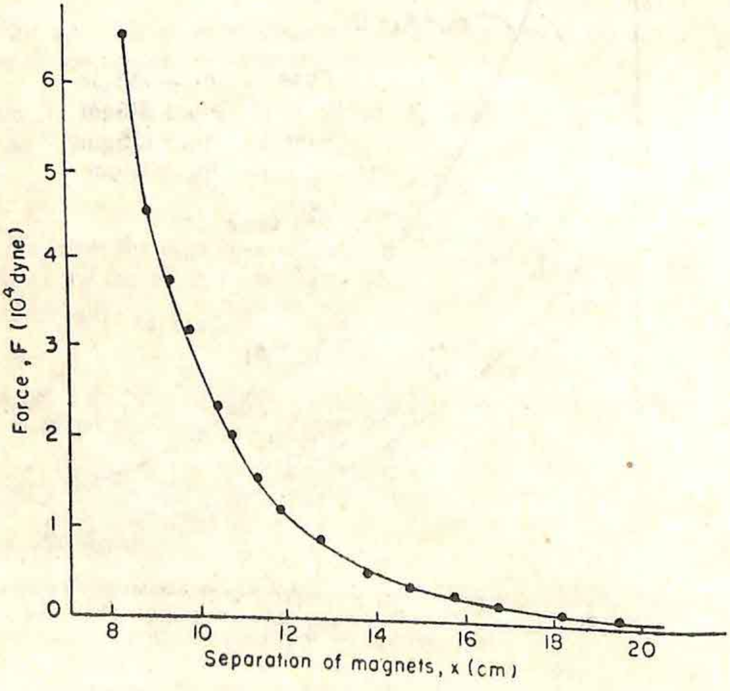

FIGURE 2.4. Force vs. distance between two magnets placed coaxially. Deduced from the U vs. x curve of Fig. 2.1.

EXERCISE 2-A(i)

From the experimental $U(x)$ vs x graph deduce $-dU/dx$ values at different values of x. Since $-dU/dx$ gives the force $F(x)$, plot a graph between $F(x)$ and x. Figure 2.4 shows the graph for force corresponding to the PE curve of Fig. 2.1.

In atomic and nuclear physics potential energy curves are not studied this way. We cannot release a projectile (say, an α particle) from a known distance from the nucleus and measure its KE outside. Nor can we measure the KE of a projectile at a given position near the nucleus. The process used is the following: (*i*) start with a model, (*ii*) assume an appropriate law of interaction, (*iii*) deduce the shape of the potential,, (*iv*) find how this potential is expected to behave with a projectile fired from outside and (*v*) *see* experimentally how far the expectations come true.

As one example, Rutherford took the model of an atom as charge Ze limited to a sphere of radius r and charge $-Ze$ distributed in some way outside this. He assumed the inverse square law to be valid up to distances as small as $\sim 10^{-12}$ cm. He deduced that for interaction with an α particle the maximum potential energy U would be $2\ Ze^2/r$. His expectation was that if α particles of kinetic energy K_0 are fired, some of them would suffer large angle scattering (up to 180°) if and only if

$$\frac{2Ze^2}{r} > K_0$$

Now, firing α particles from polonium on very thin gold foils he observed large angle scattering. Putting the constants (Z, e) and K_0 in the above relation he deduced that

$$r < 4 \times 10^{-12} \text{ cm}$$

That was the experimental discovery of the nuclear structure of the atom. (It is to be noted that by a detailed study of scattering at different angles, Rutherford established that the inverse square law is valid up to such low r values).

EXPERIMENT 2-B *To study the gravitational potential energy.*

This is a rather trivial exercise, because you are so familiar with the fact that in earth's gravitational field the potential energy of a body and earth system changes with height in accordance with

$$\triangle U = mg \triangle h$$

for heights $\leqslant$ earth's radius. But it is good to go through it, if only as a prelude to the next experiment.

Incline the track to the horizontal (inset Fig. 2.5) by raising one of its ends by a measured height H.[*] Now, release a glider[**] from a certain position A, and measure its velocity (hence kinetic energy K) at different distances x from A. U measured relative to position A, is given by $-K$. Thus the data give you U vs x curve with $U_A = 0$.

---

[*] Magnetic interaction energies for these magnets are $\sim 10^5$ erg. Since $m \sim 10^2$ gm and $g \sim 10^3$ cm/sec^2, you will note that H of the order of 1 cm or so should be large enough.

[**] One could use a brass rod or any solid in this experiment. However, to be able to use the data in the next experiment it is convenient to use a magnet itself here.

Figure 2.5 shows the results for two different slope of the air-track. Notice that both the graphs are straight lines. What quantity would the slope represent? How are the two slopes of the curves related with the slopes of the track?

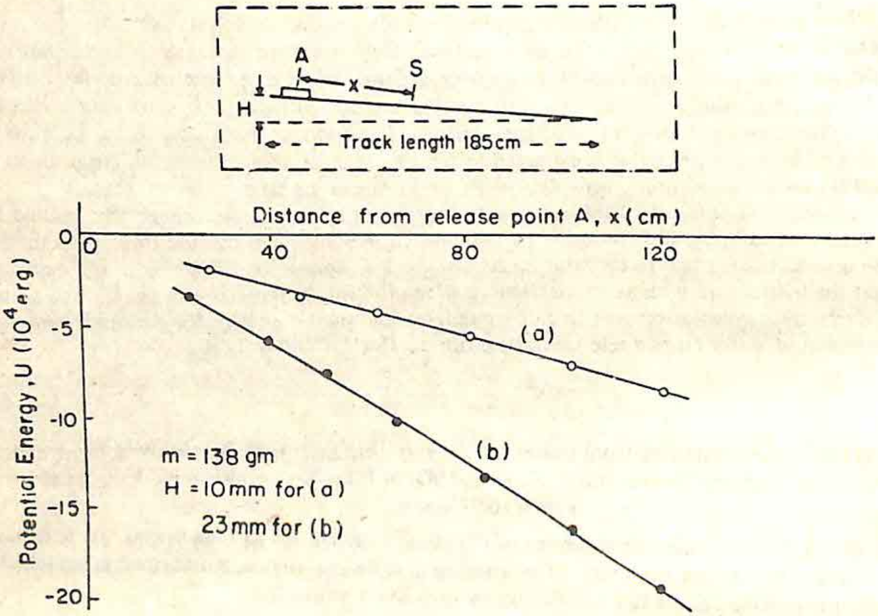

FIGURE 2.5. Variation of gravitational potential energy with distance along the air-track.

EXERCISE 2-B(i)

From the data of the two curves in Fig. 2.5, deduce the value of g. (Do not feel unhappy if the precision is not good.)

EXERCISE 2-B(ii)

From curve (*a*) in Fig. 2.5 deduce the KE imparted to a 135 gm glider in 120 cm travel if the track departs from the horizontal by 1 mm in the total length 185 cm.[*]

EXPERIMENT 2-C *Superposition of gravitational and magnetic potential energy curves.*

If you know the potential energy curves for a body in the fields of two bodies 1 and 2 separately, then the potential energy of that body in the fields of both 1 and 2 together is obtained by just adding the separate potential energies. This is the principle of superposition, and it does not matter if the nature of the fields is different for 1 and 2. This principle may be obvious from conservation of energy itself. All the same, it is a good idea to see this *experimentally*.

---

[*] This will indicate how precise you have to be in setting the track horizontal if gravitational effect has to be <1 per cent. Of course, the track construction too must have irregularities much less than, say 0.1 mm.

Set the track sloping as in Experiment 2-B, fix a magnet M_0 at the bottom end (*see* inset Fig. 2.6) and proceed as in Experiment 2-B to get the PE curve. Because of magnetic interaction between M_1 and M_0 the magnet M_1 released from A will not go beyond a certain limit. To study the potential energy curve in the farther region (*i.e.*, near M_0) release M_1 from different positions x in that region and measure the kinetic energy when M_1 reaches the position A.

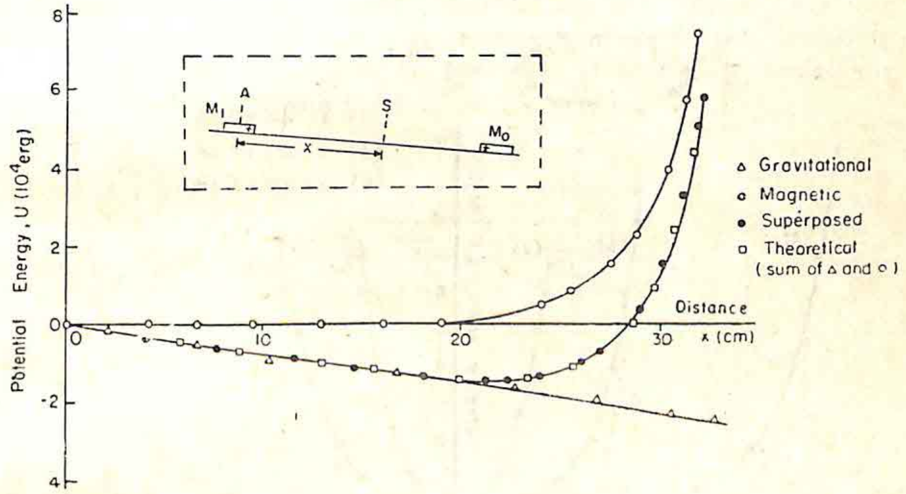

FIGURE 2.6. Superposition of gravitational and magnetic potential energies.

For M_1 in the magnetic field of M_0, the potential energy curve may be studied separately (as in Experiment 2-A), and for M_1 in earth's gravitational field, the potential energy may also be studied separately choosing the same reference point (as in Experiment 2-B). Figure 2.6 shows these two separate PE curves also. The sum of potential energies given by these two PE curves matches the observed PE curve for M_1 in the field of both M_0 and the earth.

EXPERIMENT 2-D *To study the potential energy of a magnet bounded by two fixed magnets.*

With the air-track horizontal, clamp two glider magnets M_0 and M_0' at a known separation d to confine between them a third glider magnet M_1 (Fig. 2.7, inset). You may first find the position P where M_1 comes to rest in the field of the two magnets M_0 and M_0'. Set the sensor at this position P.

Now release M_1 from different measured distances x from P (to the left as well as right) and measure the kinetic energy of M_1 as it passes P. That gives the PE when M_1 is placed at location x in the field of both M_0 and M_0', the reference level being the location of M_1 at P.

Figure 2.7 shows the PE curves for three different separations d. When d is small, the potential well is quite deep; with large d the well becomes somewhat shallow; finally with d very large the bottom of the well becomes wide and flat.

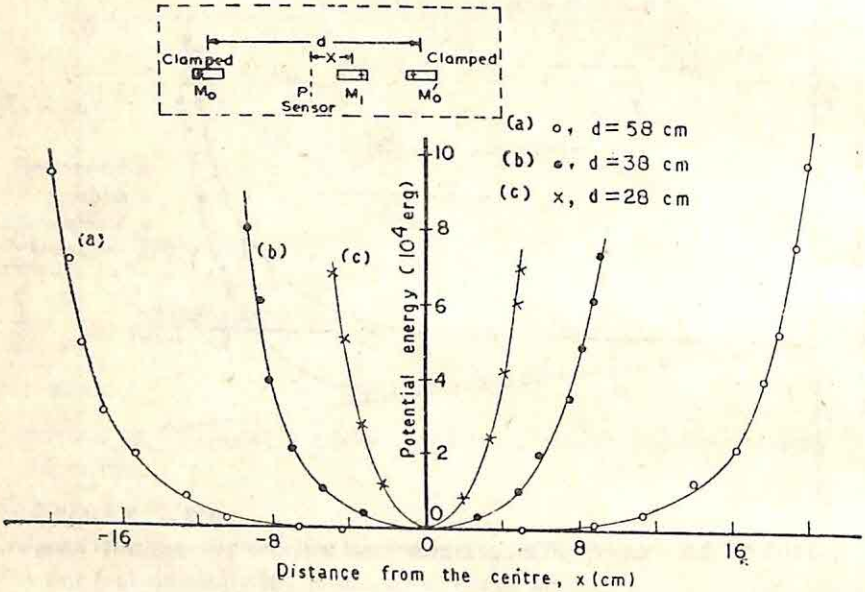

FIGURE 2.7. Potential energy of a magnet (M_1) in the field of two magnets (M_0, M'_0), shown in the inset.

In the next chapter you will study the oscillations of a magnet when placed in such potential wells. At this stage therefore it would be useful to become familiar with the nature of the potential energy curves.

The absolute value of U depends on the choice of the reference state of the system. Let Mr X choose the reference state as that at which M_0, M_0' and M are at infinite distance from each other. Now let M_0 and M_0' be brought to a distance d and clamped there. If work done in doing so is U_d and Mr Y decides to use this as the reference state, then all the U measurements by Y will differ from those made by X by this common quantity. Yet further, let M_1 be brought to the equilibrium position between M_0 and M_0'. In doing so some work U_d' is done. If Mr Z decides to use this as the reference state then his U measurements are smaller than those of Y by the amount U_d' throughout and smaller than those of Mr X by the amount $U_d + U_d'$ throughout. For a constant d these amounts are not affected by x, the displacement of M_1 from the equilibrium position. Therefore the shape of the $U(x)$ versus x curve remains independent of whether you are Mr X or Mr Y or Mr Z.

Although the isolated system comprises three bodies M_0, M_0' and M_1, the process of clamping M_0 and M_0' to the earth (which amounts to making them infinitely heavy) makes them the 'field magnets', permitting us to measure U as a function of displacement x of the magnet M_1 alone.

RELATED EXPERIMENTS

EXPERIMENT 2-D(i)

You may determine the *PE* curve for (*i*) M_1 in the field of M_0 and (*ii*) M_1 in the field of M_0'. Now with the appropriate separation d add the two PE curves and compare the resultant curve with what you got in Experiment 2-D for the given d. You would expect the shapes to match, but the reference level for U will be different. Figure 2.8 shows how the system $M_0+M_0'+M_1$ may show different PE curves depending on the separation d between M_0 and M_0'. How would you relate the varying reference level with U_d' ?

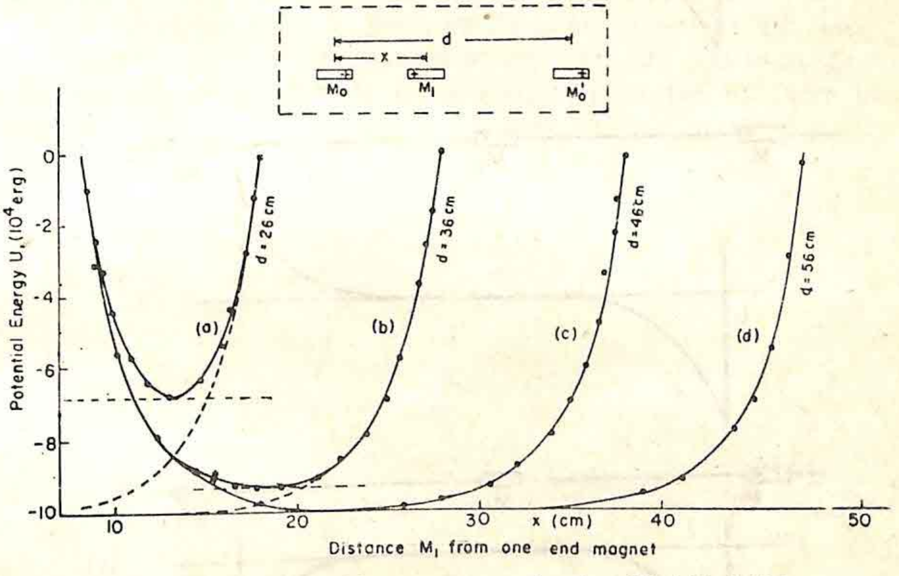

FIGURE 2.8. Potential energy curves of system $M_0+M_1+M_0'$ of d obtained by adding the PE for M_0+M_1 to that for $M_0'+M_1$.

EXPERIMENT 2-D(ii)

With M_0 and M_0' unchanged, repeat Experiment 2-D using a different magnet M_1' which has the same dimensions as M_1. Check if the U values in the old and new curves at corresponding positions bear a constant ratio.

The potential energy of the system $M_1+(M_0+M_0')$ may be considered as the product of two terms. One of these depends on M_0+M_0' and the space coordinate x only; the other is an intrinsic property of M_1 only.

The first is called the *potential** due to M_0+M_0', the second is called the *magnetic moment* of M_1. The product of magnetic moment and potential at a point x gives the potential energy when M_1 is at x. If M_1 is replaced by magnet M_1', its magnetic moment may be r-fold.** Then the value of U everywhere becomes r-fold. This is the general principle being checked here.

In the case of two electrical charges q and q' at separation r the potential energy may be written as:

$$U=K\frac{q\,q'}{r}=K\,q\left[\frac{q'}{r}\right]=Kq'\left[\frac{q}{r}\right];\qquad (K=\text{a constant})$$

Thus we may consider q' as generating the potential distribution q'/r,

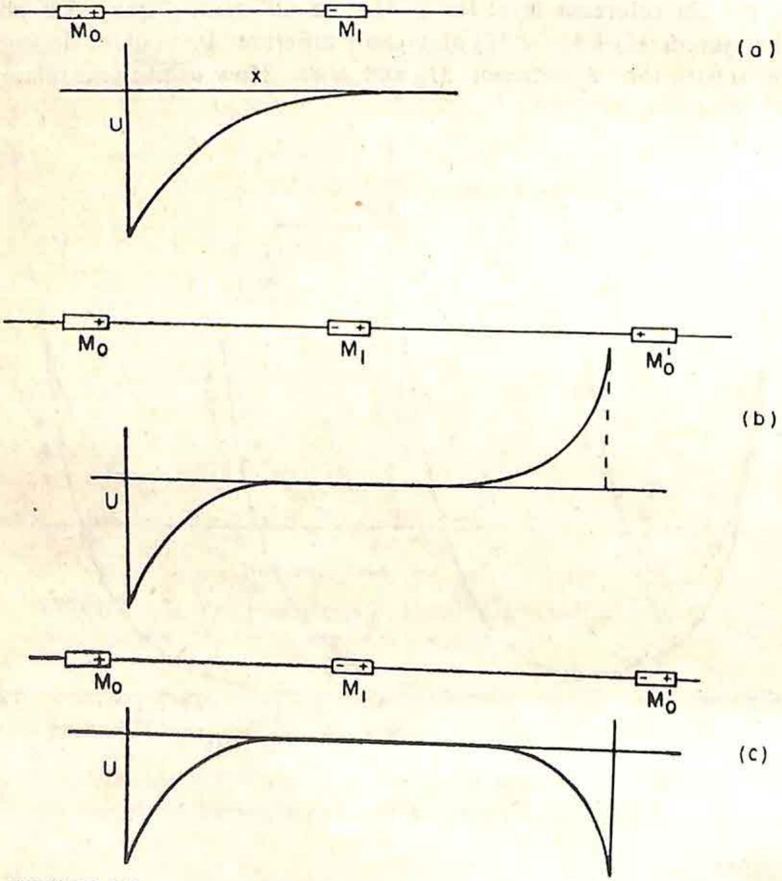

FIGURE 2.9. Other configurations and the corresponding PE curves; (*a*) M_1 in attractive mode with M_0; (*b*) M_1 in attractive mode with M_0 but repulsive mode with M_0'; (*c*) M_1 in attractive mode with both M_0 and M_0'.

---

*While 'potential energy' has the dimensions of energy (like erg or joule), 'potential' has the dimensions of 'energy per unit magnetic moment.'

**Since magnetic moment is a vector quantity, the result in general depends on the *orientation* of M_1 also. We must therefore add 'for the same orientation' in this statement. For the case of an electrical charge such qualification is not required.

which acting on q gives us the potential energy U, or we may consider the other way. They are equivalent. This is a universal truth; but quite often the convenience is in treating the clamped members as the field generating members (like M_0+M_0') and the movable member as the one which can be changed at will, as you replaced M_1 by M_1' in this experiment.

EXPERIMENT 2-D (iii)

It will be interesting to measure potential energy curves for the case of magnets in *attractive mode*. Figure 2.9 shows three geometries. In case (*a*) you have M_0 and M_1 in attractive mode; in case (*b*) M_1 is in attractive mode with M_0 but in repulsive mode with M_0'; finally in case (*c*) M_1 is in attractive mode with both M_0 and M_0'.

A particular precaution in doing these experiments is to have a rubber or sponge padding fixed at each of the two end faces of M_1 to avoid damage to the magnets in direct hits. We leave it to you to decide how you would proceed for these studies. The nature of potential energy curve you would expect is shown in Fig. 2.9 for each case.

You may note that when M_1 (with padding, as suggested) ultimately 'hits' another magnet, the *elastic interaction* comes into play in addition to the magnetic. It will be useful if one can complete the PE curve in this range also.

3

STUDY OF OSCILLATIONS IN POTENTIAL WELLS OF DIFFERENT SHAPES

3.1. POTENTIAL WELLS

In the preceding chapter we have used the equation

$$\triangle U = -\triangle K \qquad \ldots(3.1)$$

to deduce the potential energy change $\triangle U$ from the measured kinetic energy changes $\triangle K$ and thus to build up the potential energy curves for any system. Now we are going to use the PE curves in the reverse way.

Figure 3.1 shows a potential-well. Let the total energy of the system $(K+U)$ be E, as shown by the horizontal dotted line. What information does the PE curve give now? Firstly, since K cannot be negative, the intercepts of the E line with the PE curve (points P and Q, corresponding to $x=a$ and $x=b$ respectively) give the extreme limits between which the body can move. Secondly, the vertical gaps between the E line and the PE curve at different positions (the vertical full lines) give you the kinetic energy of the body at different positions in the region a to b, being obviously zero at the ends a and b. You will notice that any shift in reference level of U will effect the PE and the total energy by equal amounts, so that the information about kinetic energy K at different x values remains unchanged.

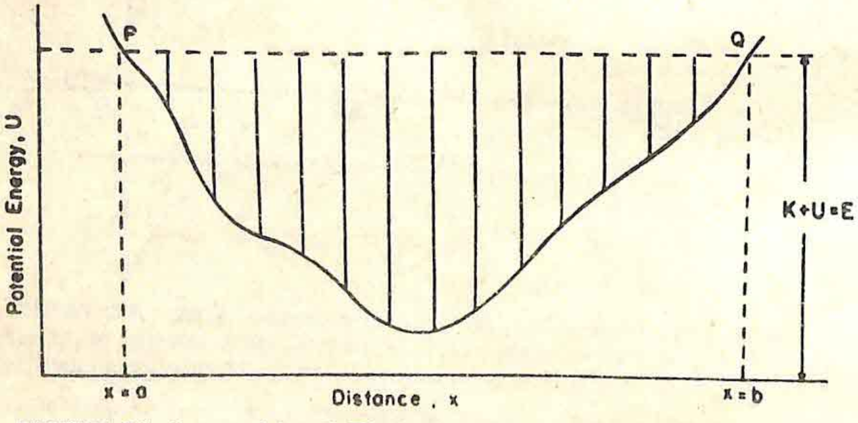

FIGURE 3.1. A potential well. The lengths of vertical lines represent the kinetic energy at different x for a given total energy E.

Figure 3.2 shows another interesting case, where the PE curve has two wells, one around $x=a$, another around $x=b$. With total energy $E=E_1$, the body can only be in the well around $x=a$, and not in the well around $x=b$; with total energy $E=E_2$ the body could be either in the well around $x=a$ or in the well around $x=b$ depending upon initial condition, but cannot pass from one well to another. We say that there is a hill (potential barrier) at $x=e$. With total energy $E=E_3$ the body moves over the wide span from $x=c$ to $x=d$, as if there is only one well, not two.* The case $E=E_2$ is of special interest because atomic particles under such conditions refuse to obey the 'either' — 'or' rule dictated by Newtonian laws; they have a finite, though small, probability for cross-over across the barrier. Explanation for this is beyond the Newtonian mechanics, but quantum mechanics explains it satisfactorily.

The process is called *tunneling* through a potential barrier. You should not, however, think that a tunnel is bored through by the particle (like a tunnel for railways through a hill). It only means that if the particle initially is on one side of the barrier, there is a finite, though small, *probability* that it may later be found on the other side.

The probability, as predicted by quantum theory, decreases with increase in the

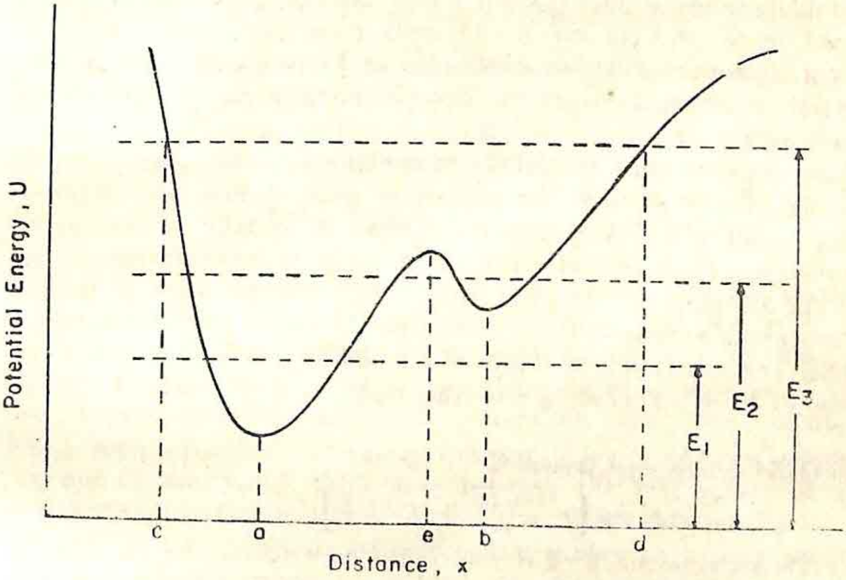

FIGURE 3.2. A double well potential.

---

*The hump at $x=e$ would show its effect in the nature of oscillation.

mass of the particle and width and height of the potential barrier.* For this reason, the probability is negligibly small for any macroscopic system. This is in agreement with 'zero probability' predicted by Newton's Laws. However, for nuclear particles, the mass is $\sim 10^{-24}$ gm, the potential width can be as small as $\sim 10^{-13}$ cm and the barrier height $\sim 10^{-6}$ erg. With all these values so small the probability becomes finite and experimentally observable.

In any case, your present experiments are with macroscopic bodies only. For any computations you will deduce the kinetic energy of the body at different positions from E and the potential energy diagrams using Equation (3.1) the other way round *i.e.*,

$$K = E - U \qquad \ldots (3.2)$$

3.2. OSCILLATIONS IN A POTENTIAL WELL

We now proceed to study the dynamics of a body in potential wells like those you obtained in Experiments 2-C and 2-D. When the motion is confined to a potential well the system exhibits periodic motion, called oscillation.**

Let us see what Newton's laws say about the oscillations. Consider a body of mass m and total energy E in a typical potential well shown in Fig 3.3, where the zeros for both U and x are taken at the bottom of the well for convenience.†

This figure shows at once that for $E=90$ units the limits for oscillation are -8.7 cm to $+6.3$ cm; for $E=40$ units these limits are $-2\ 5$ cm to $+4.3$ cm. Thus the oscillation amplitudes on the two sides are unequal in general; which one is larger may depend on the shape of the well and the value of E.

If you desire to know the details of motion—*i.e*, the time taken in traversing different parts of the path—you may at first understand it broadly from Fig. 3 3. Assume that the body is initially at rest at A. Since the force $(-dU/dx)$ at A is positive, the body starts moving to the right. The difference $E-U$ gives the kinetic energy; when it reaches $x=0$ all energy becomes kinetic. Thereafter the force $(-dU/dx)$ becomes negative. This causes slowing down of the motion, as is also shown by decrease of $E-U=K$ as we go to the right. At B we have $E-U=0$,

---

*The tunneling probability is given by:

$$P = \exp\left[-\frac{4\pi\sqrt{2m}}{h}(U-E)^{1/2}\ b\right]$$

where h is Planck's constant, $U-E$ is the amount by which the particle energy is short of the barrier height and b is the width of the barrier. Take $U-E$ and b as small as 0.1 erg and 0.1 mm and calculate P for your glider ($m=130$ gm). If the collision occurs once every second what are the chances of observing a tunneling in a million years? Compute.

**Perhaps you are already familiar with simple harmonic oscillation. But remember that not all periodic motions are simple harmonic. Most cases you are going to study here are not of simple harmonic character.

†The well is not parabolic as it is in the case of simple harmonic motion. In fact, tis not even symmetric about the U axis It is therefore a very general case.

i.e., the body comes to instantaneous rest. Thereafter the body proceeds the reverse way, and so on.

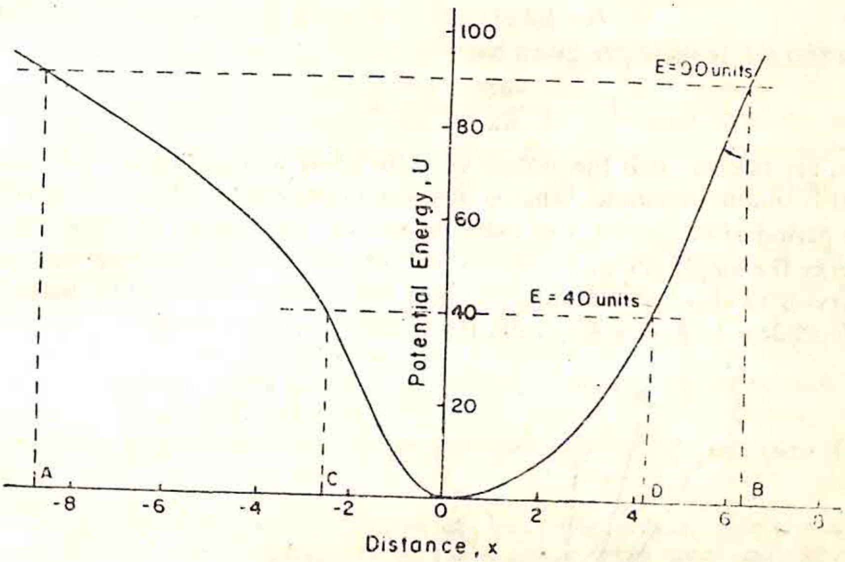

FIGURE 3.3. An asymmetric potential well.

To find out quantitatively how much time elapses in completing each part of the motion you need to do some mathematical exercise. In Equation 3.2, you may write $\frac{1}{2}\,m(dx/dt)^2$ for the kinetic energy K, and then integrate between any two positions to get*

$$t=\int dt=\sqrt{m}\int\sqrt{\frac{1}{2(E-U)}}\;dx$$

Now, integral calculus is useful only when U is a simple function of x as, for example, $U=\frac{1}{2}\,kx^2$. But in a general case the graphical or numerical integration method may be used more profitably. Briefly the method is as follows: (*i*) read U values from PE curve at several x values; (*ii*) deduce corresponding $E-U$ values for the given constant E; (*iii*) compute $1/\sqrt{2(E-U)}$ values; (*iv*) plot these against corresponding x; (*v*) find the area under this curve between the two values of x for which the travel time is desired; and (*vi*) multiply the area by $\sqrt{m}$ to get the desired t. Appendix III-A shows the procedure with a numerical example.

Proceeding in this way with the PE curve of Fig. 3.3 you would find that the travel times for the two halves A to 0 and 0 to B are not equal. Which one is larger and by what factor, will depend on the given E value. The total time T in completing one oscillation (called the *period*) will also vary with E.

---

*We have done this earlier in Chapter 2, Equation (2.15)

Figure 3.4 shows three potential wells A, B and C, all of which are symmetric about the U axis and all of them are coincident in the lowermost part. The potential curve A is parabolic, *i.e.*,

$$U=\tfrac{1}{2}kx^2 \qquad \ldots(3.4)$$

The force F is therefore given by

$$F=\frac{-dU}{dx}=-kx \qquad \ldots(3.5)$$

You are familiar that the motion corresponding to a parabolic potential well is simple harmonic. What is of special importance about it is that the period of oscillation T is independent of the energy E. With larger energy the amplitude of oscillation will become larger, but the velocity everywhere also becomes larger by just the correct amount to make T independent of E (*see* Appendix III-A; also Appendix VI-B).

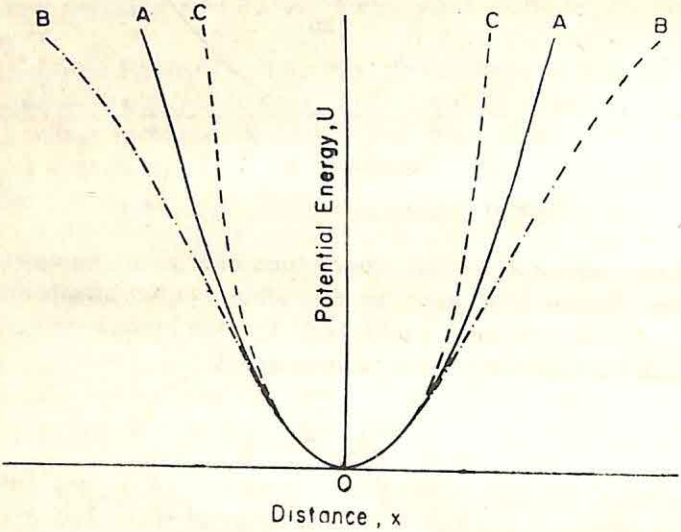

FIGURE 3.4. Three symmetrical potential wells overlapping in their low energy parts.

Now, relative to potential energy curve A the curves B and C widen and narrow down respectively at larger E values. You may apply a procedure like that of Appendix III-A to work out whether T will depend on E for these cases, and if so how. We will leave these questions unanswered for you to work out.

EXPERIMENT 3-A *To study frequency versus energy curves for oscillations in a potential well.*

Set up the arrangement used for Experiment 2-D (*see* inset of Fig. 3.5).

You may keep d in the range 20 to 40 cm so that you get a potential well whose bottom is not very flat.*

Find the equilibrium position P of glider M_1 in the system, and set the sensor there. Now release the glider from a given distance a from P. Use mode $\rfloor\overline{A}\lfloor$ of the timer to measure KE of the glider at P, which gives the total energy E of oscillations, since at P the value of U is taken as zero. Use also mode $\rfloor\overline{A}\ \rfloor\overline{A}$ of the timer to measure the times for the left half and right half oscillations, so that the sum gives the full period T. Repeat with several a values to get the T vs E data over a wide range.

Figure 3.5 shows the typical results for two separations of M_0 and M_0'. We have plotted the frequency ν $(=1/T)$ against E because in all advanced physics it is more customary to use frequency ν. In both the cases ν increases as E increases. Are the potential wells parabolic? If not, then are the upper wings of the potential curve bent-out or bent-in relative to the parabolic case? (*see* Fig. 3.4, curves B and C). Could you say why ν is in general larger for M_0 M_0' separation $d=25$ cm, than for $d=33$ cm.

In this experiment we can set the magnet M_1 oscillating with *any* value of energy E. In contrast, in molecular systems the permitted energy values in a potential well

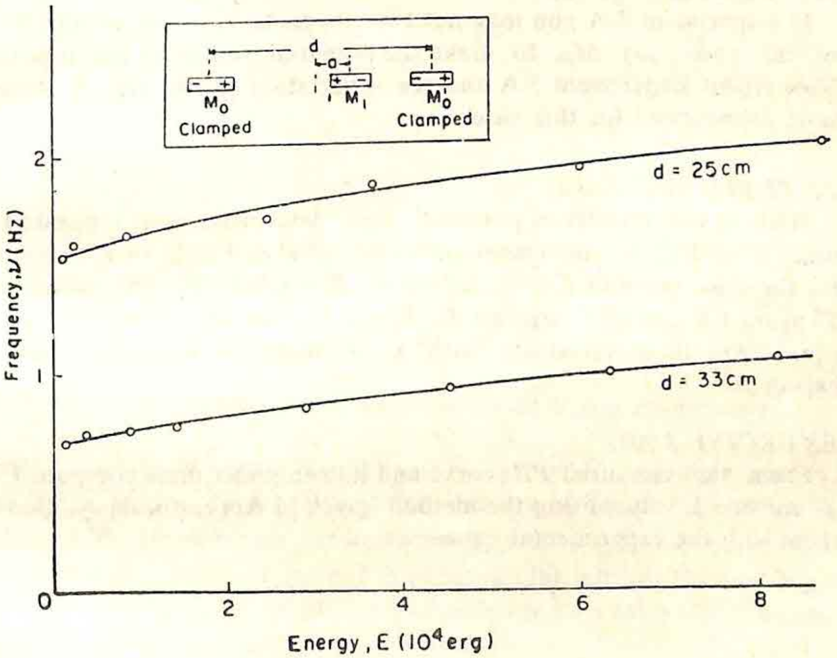

FIGURE 3.5. Variation of frequency with energy for oscillations in a potential well generated by the arrangement shown in the inset (for two values of d)

---

*It will be useful to do Experiment 2-D with the same setting, so that the potential energy curve is known. However, for the present your purpose is different.

are not found to be continuous but discrete. That is, the molecule may exist with one of a specified set of E values and no intermediate values of E are permissible. This discreteness of allowed E values is a characteristic of all bound systems when treated quantum mechanically.

Now, quantum mechanics should also be applicable to the macroscopic system of magnets you have studied. The reason why discreteness of E is not experimentally observable in this case is that the allowed energy levels, though discrete, are very close to one another.* Thus quantum mechanics approximates to Newtonian for the case under study.

There is another aspect to consider. In quantum mechanics when the analysis leads to energy values E_0, E_1, E_2, etc., one cannot assign frequencies with them. A frequency ν is associated through the equation $h\nu = E_1 - E_2$ when a system *changes* from one energy state to another. However, here again there is a principle (called *Bohr's correspondence principle*) which states that in the condition of our macroscopic experiments the quantum mechanical value would coincide with the frequency given by Newton's laws.

You thus conclude that for atomic systems quantum mechanics does give results fundamentally different from those given by Newtonian mechanics. These results are exciting. All the same, when applied to the oscillations of a magnet size body the results of quantum mechanics approximate to those of Newtonian mechanics.

RELATED EXPERIMENTS

EXPERIMENT 3-A(i)

In Experiment 3-A you may put two magnets, instead of one, at one of the ends, say M_0, to make the potential well more unsymmetrical. Now repeat Experiment 3-A and *see* if variation of ν with E becomes more pronounced for this case.

EXPERIMENT 3-A(ii)

With an unsymmetrical potential well, you may note separately the times T' and T'' for movement across left of P and right of P respectively for the same value of E (Fig. 3.5 inset). Plot separately the variations of T' against E and of T'' against E. Try to explain why T' and T'' are not equal. Are their variations with E of identical character? Do you expect it?

EXERCISE 3-A(i)

From the measured PE curve and known glider mass compute T' and T'' for one E value, using the method given in Appendix III-A. Compare them with the experimental values.

---

*For instance, in a harmonic oscillator the quantum mechanically allowed energy levels are equidistant with a gap equal to Planck's constant (h) times the frequency (ν). For oscillations of $\nu \sim 1$ Hz, the energy gaps would thus be as small as $\sim 10^{-26}$ erg.

EXPERIMENT 3-B *To study the effect of oscillator mass on the frequency.*

Repeat Experiment 3-A with varying brass loads added to the glider carrying magnet M_1. Note the total mass m of the glider in each case. Figure 3.6 (a) shows ν vs E curves for 5 different values of m. In general you note that for a given E values ν decreases as m increases.

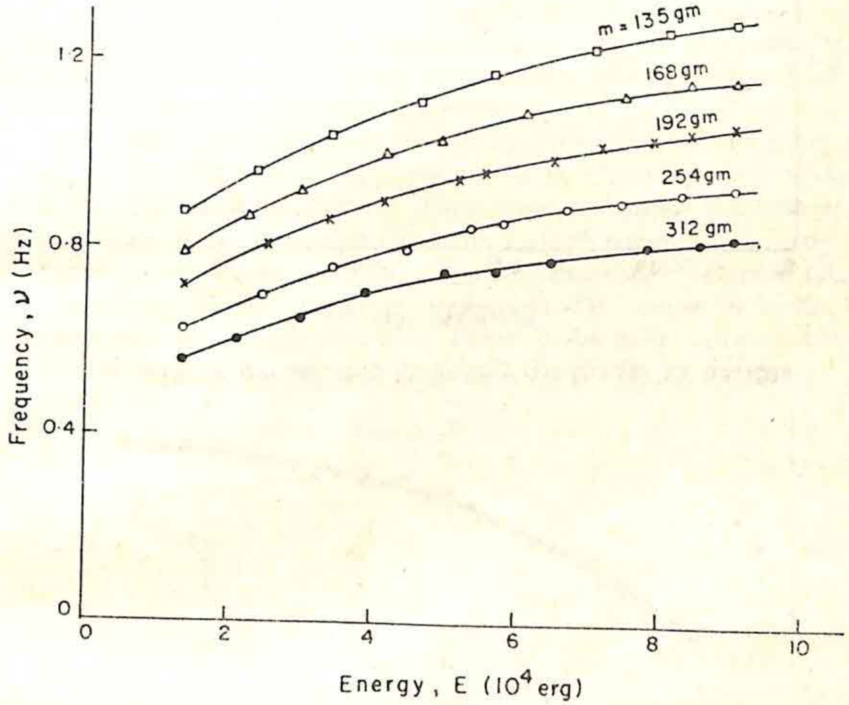

FIGURE 3.6. (a) Dependence of ν vs E curves on the mass of the oscillator.

From these data we read ν vs m data for a given E and then plot ν against $1/\sqrt{m}$ in Fig. 3.6 (b). This is done for four different E values, and in each case the graph comes out as a straight line.

In Fig. 3.6 (c), $\nu\sqrt{m}$ is plotted against E for all the data of Fig. 3.6(a). You note that the experimental points for all 5 cases (of different mass) fall on a common curve fairly well.

Figure 3.6 (b) and 3.6 (c) are just two different ways of showing that if the potential curve remains unchanged (*i.e.*, the magnets M_0, M_0', their distance d, and the glider magnet M_1 are unchanged) the oscillation frequency of the glider is proportional to $1/\sqrt{m}$ at all energy values. *See* if you can explain this using Equation (3.2).

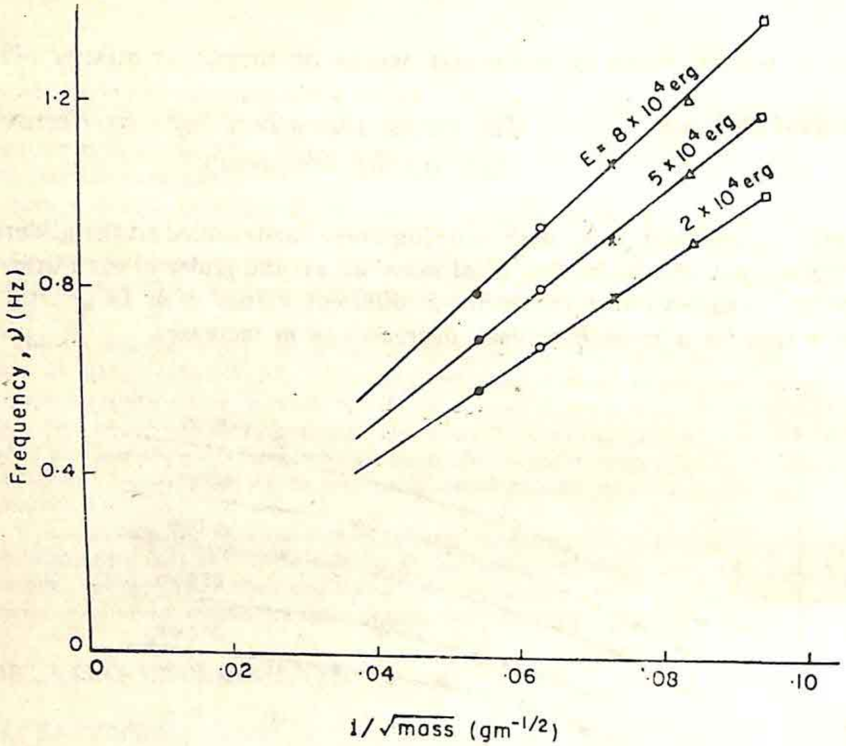

FIGURE 3.6. (b) ν vs $1/\sqrt{m}$ curves for three different E vaules.

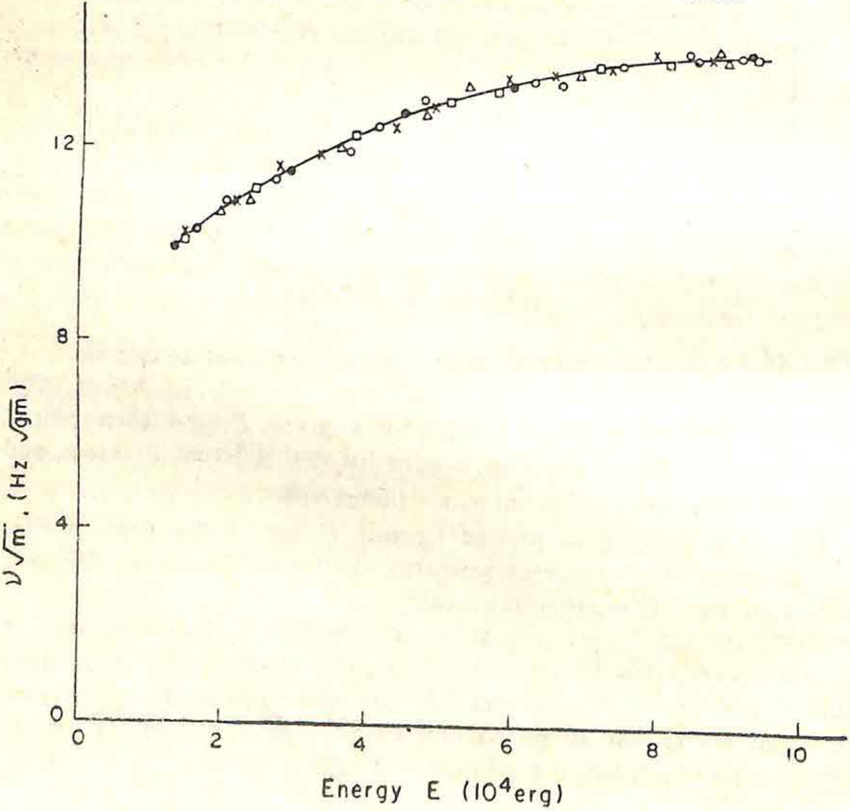

FIGURE 3.6 (*c*) $\nu\sqrt{m}$ vs. E curves for oscillators of all masses. In all the cases the potential well is the same.

EXPERIMENT 3-C *To study the frequency* vs *energy curve when two bodies oscillate against one another.*

In Experiment 3-B the field magnets M_0 and M_0' were kept clamped to the track, and M_1 alone was free to oscillate. Now unclamp M_0 and M_0' and hook them up, so that they are forced to move as one unit, M_1 being the second. There is a stable equilibrium configuration of this two-body system, and if a relative displacement x is caused and both the bodies are released simultaneously, they oscillate against one another.

The inset in Fig. 3.7 shows the arrangement. If you cover M_0 (or M_0') you may see M_0' (or M_0) and M_1 oscillating like two masses connected by a spring, or like a diatomic molecule.

Now study the ν vs E curves for the following arrangements: (*a*) when M_0+M_0' is clamped and M_1 alone oscillates; (*b*) when M_1 is clamped and M_0+M_0' oscillates; and (*c*) when none is clamped and both M_1 and M_0+M_0' oscillate. Plot these curves on a graph paper.

Figure 3.7 shows the results of a typical experiment. Curves (*a*), (*b*), (*c*) correspond to the three cases cited above. Of course (*a*) is the same as obtained in Experiment 3-A. The relation of (*b*) to (*a*) is that their ordinates bear a constant ratio, satisfying the condition

$$\frac{\nu_a}{\nu_b}=\frac{\sqrt{m_2}}{\sqrt{m_1}}=r \qquad \ldots(3.6)$$

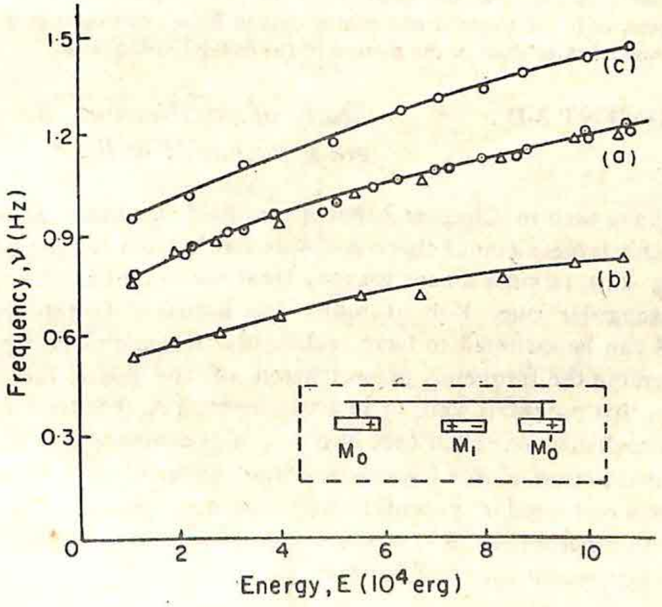

FIGURE 3.7. Dependence of ν vs E curves on the oscillating member of a two-component system.

where $m_2=m_0+m_0'$, the total mass of M_0 and M_0' with the hooking strip. This has been shown in Fig. 3.7 by multiplying the ordinates of curve (*b*) by this factor *r* and replotting; the points fall on curve (*a*) throughout the observed range.

The relation of curve (*c*) to (*a*) is again of the same kind:

$$\frac{\nu_a}{\nu_c} = \text{constant} \qquad \ldots(3.7)$$

and you may put this constant equal to $\sqrt{m}/\sqrt{m_1}$ as a parallel to Equation (3.6), and then compute m. This is called the *reduced mass* of the two-body oscillator. You may note that since curve (*c*) shows the highest ν values among the three cases, m is smaller than both m_1 and m_2.

Appendix III-B gives the relevant theory, which tells us that the reduced mass is given by

$$m=\frac{m_1\, m_2}{m_1+m_2} \qquad \ldots(3.8)$$

In Fig. 3.7 the ordinates of curve (*c*) multiplied by $\sqrt{m}/\sqrt{m_1}$ have been shown, they fall on curve (*a*) throughout, showing that the experimental value of m coincides with that given by theory.

The concept of 'reduced mass' is used widely in mechanics to simplify mathematics. Instead of both the bodies 1 and 2 oscillating (with their centre of mass unchanged) like one can talk of a single body of reduced mass m oscillating. In diatomic molecules O_2, N_2 etc., the reduced mass is half of the mass of an individual atom; in a case like HCl, the reduced mass is smaller than the mass of the H atom. Incidentally, for rotational motion also the same value of m is applicable. Thus, in the earth-and-sun case, or in the electron-and-proton case in Bohr's hydrogen atom, the use of reduced mass takes account of the motion of the heavier component.

EXPERIMENT 3-D *Study of oscillations in a rectangular potential well.*

You have seen in Chapter 2 that if the field magnets M_0 and M_0' are placed at a large distance there is a wide flat bottom for the potential well (*see* Fig 2.6). In such a case we may treat the potential well as resembling 'rectangular' one. For example, the actual potential well *ABCD* in Fig. 3.8 can be assumed to have rectangular shape defined by *A'B'C'D'*.

Determine the frequency of oscillation of the glider for different energies in this potential well, as in Experiment 3 A. Figure 3.9(a) gives the ν vs E results for one such case and you may compare this with Fig. 3.6.

The distinction of this Experiment from Experiment 3-A lies in the fact that for a rectangular potential well, we may treat $E-U=E=$constant over the length b (Fig. 3.8) where $U=0$. Now, using Equation (3.3) we get the expression for the frequency as

$$\nu=\frac{1}{\sqrt{2m}}\,\frac{\sqrt{E}}{b} \qquad \ldots(3\,9)$$

In Fig. 3.9 (a) the theoretical curve shows ν proportional $\sqrt{E}$. It may be noted that the experimental data agree fairly well with the theory in the region of large E, but there are prominent departures in the low E region. [Fig. 3.9(b) shows the ν vs $\sqrt{E}$ plot for the same case]. Why would you expect the kind of departures observed?

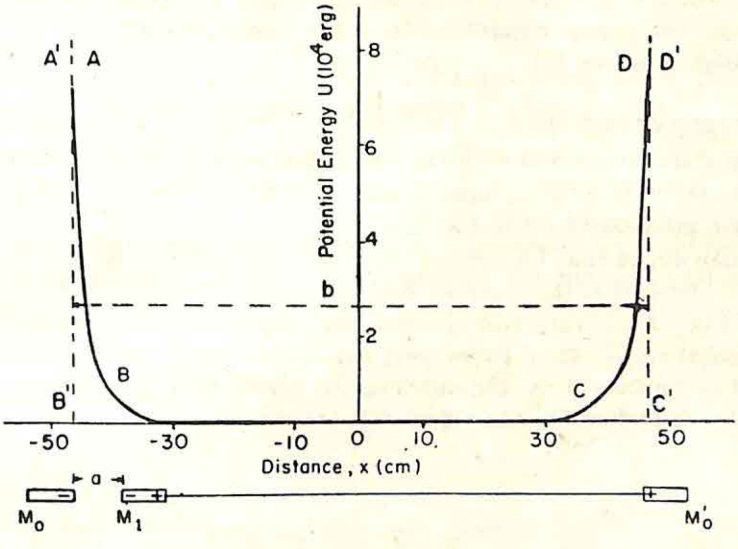

FIGURE 3.8. A nearly rectangular potential well.

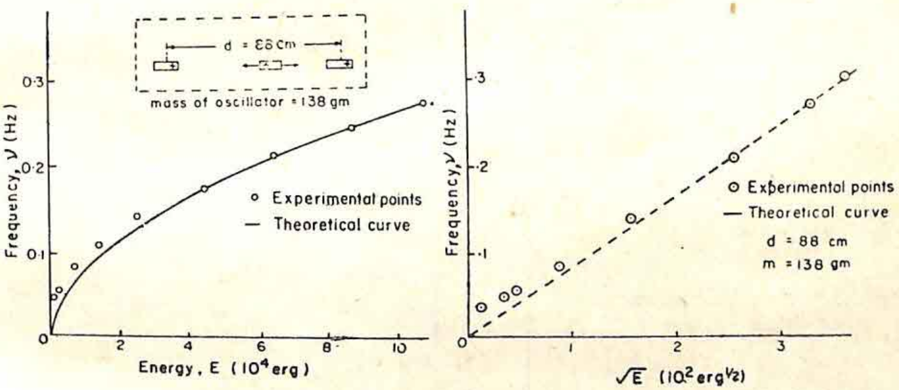

FIGURE 3.9 (a) ν vs. E plot, (b) $\nu\sqrt{E}$ plot for oscillations in a rectangular potential well.

RELATED EXPERIMENTS

EXPERIMENT 3-D (i)

Repeat Experiment 3-D varying *b* in successive steps, but keeping E

the same*, *i.e.*, releasing M_1 from a fixed separation a from M_0 each time. Thus the experiment gives ν vs b data for constant E. Would you plot ν vs b or ν vs $1/b$ graph? What do you expect the graph to be like? Why would you expect departures from the expectations? And in what region (high b or low b)?

EXPERIMENT 3-D (*ii*)

Repeat Experiment 3-D with varying glider mass m. As in Experiment 3-B, you may plot $\nu\sqrt{m}$ against E and see if the points for different m fall on the same curve [as in Fig. 3.6 (c)].

You may notice that Equation (3.9) is an approximation and Experiment 3-D shows that there are serious departure from it at smaller E values (Fig. 3.9). Yet, you do not find significant departures in the experimental $\nu\ \sqrt{m}$ vs. E curve with changing mass in the entire region for E. That means ν is proportional to $1/\sqrt{m}$ very generally. Try to guess what is so fundamental about this relation.

---

*It may be advisable to keep E large.

APPENDIX III-A

GRAPHICAL METHOD FOR DEDUCING THE DETAILS OF MOTION IN A POTENTIAL WELL

1. The Principle

If the potential energy curve $U(x)$ vs x is given and the total energy E of a body of mass m placed in this potential well is given, you can deduce all details of the oscillatory motion. The steps needed are as follows:

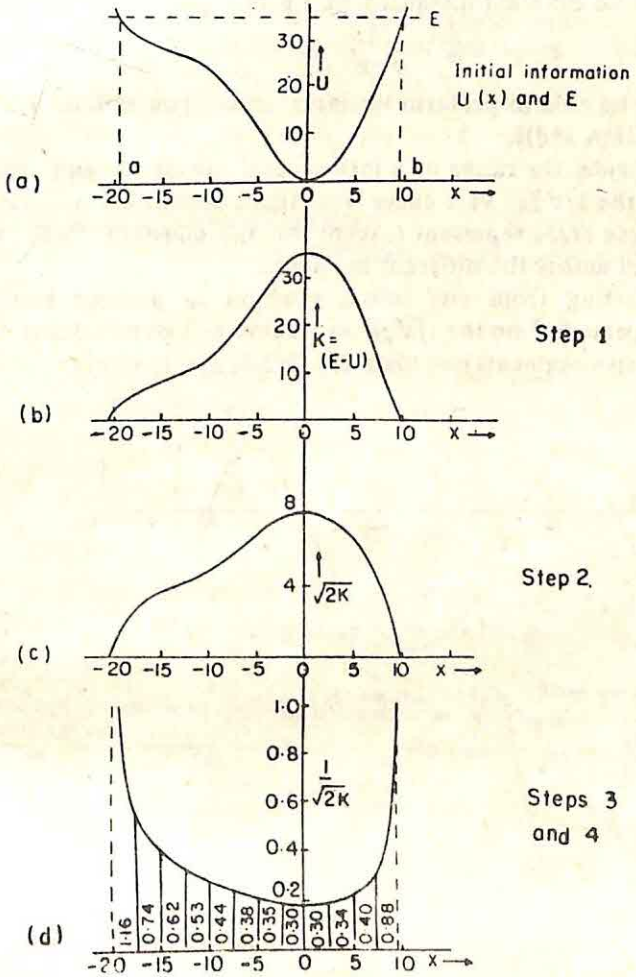

FIGURE III-A-1. Steps involved in deducing the motion of a given body with energy E in a given potential field U.

Step 1. Starting from the PE curve and the given E [Fig. III-A-1(a)] you deduce the kinetic energy at several values using

$$K(x) = E - U(x) \qquad \ldots \text{III-A (1)}$$

and thus obtain $K(x)$ vs x curve [Fig. III-A (1b)]. The limits a and b for x are set by the intersection points of E with the $U(x)$ curve shown in Fig. III-A (1a).

Step 2. Since $K = \frac{1}{2} mv^2$, you have

$$v = \frac{1}{\sqrt{m}}\sqrt{2K} \qquad \ldots \text{III-A(2)}$$

From $K(x)$ values you compute $\sqrt{2K}$ and thus get $\sqrt{2K}$ vs x curve [Fig. III-A (1c).] This, in fact, is v vs x curve, except for the constant factor $1/\sqrt{m}$.

Step 3. Since $v = dx/dt$ and your interest is in computing the time for travel across different distances, you give Equation III-A (2) the form

$$dt = \sqrt{m} \; \frac{1}{\sqrt{2K}} \; dx \qquad \ldots \text{III-A(3)}$$

Therefore to be able to perform the integration, you obtain $1/\sqrt{2K}$ vs x curve [Fig. III-A (1d)].

Step 4. Divide the range of x into several segments and deduce the areas under the $1/\sqrt{2K}$ vs x curve for these segments by counting the squares. These areas represent (except for the constant factor $\sqrt{m}$) the time of travel across the different segments.

Step 5. Starting from any initial position x_0 proceed forward and backward repeatedly* on the $1/\sqrt{2K}$ vs x curve and go on adding the areas under successive segments cumulatively. While x values repeat between the

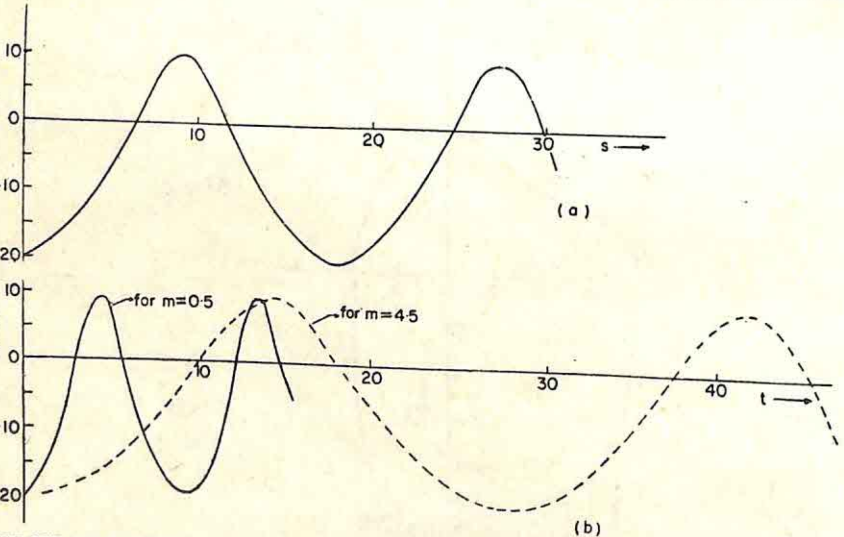

FIGURE III-A (2) (a) x vs the cumulative areas under the curve (d) of Fig. III-A (1); (b) x vs t curves for two different masses of the oscillating body.

*Just two or three scans of the region will be enough.

limits set in Step 1, the cumulative area s increases monotonously. Draw an x vs s curve, taking s along abscissa. [Fig. III-A (2a)].

Step 6. Now multiply s values by $\sqrt{m}$ throughout. That converts s values to time values (t) and you get x vs t curve [Fig. III-A (2b)]. This gives the complete information about the oscillation of the body of mass m placed in the given potential well with the given energy.

NOTES (*i*) One need not draw K vs x and $\sqrt{2K}$ vs x curves. The data may be collected in tabular form, getting $K=E-U$ then $\sqrt{2K}$ and then $1/\sqrt{2K}$. At this stage the $1/\sqrt{2K}$ vs x curve alone may be plotted to work out the areas.

(*ii*) In working out the area under the $1/\sqrt{2K}$ vs x curve you can have a lurking doubt whether the end segments would have finite areas. It can be shown mathematically[*] that although $1/\sqrt{2K}$ tends to infinity, the area does not tend to infinity so long as the inter-section of $U(x)$ curves with E line [Fig. III-A (1a)] is at non-zero slope. It may be advisable to draw the end segments separately with x-scale expanded (say) 10-fold and then to compute the area under these in (say) 5 smaller segments.

(*iii*) The $\sqrt{m}$ factor is not included at stages 2 to 5 because the s vs x curve has *general applicability for all masses*, so long as E and the *PE* curves are unchanged.

2. Example of Simple Harmonic Motion

In this case the $U(x)$ values for different x can be computed from the expression

$$U = \tfrac{1}{2}kx^2$$

We will take $k=50\ dy/\text{cm}$. Since the U values are symmetrical in x, it will be enough to tabulate U values for positive (or negative) x only. Working in steps of 0.2 cm each, we get

x(cm) =	0		.4	.6	.8	1.0	1.2	1.4	1.6	1.8	2.0
U (erg) =	0	1	4	9	16	25	36	49	64	81	100

Now we shall consider three cases (*i*) $E=16$ erg, (*ii*) $E=49$ erg, (*iii*) $E=100$ erg. We therefore deduce $K=E-U$: and corresponding $1/\sqrt{2K}$ values:

---

[*] Let the slope of $U(x)$ curve at (say) the left end x_A be $-\alpha$. Then we may write in the neighbourhood of x_A —

$$U(x) = E-\alpha(x-x_A)$$

$$\therefore \quad 2K = 2\alpha(x-x_A)$$

For a region x_A to x_A+e (where e is small), the integral of interest is

$$I= \int (2K)^{-1/2}dx = (2\alpha)^{-1/2} \int (x-x_A)^{1/2}\ dx$$

$$= 2\,(2\alpha)^{-1/2}\Big[(x-x_A)^{-1/2}\Big]_{x_A}^{x_A+e} = \sqrt{\frac{2e}{\alpha}}$$

Thus the integral is finite, except when α becomes zero, *i.e.*, when the potential curve becomes parallel to x-axis at $U=E$.

x (cm)	0	.2	.4	.6	.8	1.0	1.2	1.4	1.6	1.8	2.0
$1/\sqrt{2K}$ *values*											
Case (*i*)	.177	.182	.204	.267	∞						
(*ii*)	.101	.102	.105	.112	.123	.144	.196	∞			
(*iii*)	.070	.071	.072	.074	.077	.081	.089	.099	.118	.162	∞

The $1/\sqrt{2K}$ vs x curves are shown in Fig. III A(3) for a quarter cycle. To get the period, one has to multiply the area under the curve by 4 and

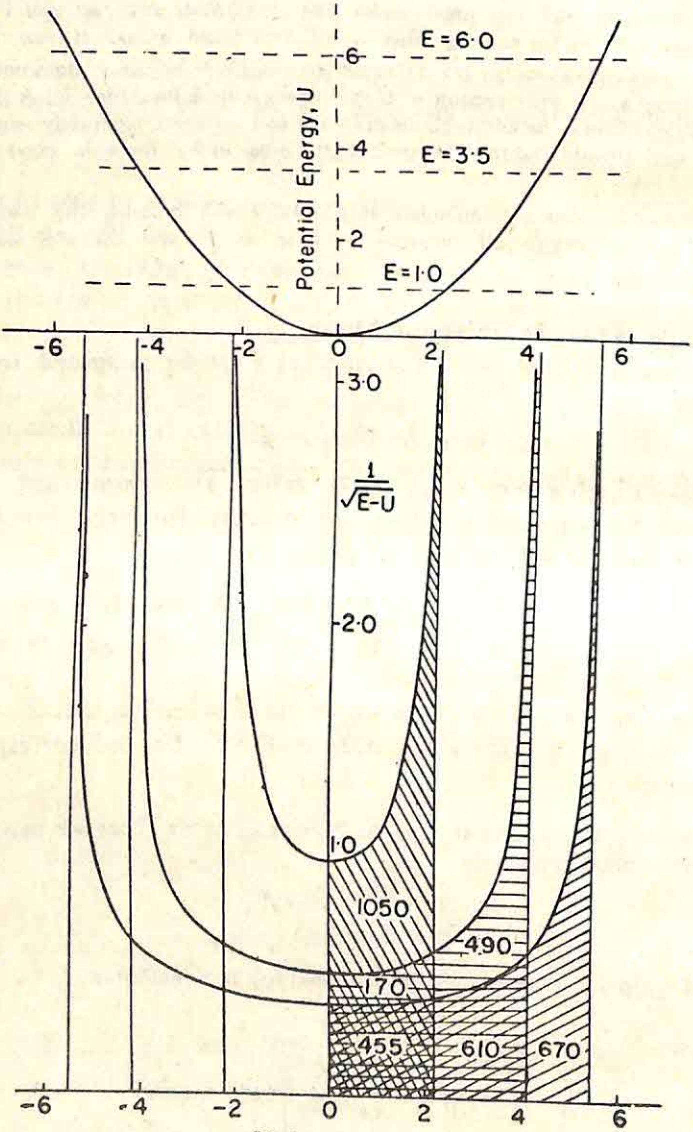

FIGURE III-A (3) $2(E-U)^{-1/2}$ versus x for a simple harmonic potential for three E values.

by $\sqrt{m}$, where m is mass of the oscillating body.

The total areas under the curve in the three cases in Fig. III-A (3) come out to be equal (within the range of error in counting the squares). This is the special feature of simple harmonic motion—the period T is independent of E.

3. Example of a General Potential Well

Figure III-A(4a) shows the case of a general type of potential well.

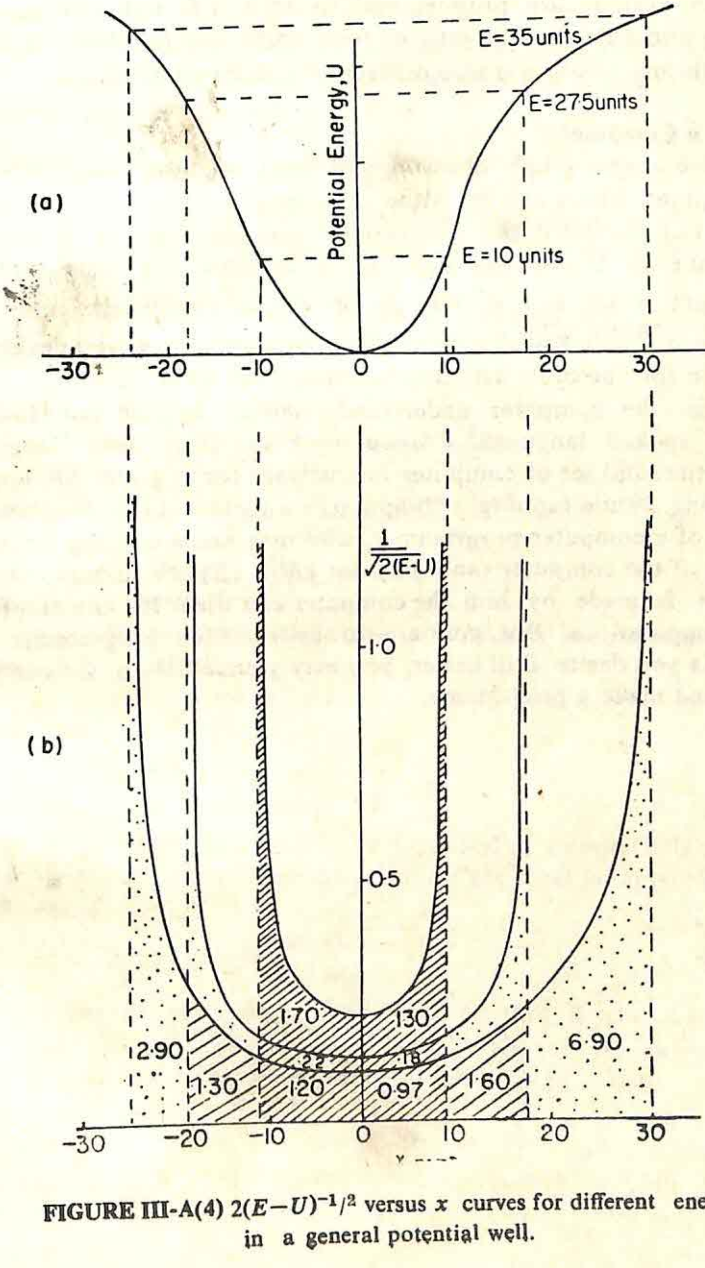

FIGURE III-A(4) $2(E-U)^{-1/2}$ versus x curves for different energies in a general potential well.

For three different energy values $E=35$, 27.5 and 10 units, we compute $E-U$ and hence $1/\sqrt{2(E-U)}$, and then plot it against x in the lower graph III-A (4b). The areas, counted in convenient segments, are shown in the figure.

The introduction of mass factor $\sqrt{m}$ would convert the 'areas' to times. Otherwise details of oscillation remain unchanged as long as E value is the same. You note that for $E=35$, 27.5 and 10 units the oscillation periods are proportional to 15.0, 7.6 and 5.8 respectively. You may also note that the ratio of time spent on the left and right of the equilibrium position is also different for different E values.

4. Using a Computer

The calculations, graph drawing and area counting can all be done by a computer. You store in it the information about U vs x; it has a memory. You then feed the instructions and the assigned E value. It will compute $E-U$ and $1/\sqrt{2(E-U)}$ at as small $\triangle x$ intervals of x as you instruct it to, and it will go on giving cumulative sum of the products $[1/\sqrt{2(E-U)}]\,\triangle x$ up to whatever stage of x you desire. The information for one cycle will also be printed out by it.

Of course, the computer understands neither English nor Hindi nor any other spoken language. Computers have their own languages. Preparing the total set of computer instructions for a given job is called programming. While running a computer is a technical job, programming is the task of a computer programmer, who may know nothing about the electronics of the computer (and may not know Physics either). Once a programme is made by him the computer can use it for any number of similar computations. But *you* are to instruct the programmer what calculations you desire. Still better, you may yourself learn the computer language and make a programme.

APPENDIX III-B

THE CONCEPT OF REDUCED MASS

Consider an isolated system of two bodies A and B in an inertial frame of reference. If the force of interaction between A and B at any time t is F, the equations of motion are

$$m_A \frac{d^2\mathbf{r}_A}{dt^2}=\mathbf{F}; \qquad m_B\frac{d^2\mathbf{r}_B}{dt^2}=-\mathbf{F} \qquad \ldots\text{III-B(1)}$$

where r_A and r_B are the position vectors of A and B respectively and m_A and m_B are their masses. We have taken care of Newton's third law in writing $-F$ in the second equation.

Let us now change the frame of reference to one fixed on the particle B. The coordinate of A is then given by

$$\mathbf{r}=\mathbf{r}_A-\mathbf{r}_B \qquad \ldots\text{III-B(2)}$$

$$\therefore \qquad m_A\frac{d^2\mathbf{r}}{dt^2}=m_A\frac{d^2\mathbf{r}_A}{dt^2}-m_A\frac{d^2\mathbf{r}_B}{dt^2}$$

$$=\mathbf{F}+\frac{m_A}{m_B}\mathbf{F}=\frac{m_A+m_B}{m_B}\mathbf{F}$$

or

$$\frac{m_A m_B}{m_A+m_B}\frac{d^2\mathbf{r}}{dt^2}=\mathbf{F} \qquad \ldots\text{III-B(3)}$$

If we change the frame of reference to one fixed on particle A, then coordinate of B is given by

$$\mathbf{r}=\mathbf{r}_B-\mathbf{r}_A$$

which again leads to

$$\frac{m_A m_B}{m_A+m_B}\frac{d^2\mathbf{r}}{dt^2}=\mathbf{F}$$

Thus the two-particle motion can be described as one-particle motion (using the other particle as reference frame) if the mass is replaced by an equivalent value.

$$m=\frac{m_A m_B}{m_A+m_B} \qquad \ldots\text{III-B(4)}$$

This is called the *reduced mass*. It is to be noted that if the interaction force between the particles is dependent on the relative displacement r alone, it is easier to deal with an equation like III-B(3) than with the two separate equations given in III-B(1).

The proof is of a general nature, irrespective of the nature of the interaction involved. The reduced mass has significance therefore for all kinds of motion where an isolated system of two particles is involved, oscillations being one class of cases.

4 STUDY OF SOME SPECIAL POTENTIALS

4.1. INTRODUCTION

You have by now learnt how an interaction can profitably be represented by a potential energy diagram. This is, in fact, the way it is always done in atomic and nuclear physics.

In the experiments of Chapters 2 and 3 the field magnets (clamped ones) were situated on the track and therefore the glider magnet could not have crossed *through* the field region. In other words, the potential energy curves had ends with $U \to \infty$. However, in a wide range of experiments in molecular, atomic, nuclear and solid state physics it is customary to fire projectiles (like protons or alpha particles or X-ray photons or neutrons) through a region of interaction and examine them as they come out of that region. There may be change in their momentum as well as energy (inelastic scattering, Chapter 5). There will also be a time-delay due to the field. Thus we collect experimental data about the interaction of projectiles with the system under examination and thence build a picture of the interaction potential from which we can deduce the internal structure and behaviour of the system under different conditions. At other times, where we have some initial idea about the interacting system, we first make a model of the potential. From it we make predictions and then use the experimental results to give final touches to the model, like determining the constants or suggesting modifications in the shape of the potential.

In this chapter you will be dealing with some special potentials which closely resemble those which are widely used as models in atomic and nuclear physics. Here the potentials will be generated with the help of magnets, whereas the actual interactions between atoms and nuclei are of different origins. So you see that the comparison will be only about the shape of the PE curve, not about the origin of the interactions. It is an experience to generate potentials of different shapes and then to see experimentally the motion of a body in or through them. Later on you can appreciate to what extent atomic systems deviate from this behaviour. The deviation of behaviour is, in fact, not due to the differences in the nature of interactions. We have stated earlier (§ 3.1, p. 42) that once the PE diagram of a system is obtained the mechanics can be discussed irrespective of what the origin of the interaction is. The deviation really occurs because at the level of atomic masses and dimensions quantum mechanics gives results which are significantly different from those given by it for macroscopic bodies* like your glider magnets. We will draw your attention to some of these differences at the appropriate places.

4.2. GENERATING REGIONS OF DIFFERENT FORMS OF POTENTIAL

Since we desire to generate regions of interaction through which a projectile may pass, the field magnets are to be mounted away from the air-track. Another consideration is to keep the magnets in pairs symmetrically about the line of the air-track so that the glider magnet (used as the projectile) may not experience torques or transverse forces, which may lead to wobbling and avoidable energy loss in friction.

Four simple geometries, with one pair of field magnets, are shown in Fig. 4.1. In cases (a) and (b) the parameter b is variable, whereas in cases (c) and (d) two parameters b and θ are variable. In each case a reversal of the polarities of the projectile produces a mirror image of the original potential. The potentials produced by them will be the subject of your study and are briefly described below:

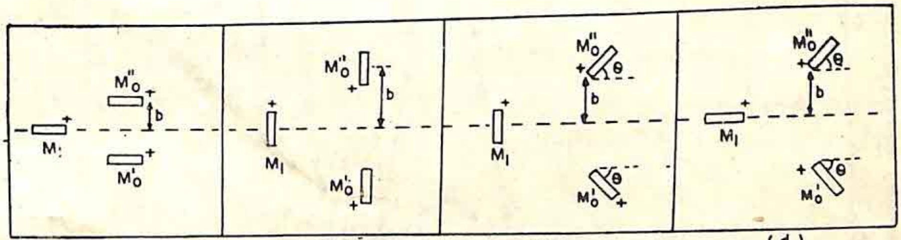

(a) (b) (c) (d)

FIGURE 4.1. Some simple geometries for field magnets (M_0' and M_0'').

(*a*) **Potential Hill with Valleys.** You get this potential when M'_0 and M_0'' are placed parallel to the track at lateral separation b each and M_1 so mounted that N poles of all the three magnets point in the same direction. When M_1 is far from the centre of M_0' and M_0'' there will be a weak attraction, but when M_1 lies in the middle of M'_0 and M_0'' there will be a strong repulsion. This means that for the $M_1+M_0'+M_0''$ system there is a large potential hill at the centre with two shallow valleys—one on each side. You may see its shape in Fig. 4.2. The details of the height and width of the potential hill, and the depth of the valleys on the two sides evidently depend on the strength of the magnets, their lengths and the lateral separation of M_0' and M_0''.

---

*For macroscopic bodies the results of quantum mechanics approximate to those of classical mechanics.

Such potentials are of special interest because they are approximately the kind of potentials used for interaction between two molecules or two atoms or two nucleons. The side dips represent the initial (weak) attraction between the particles and the potential hill corresponds to the strong repulsion when the particles are close together. The width of the hill corresponds in a way to the particle diameter. There are differences of detail—as should always be expected in such comparison. The PE curve of Fig. 4.2 is therefore only a model to illustrate how the same system can exhibit attractive as well as repulsive interaction.

(*b*) **Potential Well with side Hills.** If the polarity of magnet M_1 in the arrangement of Fig. 4.2 (a) is reversed the regions of attraction and repulsion are just interchanged, the magnitudes remaining the same. Therefore the potential now can be obtained simply by turning Fig. 4.2 upside-down about the $U=0$ axis. You now get a potential well in the centre with a hump on either side as shown in Fig. 4.3. Unlike the potential energy curves studied in the experiments on Chapter 2 this potential well is not bounded by walls of infinite height.

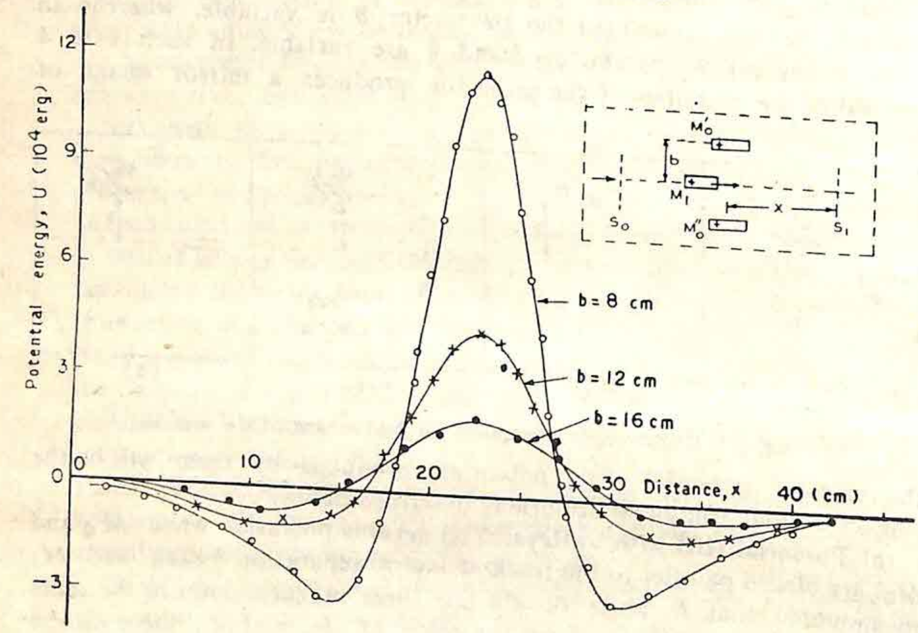

FIGURE 4.2. A potential hill with a valley on each side.

The reasons for interest in studying this kind of potential well (with side humps) is again that such potentials are used in nuclear models. For example the interaction between any charged nuclear particle and a nucleus is represented by such a potential.

A special feature of this potential is that in the energy range 0 to P the particle can be 'inside' the well, even when its energy is positive. In Newtonian mechanics a particle with such energy, if initially inside the well, will never escape. But quantum mechanics gives the result that such a particle has a chance of escaping. The present theory of emission of alpha particles by nucleus uses such a potential, and fits the experimental data quantitatively. Of course, your magnet will not escape—even if it is in this energy range—because for bodies with large mass and potential barriers of large width* quantum mechanics gives nearly zero probability or such escape.

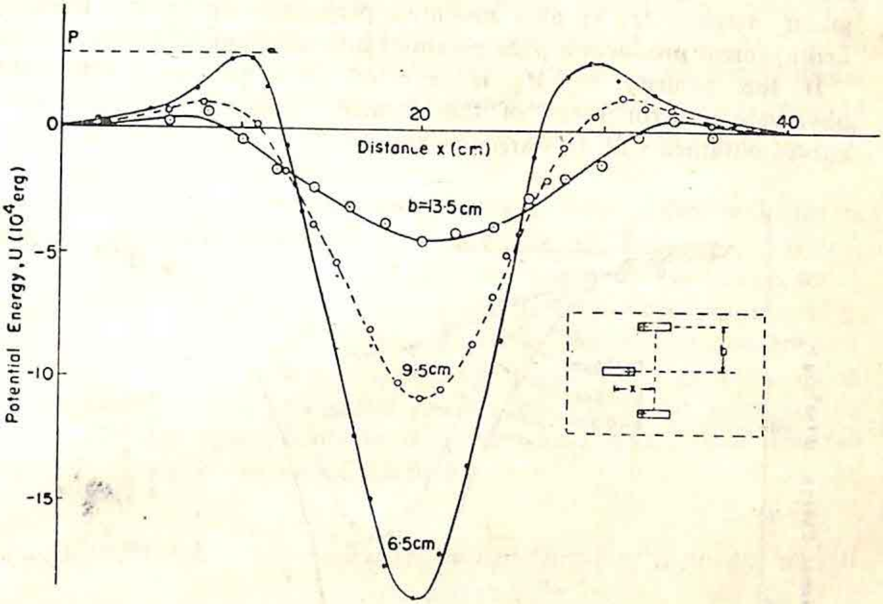

FIGURE 4.3. A potential well with a hill on each side.

(*c*) **Simple-Potential Hill or Well.** One can also generate a pure potential hill without side valleys or pure potential well without side hills.

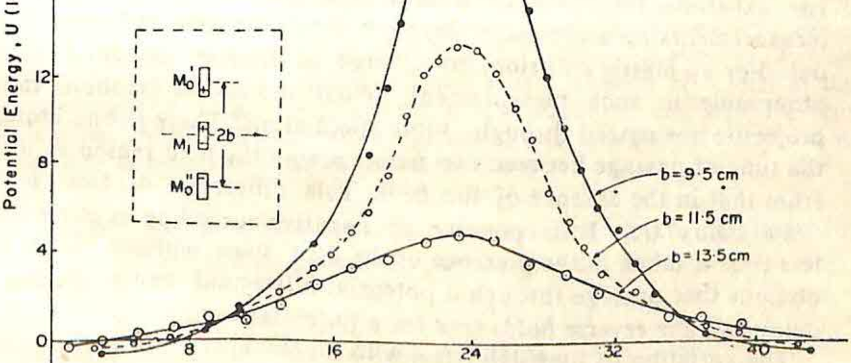

FIGURE 4.4. Simple potential hills.

---

* See footnote on p. 44 § 2 of Chap. 3

In the arrangement shown in Fig. 4.1(b) two fixed magnets M_0' and M_0'' are mounted perpendicular to the track at equal distances from it. The glider magnet M_1 is also mounted perpendicular to the track. The arrangement produces a pure potential hill, as shown in Fig. 4.4.

If the polarity of M_1 is reversed, you get a pure potential well obviously a mirror image of the former. Figure 4.5 shows some PE curves obtained with this arrangement.

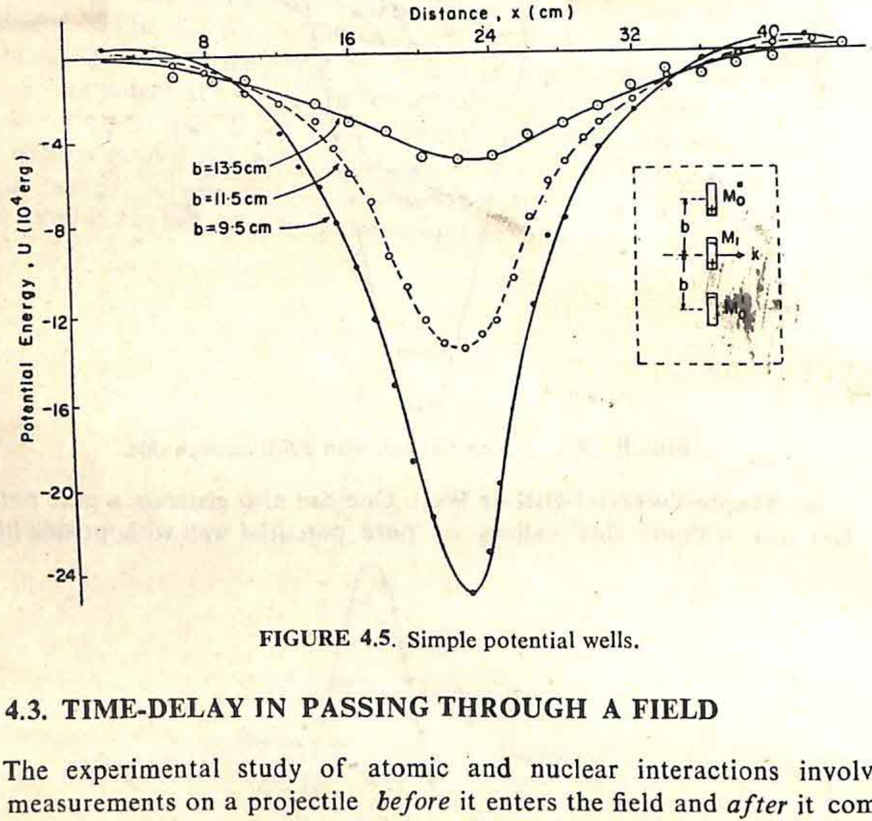

FIGURE 4.5. Simple potential wells.

4.3. TIME-DELAY IN PASSING THROUGH A FIELD

The experimental study of atomic and nuclear interactions involves measurements on a projectile *before* it enters the field and *after* it comes out. For an elastic collision, no change of kinetic energy is therefore observable in such measurement. What indication is there that the projectile has passed through some field at all? There *is* one indication: the time of passage between two points across the field region is different from that in the absence of the field. This difference of time is called '*time delay*' (t_d). It is positive or negative according as more time or less time is taken in the presence of the field than without it. It will be obvious that passage through a potential *hill* would cause *positive* time delay and the reverse holds true for a potential well.

The variation of time delay (t_d) with kinetic energy E of the projectile depends on the nature of the potential energy curve.* It will thus be clear that measurement of t_d vs E data is helpful in deducing the shape of the interaction potential. What is *not* obvious is that if two potentials are superposed, the time delays due to the two are not just additive. In other words, if t_d vs E curves for potentials A and B are separately given, you can add t_d (A) and t_d (B) only if the two fields are entirely separate in space. If they have even partial overlapping the resultant t_d vs E curve could be of very different shape.

---

* For details and snags, *see* Appendix IV-A.

Appendix IV-A shows how t_d vs E data may be used to deduce the forms of potential. But the discussion must be taken with many reservations. Firstly, in atomic and molecular physics, the Newtonian mechanics, which we have used in this Appendix, is not of sufficient validity. And, secondly, time-delays in atomic systems are measured indirectly through phase delays.* Therefore you should remember that by the experiments on time delay with macroscopic bodies you get only the broad concepts on how measurement totally outside the interaction region can lead to information about the nature of the field.

EXPERIMENT 4-A *To study the shape of a potential hill with side wells.*

Set up the arrangement shown in the inset of Fig. 4.2. In repeated trials release the glider M_1 from a fixed separation a from M_0 (not shown) and measure the velocity of M_1 at various distances x from the middle of M_0' and M_0''. You may use a point far from M_0 as well as M_0' and M_0'' as the zero reference level for U and the change in kinetic energy K relative to this position would then give you $-\triangle U$ and hence U at different x values.

Alternatively, you may release M_1 carefully from almost the middle of M_0' and M_0''. It will start off on its own either way, and you may therefore have to leave it just a bit to the left or right of the mid-point whichever way you are placing the sensor to measure the kinetic energy K of the glider M_1. Then $-K$ gives the potential energy U at the corresponding x position. This U is with reference zero level at the middle of M_0' and M_0''. After drawing the U vs x graph you can shift the zero reference to the U value at $x \to \infty$. (In this procedure magnet M_0 is not essential; it only takes care to protect M_1 from striking at the ends).

The graphs for U vs x for a set of typical experiments are shown in Fig. 4.2. From this you may measure (*i*) height of the potential hill,

---

* A notable example is that of light passing through matter. An interference experiment can measure phase delays of the order of π. For light of $\lambda = 6000$ A the time period is $\sim 1 \times 10^{-15}$ sec, so a phase delay π amounts to time delay $\sim 10^{-15}$ sec. Thin layers of glass or mica or pressure differences in gas cells would cause such phase delays, which are measured and interpreted

(*ii*) the full width at half height of the hill, and (*iii*) the depths of the valleys on either side.

You may also deduce from the U vs x curve the force F vs x curve, using $F = -dU/dx$. Figure 4.6 shows a typical result. However, since you have data on U at intervals of (say) 1 cm each, you may as well deduce F from the data and plot F vs x, without using the U vs x curve. Note the difference it makes in the scatter of F data. Why does it occur?

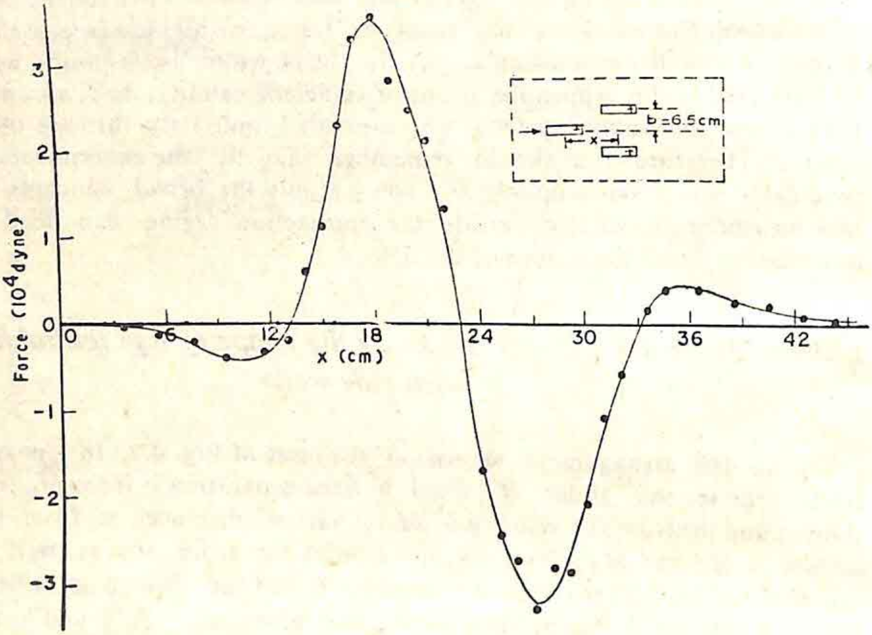

FIGURE 4.6. The force F vs x curve corresponding to the potential energy curve of Fig. 4.2.

RELATED EXPERIMENTS

EXPERIMENT 4-A (*i*)

With the same set up you may use a different spacer to fire M_1 or a different firing magnet M_0 and repeat the experiment. Check if the *PE* curve which you get is independent of these.

EXPERIMENT 4-A (*ii*)

With the same set up you may use a double timer, one measuring the kinetic energy of the glider M_1 at a fixed position and the other at a variable x position. Now you need not take care to keep a the same in repeated firing;* from the difference of K you get the U vs x data uniquely.

* In fact you may even dispense with the firing magnet M_0 and set M_1 in motion by a push of your hand.

EXPERIMENT 4-A (iii)

Take another rider with a brass load and hook it up to M_1 to increase the mass. Repeat the experiment. See if the PE curve comes out to be the same as before.

EXPERIMENT 4-A (iv)

Change the sideways separation b of M_0' and M_0'' (*see* inset, Fig. 4.2) in 4 or 5 steps of (say) 2 cm each. Repeat the Experiment 4-A. Deduce general conclusions about the variations with b in the hill height, full width at half-height and the ratio of hill height to valley depth.

EXPERIMENT 4-B *To study the shape of a potential well with shoulders.*

The arrangement for this is the same as for Experiment 4-A, except that the polarity of M_1 (and hence of M_0, if used) is reversed. The experiment is also to be done in the same way as Experiment 4-A.* The results of a typical experiment are presented in Fig. 4·3. Measure the well depth and width, and also the shoulder heights.

If Experiment 4-B is done with the same magnets and separation as 4-A the potential energy curve should come out to be the mirror reflection of Fig. 4.2. Check if your results show this.

EXPERIMENT 4·C *To study a simple potential hill or well.*

Repeat experiment 4-A (or 4-B) with the arrangement of inset of Fig. 4.4, where the magnets are placed perpendicular to the air track. You may use a firing magnet M_0 at one end, placed parallel to M_1 and in repulsive mode with it.**

Obtain several potential hills (or wells) by varying the separation b of the magnets M_0' and M_0'' from the air track. Obtain one plot to show how the potential hill height (or well depth) U_{max} changes with b, and another plot to show how the half-width of the hill (or well) changes with b.

Further experiments like 4-A (*i*) to 4-A (*iii*) may also be done with this arrangement.

Figures 4.4 and 4.5 show the typical U vs x curves for three different b values. The U_{max} vs b and half width vs b curves are not shown.

You may also obtain the force F vs α curves for this arrangement as in Experiment 4-A (Fig. 4.6), and note the differences.

---

* The alternative procedure stated with Experiment 4-A is, however, not applicable here

** For the 'hill' experiment you may also use the alternative method as suggested under Experiment 4-A.

EXPERIMENT 4-D *To study the oscillations in a potential well with shoulder hills.*

This experiment may be done in the same way as Experiment 3-A to find the oscillation frequency ν for different energy values E. Figure 4.7 shows a typical set of results. Frequency of oscillation *decreases* as energy increases. You may compare this ν vs E curve with that obtained in Experiment 3-C and note that the departure from harmonic character is of an opposite kind. Here ν decreases as E increases. Further if you increases the energy in this case a limit comes when the glider M_1 flies off, rather than oscillate. Just near this energy value the decrease in frequency with increasing E becomes quite rapid.

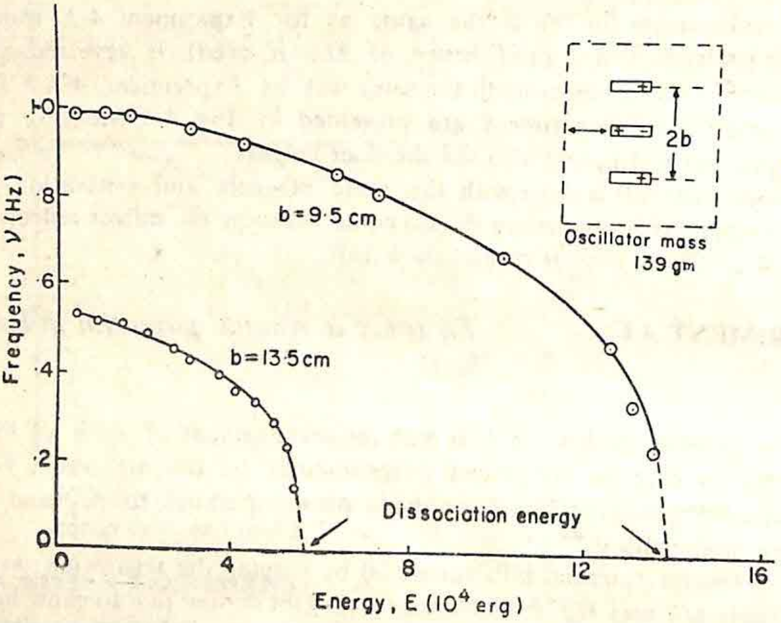

FIGURE 4.7. ν vs. E curves for oscillations in the potential well of Fig. 4.3.

EXPERIMENT 4-E *Study of oscillations in a simple potential well.*

This experiment may be done in the same way as Experiment 4-D, but with the arrangement shown in the inset of Fig. 4.8, which corresponds to the potential shape of Fig. 4.5. The typical ν vs E curve (Fig. 4.8) shows that the frequency falls as the energy increases, tending to zero at a limiting energy.

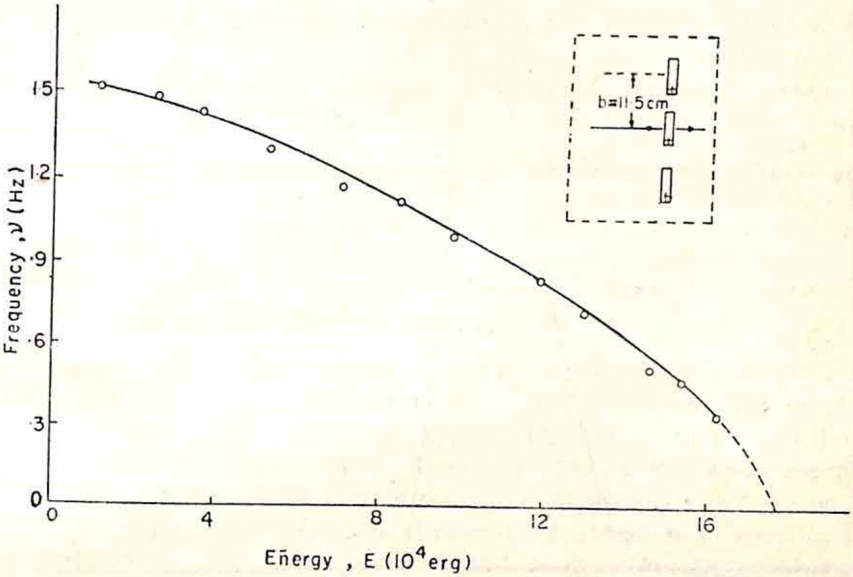

FIGURE 4.8. ν vs. E curves for oscillations in the potential well of Fig. 4.5.

The ν vs E curves of Experiments 3-C, 4-D and 4-E are of different character and the explanation lies in the corresponding PE curves. Newtonian mechanics shows that in a potential well of parabolic shape ν does not change with E; if the shape narrows down at higher E values, ν increases; and if the shape widens out at higher E values, ν decreases. Experiment 3-C corresponds to one kind of departure from the parabolic potential, Experiments 4-D and 4-E correspond to the opposite kind of departure.

There is also a difference between the ν vs E curves of Experiments 4-D and 4-E. In the first case the fall of ν is slow at first and major part of the fall occurs in a narrow range of E near the top. In the second case the fall of ν with increasing E is distributed over a wide range of E. You may explain them by looking at the corresponding PE curves.

EXPERIMENT 4-F *To generate some other potential shapes and study oscillations in them.*

Arrange the field magnets M_0' and M_0'' in the geometry shown in the inset of Fig. 4.9. Study the PE curve for a glider M_1 interacting with the field of these magnets. Figure 4.9 shows a typical result.

What is important about this potential curve is that its right half is so close in shape to the famous Lennard-Jones (L-J) potential used in molecular physics. (Compared with the right half of Fig. 4.2, the hill part is much steeper here, and hence the valley shape has very large slope on one side and quite a gradual one on the other, as it is in the L-J potential).

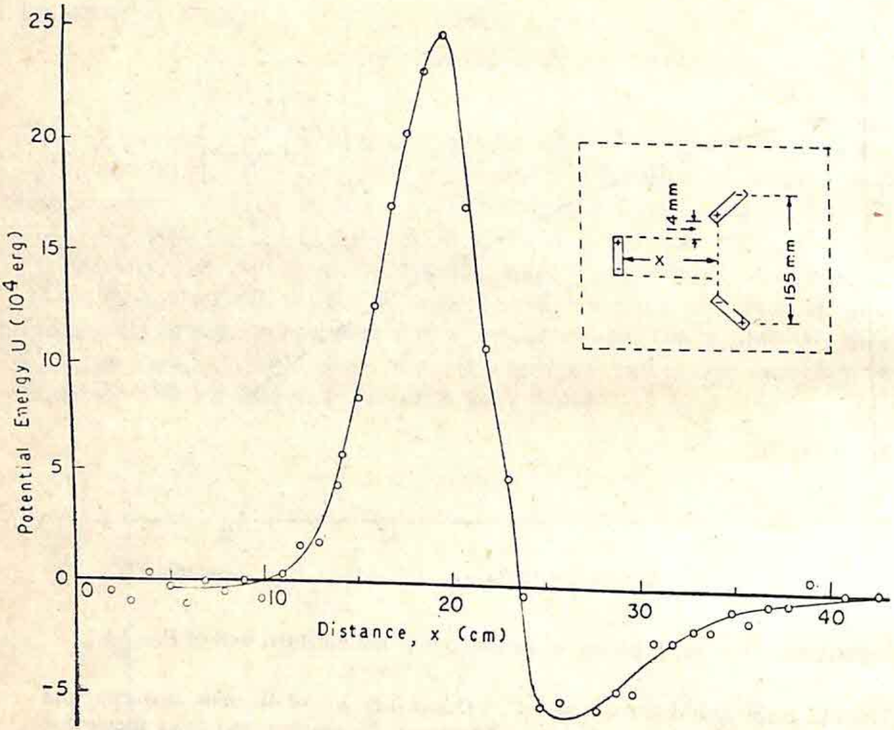

FIGURE 4.9. A potential hill with a single valley on one side only.

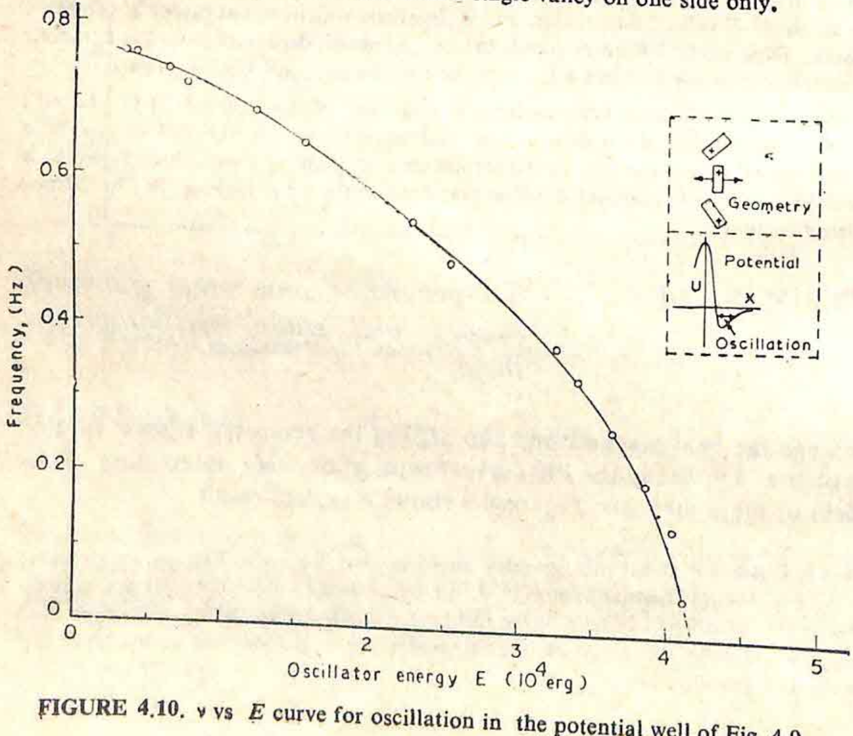

FIGURE 4.10. ν vs E curve for oscillation in the potential well of Fig. 4.9.

You may now study the oscillations in the potential valley of Fig. 4.9. The ν vs E curve now should be much nearer to what is observed in the vibrational spectra of diatomic molecules. Fig. 4.10 shows the results of a typical experiment.

In diatomic molecules as the vibration energy reaches a limit the molecule dissociates; *i.e.*, one part flies off from the rest. This limiting energy is called *dissociation energy* of the molecule. Not only this. The quantum mechanically *allowed* energy levels come closer and closer together as the oscillation energy increases. Since $h\nu$ in quantum mechanics refers to energy gaps, we may see ν tending to zero as the dissociation stage is approached. Figure 4.10 is thus a good parallel.

Arrange a chain of magnets as shown in the inset of Fig. 4.11 and study the potential energy curve for a glider in the field of these magnets. Figure 4.11 shows a typical PE curve, which is a broad potential hill with several small valleys and hills on its top. Depending upon the number of magnet-pairs and their spacing you can alter the total width, the height and valley depths. Oscillations in a valley in this potential have one character: when the energy of oscillation crosses a limit, the glider would escape with energy much larger than the energy of oscillation.

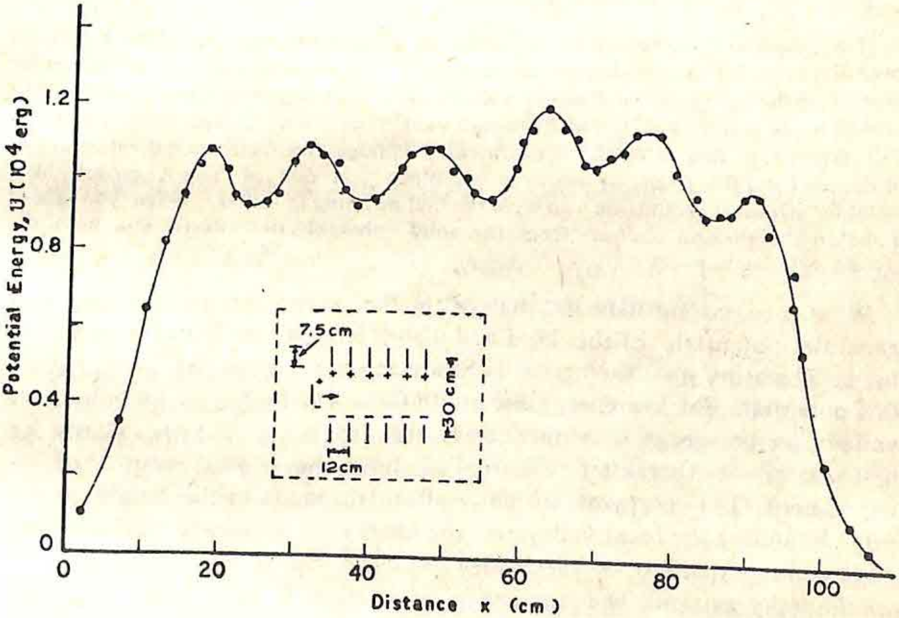

FIGURE 4.11. A potential hill with several small valleys or hills on its top.

Reverse the glider polarity relative to the last case and obtain the PE curve. Figure 4.12 shows the result of a typical experiment with 5 pairs of field magnets. This is a broad potential well with periodic valleys and hills inside it.

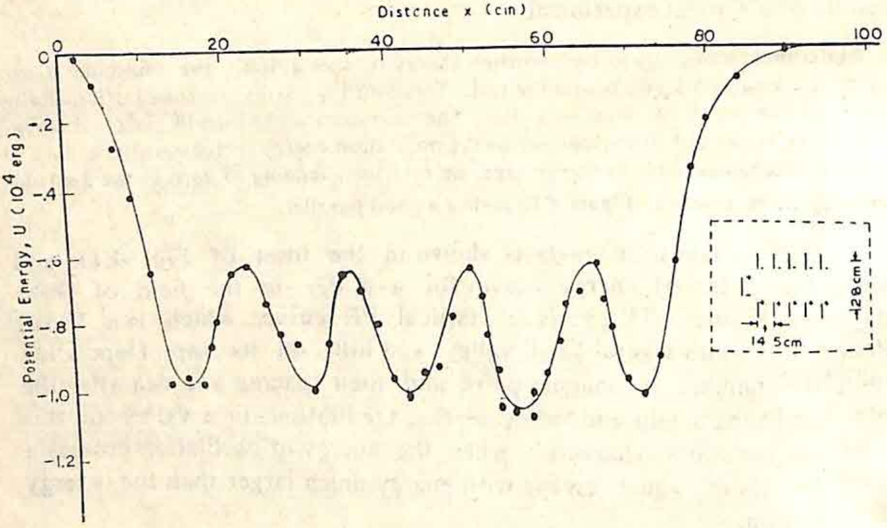

FIGURE 4.12. A potential well with several smaller hills and valleys inside it.

This potential energy curve has a parallel in solid state physics, where a periodic potential exists for electron-lattice interaction.* The electron may be bound to an atom (oscillating in the individual valleys of Fig. 4.12), or it may be free to move around in the entire solid (the wider overall valley), or it may escape from the solid. The expression 'free electron' has now two meanings: free from the individual atoms of the solid and free from the entire solid. When you talk of 'free electrons' in a metal for electrical conduction you have the first meaning in mind. When you talk of a photon liberating an electron from the solid (photoelectric effect), you have the second meaning in mind.

What is important here is that with the magnetic dipoles you can generate potentials of this kind and also study the motion of a glider in them. The story goes farther still. Study the oscillations of a glider in this potential. For low energy the oscillations are limited to an individual valley. As the energy E is increased, the frequency ν falls, slowly at first and rapidly thereafter. Figure 4.13 shows the typical results of an experiment. The energy at which $\nu \to 0$ corresponds to the height of the ridge bounding the local valley. As the energy is increased further, the oscillations extend over the wider well and it is an interesting sight to see the jerky motion. The frequency now starts from a low value, increases as E increases, but later on again starts falling off as E approaches the top of the potential well.

---

* In solids the periodic 'valleys' are much deeper compared with the average depth. You can get nearer to that in your experiment by increasing the longitudinal separation of magnets (say, from 14.5 cm to 30 cm).

Figure 4.13 is like a 'dispersion curve'. In this experiment you *know* why all these changes are occurring. But imagine a solid state physicist just getting experimentally *a* ν vs E curve with ν dipping to zero at some energy E_1 (Fig. 4.13) and again rising, but upto a much lower value than before. Then he must apply logic and imagination (*i.e.*, try some models) to understand why such behaviour may occur.

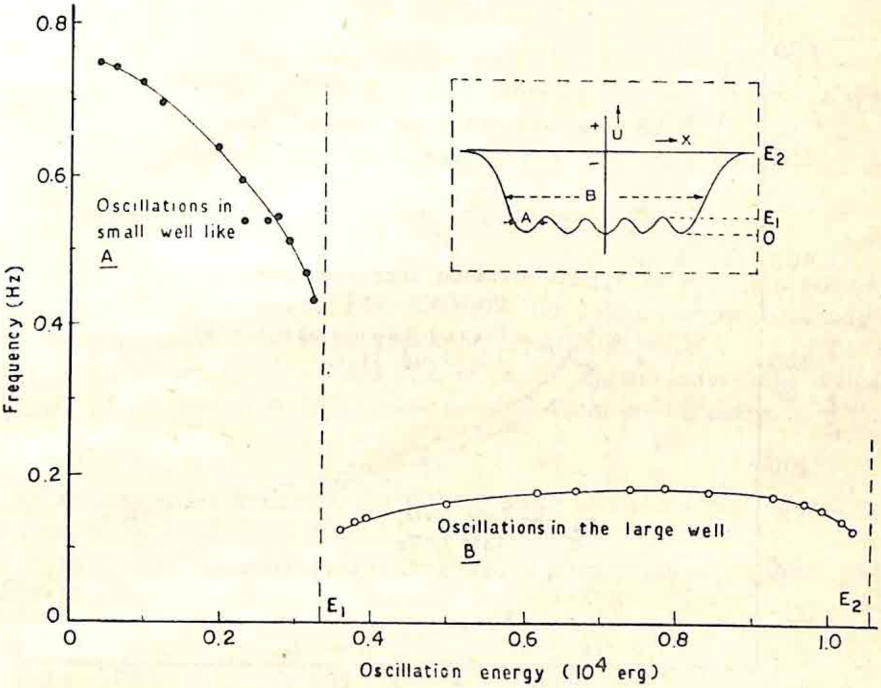

FIGURE 4.13. ν vs. E curve for oscillations in the potential well of Fig. 4.12.

EXPERIMENT 4-G *To study time-delay in passing through a potential hill.*

Set up the arrangement for a potential hill, as shown in the inset in Fig. 4.14. Set the sensors S_1 and S_2 far enough from M_0', M_0'' and M_0 so that the sensors are in field-free space. In the double timer, use one timer in $\rfloor\overline{A}\llcorner$ mode to determine the projectile energy E at S_1 and the other in $\rfloor\overline{A}\ \rfloor\overline{B}$ mode to determine the time of travel t across distance $S_1 S_2$. Plot a graph between t and E.

Now remove the field magnets M_0' and M_0'' and repeat the whole experiment, keeping S_1 and S_2 *positions unchanged*. The travel time for $S_1 S_2$ distance may be called t_0 now. Plot a graph between t_0 and E. From the two graphs deduce $t-t_0=t_d$ (the time delay) for different E values.

Figure 4.14 shows the data for an actual case. You note that t_d increases as E decreases and tends to infinity as E approaches a certain value. Theory (Appendix IV-A) would show that this E value is the height U_0 of the potential barrier. (Of course, for $E<U_0$ the projectile would not reach sensor S_2 at all.)

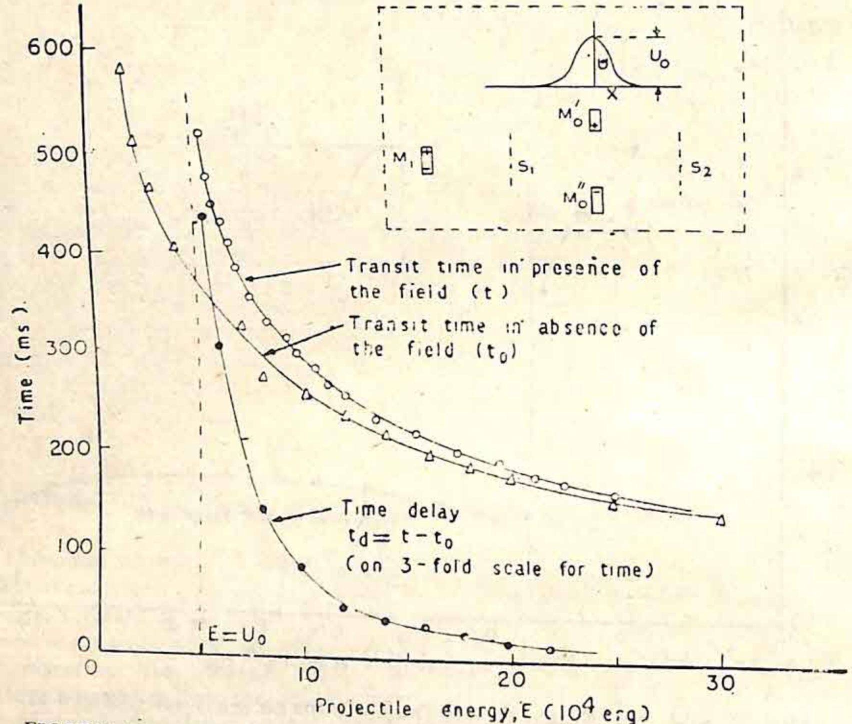

FIGURE 4.14. Variation of time delay *vs.* kinetic energy for a projectile passing through a potential hill region.

RELATED EXPERIMENTS

EXPERIMENT 4-G(i)

Change the positions of sensors S_1 and S_2 (Fig. 4.14) such that they are still away from the fields of M_0 as well $M_0'+M_0''$. Repeat the Experiment 4-G. See if t_d vs E relationship is independent of the sensor positions.

NOTE. t_0 and t individually would, of course, depend on S_1 S_2 separation; but t_d should not.

EXPERIMENT 4·G(ii)

Repeat the experiment with glider M_1 loaded to change its mass, but keeping the arrangement unchanged otherwise. See how the t_d vs E curve changes with m. Check if t_d changes by a constant factor at all E values; if so, guess the relation of this factor to the change in mass (*see* Appendix IV-A).

EXPERIMENT 4-G (iii)

You may do the same experiment with any other potential involving a hill, like those of Figs. 4.2, 4.9 and 4.11. (The last one may be good to get large time delay).

EXPERIMENT 4-G(iv)

You may repeat Experiment 4-G, keeping the potential hill low (by increasing M_0' M_0'' separation), and working in the energy range $E \gg U_{max}$. Plot a graph between the observed t_d and $E^{-3/2}$.

Appendix IV-A shows that for $E \gg U_0$ the time delay is given by

$$t_d \approx \frac{1}{2}\sqrt{\frac{m}{2}}\cdot(U_0\, b)E^{-3/2} = \tfrac{1}{2}\sqrt{\frac{m}{2}}\left[\int U\, db\right]E^{-3/2}$$

At large E values t_d becomes small and therefore errors may not remain insignificant. But it is good to see how far your experiment may approach the condition for which this approximation is valid.

From an estimate of the slope of t_d vs $E^{-3/2}$ curve deduce the value $\int U\, db$ and compare it with the value deduced from the PE curve.

EXERCISE 4-G(i)

In the experimental t_d vs E curve the F value at $t_d \to \infty$ gives the peak height U_0 of the potential hill.

If the actual potential hill is replaced by a rectangular potential hill of height U_0 and width b,

$$t_d = \sqrt{\frac{m}{2}}\cdot b\left[\frac{1}{\sqrt{E-U_0}} - \frac{1}{\sqrt{E}}\right]$$

(*see* Appendix IV-A for details). From your data compute b and compare this rectangular potential shape with the experimental one (Experiment 4-C) for the same system.

From the U_0 and b values deduced above, now deduce a complete t_d (calculated) vs E curve. Notice the departures and qualitatively suggest what changes in potential shapes would explain them.

Do not feel bothered if no single suggestion explains even qualitatively the departures in different regions of E. A given model leads to a unique prediction about the result; but a given result may follow from several different models. That is why scientific research is a continuing process.

EXERCISE 4-G (ii)

Using the *experimental* U vs x curve for the same system (Experiment 4-C) deduce the theoretical time-delays for two or three E values. Compare them with the experimental values.

In Exercise 4-G (*i*) you were trying a 'fit' of t_d vs E data with a model—the rectangular PE barrier. Here you are trying a 'fit' of observed t_d vs E data with the expectations from the *experimental* PE barrier, so as to see the validity of Newtonian mechanics. Why is an Exercise like 4-G(ii) not feasible in atomic interactions?

EXPERIMENT 4-H *To study time-delay in passing through a simple potential well.*

The experimental details are the same as for Experiment 4-G. Only, the polarities of both M_0 and M_1 have to be reversed. One practical difference is that much smaller glider energies are needed in this case.

Figure 4.15 gives the typical data of t_o vs E, t vs E and $t-t_o=t_d$ vs E. Examine the curves closely. Firstly, you note that t_d is negative. It means that presence of this potential makes the projectile go faster than without the field. Secondly, as E becomes smaller, the magnitude of t_d becomes larger, tending to infinity as $E\to0$.

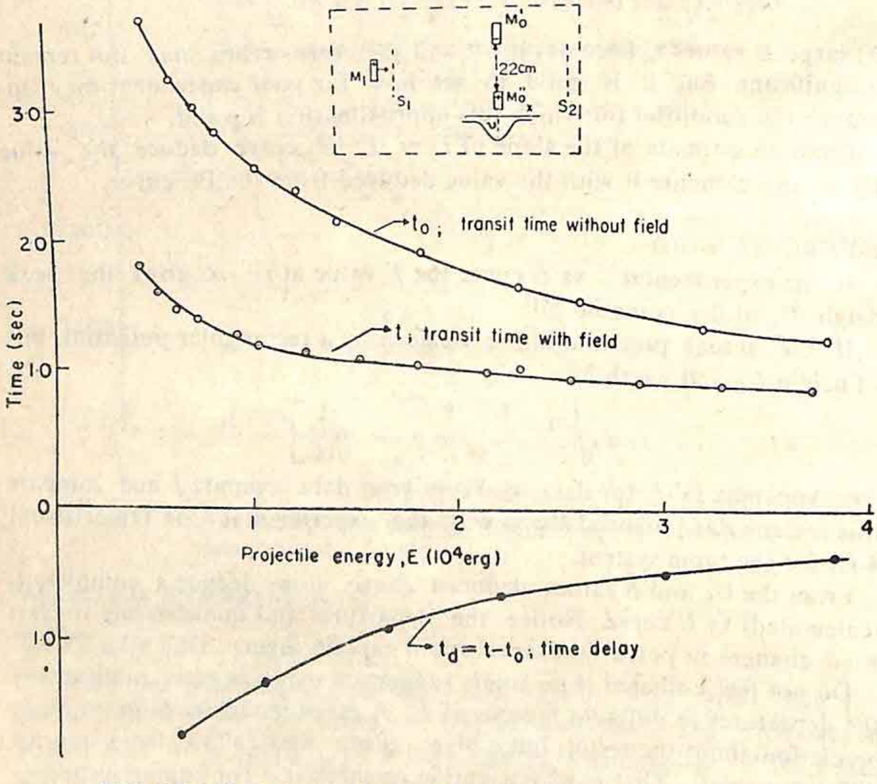

FIGURE 4.15 Variation of time delay with kinetic energy for a projectile passing through a potential well region.

RELATED EXPERIMENTS

EXPERIMENTS 4-H (i) and (ii)

Check the effects of changing the sensor positions, and glider mass on the t_d vs E curve, as in Experiments 4-G(*i*) and (*ii*) respectively.

EXERCISES 4-H(i) and 4-H(ii)

These may be done exactly as Exercises 4-G (*ii*) and (*iii*) respectively, using the potential well as shown in the inset of Fig. (4.15).

EXPERIMENT 4-H(iii)

Consider a rectangular potential well of width b and depth U_0. The experimental t_d vs E curve gives no clue for U_0 as it did in Experiment 4-G. Therefore use t_d values at one pair of E (say E_1 and E_2) to deduce a pair of U_0 and b values, as explained in Appendix IV-A. That describes the rectangular potential well fitting into the observed t_d *at the chosen pair of E values.*

You will notice, however, that for different pairs of E_1 and E_2, you do *not* get identical U_0, b pairs. It only means that the rectangular—well model needs refinement. That is how a theoretical physicist collaborates with the experimental physicist. Model, predictions, observed deviations, improved model, revised predictions, finer observations, further improved model, and so on! Sometimes the whole structure of the model breaks down and we have to start afresh—the final test is of experiment alone. Science is experiment. No model which does not bear the scrutiny of experiment can survive.

APPENDIX IV-A

DEDUCTION OF POTENTIAL PARAMETERS FROM TIME-DELAY

1. The Basic Equation

In Chapter 2 we have shown how the travel time of a body may be computed from a knowledge of its total energy and the potential energy diagram. Equation (2.8) may be put as

$$t = \sqrt{\frac{m}{2}} \int_1^2 \frac{1}{\sqrt{E-U}}\, dx$$

where m is mass of the body, E its total energy, U is the potential energy as a function of x, and t is the time of travel between two locations 1 and 2. If t_o is the time of passage over the same region in the absence of the field ($U=0$), we get

$$t_0 = \sqrt{\frac{m}{2}} \int_1^2 \frac{1}{\sqrt{E}}\, dx$$

Hence time-delay is given by

$$t_d = t - t_o = \sqrt{\frac{m}{2}} \int_1^2 \left[\frac{1}{\sqrt{E-U}} - \frac{1}{\sqrt{E}}\right] dx \quad \ldots \text{IV-A(1)}$$

For a given form of the potential U, the time delay thus depends on the initial kinetic energy $K_o = E$ of the projectile.

2. Case of a Rectangular Potential Hill or Well

Consider a rectangular potential hill of height U_0 and width b

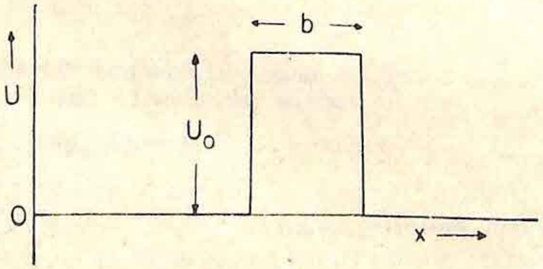

FIGURE IV-A (1) A rectangular potential barrier.

[Fig. IV-A(1)]. The potential is uniquely defined by these two parameters only.

Since $U = U_0$ throughout the width b, Equation IV-A(1) gives

$$t_d = \sqrt{\frac{m}{2}}\left[\frac{1}{\sqrt{E-U_0}} - \frac{1}{\sqrt{E}}\right] b \qquad \ldots \text{IV-A(2)}$$

From the t_d vs E data we may now choose any pair of E values with corresponding experimental t_d values, so that two constants U_0 and b can, *in principle*, be uniquely determined from the observations.

The same procedure will apply for a potential well of rectangular shape.

If the experimental t_d vs E data are collected for a rectangular potential well or hill, then the computed U_0 and b values should be independent of what pair of E (and corresponding t_d) was chosen for the computation. You may think of the converse that if all pairs of observed t_d and E values substituted in Equation IV-A(2) lead to the same values of U_0 and b the potential may be of the rectangular shape defined by U_0 and b. This converse, however, may not hold, as you will see later (§ 5).

3. An Actual Potential Hill or Well

For simplicity of mathematical treatment any real unknown potential may, in general, be approximated to a rectangular hill or well. Figures IV-A (2a and 2b) show that no unique approximation may be satisfactory. In such cases the values of U_0 and b deduced from Equation IV-A(2) will be found to vary with the pair of E and t_d values used in their deduction.

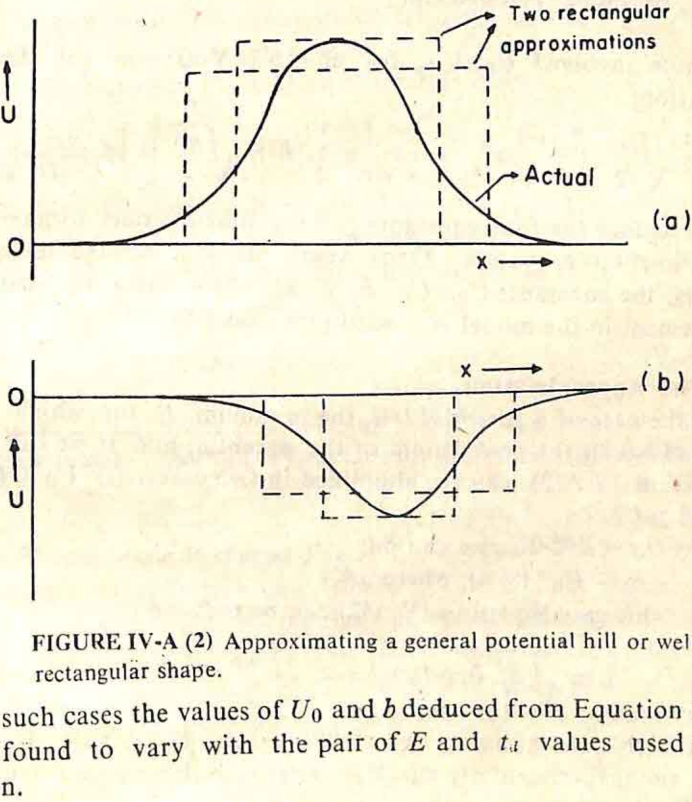

FIGURE IV-A (2) Approximating a general potential hill or well to a rectangular shape.

For a potential *hill* there is one special feature. The experimental t_d vs E curve would show $t_d \to \infty$ at a lower limit for E, which therefore gives you an upper limit for U_0. Then one deduces the corresponding b by using t_d for any one value of E in Equation IV-A(2). This b, for an actual potential hill, will be found to vary with E—indicating that the actual hill is different from the rectangular shape.

A refinement of the model may proceed as explained below for a potential hill. We approximate the actual potential to a two-step rectangular shape. [Fig. IV-A (3)]. Assuming symmetrical form, four constants are now involved U_0, U'_0, b'_0. and b'_0 You now get the time-delay equation:

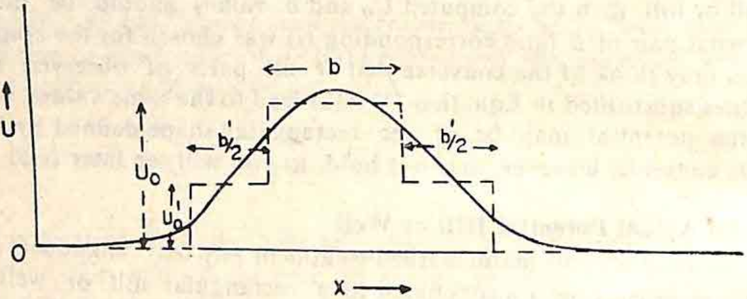

FIGURE IV-A (3) Approximating an actual potential hill to a two-step rectangular potential hill.

$$t_d = \sqrt{\frac{m}{2}}\left[\frac{1}{\sqrt{E-U_0}} - \frac{1}{\sqrt{E}}\right] b + \sqrt{\frac{m}{2}}\left[\frac{1}{\sqrt{E-U}} - \frac{1}{\sqrt{E}}\right] b'_0$$

To deduce the four constants you use four E values with corresponding experimental t_d values. Once again, as you change the quartet of E values, the constants U_0, U_0', b, b' change—indicating that a further refinement in the model is needed (see also § 5).

4. Two Approximations

In the case of a *potential hill*, the minimum E for which t_d data can be had equals the peak height of the potential hill. If we call it U_0 then Equation IV-A(2) can be simplified in two cases: (*i*) $U_0 < E \ll 2U_0$; and (*ii*) $E \gg U_0$.

For $U_0 < E \ll 2U_0$ we can put

$$E = U_0\,(1+\alpha), \text{ where } \alpha \ll 1$$

For this case Equation IV-A(3) can be reduced to

$$t_d \approx \sqrt{\frac{m}{2}}.\, b\,(\alpha U_0)^{-1/2} \approx \sqrt{\frac{m}{2}}.\, b\,(E-U_0)^{-1/2} \qquad \ldots\text{IV-A(3)}$$

Thus in this energy range one would expect t_d to vary as $(E-U)^{-1/2}$. You may experimentally check it. Alternatively you may take several E

values in the neighbourhood of U_0 and deduce b values from this equation. The variation of b will show the extent of departure of the *actual* potential from the rectangular *model*.

For $E \gg U_0$. For this case Equation IV-A (2) gives

$$t_d = \frac{1}{2}\sqrt{\frac{m}{2}}\,(U_0 b)\,E^{-3/2} \qquad \ldots\text{IV-A(4)}$$

Thus for large E values the time-delay varies as $E^{-3/2}$. Since the product $U_0 b$ comes out now as a single constant, you may see that the observed t_d for a given E does not give U_0 and b separately. In effect this means that what you get as $U_0\, b$ is $\Sigma\, U_i\, b_i$ for a multistep potential or $\int U\, db$ (area under the U vs b curve) for a smooth curve. Data at large E will therefore not distinguish between different potential shapes with same area. (If U_0 is determined from $t_d \rightarrow \infty$ at $E = U_0$, you would get a unique b so far as data in the range $E \gg U_0$ are concerned). It means that only the data at E near U_0 will tell you how far the actual potential departs from the rectangular model.

In the case of a *potential well* U is negative. If U_0 is the *magnitude* of this depth, Equation IV-A(2) becomes

$$t_d = \sqrt{\frac{m}{2}}\left[\frac{1}{\sqrt{E+U_0}} - \frac{1}{\sqrt{E}}\right]b \qquad \ldots\text{IV-A(5)}$$

The two cases of interest in this situation are (*i*) $E \ll U_0$, where we may put $E = \alpha U_0$, where $\alpha \ll 1$; (*ii*) when $E \gg U_0$.

For $E = \alpha U_0$, $\alpha \ll 1$. Equation IV-A(5) gives for this case

$$t_d = -\sqrt{\frac{m}{2}}\cdot b\left[E^{-1/2} - U^{-1/2}\right] \approx -\sqrt{\frac{m}{2}}\,.\,b\,.\,E^{-1/2} \qquad \ldots\text{IV-A(6)}$$

Thus one may think of checking $E^{-1/2}$ dependence of t_d in the very low energy range. However, for an actual potential (which is not of rectangular shape) the departures start from quite low values of E.

For $E \gg U_0$. Equation IV-A(5) now gives

$$t_d = -\frac{1}{2}\sqrt{\frac{m}{2}}\,(U_0 b)\,E^{-3/2} \qquad \ldots\text{IV-A(7)}$$

which is the same as Equation IV-A(4), except for the negative sign. Comments made under Equation IV-A(4) are therefore applicable for this case also.

5. A Snag in Deducing the Potential Form

Let us consider a hypothetical case where t_d vs E data for (say) a potential hill fit into a 2-step rectangular potential like that of Fig. IV-A(4i) *for all E values*. It means that from observed t_d at four E values you got the four parameters U_0, U_0', b, b' and then you checked that for all other E values the observed t_d matched with the calculated t_d.

Now, let us have a look at the potentials of Figs. IV-A (4 ii to iv). Each involves only two heights as in Fig. IV-A (4i), but the widths are distributed differently, total widths remaining unaltered for each *U* value, Since time-delay is additive for *non overlapping potentials*, the

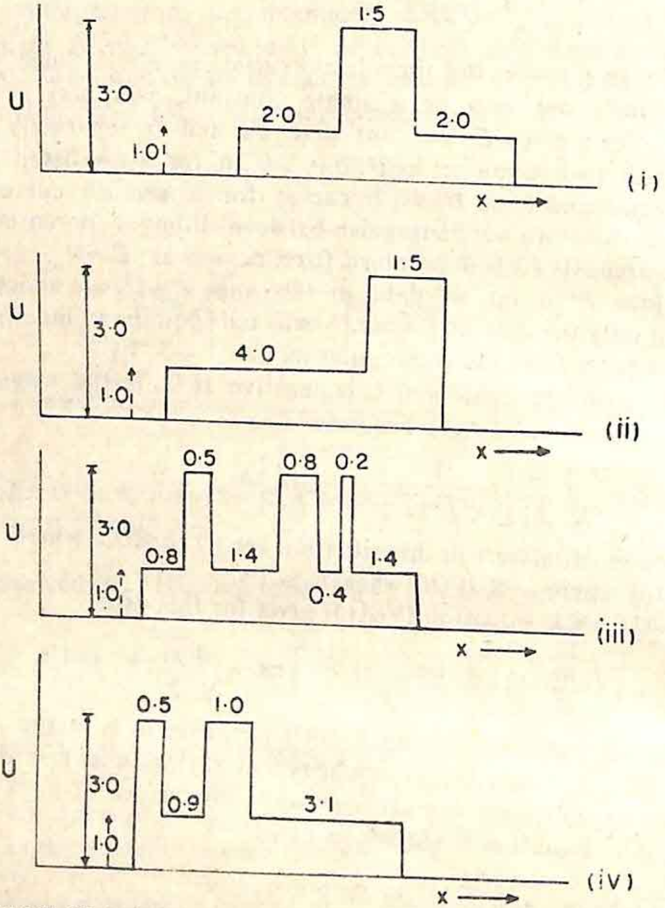

FIGURE IV-A (4) Alternative equivalents for a two-step rectangular potential for idential time-delay.

measurements—whether at low, high, or intermediate *E* values—will make absolutely no distinction between these four potential shapes and an infinity of alternative potentials satisfying this condition. Thus the deduction of the potential form from time-delay studies is—even in principle—not unique, although it could be a rigorous check on whether a suggested potential is valid or not from this point of view.

5

INELASTIC COLLISIONS

5.1. INTRODUCTION

So far you have dealt with collisions in which the target was rigidly clamped and the kinetic energy K of a projectile *after* passing through a field was equal to that *before* entering the field. In such cases the collision is said to be elastic.*

An *inelastic collision* is one in which the equality of ΣK_1 before and after the collision does not hold. For a single projectile interacting with a field it means that $\triangle K$ defined by

$$K\ (\text{after}) - K\ (\text{before}) = \triangle K \qquad \ldots (5.1)$$

is not zero. $\triangle K$ negative would mean that some part of K (before) has gone into some *internal modes* of excitation of either the field magnets or the projectile or both.** $\triangle K$ positive would mean that some energy is transferred from the internal modes to the kinetic energy of translation.

5.2. INTERNAL MODES OF A SYSTEM

Consider the arrangement of Fig. 5.1, in which one of the field magnets (here M_0') is so mounted that it can oscillate about a mean position. The oscillations could be linear ones ($\parallel$ or $\perp$ to the track, or in any direction), or angular ones, depending on how M_0' is mounted. In general these oscillation modes are called *internal modes* of M'_0. In fact both M_0' and M_0'' could be mounted so as to be free for oscillations, either jointly or separately, and one of them could have linear and the other an angular degree of freedom. In general every motion other than translational is defined as an internal mode and each such internal mode will have its own energy, called *internal energy* E_{int}, depending on the amplitude of oscillations.* Conservation of energy then gives us.

---

* In the experiments of Chapter 1 the target was not clamped and could share kinetic energy with the projectile, but the sums ΣK_1 *before* and ΣK_f *after* the collision were equal. That too was a case of *elastic collision*.

** We are excluding dissipative interactions, *i.e.*, those in which part of the energy gets converted into heat.

$$\triangle E_{int} = -\triangle K \qquad \ldots (5.2)$$

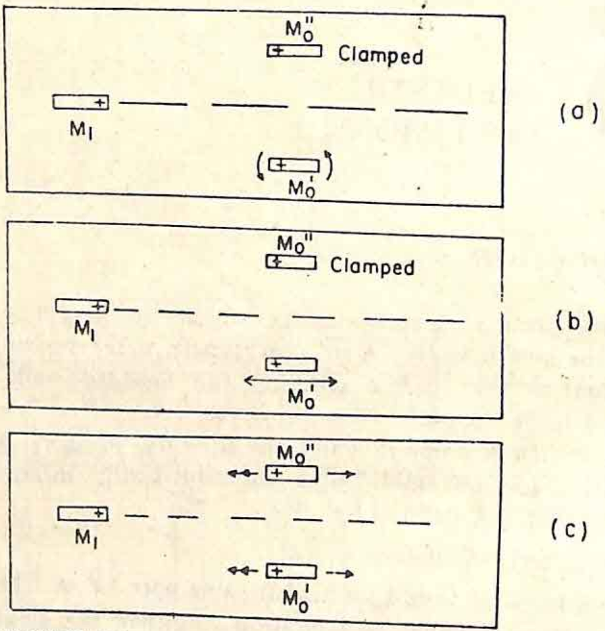

FIGURE 5.1. Three of the many possible ways in which an internal mode may exist in the 'target' (the field magnets).

If you experiment with a projectile and a target, then a non-zero value of $\triangle K$ would give you the information that the target (or the projectile) has an internal degree of freedom or an internal mode. From a study of how $\triangle K$ depends on various parameters, you may get valuable information about these internal modes.

In atomic, molecular and nuclear physics very often you come across internal modes. Atoms have internal modes corresponding to electronic configurations. In the collision of two atoms (or an electron and an atom) an atom can go to a higher or lower internal energy state. In molecules, the vibrations of the atoms relative to each other and rotation of the molecule about an axis are internal modes. Inelastic collisions are widely used to extract information about these modes.

One good example of inelastic collisions is the Franck and. Hertz experiment. Electrons of kinetic energy K_0 are sent into an elemental gas and, their kinetic energy K after collisions with the gas atoms is measured. Experimental evidence is that K comes out to be either K_0 or $K_0 - \epsilon_1$ or $K_0 - \epsilon_2$ or $K_0 - \epsilon_3 \ldots$ where ϵ_1, ϵ_2, ϵ_3 .... have definite discrete values for the given element. It is thus an experimental evidence that the atoms of the element concerned have internal states with energy differences given by ϵ_1, ϵ_2, $\epsilon_3 \ldots$ and can have no intermediate energy states.

---

* If the projectile has a 'structure' (is made up of components) there could be 'internal modes' there too. For example an atom used as a projectile can itself go to an excited state,

Another good example is Raman effect. When photons with energy $h\nu_0$ are sent through the sample their energy after collisions comes out to be $h\nu_0$ or $h(\nu_0 - \nu_1)$ or $h(\nu_0 - \nu_2)$ or $h(\nu_0 - \nu_3)$, etc., where ν_1, ν_2, ν_3 etc., have discrete values for molecules of the sample. So we learn that the molecules of the sample have internal modes with energy differences given by $h\nu_1$, $h\nu_2$, $h\nu_3$, etc.

The experiments in this chapter are meant to understand macroscopically how the energy transfer in inelastic collisions may depend on various parameters of the projectile or the target. For this purpose an internal mode with variable parameters is provided to one or both the field magnets, which act as the target.

5.3. GENERAL DESCRIPTION OF THE ARRANGEMENTS

There is a wide variety of methods for providing an 'internal mode' in the kind of systems you have been studying. Of these, two are described below.

In Fig. 5.2 (a) a pair of magnets M_0' and M_0'' is shown mounted in a rigid frame capable of oscillating about an axis $O\,O'$ such that the magnets oscillate jointly on the two sides of the track and parallel to it. The interaction energy (*PE*) is again like that of Experiment 4-A or 4-B. The oscillation frequency and energy are given by expressions applicable for a rigid pendulum. However, one could replace the rigid rod *OA* by a steel strip clamped at end 0.

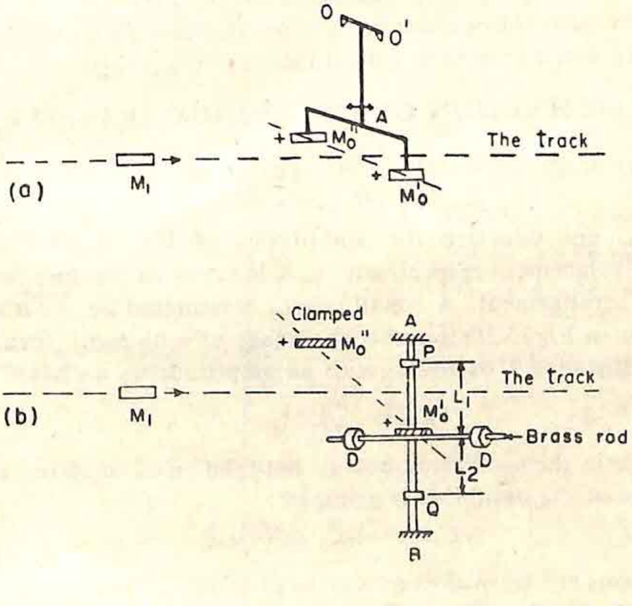

FIGURE 5.2. Two internal mode mechanisms used in the experiments described in this book, (*a*) Pendulum like oscillations of the system of field magnets (*b*) Torsional oscillations of one of the two field magnets.

Figure 5.2 (b) shows the arrangement devised for giving one of the two field magnets a torsional degree of freedom. A steel strip AB is held vertically between two clamps A and B and the magnet M_0' is mounted horizontally on it. The restoring factor C may be changed by shifting the sliding clamps P and Q and the moment of inertia I may be changed by mounting loads D, D at variable distance on a brass rod attached rigidly with the magnet mount. Figure 5.2(c) shows a photograph of this set-up.

The frequency of torsional oscillations is given by

$$\nu = \frac{1}{2\pi}\sqrt{\frac{C}{I}} \qquad \ldots (5.3)$$

and the oscillation energy by

$$E_{int} = \tfrac{1}{2}C\theta_0^2 \qquad \ldots (5.4)$$

where θ_0 is the angular amplitude of oscillations.

Some of the special features of this arrangement are that the inertia factor I and restoring factor C can be varied independently, and that ν can be varied over a wide range and with ease.

The projectile M_1 has no freedom for rotatory motion about a vertical axis; this amounts to saying that the projectile effectively has 'infinite' moment of inertia* about this axis. This makes the analysis of energy transfer simpler.

We shall concentrate our attention for most part on the use of this system. However, the system of Fig. 5.2(a) has a feature that M_1 does not have infinite moment of inertia about the axis OO'. On this account some different features show up in experiments with it. We shall describe just one typical experiment with it later as an example.

5.4. DETERMINATION OF THE ENERGY TRANSFER

The energy of torsional oscillations is given by

$$E_{int} = \tfrac{1}{2}\, I\dot{\theta}^2_{max} = \tfrac{1}{2}\, C\theta^2_{max} \qquad \ldots (5.5)$$

where $\dot{\theta}_{max}$ and θ_{max} are the amplitudes of the angular velocity and angular displacement respectively. θ_{max} is easier to measure, using a lamp-and-scale arrangement. A small mirror is mounted on the magnet holder [not shown in Fig. 5.2(b)] and if the image of a filament formed by this mirror at distance L oscillates with an amplitude w_0 we have**

$$\theta_{max} = \frac{w_0}{2L} \qquad \ldots (5.6)$$

The *change* in the oscillation energy between any two states of different amplitudes of the oscillator is given by

$$\triangle E_{int} = \tfrac{1}{2}\, C.\ \triangle(\theta^2_{max}) \qquad \ldots (5.7)$$

---

* This means that for rotatory motion the glider M_1 is to be taken as 'clamped' to the track, and hence to the earth. It is an example how the term 'free' changes meaning with the context.

** Within the limits of accuracy desired.

In Equation (5.2) we have suggested that a measurement of $\triangle K$ leads to an evaluation of $\triangle E_{int}$. In the experiments on molecular and nuclear physics the measurements are made that way, *i.e.*, we measure K (before) and K (after) and from the measured $\triangle K$ we infer $\triangle E_{int}$. However, as you will see in the present experiments, the magnitude of $\triangle K$ is quite small relative to the K values. Therefore even small errors in measurements of K (before) and K (after) can make a big error in $\triangle K$ and hence in $\triangle E_{int}$. For this reason we propose to measure $\triangle E_{int}$ directly by measuring θ_{max} (before) and θ_{max} (after) and using Equation (5.7).

5.5. PRELIMINARY EXPERIMENTS

(*a*) Determination of Constants of the Internal Mode

For the torsional oscillator [Fig. 5.2(b)] measure the period of oscillation (T). Then increase the moment of inertia by adding two equal masses (m each) on two sides of the brass rod at equal distances (a each) from the strip axis. Measure the period again (T'). Since increase in the moment of inertia is $2ma^2$, Equation (5.3) gives

$$T'^2 - T^2 = \frac{4\pi^2}{C}\ (I'-I) = \frac{8\pi^2 ma^2}{C} \qquad \ldots(5.8)$$

Thus the torsional couple per unit twist (C) is determined. Then using Equation (5.3) you can deduce I.

(*b*) Determination of the Torque Ω vs Projectile Distance x

Set up the arrangement shown in inset of Fig. 5.3. Hold the glider M_1 at different distances x from the centre of M_0' M_0'' and measure the steady angular deflection of M_0' (*see* § 5.4). If the deflection is 0, the

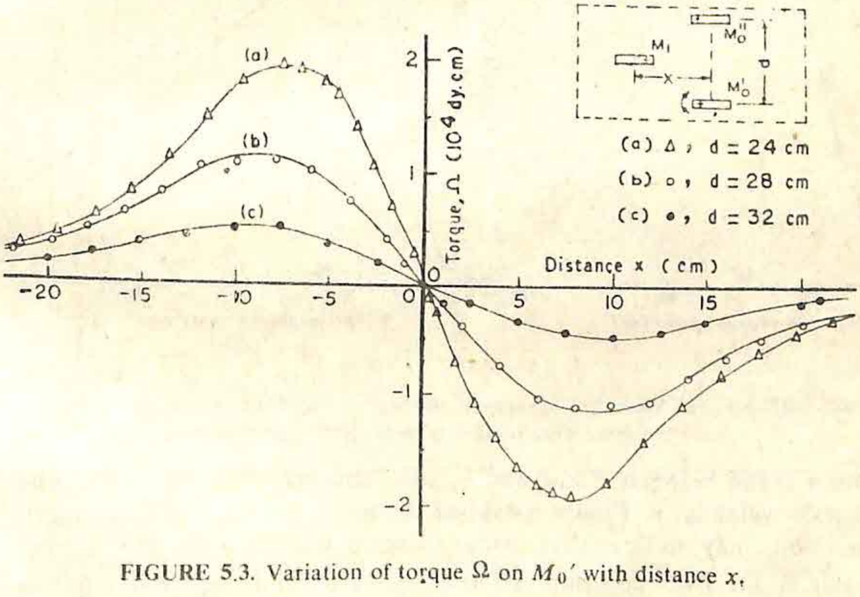

FIGURE 5.3. Variation of torque Ω on M_0' with distance x.

torque is given by

$$\Omega = C\theta \qquad \ldots(5.9)$$

where C is known from Experiment (a). Thus the Ω vs x curve is obtained. This will depend on the separation d between M_0' and M_0''. Figure 5.3 shows the typical Ω vs x curves for three different d values.

It will be a good idea to change the C of the torsional oscillator [by changing the strip length, Fig. 5.2(b)] and to repeat the Ω vs x measurements to see that the results are independent of C.

The Ω vs x measurements may also be done with the transverse arrangement of M'_0 and M_0'' (Fig. 4.4). The shape of the curve may be quite different.

EXPERIMENT 5-A *To study the energy transfer as a function of projectile energy or velocity.*

With the arrangement shown in the inset of Fig. 5.4(a), keep M_0' initially in the non-oscillating state, fire M_1 with different kinetic energies K (sensor not shown) and measure the resultant oscillation amplitude θ_{max} developed in M_0' (*see* Equation 5.6). The energy absorption $\triangle E_{int}$ is given by $\frac{1}{2}C\theta^2_{max}$ where C is known from preliminary experiment [§ 5.5 (a)].

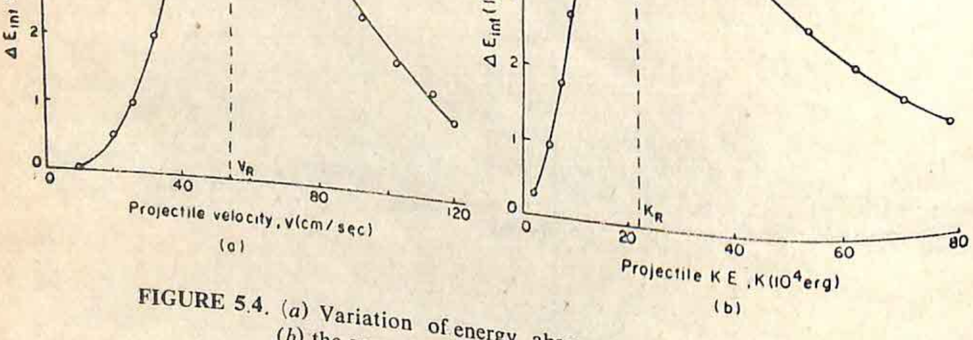

FIGURE 5.4. (*a*) Variation of energy absorption with projectile velocity. (*b*) the same data plotted with projectile kinetic energy as abscissa.

Plot a graph between $\triangle E_{int}$ and K, and another between $\triangle E_{int}$ and projectile velocity v: Figure 5.4 shows the typical results of an experiment. You may notice that with increase of v (or K) the energy transfer in inelastic collision at first increases and then starts falling off. The v (or K) where $\triangle E_{int}$ becomes maximum may be called the resonance value v_R (or K_R). The corresponding energy absorption may be called the resonant absorption.

When does a resonance phenomena occur? What factors govern the energy absorption curve? The next few experiments are meant to investigate this.

RELATED EXPERIMENTS

EXPERIMENT 5-A(i)

Experiment 5-A may be repeated with magnet M_1 reversed in polarity but with the same geometry otherwise. See whether the results remain invariant. Would you expect that?

EXPERIMENT 5-A(ii)

Experiments 5-A and 5-A(i) may be repeated with the magnets perpendicular to the track like Fig. 4.4.

EXPERIMENT 5-B *To study the dependence of the absorption curve on the projectile mass.*

Repeat Experiment 5-A with the same geometry, but with mass of

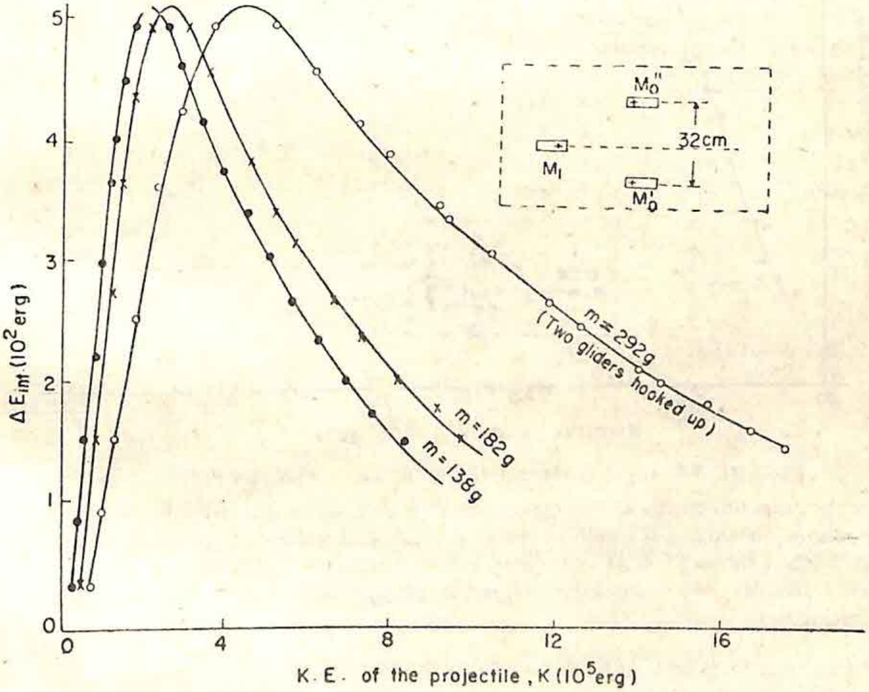

FIGURE 5.5. (*a*) Variation in ΔE_{int} with kinetic energy for different projectile masses.

the glider changed in a few steps. Thus a given velocity v now corresponds to different K values and *vice versa*. Figures 5.5(a) and 5.5(b) show the $\triangle E_{int}$ vs K and $\triangle E_{int}$ vs v plots of the data of an experiment with three different masses of the glider.

You note that the absorption curve showing $\triangle E_{int}$ vs v is independent of the glider mass. Thus the energy transfer for a given geometry is a function of glider velocity v and not of the glider kinetic energy K.

You may note that the energy fed to M_0' is in torsional oscillations. As M_0' experiences a torque the glider M_1 experiences an equal and opposite torque. But it is not free for angular displacement: *i.e.*, its related moment of inertia I is infinite. The 'collision' therefore does not change in nature with changing *mass*: it depends on I and that is infinite for all projectile masses.*

However, it is advantageous to use a more massive projectile for another reason. You often use the approximations**

$$K \gg U \text{ and } K \gg \triangle E_{int}$$

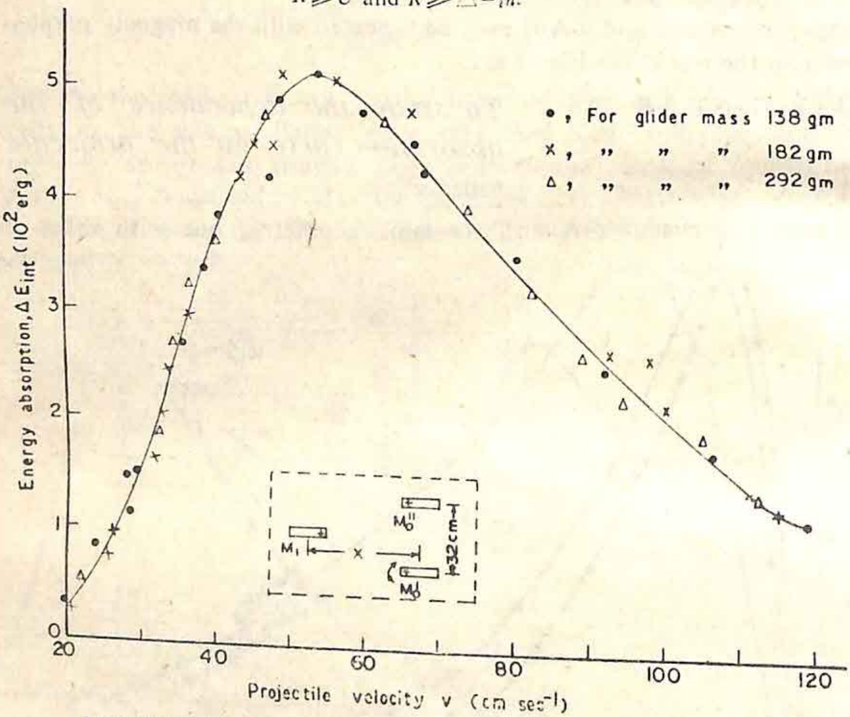

FIGURE 5.5. (*b*) The same data plotted on $\triangle E_{int}$ vs v graph.

Since the potential energy U and energy transfer $\triangle E_{int}$ are primarily due to magnetic interactions, increasing m would increases K alone and make the approximations more valid. Typical values of K, U and $\triangle E_{int}$ are $\approx 10,^5$ $\approx 10^4$ and $\approx 10^3$ erg respectively. Making the M_0' M_0'' separation larger takes you nearer the approximation by decreasing both U and $\triangle E_{int}$.

---

* You may expect a different result if the oscillator is of the kind shown in Fig. 5.2(a). Thus the same projectile responds differently with different modes. See Experiment 5-F.

** *See* Appendix V-A(2).

EXPERIMENT 5-C *To study the dependence of energy absorption on the restoring factor C of the internal mode.*

Repeat Experiment 5-A changing C in steps, but keeping the moment of inertia I unchanged. In each case measure C as described in § 5.5 (a).

Figure 5.6 shows the typical results of an experiment. You notice that as C increases the energy transfer decreases at all values of the projectile velocity. Also the resonance velocity v_R increases with increasing C. You may list the corresponding v_R and C values and then hunt for a possible relation between them. Similarly you may list the peak values $(\triangle E_{max})$ of the absorbed energy and the corresponding C values and hunt for a possible relation between them. In experimental work these are called correlations, and they help you in building up a model.

You will find, for example, that v_R comes out closely proportional to $\sqrt{C}$. You do not know whether this will hold for all ranges of C and for all similar systems. So you may say that *in the observed range* $v_R \propto \sqrt{C}$. But a little thought may tell you that this is as good as saying that $v_R.T$ is constant (why?) In the latter relation both v_R and T are measured quantities, and the product has the dimensions of length.

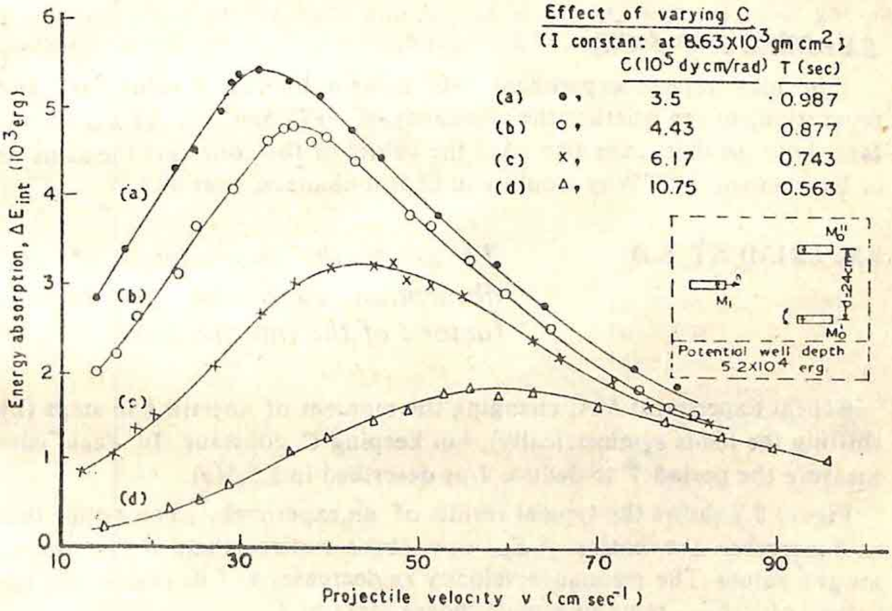

FIGURE 5.6. Variation in curves 5.5 (a) for different C.

From the data of Fig. 5.6, $v_R T$ comes out to be $\sim$32 cm. Since the energy take-up is related with torque Ω, you may have a look at Fig. 5.3. For $d=24$ cm, Ω(max) and Ω(min) occur at a separation of $\sim$16 cm.

($=b$, say) and thus you may infer that $v_R T/2$ equals this length. We repeat that this may not be a general truth; only experiment will tell you. But such inferences are useful for interpretation. For instance $v_R T/2=b$ would mean $b/v_R=T/2$, that is, the energy transfer is maximum when the time taken by the projectile to travel from Ω(max) to Ω(min) position equals half the oscillation period of M_0'.

Notice that we have not yet gone into the mechanics of the energy transfer. Yet the experimental data lead us to inferences if we study the effect of varying the parameters.

As regards $\triangle E_{max}$ you may find that it comes out proportional to $1/C$. You do not yet know why. But in the range of the observations you find the correlation $C\triangle E_{max}=$constant for a given I. As an experimental step this is in itself significant. We note the two correlations:

$$\left.\begin{array}{r} v_R \,.\, T=\text{constant} \\ \text{and } C \,.\, \triangle E_{max}=\text{constant} \end{array}\right| \quad \text{(for a given } I\text{)}$$

You may wonder whether the entire curves can be correlated with one another, rather than only the peaks.* But we shall wait for more data before we go into that attempt.

RELATED EXPERIMENTS

EXPERIMENT 5-C(i)

You may repeat experiment 5-C using a different d value (M_0' M_0'' separation) to see whether the constancy of $v_R T$ and $C \,.\, \triangle E_{max}=$constant hold in that case also. Are the values of the constants the same as in Experiment 5-C? Why would you expect changes, it at all?

EXPERIMENT 5-D

To study the dependence of the absorption curve on the inertia factor I of the internal mode.

Repeat Experiment 5-A, changing the moment of inertia I in steps (by shifting the loads symmetrically), but keeping C constant. In each case measure the period T to deduce I as described in § 5.5(a).

Figure 5.7 shows the typical results of an experiment. You notice that as I increases the entire $\triangle E_{int}$ vs v curve contracts and shifts towards lower v values. The resonance velocity v_R decreases as I increases. But the values of $\triangle E_{max}$ remains almost independent of I.

---

* Such correlations have been found in physics in many cases—like, the blackbody spectra at different temperatures or the specific heat curves for simple solids at low temperatures.

List the corresponding ν_R and I values and search for a correlation. Or, you may try a correlation between ν_R and T. You will find that in the

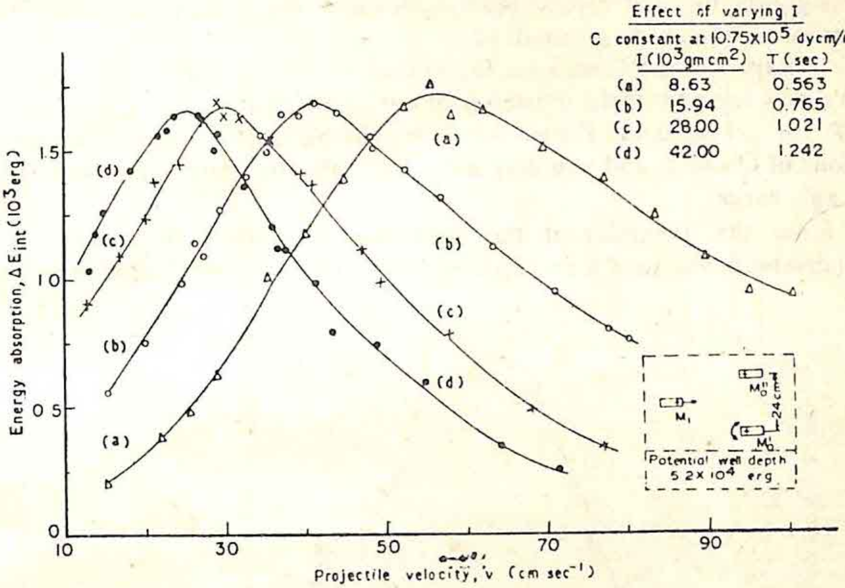

FIGURE 5.7. Variation in curve 5.5 (a) for different I.

range of observations $\nu_R T$ comes out constant, just as you got in Experiment 5-C, where T was changed by altering the spring factor C.

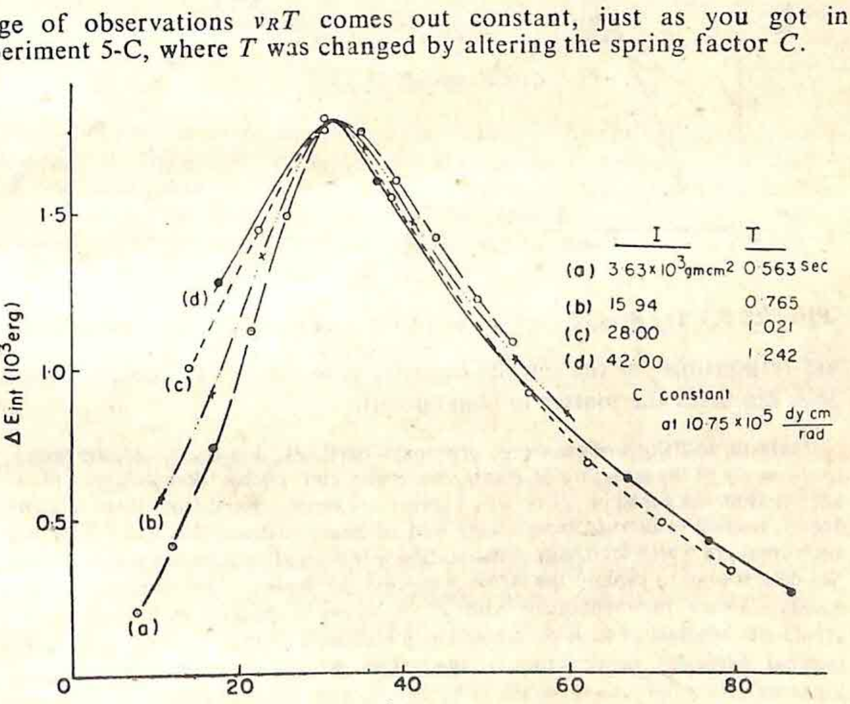

FIGURE 5.8. Variation of ΔE_{int} with νT for different I

There may be more in the data than what catches the eye. In Fig. 5.8 we show a plot of $\triangle E_{int}$ against νT (instead of ν). You may note that the graphs for all I values nearly coincide, the departures being more serious in the range of small νT.

In Experiment 5-C we have found that $C \triangle E_{max}$ comes out constant. We now try a fit of the entire set of curves by plotting $C \,.\, \triangle E_{int}$ against νT for all the data. Figure 5.9 shows the plots for 7 different combinations of C and I, and you may note that all the points fit close to a single curve.

Since the dynamics of the interaction is known, you may try to understand why such a correlation should exist, and what approximations

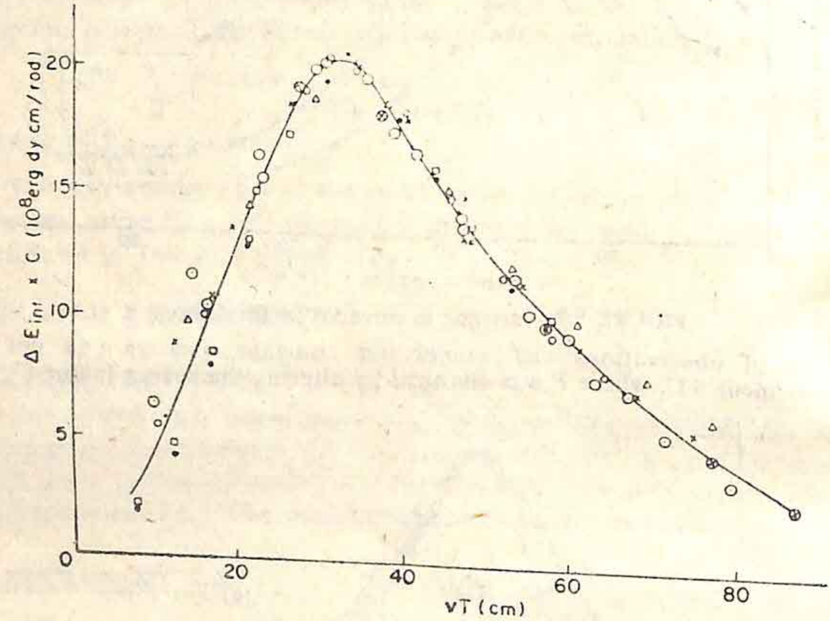

FIGURE 5.9 The data of Figs. 5.6 and 5.7 plotted on a $C.\ \triangle\ E_{int}$ vs. ν graph.

are responsible for the serious departures in the low νT range. Appendix V-A discusses the matter in some detail.

Inelastic collisions of electrons, protons, α particles, ion beams etc. are widely used in the study of the structure of atoms, molecules and nuclei. 'Resonances' of a wide variety (like the peaks in $\triangle E_{int}$ vs ν curves) are observed and from them inferences are drawn, leading to further experiments and advances in theory.* Figure 5.10 gives one such curve, in which scattering cross-section σ is plotted against the projectile energy E. We do not plan to explain the terms or discuss the details. The essential point is that σ does not vary monotonously with E; it shows a peak (called resonance), and a systematic analysis of such occurrence is a standard method for learning about the internal dynamics or structure of the system. An important stage in such analysis is the search for empirical correlations between a wide range of data.

---

* See also Chapter 6 for a closer look at 'resonances' from another angle.

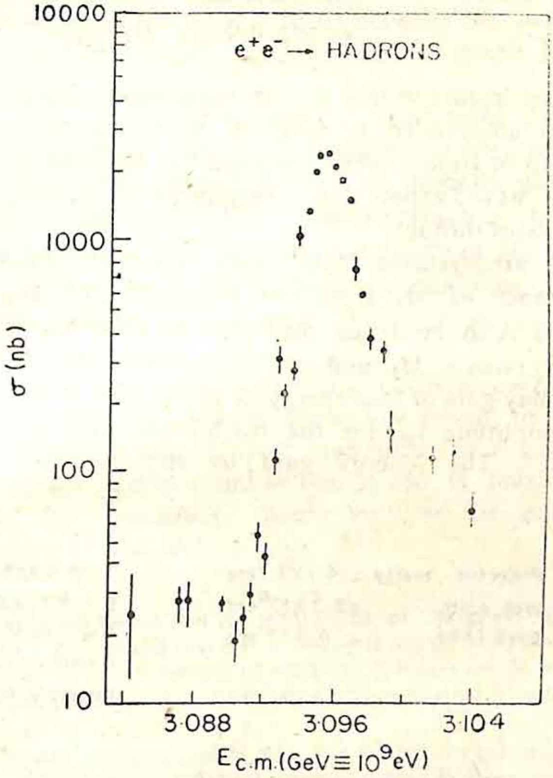

FIGURE 5.10. The resonance observed when beams of high energy electrons and positrons collide. The ordinate shows the cross-section for annihilation of e and e^-. This resonance led to the discovery of a new elementary particle (named [illegible]) by B. Ritcher and S.C. Ting independently in 1974. The Nobel Prize in Physics for 1976 was awarded to both of them. This graph is taken from a review by A.M. Boyarski and others, Phy. Rev. Lett. *34*. 1357, (1975)]

In your present experiment the model has so many constraints.* Even so, the richness of information may be noted. Without any correlation, the richness would be like that of a forest; with the correlation found, the picture becomes attractive, like a well-laid garden.

RELATED EXPERIMENT

EXPERIMENT 5-D(i)

Change C in several steps and each time adjust I in such a way that period T remains the same. Now repeat Experiment 5-A for all combination and plot $\triangle E_{int}$ vs ν data on the same graph. Comment on the results.

---

*Two of them being that M_1 is constrained for linear motion along the track only and M_0' is constrained to have only rotatory oscillation about one axis.

EXPERIMENT 5-E *To study the effect of phase relation on the energy transfer.*

Unlike the experiments so far, in this experiment you have to keep M_0' initially in an excited (oscillating) state and then measure the energy transfer to or from it when the projectile M_1 is fired with a given velocity v. You would expect $\triangle E_{int}$ to depend strongly on the phase of M_0' when M_1 passes through.

Set the firing arrangement M_0M_1 with spacer of width s, keeping the release distance of M_1 from the centre of M_0' M_0'' at a large value ($>$100 cm). Also hold the oscillator magnet M_0' turned by an angle θ_0. Now release M_1 and M_0' *simultaneously*. M_0' will start oscillating and may gain or lose energy as M_1 passes through the field. Measure the amplitude θ_0' for the oscillations of M_0' after M_1 has passed through.* The energy gain by the oscillator is $\triangle E_{int} = \frac{1}{2} C (\theta_0' - \theta_0^2)$.

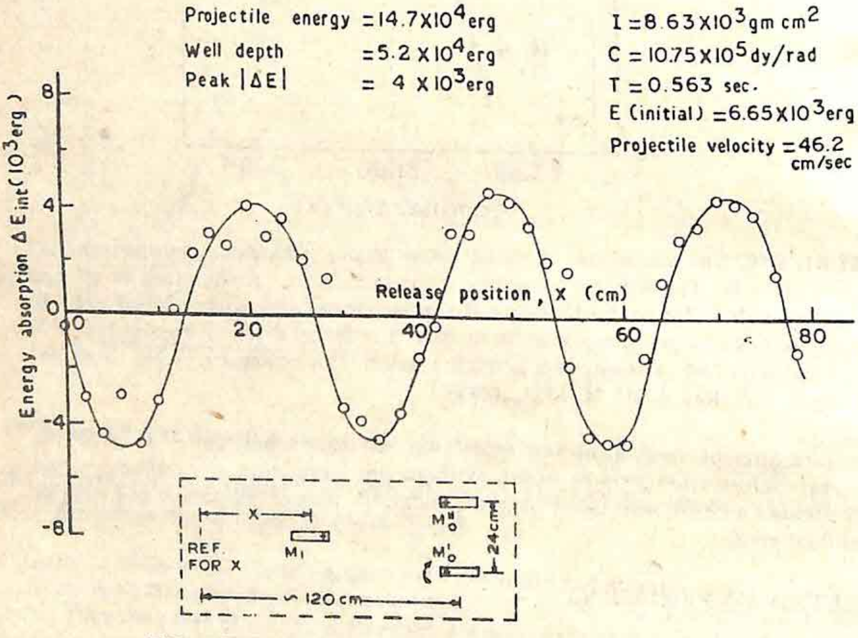

FIGURE 5.11. Effect of phase relation on energy absorption.

You now change the release distance (x) by successive equal steps $\triangle x$ (say, 1 or 2 cm) and repeat the experiment, keeping the release velocity v of M_1 the same every time (*i.e.*, using spacer of a constant width s). In doing so you are changing the time of arrival of M_1 at the field centre by steps of $\triangle x/v$, and thus the relative *phase* between the projectile and the oscillator by time intervals of $\triangle x/v$.* Draw a graph between $\triangle E_{int}$ and x.

---

*Damping of the oscillator is so small that energy loss due to it in a few oscillations may be neglected.

Figure 5.11 shows the results of one such experiment. You find that the energy transfer becomes alternately positive and negative as x changes Thus for the same system the energy transfer depends on the *phase* of the oscillator at the instant the projectile reaches the field centre. The projectile takes time x/v** to reach the centre of $M_0' \, M_0''$. This time divided by period T gives the number of oscillations (n) completed by M_0' as M_1 reaches the field centre. This n provides a measure of the phase.

Figure 5.11 shows that maxima of $\triangle E_{int}$ occur at $x=22$,48 and 73 cm. For $v=46$ cm/sec and $T=0.563$ sec, these correspond to times $n=0.85$, 1.86 and 2.82 respectively. If you take these as roughly† 2, 3 and 4 respectively, the conclusion would be that $\triangle E_{int}$ is maximum when the oscillator has $|\theta|$ maximum (hence $\dot{\theta}=0$) at the time the projectile reaches the centre of $M_0' \, M_0''$.

In Fig. 5.11 you may notice that the separations of the peaks of E_{int} on the x scale are equal ($\sim$ 26 cm) and that this quantity is equal to vT ($\sim$ 26 cm). Should this be a general truth, irrespective of what v or T values are chosen for the experiment, and irrespective of the C and I values of the oscillator? Should the peak value of E_{int} depend on v?

Another fact may be noted in Fig. 5.11. The scatter of experimental data is quite large initially (at large x), but reduces considerably as the release point nears $M_0'M_0''$. This is because v is not rigorously reproducible for a given spacer separation s. An error $\triangle v$ causes a greater error in phase when the distance is larger.

RELATED EXPERIMENTS

EXPERIMENTS 5-E(i)

With the same set-up repeat Experiment 5-E with a different projectile velocity v' (*i.e.*, using a different spacer for firing M_1). Notice and interpret the changes in (*i*) the repeat distance of the $\triangle E_{int}$ vs x curves (*ii*) the height of the maxima of $\triangle E_{int}$. Figure 5.12 shows the results of a typical experiment.

---

*Although the travel time of M_1 to the middle of $M_0' \, M_0''$ is *not* equal to x/v, the *change* in this time is equal to $\triangle x/v$, so long as the release position is well outside the field region.

**Assuming that the energy transfer and the PE of the system are both much smaller than the KE of the glider.

†This is not a good approximation and the data may really need more analysis. Possibly the effect of the PE curve in changing the projectile velocity may also have to be taken into account. More important is that n change in steps of 1.

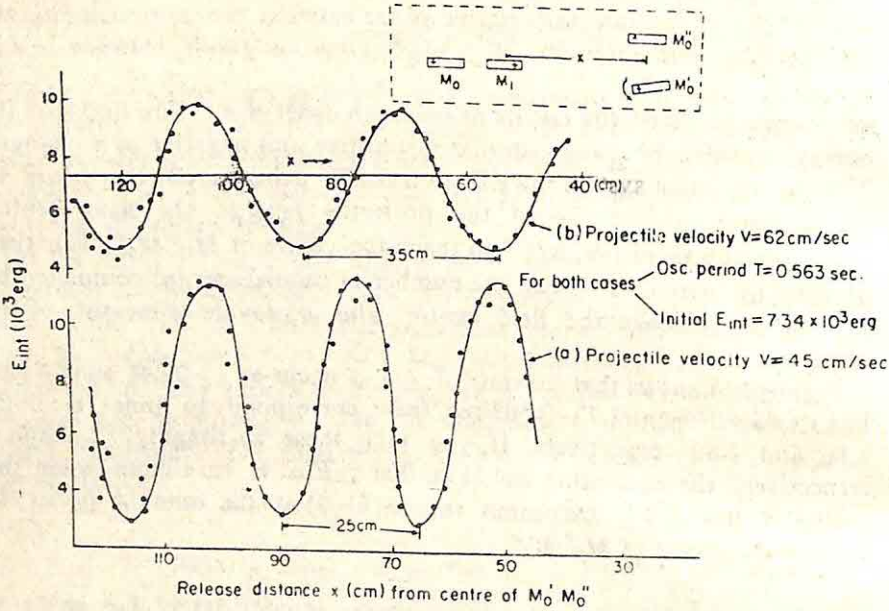

FIGURE 5.12. Dependence of $\triangle E_{int}$ amplitude and its periodicity on the projectile velocity.

EXPERIMENT 5-E(ii)

With the same set-up repeat Experiment 5-E with a different initial amplitude θ_0 of the oscillator. See whether the repeat distance of the $\triangle E_{int}$ vs x curve changes and whether the peak values of $\triangle E_{int}$ depend on θ_0; if so, how.

There is a special interest in this. The initial oscillation energy is $\frac{1}{2}C\theta_0^2$ and while the increase of E_{int} could be of any magnitude, the decrease cannot be larger than $\frac{1}{2}C\theta_0^2$. Therefore the symmetry about the x-axis seen in Fig. 5.11 may not always be observed. From this point of view 'emission' and 'absorption' of energy by an oscillating system like M_0' are not fully symmetrical processes. But it is instructive to do the experiment. Having observed the maximum $\triangle E_{int}$ is an Experiment like 5-E, you may set θ_0 for this experiment at 1.0, 0.8, 0.6 times of that value and see the results.

EXERCISE 5-E(i)

From the data given in Fig. 5.11 compute the extreme per cent changes in the projectile velocity due to the energy transfer $\triangle E_{int}$. You may make a similar calculation for change arising from the PE of the system $M_1+M_0'-M_0''$. How will the latter calculation change if you had a potential hill arrangement of polarities instead of a well?

In atomic and nuclear experiments you are generally dealing with projectiles of all kinds—electric monopoles (charged particles), magnetic dipoles (as in neutrons), etc. These projectiles pass at various distances from the nuclei and the induced dipole is generally a serious matter for consideration of the interaction. Therefore there is no reason to expect that the experiments done by you with magnetic dipoles will have direct correlation with what you observe in atomic and nuclear experiments But the fact that *resonances* occur for energy transfer is the most significant part of the experiments. The dependence of these resonances on the various parameters is a game any experimentalist must play before he can use the data for interpretation. In fact, at the moment it appears that in physics the experimentalists have outstripped the theorists by collecting a large volume of data on resonances of all kinds, which have yet to be satisiactorily explained. Mysteries of nature are unlimited—the more we learn, the more we come to know of things that have to be learnt about.

EXPERIMENT 5-F *To study the energy transfer to a different mode of the target oscillator.*

All the Experiments 5-A to 5-E described so far relate to the arrangement of Fig. 5.2(b) for the oscillations of the field magnet M_0'. Now, you may mount M'_0 M_0'' in the manner shown in Fig. 5.2(a) and repeat all the experiments.

Figure 5.13 shows the results of one experiment with the oscillating system working as a compound pendulum. Since the spring factor C and inertia factor I cannot be changed independently in this case, analysis is difficult. (You may use a steel strip arrangement as suggested earlier). But all the same the rule '$v_R T$=constant' appears to be obeyed here also.

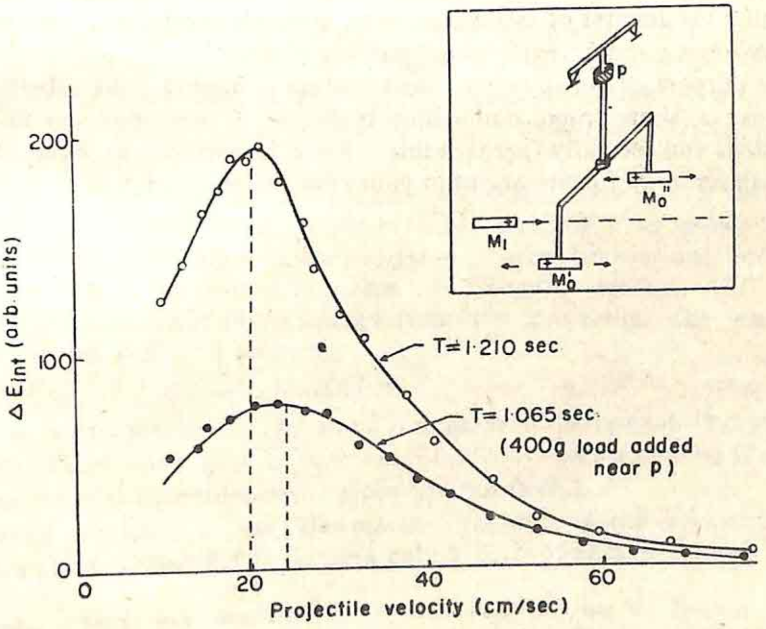

FIGURE 5.13. ΔE_{int} vs v curves for a different internal mode of the field magnets M_0' M_0''.

Since the mode of oscillation is different in this case you may get some results different from those you got earlier. For instance, Experiment 5-B may have special features. We will not take away your joy of discovery and intelligent analysis by describing the results.

In any experiment in Physics a given projectile may interact with different modes of the system under study in different ways. Conversely, a given mode of the system may interact with different projectiles in different ways. As one example, infra-red light passed through CO_2 gas would not excite the symmetric vibration, though it excites the antisymmetric ones. In contrast, in Raman effect (modified scattering of visible and ultraviolet light) it is just the reverse. Nature of the mode and the projectile is thus a matter of some importance in inelastic scattering.

A Note of Caution on Analogies

Analogies from elementary physics are of great use in enriching your awareness so that when new physics is to be explained, you have a whole lot of ideas stacked away in your mind to draw upon. True, there have been cases in history when scientists, not completely conversant with earlier theories, have come up with new ideas that work excellently for the latest developments. But this is very rare.

At the same time, you ought to be very cautious in jumping to extrapolations from elementary ideas. It would be tempting for you after studying Newtonian systems and resonances to look at the particle resonances and say "I will start on a classical model now." We would strongly urge that it would be much better to spend your time to learn a considerable amount of modern physics, quantum mechanics, etc. before even worrying about "explaining" particle physics.

The purpose of our drawing your attention to atomic (and sub-atomic) systems to show some similarities is firstly to accustom you to such situations and secondly (perhaps this is more important) to build up an enthusiasm to go further ahead in your exploration of physics.

APPENDIX V-A

ANALYSIS OF ENERGY TRANSFER IN INELASTIC COLLISIONS OF DIPOLES

1. General Considerations

Figure V-A (1) shows a magnetic dipole M_1 (hereafter called *the projectile*) passing between a pair of identical dipoles M_0', M_0''. The constraints are : (*i*) M_1 is free only for motion along with the track *AB*; (*ii*) M_0'' is neither free for linear motion nor for rotation; (*iii*) M'_0 is not free for linear motion, but can have torsional oscillations in a plane containing M_0' and the track, for which it has a specified inertia factor *I* and spring factor *C*.

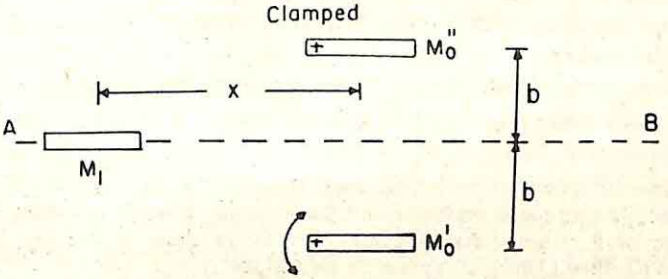

FIGURE V-A (1) The configuration used in energy transfer experiments. M_1 is the projectile; M_0' has an internal mode.

Between the projectile M_1 and the pair $M_0'+M_0''$ there is (*i*) a mutual force and (*ii*) a mutual torque. Since both M_0' and M_0'' have $m \rightarrow \infty$ (no freedom for linear motion), neither of them shares translational energy on this account as the projectile passes. For angular motion, M_0' has finite *I* and therefore it shares energy from the projectile. The energy transfer, called $\triangle E_{int}$, is given by:

$$\triangle E_{int} = \int \Omega d\theta = \int \Omega \dot{\theta}\, dt \qquad \ldots \text{V-A (1)}$$

where Ω is the torque on M_0' and θ is angular displacement. However, since we neither know Ω as a function of θ, nor corresponding Ω and $\dot{\theta}$ as functions of time these expressions are not useful.

Actually we have to use Newtonian dynamics in the original way in which Newton used it.* It is now called The Method of Numerical

---

*Integral calculus was developed by Newton. Prior to that his method for deducing planetary motion (and all dynamics for that matter) was the one being described here. With computers this method has now become of wide use again, particularly where integration is not feasible.

Integration. In this method time is divided into a series of equal small intervals ($\triangle t$) and changes in the velocity and position coordinates in successive intervals are computed step by step.

2. Energy Transfer when the Oscillator is Initially Unexcited

(*a*) *The numerical integration.* The initial conditions are $\theta=0$ and $\dot{\theta}=0$, and you have to use the equation

$$\ddot{\theta}=\frac{\Omega-C\theta}{I} \qquad \ldots \text{V-A (2)}$$

to deduce $\dot{\theta}$ and θ at successive stages as the projectile passes in the field of M_0' and M_0'' to exert a torque Ω.

Before we proceed ahead we make two simplifying assumptions

(*i*) Ω is a function of x alone, *i.e.*, its variation with θ is relatively much smaller.

(*ii*) The projectile velocity v is not appreciably changed due to the potential energy in the field and the energy transfer.

Assumption (*i*) is better satisfied if the separation d of the magnets M_0' and M_0'' is kept large. The torque Ω on M_0' is not the same at different θ values; but if the total range of θ is small and the sideways shift of poles is consequently small (relative to d), then Ω depends primarily on x alone.

Assumption (*ii*) needs a closer examination. Consider the data of Fig. 5.11. Projectile energy is 1.5×10^5 erg and the potential well has depth 0.5×10^5 erg. Thus the potential well increases the velocity by ~ 15 per cent.* The maximum energy transfer is 0.04×10^5 erg and therefore its effect on v is not appreciable. To make assumption (*ii*) more valid you may keep d larger, *i.e.*, the potential well shallower; but the energy transfer (which you desire to measure) will then become smaller. Thus the effective change in v is 10-15 per cent. Neglecting this could be serious, but this change is the upper limit and is over a small range of x.

With these assumptions the Ω vs x curve is converted to Ω vs t curve using the relation $\triangle t=(1/v)\ \triangle x$. The zero of time may be chosen anywhere.

Numerical integration now proceeds in the following steps:

Step 1. Divide the time scale into a series of small parts $\triangle t_1$, $\triangle t_2$, ... $\triangle t_i$ ... **. Determine from the Ω vs t curve the values of Ω_i at the middle of the i^{th} intervals.

Step 2. Let $\dot{\theta}$ and θ at the start of the i^{th} interval to be $\dot{\theta}_i$ and θ_i respectively. Then compute $C\theta_i$, thence $(\Omega_i-C\theta_i)/I$. That gives $\ddot{\theta}_i$, the angular acceleration during the i^{th} interval.

Step 3. Multiply $\ddot{\theta}_i$ by $\triangle t_i$. That gives $\triangle\dot{\theta}_i$, the change in angular velocity during the i^{th} interval. $\dot{\theta}_i+\triangle\dot{\theta}_i$ gives $\dot{\theta}_{i+1}$.

---

*If the well were changed to a hill, the velocity would decrease by 23 per cent,

**These may or may not be equal. But they must *be small*.

Step 4. Deduce the mean* of $\dot{\theta}_i$ and $\dot{\theta}_{i+1}$ and multiply it by $\triangle t_i$. That gives $\triangle \theta_i$, the change in angular displacement during the i^{th} interval. $\theta_i + \triangle \theta_i$ gives θ_{i+1}.

The process may be started from the moment where Ω is nearly zero and may be carried on till Ω ceases to be significant.** Thus you get a complete description of the dynamics: $\dot{\theta}$ vs t and θ vs t.

The energy at any stage may be deduced using

$$E_{int} = \tfrac{1}{2} C\theta^2 + \tfrac{1}{2} I\dot{\theta}^2$$

But it is instructive to plot $\Omega\dot{\theta}$ against t to appreciate the variations in the rate of energy transfer in different time spans.

Table V-1 (p. 111) gives a section of the complete table of computations with the parameters C and I corresponding to curve (a) in Fig. 5.6 and $v = 30$ cm/sec. Time intervals of width 1/30 sec were taken for the computation. You may notice how $\dot{\theta}$ and θ deduced in each stage are used as the initial $\dot{\theta}$ and θ for the next stage.

(*b*) *Graphical representation of the results.* Graphical plots of the computations of Table V-1 are shown in Fig. V-A(2). The x coordinate shows the glider position† and y coordinate shows the corresponding state of the oscillator in terms of (*a*) the torque Ω applied by the glider; (*b*) the angular acceleration $\ddot{\theta} = (\Omega - C\,\theta)/I$; (*c*) the angular velocity $\dot{\theta}$; (*d*) the angular displacement θ; (*e*) the power $\Omega\dot{\theta}$, *i.e.*, the rate at which energy is fed to the oscillator; and (*f*) the energy E_{int} of the oscillator.†† You may note from curve (*e*) that the major part of the energy transfer occurs in those two time spans during which the *magnitude* of Ω is large.

The dotted curves in Fig. V-A(2) belong to the case of a projectile with $v = 60$ cm/sec in the same geometry of M_0' and M_0''. By the time $\dot{\theta}$ goes from positive peak to negative dip, the projectile moves farther ahead than the position where Ω has maximum negative value; hence the dips in Ω and $\dot{\theta}$ do not match well now and the second peak in $\Omega\dot{\theta}$ vs x curve is much smaller. That accounts for smaller energy transfer in this case than with $v = 30$ cm/sec.

(*c*) *Condition for resonance.* The condition for resonance (maximum

---

*You may note that while Ω_i and $\dot{\theta}_i$ could be taken for the *middle* of the i^{th} interval, $C\theta_i$ could be taken only for the start of the interval. At the stage where $C\theta_i$ is needed you do not know θ_{i+1}. Of [course, after step 4 you can go back to step 2 and make an improved calculation using mean θ_i there. This is called *the method of iteration.*

**After that $\ddot{\theta}$ will be given by just $-(C/I)\theta$, which is the equation for simple harmonic oscillation without any change in energy.

†Division by glider velocity (30 cm/sec) will convert the x-scale to time scale. Thus the separation of successive θ peaks or $\dot{\theta}$ peaks is ~ 30 cm, which is equivalent to ~ 1 second. As listed on Fig. 5.6 the period for the oscillator in this case is 0.987 sec.

††The computed energy transfer comes to 6×10^3 erg, compared with the experimental value 5.5×10^3 erg [*see* curve (a), Fig. 5.6].

energy transfer) is now easy to see. Comparison of the $\ddot{\theta}$ curve with the Ω curve on one side and the θ curve on the other shows that after the

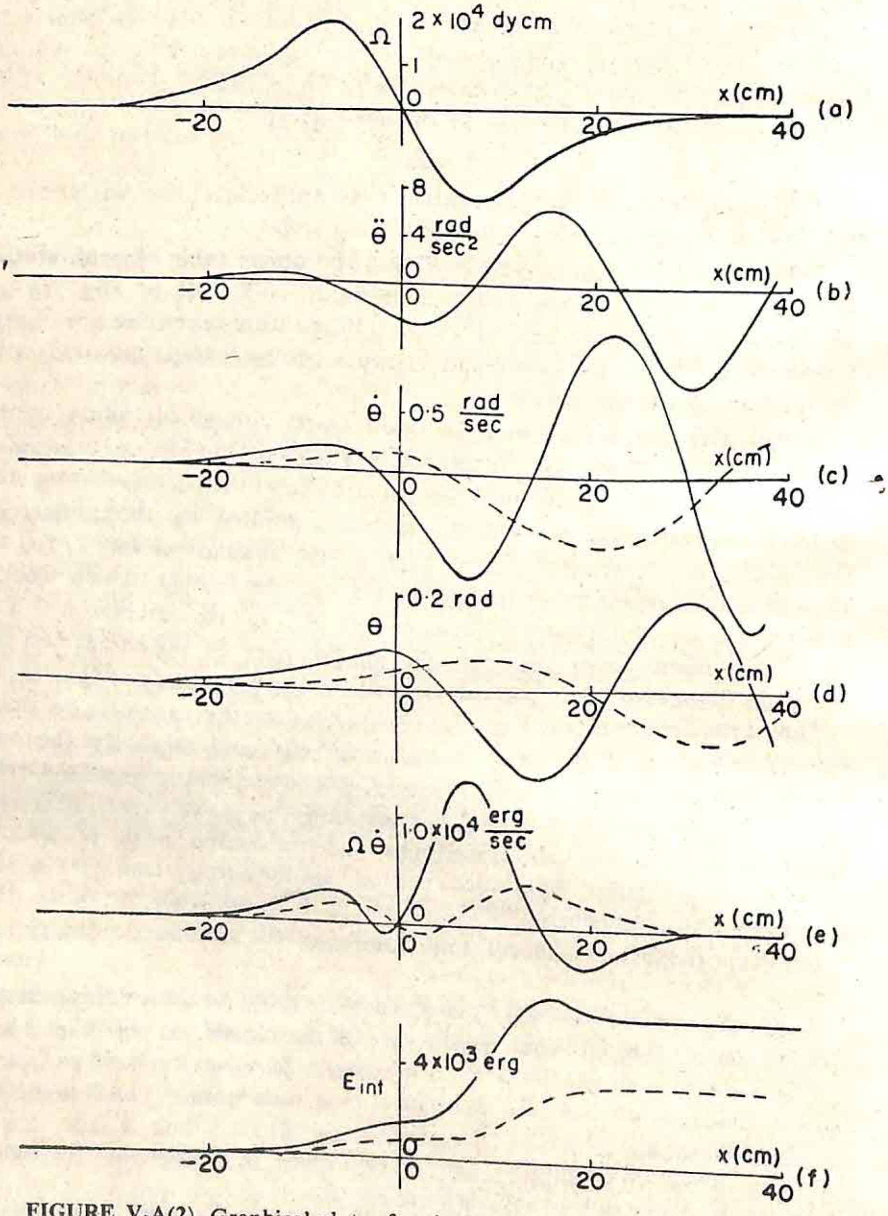

FIGURE V-A(2). Graphical plots of various parameters computed in Table V-1.

initial stages $\ddot{\theta}$ is dominantly governed by the $-C\theta$ term (in $\Omega - C\theta$), *i.e.*, the internal spring factor of the oscillator. Thus the time for $\dot{\theta}$ changing from maximum positive to maximum negative value is close to $T/2$. The Ω value changes from maximum positive to maximum negative over a distance approximately $2L$, where L is the length of the magnet. Thus the peaks and dips of Ω and $\dot{\theta}$ curves would match if the projectile velocity is such that $2L/v \approx T/2$, that is $vT \approx 4L$. You may note, however, that a number of approximations are involved in this relation.

3. Changes in the Energy Transfer Curves with Changes in the Oscillator Constants

To see the effect of changing C or I or both on the energy transfer curves we will use a method in which multiple parameters in the numerical computation are changed in such a way that a given series of computations remains valid for the new situation except for change by constant common factors.

Let us recall the steps in the numerical integration. The Ω vs x curve is changed to Ω vs t using the relation

$$\triangle x_i = v \triangle t_i \qquad \ldots \text{V-A(3)}$$

The Ω vs t curve is then divided into small intervals $\triangle t_i$ and the steps of computation are

$$\ddot{\theta}_i = \frac{\Omega_i - C\theta_i}{I}$$

$$\triangle \dot{\theta}_i = \ddot{\theta}_i \, \triangle t_i$$

$$\triangle \theta_i = \tfrac{1}{2}(\dot{\theta}_i + \dot{\theta}_{i+1}) \triangle t_i$$

We shall now consider separately the effect of changing C and I.

(*a*) **Effect of changing the spring factor C**. Let C change to C' such that

$$C' = rC$$

We shall find what change in v would, if at all, keep the steps of numerical integration valid for the new situation. Let us try

$$v' = qv$$

Then to keep the same Ω_i values valid you have to change the intervals of time to

$$\triangle t'_i = \frac{1}{q} \triangle t_i$$

We also need $C'' \theta'_i = C\theta_i$ if $\ddot{\theta}_i$ values have to remain unchanged. We will see later what relation of q and r factors satisfies this requirement. Now,

$$\ddot{\theta}_i' = \ddot{\theta}_i$$

leads to $$\triangle \dot{\theta}'_i = \frac{1}{q} \triangle \dot{\theta}_i \text{ (hence } \dot{\theta}'_i = \frac{1}{q} \dot{\theta}_i)^* \qquad \ldots \text{V-A(4)}$$

and $$\triangle \theta'_i = \frac{1}{q^2} \triangle \theta \text{ (hence } \theta'_i = \frac{1}{q^2} \theta_i)^*$$

---

*What applies to $\triangle\dot{\theta}$ and $\triangle\theta$ applies to $\dot{\theta}$ and θ also in this case, where both $\dot{\theta}$ and θ are initially zero.

This is because the change $\triangle t_i$ to $\triangle t_i$ brings in a factor $1/q$ at each step.

The requirement $C'\theta'_i = C\theta_i$ now leads to

$$r = \frac{C'}{C} = \frac{\theta_i}{\theta'_i} = q^2 = \left(\frac{\nu'}{\nu}\right)^2$$

or

$$\frac{\nu'}{\nu} = \sqrt{\frac{C'}{C}} = \frac{T}{T'} \text{ (since } I = I'\text{)}$$

$$\nu'T' = \nu T \qquad \text{. . . V-A(5)}$$

Thus with change of C, if the condition V-A(5) is satisfied, the entire computation remains valid, with change factors given by Equation V-A(4). The new energy transfer is given by

$$\triangle E'_{int} = \tfrac{1}{2}\, C'\, (\theta')^2 + \tfrac{1}{2}\, I\, (\dot{\theta}')^2 = \frac{C}{C'} \triangle E_{int}$$

as can be seen by using Equation V-A(4). This means

$$C' \triangle E'_{int} = C \triangle E_{int} \qquad \text{. . . V-A(6)}$$

In essence, therefore, $C' \triangle E'_{int}$ has the same functional dependence on ν', C' as $C \triangle E_{int}$ has on ν, C provided that relation V-A(5) is satisfied.

(*b*) **Effect of changing the inertia factor I** Let I change to I' such that

$$I' = rI$$

We have to see what change in ν keeps the steps of numerical integration valid for the new situation.

Let ν change to $\nu' = q\nu$. To keep the same Ω_i values valid, we have to change $\triangle t_i$ to $\triangle t'_i = (1/q) \triangle t_i$. Since C is unchanged in this case, we require to arrange so that $\theta'_i = \theta_i$. We shall soon see what relation of r and q fulfils this. We have, considering $I' = rI$, and $\triangle t' = (1/q) \triangle t_i$—

$$\ddot{\theta}_i' = \frac{1}{r}\, \ddot{\theta}_i \,;\ \dot{\theta}_i' = \frac{1}{qr}\, \dot{\theta}_i \,;\ \theta'_i = \frac{1}{q^2 r}\, \theta_i$$

The last relation, in view of $\theta_i' = \theta_i$, means $q^2 r = 1$

$$\therefore \qquad \frac{\nu'}{\nu} = q = \sqrt{\frac{1}{r}} = \sqrt{\frac{I}{I'}} = \frac{T}{T'}$$

where T is period of the oscillator. This means

$$\nu'T' = \nu T$$

which is exactly the same as Equation V-A(5). Thus whether C changes or I changes, the entire computation remains valid if ν is so changed as to keep νT constant.

The energy transfer is given by

$$\triangle E'_{int} = \tfrac{1}{2}\, C\, (\theta')^2 + \tfrac{1}{2}\, I\, (\dot{\theta}')^2 = \triangle E_{int}$$

as can be seen by simple substitution.

Combining with the earlier result we can say that the quantity $C \triangle E_{int}$ does not depend on ν, C and I separately, but is a function of a single variable νT.

Let us remember, however, that the results are valid only under the assumption that the projectile moves with uniform velocity. The validity of this assumption is less at lower velocities. Hence you may expect serious departures in that region.

4. Energy Transfer when the Oscillator is Initially Excited

Let the oscillator have initial oscillations with amplitude θ_0 so that we write

$$\theta = \theta_0 \cos \frac{2\pi t}{T} \qquad \text{. . .V-A(7)}$$

assuming that time is counted from the instant when $\theta = \theta_0$. The Ω vs x data may be converted into Ω vs t data in the manner described before.

Then we may use Equation V-A(1) to compute the energy transfer.

$$\triangle E_{int} = \int \Omega\ \dot{\theta}\ dt = -\frac{2\pi\theta_0}{T} \int \Omega\ \sin \frac{2\pi t}{T}\, dt \qquad \text{. . . V-A(8)}$$

In this we assume that the energy transfer (to or from the oscillator) is a small fraction of the initial energy of the oscillator to enable us to take θ_0 outside the integral sign. The method to use Equation V-A(8) is to get the corresponding values of Ω and $\sin 2\pi \frac{t}{T}$ at different times, then to plot the product against time, and finally to find the area under the curve. Let us consider some typical cases.

(*a*) *Projectile velocity very low*. For this case the time scale of Ω vs t curve becomes very narrow; thus the case is equivalent to oscillator period becoming very large. In this case $\dot{\theta}$ changes very little during the passage of the projectile through the field region. Equation V-A(8) then becomes

$$\triangle E_{int} = \dot{\theta} \int \Omega\ d\theta \therefore \triangle E_{int} = 0$$

since Ω is negative for as much time as that for which it is positive.

(*b*) *Maximum response condition*. Figure 5.3 shows that the torque Ω changes from the +ve peak value to −ve peak value as the projectile travels a length *nearly* $2L$, where L is the length of the magnets. For projectile velocity v (neglecting the effect of the potential hill or well) this corresponds to time interval $2L/v$. If the oscillator period T is such that $\dot{\theta}$ reverses sign in just this time, then the product $\Omega\dot{\theta}$ is positive in both regions or negative in both so that $\triangle E_{int}$ gets the extreme +ve or −ve value respectively. Thus for extreme energy transfer we need

$$\frac{2L}{v} \approx \frac{T}{2}$$

The actual $\triangle E_{int}$ depends also on the proper phase condition. Figure V-A-3 shows (Ω, t), $(\dot{\theta}, t)$ and $(\Omega\dot{\theta}, t)$ curves for three relative phases. The areas under the last curve are shaded and they give you $\triangle E_{int}$. You may see that for the three cases $\triangle E_{int}$ is maximum, zero and minimum.

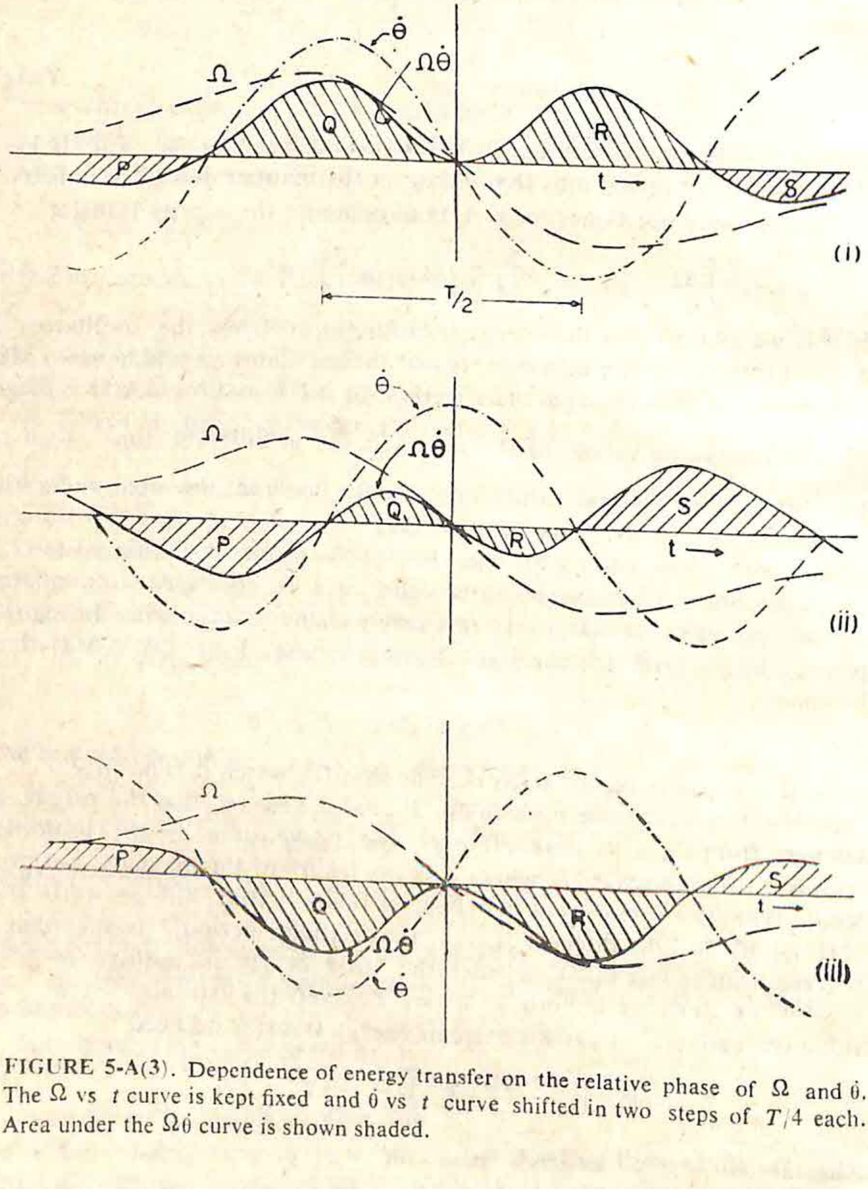

FIGURE 5-A(3). Dependence of energy transfer on the relative phase of Ω and $\dot{\theta}$. The Ω vs t curve is kept fixed and $\dot{\theta}$ vs t curve shifted in two steps of $T/4$ each. Area under the $\Omega\dot{\theta}$ curve is shown shaded.

TABLE V-1

NUMERICAL COMPUTATION OF THE DYNAMICS OF ACTIVATION OF TORSIONAL OSCILLATIONS IN A DIPOLE BY THE PASSAGE OF A PROJECTILE

$I = 8.63 \times 10^3$ gm cm^2 $v = 30$ cm/sec

$C = 3.50 \times 10^5$ dy cm/rad $\triangle t = 1/30$ sec

x_i cm £	Ω_i dy.cm $\times 10^{-4}$	θ_i rad $\times 10^2$	$\dot\theta_i$ rad s^{-1}	$C\theta_i$ dy cm $\times 10^{-1}$	$\ddot\theta_i$ rad s^{-2}	$\triangle\dot\theta_i$ rad s^{-1} $\times 10^2$	$\dot\theta_{i+1}$ rad s^{-1}	$\triangle\theta_1$ rad $\times 10^2$	θ_{i+1} rad $\times 10^2$
...	...	...	...	...	...	...	...	...	...
−4	1.47	7.52	.164	2.63	−1.35	−4.49	.119	.473	7.99
−3	1.10	7.99	.119	2.80	−1.97	−6.57	.054	.288	8.28
−2	0.80	8.28	.054	2.90	−2.43	−8.11	−.028	.043	8.32
−1	0.40	8.32	−.028	2.91	−2.91	−9.71	−.125	−.254	8.07
0	0	8.07	−.125	2.82	−3.28	−10.9	−.234	−.598	7.47
1	−0.40	7.47	−.234	2.61	−3.50	−11.7	−.351	−.975	6.49
2	−0.80	6.49	−.351	2.27	−3.57	−11.9	−.469	−1.37	5.13
3	−1.10	5.13	−.469	1.79	−3.36	−11.2	−.581	−1.75	3.38
4	−1.47	3.38	−.581	1.18	−3.08	−10.3	−.684	−2.11	1.27
5	−1.70	1.27	−.684	0.44	−2.49	−8.29	−.767	−2.42	−1.15
6	−1.87	−1.15	−.767	−0.40	−1.70	−5.67	−.823	−2.65	−3.80
7	−1.92	−3.80	−.823	−1.33	−0.68	−2.28	−.846	−2.78	−6.58
8	−1.93	−6.58	−.846	−2.30	+0.43	+1.45	−.832	−2.80	−9.38
9	−1.83	−9.38	−.832	−3.28	1.69	5.62	−.776	−2.68	−12.1
10	−1.73	−12.1	−.776	−4.22	2.85	9.50	−.681	−2.43	−14.5
11	−1.60	−14.5	−.681	−5.07	4.03	13.4	−.546	−2.05	−16.5
12	−1.40	−16.5	−.546	−5.79	5.09	17.0	−.377	−1.54	−18.1
13	−1.20	−18.1	−.377	−6.33	5.95	19.8	−.179	−.925	−19.0
14	−1.07	−19.0	−.179	−6.65	6.47	21.6	+.037	−.235	−19.2
15	−0.92	−19.2	+.037	−6.73	6.74	22.5	.262	+.499	−18.7
16	−0.78	−18.7	.262	−6.56	6.70	22.3	.485	1.24	−17.5
17	−0.68	−17.5	.485	−6.12	6.31	21.0	.696	1.97	−15.5
18	−0.59	−15.5	.696	−5.43	5.61	18.7	.883	2.63	−12.9
...	...	...	...	...	...	...	...	...	...

NOTE. Computation was made up to five significant places to avoid cumulative errors. But values are shown to only three significant places, which is the range of validity. Computation was made from $x_i = -30$ cm to $+30$ cm: only a section of it is shown here.

6 STUDY OF DAMPING IN A HARMONIC OSCILLATOR

6.1. INTRODUCTION

In the experiments of Chapter 3 and 4 you have seen that for oscillations in a general potential well the frequency ν varies with energy E. In contrast, the oscillator used for the inelastic collision experiments of Chapter 5 was essentially harmonic, for which ν is independent of E. In this chapter we shall study a harmonic oscillator.

Ideal harmonic oscillations occur under a parabolic potential*

$$U=\tfrac{1}{2}\,C\theta^2 \qquad \ldots (6.1)$$

where C is called *the torque constant*, or *the restoring factor* and θ is the angular displacement. It is notable that oscillations in any general potential well, in the limit of small amplitude, approximate to the harmonic character (*see* Appendix VI-A).

For a system with moment of inertia I about the axis of oscillation the equation of motion in the absence of an external torque is

$$I\ddot{\theta}=-C\theta \qquad \ldots (6.2)$$

The frequency of oscillation, as shown in Appendix VI-B, is given by

$$\nu=\frac{1}{2\pi}\sqrt{\frac{C}{I}} \qquad \ldots (6.3)$$

The energy of oscillation (E) is given by

$$E=\tfrac{1}{2}C\theta^2+\tfrac{1}{2}I\dot{\theta}^2=\tfrac{1}{2}C\theta_0^2=\tfrac{1}{2}I\dot{\theta}_0^2 \qquad \ldots (6.4)$$

where θ_0 and $\dot{\theta}_0$ are the amplitude of the angular displacement and angular velocity respectively. You have already used these expressions in Chapter 5.

Analytically, the harmonic oscillation has the special feature that the displacement can be expressed in terms of a *single* sine or cosine term. Any general oscillation can be expressed as a sum of different sine or cosine terms. Thus for a proper understanding of oscillations of a general kind, a study of harmonic oscillations is of fundamental importance.

---

*We will use angular coordinates, because the experiments in this chapter involve angular oscillations.

6.2. THE DAMPED HARMONIC OSCILLATOR

An actual oscillator may differ from the ideal harmonic character in two ways:

(*a*) The potential energy function may depart from the parabolic character appreciably (*e.g.*, when the amplitude is large).

(*b*) Some source of dissipation of energy may be present causing damping *i.e.*, fall of amplitude with passage of time.

We will describe just one experiment concerning (*a*), primarily to enable you to judge to what extent anharmonicity (departure from harmonic nature) may be neglected. For most part the experiments will be centred on (*b*), *i.e.*, damping or dissipation of energy in an otherwise harmonic oscillator.

If an external torque Ω' acts on the oscillator when its angular velocity is $\dot{\theta}$, the energy transfer to the pendulum is*

$$\triangle E = \int \Omega' \dot{\theta}\, dt \qquad \ldots (6.5)$$

If Ω' has a sign opposite to that of $\dot{\theta}$ we have $\triangle E$ negative, *i.e.*, there is dissipation of energy.

In the simplest treatment of damping one takes Ω' as proportional to the angular velocity and directed opposite to it. Thus

$$\Omega' = -r\dot{\theta} \qquad \ldots (6.6)$$

where r is a constant of the system, called the *damping factor*. As shown in Appendix VI-C, the oscillation is then modified to the form

$$\dot{\theta} = \dot{\theta}_0 e^{-\alpha t} \cos(\omega_0' t + \delta) \qquad \ldots (6.7)$$

with

$$\alpha = \frac{r}{2I} \qquad \ldots (6.8a)$$

and

$$\omega_0' = (\omega_0^2 - \alpha^2)^{1/2} \qquad \ldots (6.8b)$$

α is called the *damping coefficient* and the resultant oscillation has its velocity amplitude falling with time according to

$$\dot{\theta}_0(t) = \dot{\theta}_0(0) e^{-\alpha t} \qquad \ldots (6.9)$$

or with number of oscillations according to

$$\dot{\theta}_0(n) = \dot{\theta}_0(0)\, e^{-\alpha' n} \qquad \ldots (6.10)$$

where

$$\alpha' = \alpha\, T \qquad \ldots (6.11)$$

T being the period of oscillation.

Appendix VI-C defines, among other quantities, the *quality factor* Q of an oscillator and shows that it is related with α', α and r through the relations

$$Q = \frac{\pi}{\alpha'} = \frac{\pi}{\alpha T} = \frac{\pi . 2I}{rT} \qquad \ldots (6.12)$$

Thus high damping coefficient means low Q and *vice versa*.

---

*Like Equation (Y-I), used earlier in discussing the energy transfer.

EXPERIMENT 6-A* *To study the variation of period with amplitude in large angle oscillations.*

Figure 6.1 shows a rigid pendulum *AB hinged* at *O* so that it can oscillate in a vertical plane, A_0B_0 being the equilibrium position. You may release the pendulum from θ as large as near 180°. It will oscillate, but the amplitude falls off rather quickly, because in hinged systems frictional loss cannot be made very small. For this reason period T cannot be determined by timing (say) 10 oscillations with a stop watch.*

Set up a sensor at the position B_0 and connect it to the timer, setting the latter in the $\rfloor\overline{A}\ \rfloor\overline{A}$ mode. The timer will now measure the time for half a swing (*i.e.*, $T/2$). Release the pendulum from some initial deflection θ_0', and measure the maximum deflection θ_0 reached on the other side. The $T/2$ measured by the timer is to be taken as the half period corresponding nearly to amplitude θ_0 (not θ_0'). Taking several data like this, plot a graph between amplitude θ_0 and period T.

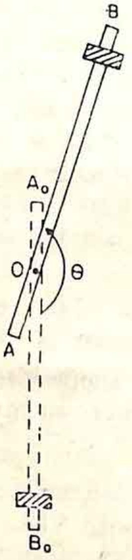

FIGURE 6.1. The rigid pendulum for large-angle oscillations.

Figure 6.2 gives the typical results of an experiment. Notice that T rises to over 3-fold as the amplitude approaches near 170^0 and the slope $dT/d\theta_0$ there indicates that $T \to \infty$ as $\theta_0 \to 180^0$. (See if you can explain it by some simple logic.)

However, in the lower range of θ_0, the slope $dT/d\theta_0$ starts from zero and shows a very slow change. You may compute the range of θ_0 permissible if period T is to vary relative to T_0 (*i.e.*, T at $\theta_0 \to 0$) by (*i*) less than 50 per cent, (*ii*) less than 10 per cent, (*iii*) less than 0.5 per cent.

SUPPLEMENTARY EXPERIMENT

EXPERIMENT 6-A (*i*)

Vary the period of the pendulum (by shifting the load) and check if the results of Fig. 6.2 are valid for all cases if T is replaced by the fraction T/T_0.

---

*Friction being large in this case, one needs to measure the period T by timing as small as half an oscillation. The timer makes this possible.

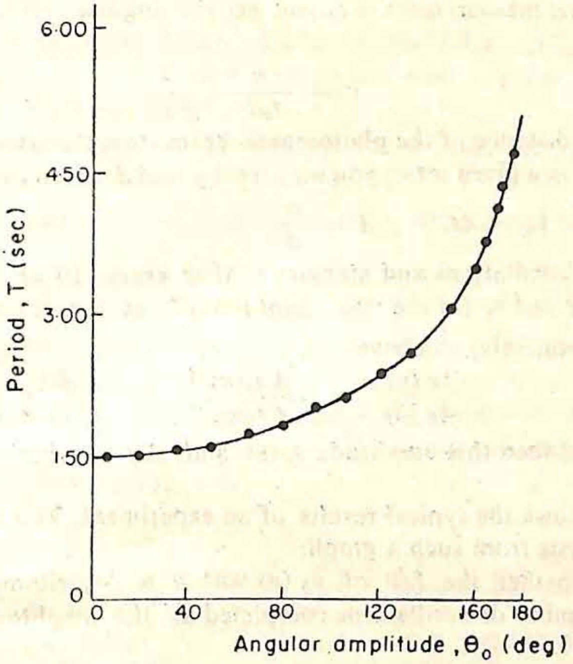

FIGURE 6.2. Period T vs amplitude θ_0 for the pendulum of Fig. 6.1.

EXPERIMENT 6-B* *To study the damping of an oscillator.*

Figure 6.3 shows a rigid pendulum oscillating on the pair of pivots PP', supported on a base BB'. Two loads M_1, M_2 can be clamped at variable distances from the axis of oscillation PP'. This changes the moment of inertia I and also the restoring factor $C=mgl$ (*see* Appendix VI-B).

With hard and sharp pins as pivots and hard base BB', the damping becomes quite small. Part of the damping is at the pivot support and part is due to air friction.

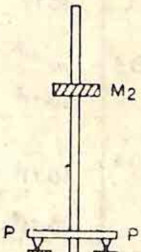

FIGURE 6.3. The rigid pendulum.

Attach a pin of diameter 3 to 5 mm at the lower end of the pendulum and set up a photosensor so that the pin intercepts the sensor beam when the pendulum passes through the equilibrium position. Set the timer in the $\rfloor\overline{A}\lfloor$ mode. If the pin diameter is x and the time measurement is t_v you get the angular velocity amplitude as

---

* In this and all later experiments we shall deal only with oscillations of small amplitude, so that period T is independent of the amplitude.

$$\dot{\theta}_0 = \frac{w}{t_v d}$$

where d is the distance of the photosensor beam from the axis of oscillation. However, in a given series you may treat w and d as constant, so that

$$\dot{\theta}_0 = A t_v^{-1} \; ; \; A = \frac{w}{d} \qquad \ldots (6.13)$$

Now, start the oscillations and measure t_v after every 10 or 20 oscillations*. If $\dot{\theta}_0\,(0)$ and $\dot{\theta}_0\,(n)$ are the amplitudes** at the zeroth and *nth* oscillation respectively, you have

$$\frac{\dot{\theta}_0\,(n)}{\dot{\theta}_0\,(0)} = \frac{A\,t_v(n)^{-1}}{A\,t_v(0)^{-1}} = \frac{t_v(0)}{t_v(n)}$$

Plot a graph between this amplitude ratio and the number of oscillations n.

Figure 6.4 shows the typical results of an experiment. You may do the following analysis from such a graph:

(*a*) Check whether the fall of $\dot{\theta}_0\,(n)$ with n is logarithmic. For this find out the number of oscillations completed as the amplitude falls in

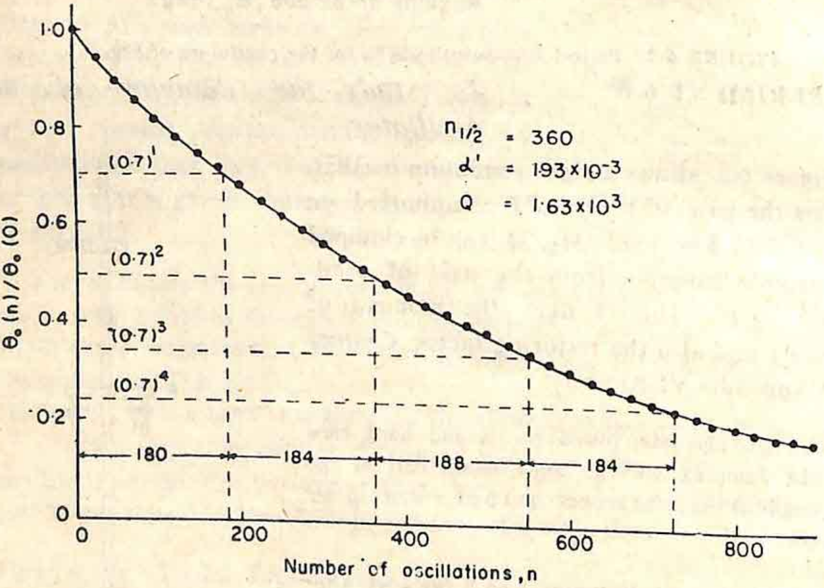

FIGURE 6.4. Angular velocity amplitude *vs* number of oscillations for the pendulum of Fig. 6.3.

---

* The period T is large enough to permit you to reset the timer to zero between any two passages.

** In the following discussion 'amplitude' will refer to the 'angular *velocity* amplitude.' With a timer it is far easier to measure this than to measure the angular *displacement* amplitude.

geometric progression. Figure 6.4 shows this for a typical value 0 7 for the geometric ratio. The numbers come out nearly equal, showing that $\dot{\theta}_0\ (n)$ varies logarithmically*.

(*b*) Determine $n_{1/2}$, the number of oscillations completed as the amplitude falls to half the original value.**

(*c*) Determine α', α and Q using the relations (see Appendix VI-C)

$$\alpha' = \frac{0.693}{n_{1/2}}\ ;\quad \alpha = \frac{\alpha'}{T}\ ;\quad Q = \frac{\pi}{\alpha'}$$

You may also plot a graph between the logarithm of the ratio $\dot{\theta}_0\ (n)/\dot{\theta}_0\ (0)$ against n. If this graph is a straight line it verifies Equation (6.10) straightaway. The negative slope multiplied by $\log_e 10$ gives α' and thence you get α and Q. Figure 6.5 shows the semilog plot for the case corresponding to Fig. 6.4.

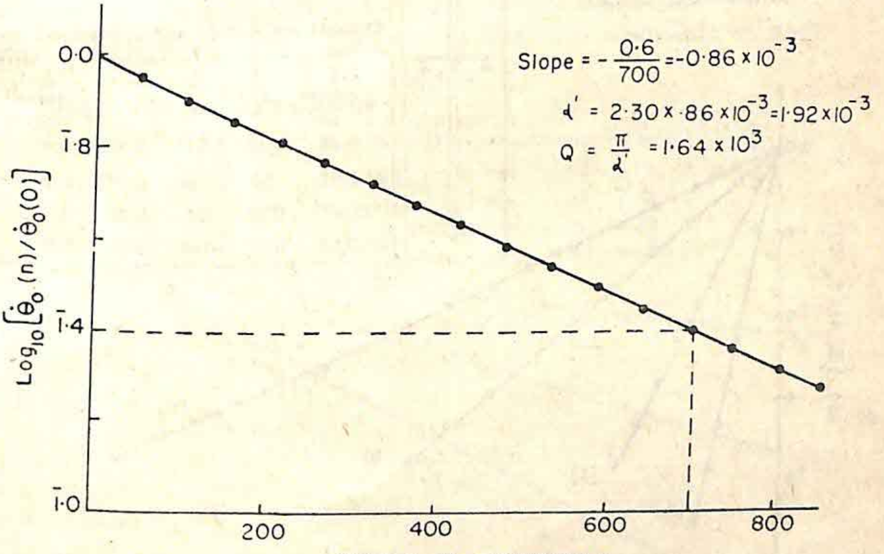

FIGURE 6.5. Semilog plot for the data of Fig. 6.4.

EXPERIMENT 6-C

To study the dependence of damping coefficient α on I and C of the oscillator.

Perform Experiment 6-B with a given pendulum and draw a semilog

---

*See, for example, *Physics Through Experiment*, Vol. I, Experiment 2-A.

**You could start from *any* $\dot{\theta}_0\ (n)$ and go up to half its value. If Equation (6.10) is true, the result in (*b*) should be independent of where the starting point is chosen.

plot like that of Fig. 6.5. Now repeat the process a number of times after shifting the position of the load M_1 (Fig. 6.3) in steps. Deduce the damping coefficient α in each case. Observe also the period T for each case.

Figure 6.6 shows the typical result of one such experiment. You may note that as the mass moves nearer the axis of oscillation, the α value increases: about 10-fold increase is seen in the range in which the experiment was done.

Now, the theory of damped oscillations (*see* Appendix VI-C) shows that $\alpha = r/2I$ (Equation 6.8a). You would therefore desire to know how r varies with the shift of load M_1. For this you need a knowledge of I. This may be computed from the distribution of mass. But we suggest an experimental procedure:

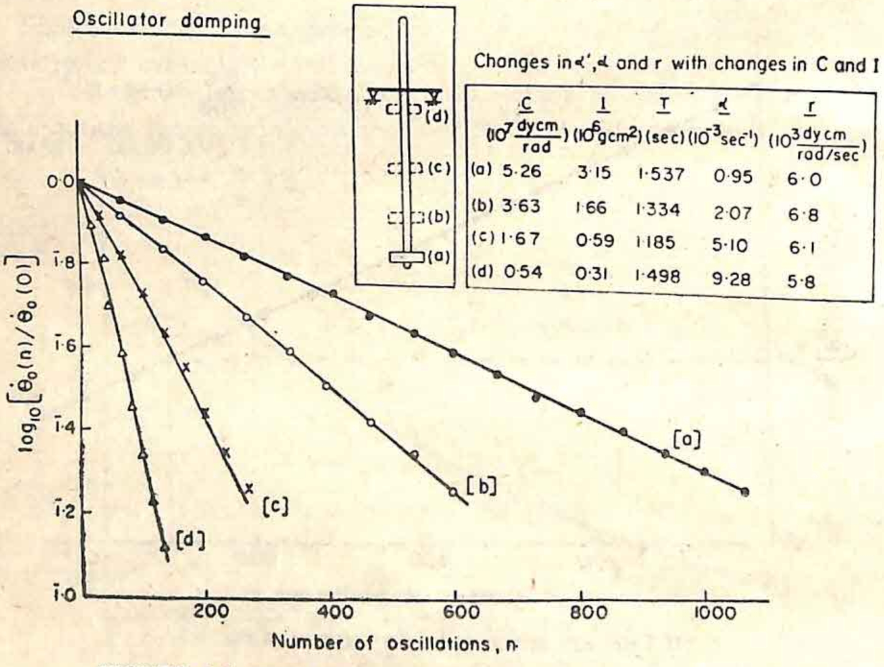

Changes in α', α and r with changes in C and I

	C ($10^7 \frac{\text{dycm}}{\text{rad}}$)	I (10^6 gcm^2)	T (sec)	α (10^{-3} sec^{-1})	r ($10^3 \frac{\text{dy cm}}{\text{rad/sec}}$)
(a)	5·26	3·15	1·537	0·95	6·0
(b)	3·63	1·66	1·334	2·07	6·8
(c)	1·67	0·59	1·185	5·10	6·1
(d)	0·54	0·31	1·498	9·28	5·8

FIGURE 6.6. Effect of redistribution of a given total mass of pendulum on damping.

Shift the loads M_1 and M_2 in opposite directions in such a way that $m_1 \Delta d_1 = m_2 \Delta d_2$. That keeps the centre of mass G (Fig. 6.3) unchanged. Hence if T and T' are the periods for the two cases, we have

$$\left(\frac{T}{T'}\right)^2 = \frac{I}{I+\Delta I} \qquad \ldots (6.14)$$

This leads to the determination of I, since ΔI is given by $m_1\Delta(d_1^2) + m_2\Delta(d_2^2)$.

The results of such deduction of *I* and *r* are shown in the inset in Fig. 6.6. You may note that although α varies so widely, *r* comes out constant within the limits of experimental error.

The analysis shows that for a given total mass of the oscillator the distribution of mass does not appreciably affect the damping factor *r*.

EXPERIMENT 6-D *To study the effect of the total mass on the damping factor r.*

Repeat Experiment 6-B, changing the total mass of the pendulum by mounting other loads. Estimate *I* each time by geometry; you can then convert the observed α values to *r* values (Equation 6·8a).

Figure 6.7 shows the graphs for a typical experiment. We note that the damping factor *r* increases considerably with the increase of the total mass *m*. The inset in Fig. 6.7 gives the relevant data and Fig. 6.8 shows a graphical plot of *r* against *m* in search of a possible relation.

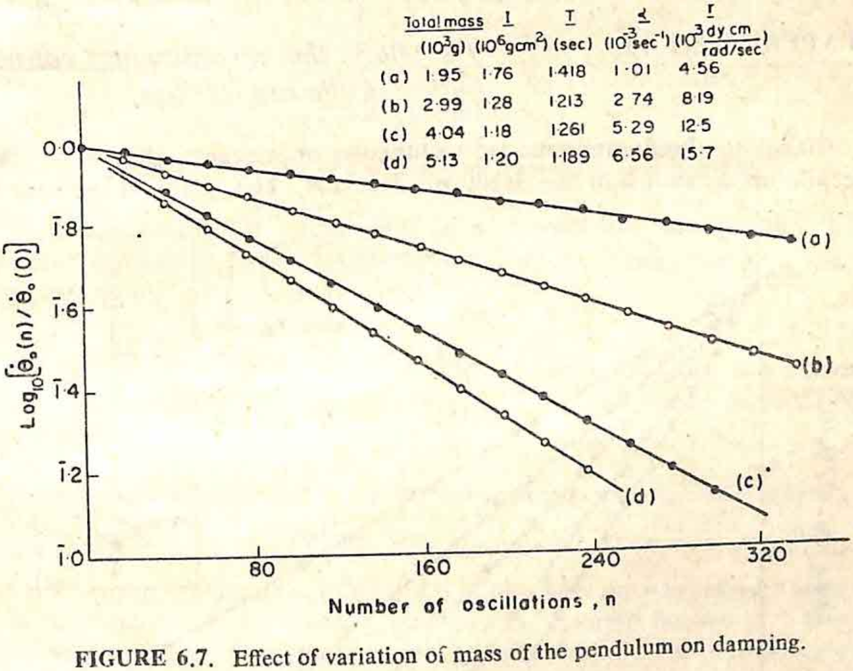

	Total mass (10^3g)	I (10^6gcm^2)	T (sec)	α (10^{-3}sec^{-1})	r ($10^3\frac{\text{dy cm}}{\text{rad/sec}}$)
(a)	1·95	1·76	1·418	1·01	4·56
(b)	2·99	1·28	1213	2 74	8·19
(c)	4·04	1·18	1·261	5·29	12·5
(d)	5·13	1·20	1·189	6·56	15·7

FIGURE 6.7. Effect of variation of mass of the pendulum on damping.

Within the range of experimental errors, one can draw a straight line in Fig. 6.8 through the observed points. However, extending it as such would lead to $r \rightarrow$ negative as $m \rightarrow 0$, which would hardly make sense. In fact there must be some contribution in *r* from air friction, which is size-dependent, not mass dependent. A finite positive intersection on the *r* axis is therefore to be expected. Hence one must collect more data before any relation can be found.

All the same one fact appears established from the experiment; the major contribution to r in a rigid pendulum is not due to air friction (viscosity), but is at the points of support. Any improvement in Q must therefore be sought there.

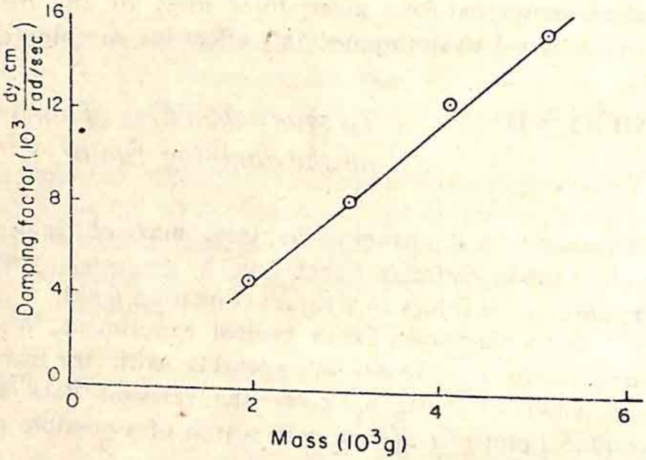

FIGURE 6.8. Variation of damping factor with mass (from the data of Fig. 6.7)

EXPERIMENT 6-E *To study the air-damping contribution in the oscillations.*

Clamp an aluminium vane (of rectangular or circular shape) on the pendulum as shown in the inset of Fig. 6.9. The plane of the vane is

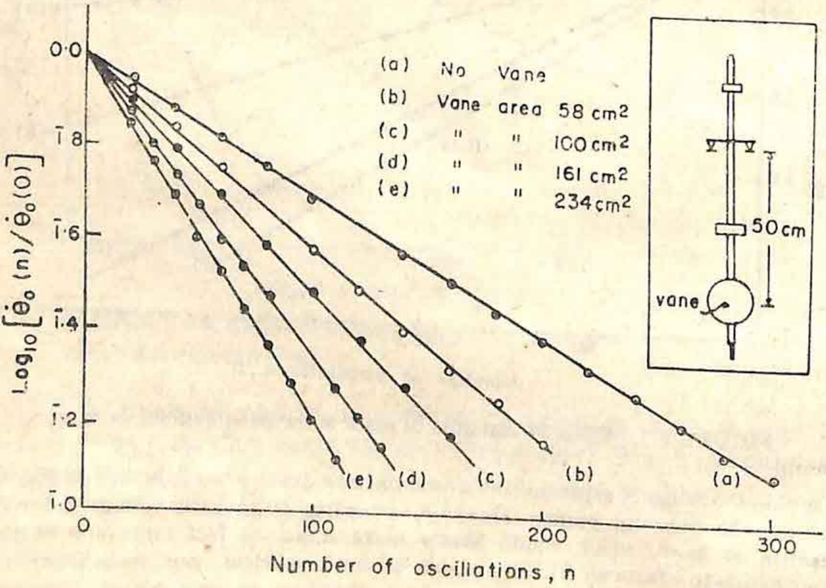

FIGURE 6.9, Effect of vane area on the oscillator damping.

perpendicular to the plane of oscillations. Measure the distance p_1 of the centre of the vane from the axis of oscillation. Measure also the period of oscillation T. Now repeat the damping study as in Experiment 6-B, with vanes of different areas mounted with the centre at the same distance p_1.

Figure 6.9 shows the typical results of an experiment like this. As the vane area increases the damping increases. Figure 6.10 shows a graph of α' *vs* vane area s. It comes out as a straight line, showing that the damping force on the vane is proportional to the vane area. You may therefore write

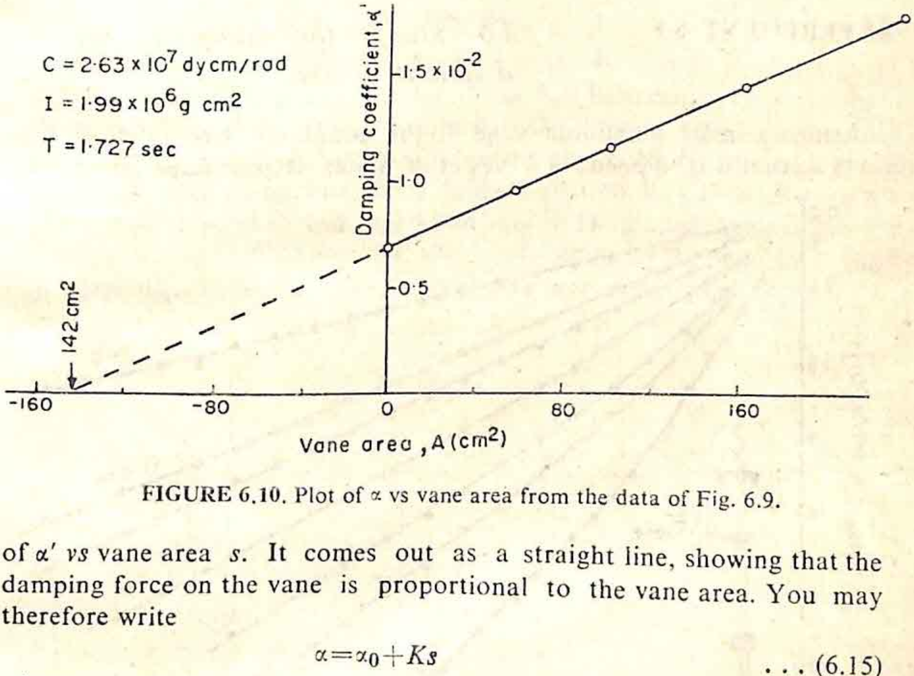

FIGURE 6.10. Plot of α vs vane area from the data of Fig. 6.9.

$$\alpha = \alpha_0 + Ks \qquad \ldots (6.15)$$

where α_0 is the damping constant without the vane and K is a constant depending on the medium and the distance of the vane from the axis of oscillation.

In the case of a sphere moving in a fluid the drag force is given by Stokes relation

$$F = -6\pi\eta\, av \qquad \ldots (6.16)$$

where η is viscosity of the fluid, v the velocity of the sphere and a its radius. Thus F is proportional to a, a linear dimension and not area. Obviously the case of a vane is distinctly different. Hydrodynamics tells us that for a flat vane moving along its normal the drag force is

$$F = -C_D \,.\, s\,\rho \frac{v^2}{2} \qquad \ldots (6.17)$$

where ρ is density of the medium and C_D is a numerical constant, whose value is 1.1 in our range of work. This shows that $F \propto s$, as our experiment would seem to confirm. But there is a serious difficulty: dependence on v goes to the second power

(v^2). This would need revision of the entire theory as given in Appendix VI-C, since Equation VI-C (1) would change to

$$\Omega' = -r_0\,\dot{\theta} - r\,\dot{\theta}^2 \qquad \ldots (6.18)$$

the first term belonging to the original drag (without the vane) and the second being the contribution due to the vane.

We shall not go farther in the analysis, except to mention that shape of the drag device (vane or sphere or cylinder) makes a major difference in the parametric dependence of the drag force, and can therefore be a subject of detailed study by itself.

EXPERIMENT 6-F *To study the damping due to a vane in water.*

Attach a small aluminium vane to the pendulum (*see* inset of Fig. 6.11) so that it is dipped in a vessel of water. Repeat Experiment 6-E, with the difference that this time you may study the dependence of damping on the distance p_1 of the centre of the vane from the axis of oscillation.

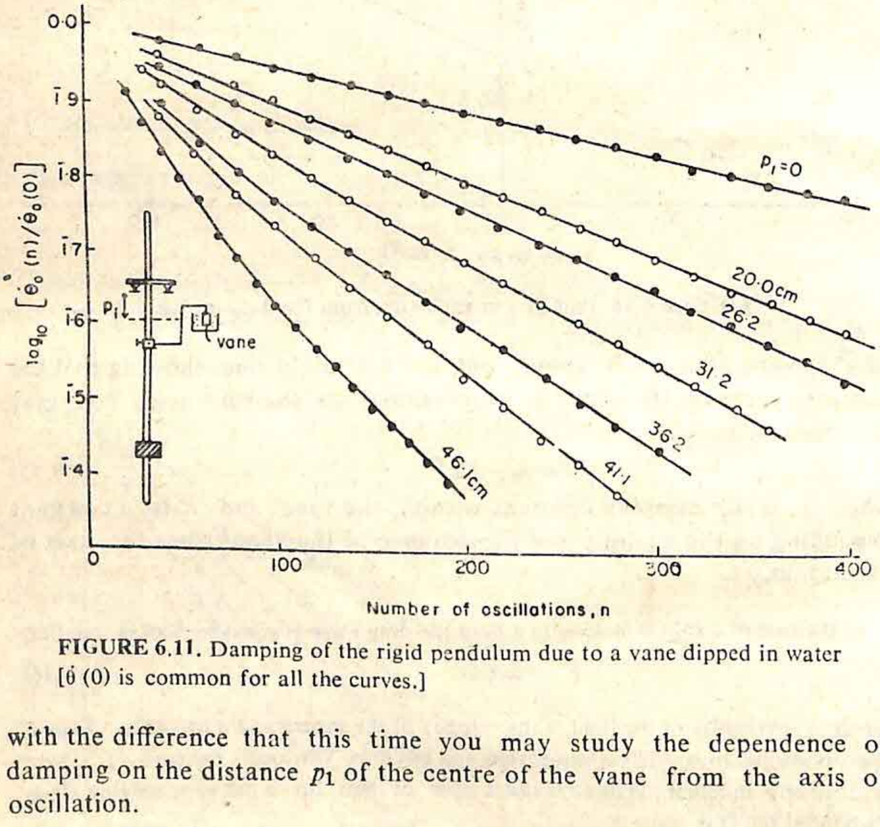

FIGURE 6.11. Damping of the rigid pendulum due to a vane dipped in water [$\dot{\theta}$ (0) is common for all the curves.]

Figure 6.11 shows the results of an experiment with a flat vane of area 4 cm^2. The initial angular velocity amplitude was kept the same in all the cases, so that a given line parallel to the n axis in the graph corresponds to a given $\dot{\theta}_0$. You may notice that while the semilog plots come out close to straight line in the low p_1 range, they show curvatures in the high p_1 range—the curvature decreasing as $\dot{\theta}$ decreases. Obviously the amplitude fall is not logarithmic and the theory of Appendix VI-C breaks down more seriously.

If we accept Equation (6.17) and remember that $v=p_1\dot{\theta}$, the damping torque now becomes

$$\Omega'(\text{vane})=\text{force}\times p_1=-Kp_1{}^3\,\dot{\theta}^2 \qquad \ldots (6.19)$$

where $K=C_D\, S\rho/2$. Equation VI-C(1) of Appendix VI-C now changes to

$$\Omega'=-r_0\dot{\theta}-Kp_1{}^3\,\dot{\theta}^2 \qquad \ldots (6.20)$$

If the second term is dominant—as it would be at high p_1 and high $\dot{\theta}$—the departures from exponential decay will be serious. This is what is observed. The slope of log $\dot{\theta}$ vs n curve at a given point on the curve may still be called α', but it will not be admissible to equate this with $TKp_1{}^3/2I$ as a parallel to $Tr/2I$ [vide Equation VI C(11)]. Figure 6.12 shows the slope α' at ordinate I.8 in Fig. 6.11 plotted against $p_1{}^3$. The straight line fit would show that the contribution of the vane in α' shows $p_1{}^3$ dependence, although the decay is now not exponential.

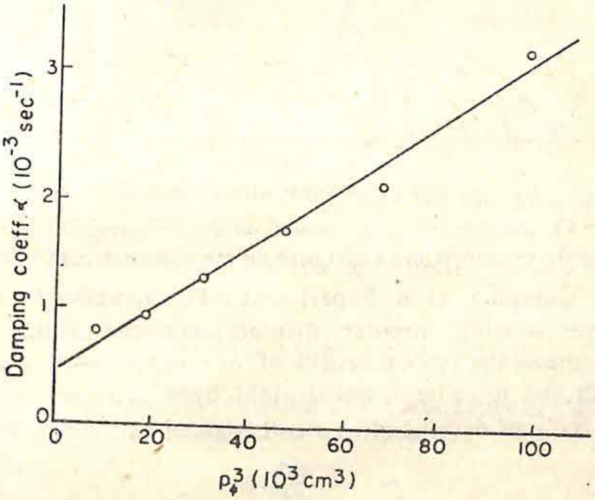

FIGURE 6.12. Variation of damping factor with $P_1{}^3$ (The α values corresponding to ordinate $\bar{1}$.8 in Fig. 6.11 are used here)

EXPERIMENT 6-G *To study the electromagnetic damping using a coil.*

Mount a magnet on the pendulum with its length horizontal and in the plane of oscillation. Place a pair of coils C_1, C_2 (Inset, Fig. 6.13) symmetrically, such that during the oscillations the magnet moves along the common axis of the coils. The coils may be connected in series* and the circuit completed through a variable resistance R (not shown).

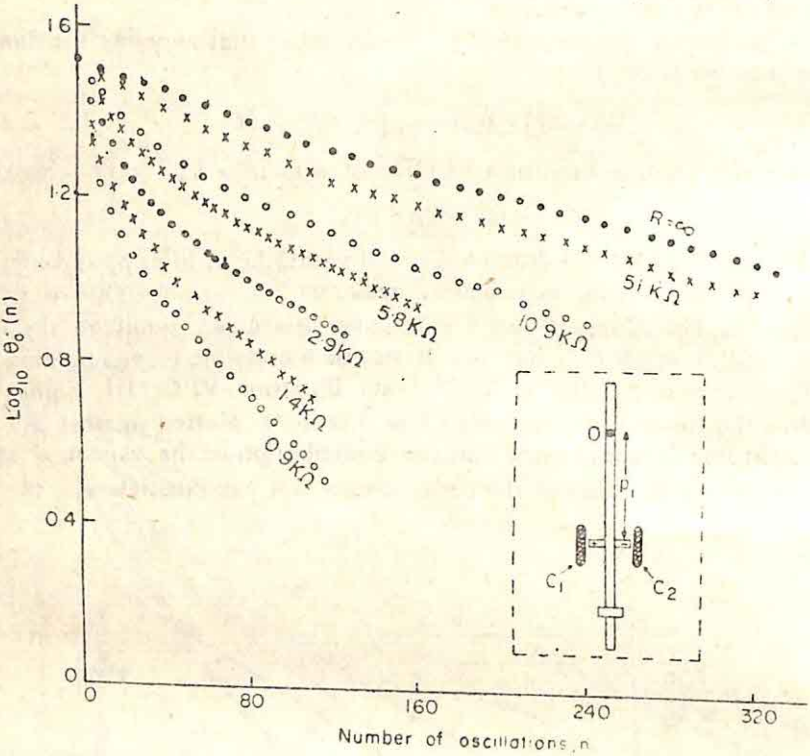

FIGURE. 6.13. Damping of a rigid pendulum due to interaction between a magnet mounted on the pendulum and a coil with different resistance in series with it.

Study the damping as in Experiment 6-F, changing R each time, but keeping the starting angular displacement the same in all cases. Figure 6.13 shows the typical results of one experiment. Note that the semilog plots are, in general, not straight lines.

The induced emf developed in a coil is given by

$$e = -\frac{d\phi}{dt} \qquad \ldots (6.21)$$

where ϕ is magnetic flux through the coil. The current produced is

$$i = \frac{e}{R} = -\frac{1}{R}\,\frac{d\phi}{dt}$$

This current interacts with the magnet to produce a damping force

$$F = Ai = -\frac{A}{R}\,\frac{d\phi}{dt}$$

---

*Two coils may be connected in series in two days. If c_1, d_1 are the terminals of one and c_2, d_2 of the other, you can connect d_1 to either c_2 or d_2. For resistance this make no difference; for this experiment the two are very different. Learn it by doing, and then try to explain why?

where A is dependent on the strength of the magnet and its geometric placement relative to the coil. If the magnet is at distance p_1 from the axis of oscillation, the damping torque is

$$\Omega' = -\frac{Ap_1}{R}\frac{d\phi}{dt}$$

The $-r\dot{\theta}$ term in the theory of damped oscillator (Appendix VI-C) is this torque.

Now, $d\phi/dt$ is not just proportional to $\dot{\theta}$ (*i.e.*, $d\theta/dt$) in this case. Figure 6.14 shows schematically the lines of magnetic induction due to a magnet. For a coil placed as shown in this figure the rate of change of flux $(-d\phi/dt)$ will not be proportional to velocity of the magnet. For this reason the theory of Appendix VI-C is no longer valid, and the plot of $\log \dot{\theta}_0(n)$ against n is not expected to be a straight line. That is in line with the experimental results (Fig. 6.13).

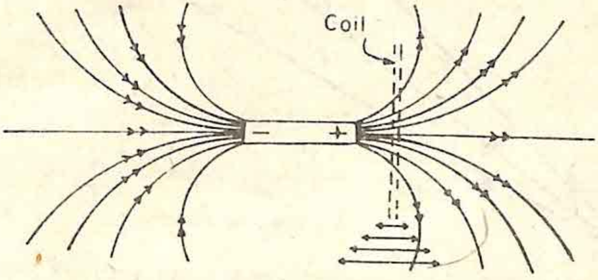

FIGURE 6.14. Magnetic flux lines through a coil placed coaxially.

However, for oscillations of a given amplitude we may introduce a relation like

$$\frac{d\phi}{dt} = A'v = A'p_1\dot{\theta}$$

where A' is some constant representing the mean ratio of $d\phi/dt$ and v*. Using this in Equation (6.20) with $\Omega' = -r\dot{\theta}$ leads to

$$r = -\frac{AA'p_1^2}{R} \qquad \dots (6.22)$$

and a corresponding value of $\alpha' = rT/2I$

Now in Figure 6.13 draw a horizontal line which corresponds to a given amplitude $\dot{\theta}_0$ At the intercepts determine the slopes (α') of the curves, whence you get α $(= \alpha'/T)$. Plot a graph showing α against $1/R$. Different horizontal lines correspond to different $\dot{\theta}_0$ and each may have a different α vs $1/R$ curve. See if these graphs come out as straight lines. If so, it shows that the electromagnetic damping is proportional to $1/R$.

---

* This mean value will *not* be the same for oscillations of different amplitudes.

Figure 6.15 shows the α vs $1/R$ plots for three $\dot{\theta}_0$ values in Fig. 6 13. The points fit nearly to a straight line in each case. The increase of slope with increasing $\dot{\theta}_0$ shows that A' in Equation 6.22 increases in the same order.

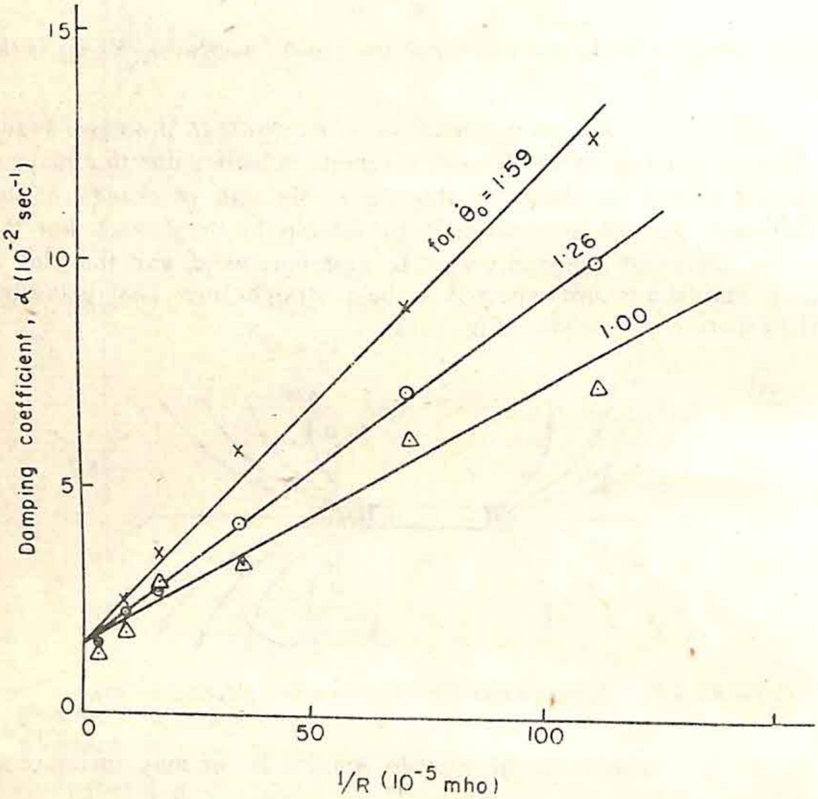

FIGURE 6.15. Variation of damping coefficient with $1/R$ (using the data of Figure 6.13).

EXPERIMENT 6-H . *To study electromagnetic damping using a metal sheet.*

In the arrangement for Experiment 6-G replace the coils with a plane metal sheet standing parallel to the plane of oscillation. Let the lateral separation between the magnet and the plane of the sheet be d.

Make the damping study for different values of d and plot the log $\dot{\theta}_0$ vs n graphs for each case. Figure 6.16 gives the typical results of one such study. The sheet used was that of aluminium and was 2 mm thick. You may note that, unlike Experiment 6-G, the graphs come out as straight lines. Try to explain this significant difference. Figure 6.17 shows the plate relative to the magnetic lines of induction. Treating the plate oscillating (relative to the magnet) you may see how this case differs from that of the coil oscillating.

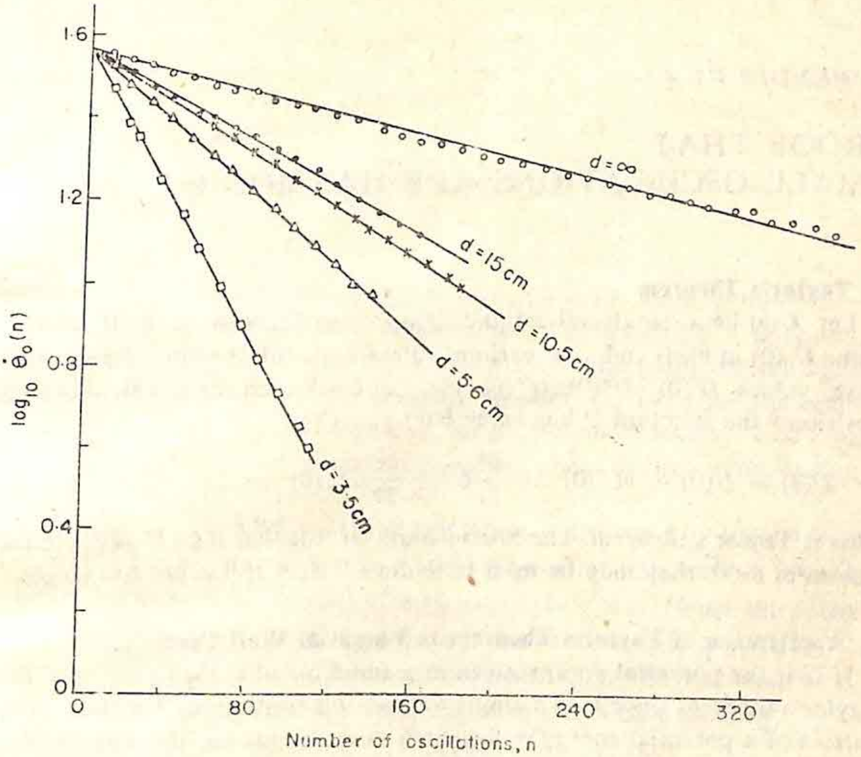

FIGURE 6.16. Electromagnetic damping of a rigid pendulum carrying a magnet oscillating close to a metal sheet.

From Fig. 6.16 you may observe that the damping increases rapidly as the plate to magnet separation decreases. You may draw a graph between α and $1/d$ to represent this fact. What should α tend to as $d \to \infty$?

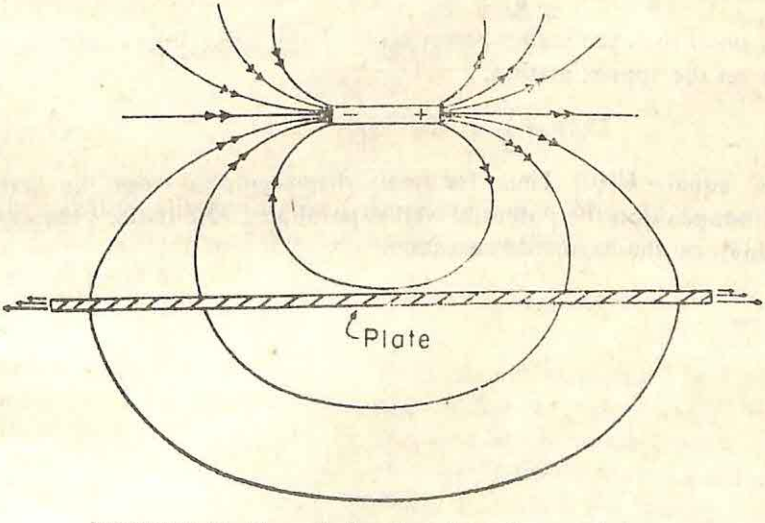

FIGURE 6.17. Magnetic flux lines through a metal sheet.

APPENDIX VI-A

PROOF THAT SMALL OSCILLATIONS ARE HARMONIC

1. Taylor's Theorem

Let $U(\theta)$ be a single-valued and continuous function of θ. If it has a value $U(0)$ at $\theta=0$ and the various differentials of U with respect to θ have values $U'(0)$, $U''(0)$, $U'''(0)$ etc., at $\theta=0$, then for a neighbouring position θ the function U has value $U(\theta)$ given by

$$U(\theta) = U(0) + \theta U'(0) + \frac{\theta^2}{2!}U'' + \frac{\theta^3}{3!}U'''(0) + \dots \qquad \dots \text{VI-A (1)}$$

This is Taylor's theorem. The salient point of it is that if U, U', U''' etc are known *at* $\theta=0$, they may be used to deduce U at θ, if θ is not too large.

2. Application of Taylor's Theorem to Potential Well Case

If U is the potential energy given as a function of θ, then you may use Taylor's theorem since U is a single-valued and continuous function. The *bottom* of a potential energy well (which corresponds to the equilibrium state) has $U'=0$ and U'' positive. If this bottom is taken as the origin for both U and θ we also have $U(0)=0$, and θ is then the displacement coordinate relative to the equilibrium position.

Equation VI-A (1) then becomes

$$U(\theta) = \frac{\theta^2}{2}U''(0) + \frac{\theta^3}{6}U'''(0) + \frac{\theta^4}{24}U''''(0) + \dots \qquad \dots \text{VI-A (2)}$$

If θ is *small* then the higher power terms have negligible contribution, and you get the approximation:

$$U(\theta) = \frac{\theta^2}{2}U''(0) = \tfrac{1}{2}C\theta^2 \qquad \dots \text{VI-A (3)}$$

where C equals $U''(0)$. Thus for small displacements from the stable equilibrium position the potential well is parabolic. Oscillations therefore approximate to the harmonic character.

APPENDIX VI-B

THEORY OF THE RIGID PENDULUM

Figure VI-B (1) shows the essential features of a rigid pendulum. A rigid bar carries two adjustable masses and oscillates about a horizontal axis perpendicular to the plane of the figure and passing through O. Let G be the centre of mass of the pendulum, m its mass and I the moment of inertia about the axis of oscillation. Let $GO=l$.

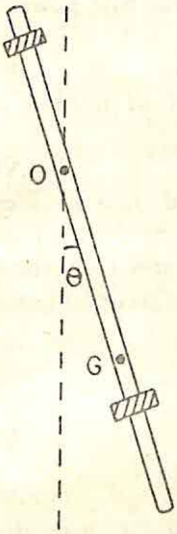

FIGURE VI-B (1). A rigid pendulum.

If the pendulum is displaced by angle θ from the equilibrium position, the centre of mass rises up by height $l\,(1-\cos\theta)$. Hence the potential energy relative to $\theta=0$ state is given by

$$U=mgl\,(1-\cos\theta)=\tfrac{1}{2}(mgl)\theta^2, \text{ for small } \theta.$$

The restoring couple Ω is thus given by

$$\Omega=-\frac{dU}{d\theta}=-C\theta \qquad \text{. . . VI-B (1)}$$

where $C=mgl$ . . . VI-B (2)

The equation of motion, neglecting friction, is therefore

$$I\ddot{\theta}+C\theta=0 \qquad \text{. . . VI-B (3)}$$

This equation has the general solution

$$\theta=\theta_0\cos(\omega_0 t+\delta) \qquad \text{. . . VI-B (4)}$$

where ω_0 is given by

$$\omega_0=\sqrt{\frac{C}{I}} \qquad \text{. . . VI-B (5)}$$

as can be seen by substitution from Equation (4) into (3). θ_0 and δ are constants of integration, determined by the initial conditions. The frequency ν is given by

$$\nu=\frac{\omega_0}{2\pi}=\frac{1}{2\pi}\sqrt{\frac{C}{I}} \qquad \text{. . . VI-B (6)}$$

The frequency of oscillation may be changed by changing C or I or both. From Fig. VI-B (1) you may note that sliding the upper mass is more effective in this: raising it up would increase I and decrease C (since G rises up, whence l decreases), thus reducing ν considerably; lowering it does the opposite. The effect of moving the lower mass does not change ν appreciably, because I and C change in the same direction, though unequally.

APPENDIX VI-C

THEORY OF DAMPED OSCILLATIONS

1. The Assumptions

We shall assume that the oscillations are in a range of amplitude for which the restoring torque is proportional to the displacement. We also take the damping torque Ω' to be proportional to the first power of the angular velocity $\dot{\theta}$, so that we write

$$\Omega' = -r\,\dot{\theta} \qquad \ldots\text{VI-C(1)}$$

where r is called *the damping factor.* The equation of motion of the oscillator [VI-A (3)] then becomes

$$I\,\ddot{\theta} + r\,\dot{\theta} + C\theta = 0 \qquad \ldots\text{VI-C(2)}$$

The Assumption $\Omega' = -r\dot{\theta}$ may or may not be valid in a given case. It must be remembered that what follows is based on the validity of this assumption. Conversely, any experimental departures from the theory given below may be related with deviations from this assumption.

2. Solution of the Equation of Motion

Equation VI-C(2) may be put in the form

$$\ddot{\theta} + 2\alpha\dot{\theta} + \omega^2{}_0 = 0 \qquad \ldots\text{VI-C(3)}$$

where

$$\alpha = \frac{r}{2I} \qquad \ldots\text{VI-C(4)}$$

and ω_0 has the same meaning as in Equation VI-A(5). If we try the solution

$$\theta(t) = ae^{\beta t}$$

Equation VI-C(3) leads to

$$\beta^2 + 2\alpha\beta + \omega^2{}_0 = 0$$

or

$$\beta = -\alpha \pm i\sqrt{\omega^2{}_0 - \alpha^2}$$

The most general solution of Equation VI-C(3) is therefore

$$\theta(t) = a_1 e^{(-\alpha + i\sqrt{\omega_0{}^2 - \alpha^2})t} + a_2 e^{(-\alpha - i\sqrt{\omega_0{}^2 - \alpha^2})t}$$

or

$$\theta(t) = \theta_0(0)e^{-\alpha t}\cos(\omega_0{}'t + \delta) \qquad \ldots\text{VI-C(5)}$$

where

$$\omega'{}_0 = \sqrt{\omega_0{}^2 - \alpha^2}$$

and $\theta_0(t)$ and δ are constants (related with a_1 and a_2) decided by the initial conditions. Comparing Equation VI-C(5) with Equation VI-B(4), which applies in the damping-free case, one finds that there are two differences: (*i*) the frequency decreases from ω_0 to $\sqrt{\omega_0{}^2 - \alpha^2}$ and (*ii*) the amplitude falls with time according to $e^{-\alpha t}$ term.

The corresponding equation for angular velocity $\dot{\theta}(t)$ will be

$$\dot{\theta}(t)=\dot{\theta}_0(0)e^{-\alpha t}\cos(\omega_0' t+\delta') \qquad \ldots\text{VI-C(6)}$$

$\dot{\theta}_0(0)$ and δ' are related with $\theta_0(0)$ and δ through*

$$\dot{\theta}_0(0)=\omega_0'\,\theta_0(0) \quad \text{and} \quad \delta'=\delta+\frac{\pi}{2}$$

3. The Decay of Amplitudes

For displacement amplitude and angular velocity amplitude at time t, Equations VI-C(5) and VI-C(6) above give

$$\theta_0(t)=\theta_0(0)e^{-\alpha t} \qquad \ldots\text{VI-C(7a)}$$

$$\dot{\theta}_0(t)=\dot{\theta}_0(0)e^{-\alpha t} \qquad \ldots\text{VI-C(7b)}$$

Thus both θ_0 and $\dot{\theta}_0$ fall exponentially and at the same rate. The constant α is called the *damping coefficient* for amplitude.

The times in which the amplitude falls to $1/e$ and $\frac{1}{2}$ of the original are designated by $t_{1/e}$ and $t_{1/2}$ respectively, and you can see that

$$t_{1/e}=\frac{1}{\alpha} \quad \text{and} \quad t_{1/2}=\frac{0.693}{\alpha} \qquad \ldots\text{VI-C(8)}$$

The amplitude may also be expressed in terms of the number of oscillations completed (n), using $n=t/T$, where T is the period of oscillation. Equation VI-C(7b), for instance, then becomes

$$\dot{\theta}_0(n)=\dot{\theta}_0(0)e^{-\alpha' n} \qquad \ldots\text{VI-C(9)}$$

where $$\alpha'=\alpha T \Rightarrow n_{1/2}=\frac{0.693}{\alpha'} \qquad \ldots\text{VI-C(10)}$$

Combining Equation VI-C(10), (8) and (4) you may note the interrelations

$$\alpha'=\alpha T=\frac{0.693}{n_{1/2}}=\frac{r}{2I}\,T \qquad \ldots\text{VI-C(11)}$$

4. Energy Dissipation

The energy of oscillation (E) is proportional to $(\dot{\theta}_0)^2$. Hence Equation VI-C(9) gives

$$E(n)=E(0)e^{-2\alpha' n} \qquad \ldots\text{VI-C(12)}$$

The energy dissipation *per cycle* is thus given by

$$-\frac{dE}{dn}=2\alpha'.E \qquad \ldots\text{VI-C(13)}$$

and the energy dissipation *per unit time* (called power loss) is given by

$$P=-\frac{dE}{dt}=\frac{2\alpha'}{T}.E=2\alpha E \qquad \ldots\text{VI-C(14)}$$

---

* These are first approximations, valid for low α.

The power loss may also be deduced from first principles, using Equation VI-C(1). If the instantaneous power loss is P_{inst}, we have

$$P_{inst} = -\Omega'\dot{\theta} = -r(\dot{\theta})^2$$

$$P = \text{average of } P_{inst} = -\tfrac{1}{2}r(\dot{\theta}_0)^2$$

because *average* $(\dot{\theta})^2 = \frac{1}{2}(\dot{\theta}_0)^2$ in harmonic oscillations. Now use of Equation VI-C(4) and $\frac{1}{2}I(\dot{\theta}_0)^2 = E$ leads to the result VI-C(14).

5. Quality Factor

An oscillator will be called *good* if it can complete a larger number of oscillations before its energy falls to a given fraction. A quantitative measure of the 'quality' is the '*quality factor*' Q defined as 2π times the number of oscillations completed by the oscillator as the energy falls to $1/e$ times the initial value. In view of Equation VI-C(12) we thus get

$$Q = 2\pi \times \frac{1}{2\alpha'} = \frac{\pi}{\alpha'} \qquad \text{. . .VI-C(15)}$$

In view of the relations VI-C(11) and $w'_0 = 2\pi/T$, the expression for Q can be put in several forms:

$$Q = \frac{\pi}{\alpha'} = \frac{\pi}{\alpha T} = \frac{\pi . 2I}{r . T} = \frac{w'_0}{2\alpha} \qquad \text{. . .VI-C(16)}$$

It may be noted that in the equation of motion the damping is expressed as proportional to the damping factor r. The directly observed parameter is the damping coefficient α which is given by $r/2I$. Therefore, among two oscillators with equal r, the one with larger I has smaller damping and hence higher Q.

It may also be noted that Q is proportional to $1/\alpha'$ and not to $1/\alpha$. Therefore, for equal α the system with smaller period T (higher frequency ν) will have higher Q. As an example you may compare a good pendulum of $1/\alpha \approx 500\ s$ with an excited sodium atom for which $1/\alpha$ is much smaller, being $\sim 10^{-10}\ s$. But since the corresponding periods T are $\sim 1 s$ and $\sim 10^{-15}\ s$ respectively, the Q values in the two cases come to $\sim 500\ \pi$ and $10^5\ \pi$ respectively. Thus the Na atom (treated as a classical oscillator) has a much higher Q, although its $1/\alpha$ is much smaller than that of the pendulum.

7

STUDY OF FORCED OSCILLATIONS

7.1. GENERAL

Consider an oscillator A of natural frequency ω_0. Once set in oscillations it loses energy, as you have seen in the experiments of Chapter 6. To maintain oscillations energy may be fed to A in many ways, two of which are the following:

(*a*) An oscillator B may apply a periodic torque of frequency ω which is independent of ω_0.

(*b*) A non-periodic energy source C may apply a torque on A with the frequency ω_0, determined by A itself.

In the second case A is called a *maintained oscillator*, in the sense that C has no frequency of its own but just serves to maintain the vibrations of A. In the first case A becomes a *forced oscillator*, that is, it gives up the oscillations of its own frequency ω_0 and oscillates with frequency ω of the oscillator B. It is customary to call B the driver and A the driven oscillator.

Through the experiments in this chapter you will study the nature of forced oscillations, *i.e.*, how the amplitude and phase of the oscillations of A depend on the frequency ω and the parameters of A, like its I and Q (cf. Chapter 6).

7.2. FORCED OSCILLATIONS

Let the oscillator B apply on A a torque given by

$$\Omega_{BA} = \Omega_0 \cos \omega t \qquad \ldots (7.1)$$

Appendix VII-A gives the theory of oscillations under this torque and the salient results are as follows:

(*a*) The natural vibrations of A (frequency ω_0) die out with time and it starts oscillating with frequency ω of the driver B.

(*b*) The amplitude of A goes on increasing with time, till it reaches a steady value. The oscillations of A after this stage are called the *steady state* oscillations. The stages passed through by A before this are called *transients*.

(*c*) The displacement amplitude of the driven oscillator in the steady state is given by

$$\theta_0 = \frac{\Omega_0/I}{[(\omega_0^2-\omega^2)^2+4\kappa^2\omega^2]^{1/2}} \qquad \ldots (7.2)$$

where I is inertia factor and κ the damping coefficient of oscillator A.

(*d*) The phase of the driven oscillator lags behind that of the driver by angle δ given by

$$\tan\delta = \frac{2\kappa\,\omega}{\omega_0^2-\omega^2} \qquad \ldots (7.3)$$

(*e*) The velocity amplitude $\dot{\theta}_0$ is given by

$$\dot{\theta}_0 = \omega\theta_0 = \frac{\omega\Omega_0/I}{[(\omega_0^2-\omega^2)^2+4\kappa^2\omega^2]^{1/2}} \qquad \ldots (7.4)$$

You have to measure θ_0, δ and $\dot{\theta}_0$ for different frequencies ω of the driver to see if the forced oscillations show the expected behaviour. The theory assumes that the only effect of coupling A with the driver B is the imposition of the torque Ω_{BA}. It is possible that the coupling may produce other effects too on A, and it is also possible that the torque may not be harmonic as assumed in Equation (7.1). You may therefore consider the experimental results with an open mind, the theory being only a broad framework.

7.3. DESCRIPTION OF THE APPARATUS

Figure 7.1 gives a photograph of the system used. On the left is shown the maintained oscillator used as the driver, and on the right is the driven oscillator. One thread joining the two oscillators carries a small load, which provides the 'coupling' between the two oscillators, *i.e.*, the application of torque Ω_{BA} on A due to B. A separate pair of threads attached to two oscillators carries a convergent lens. The image of a point source (a torch bulb) made by this lens on a vertical screen produces Lissajous figures as the pendulums oscillate. The details of these are as follows:

(*a*) Maintained Oscillator

The amplitude of the torque Ω_{BA} (Equation 7.1) is proportional to the amplitude of the driver, if other things are constant. In our study the amplitude of the driver should therefore remain constant not only with time but also with the change in its frequency ω, which will be effected by sliding the loads on it. The device used is shown in Fig. 7.2. A magnet is attached to the pendulum so that the axis of the magnet is horizontal and in the plane of oscillation. The coils P_1 and P_2 are provided on the two sides and connected to a circuit, which works as follows. Oscillations of the magnet generate an emf in coil P_1; this is amplified and fed to coil P_2 to generate a current which applies a force on the magnet. Now one requirement is that this current should be in the proper phase so that in each oscillation some energy is fed to the oscillator. The second requirement is that the energy feeding should decrease to just the maintenance level as the amplitude reaches the desired preset value. The electronic circuit is arranged to meet these requirements. If desired, the preset value of the amplitude may be changed by turning a knob on the control panel.

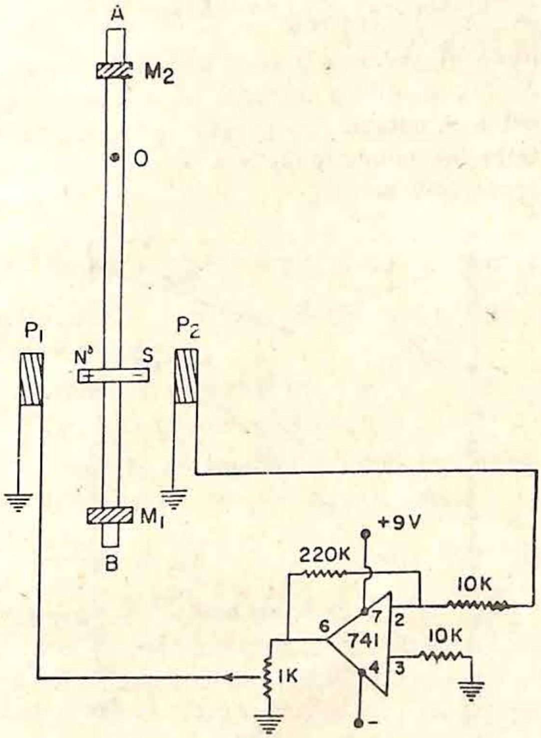

FIGURE 7.2. The maintained oscillator and the related circuit.

In forced oscillations one desires that the 'driver' have far greater inertia than the 'driven', so that for a given energy drawn from it by the driven oscillator, the driver's loss of amplitude may not be large.* For this reason the driver pendulum may be loaded with about three times the loads on the driven pendulum. Since both I and C increase with the load, the frequency still has the same order of magnitude and may be varied by shifting the masses.

(*b*) The Coupling

Details of how the torque Ω_{BA} on A due to B depends on the geometry of the threads (Fig. 7.1) and the coupling mass m are discussed in Appendix VII-B. Figure 7.3 shows the essential geometry and the parameters l, p, m and ϕ. The torque Ω_{BA} comes out to be

---

*You may appreciate this point more after studying coupled oscillators (Chapter 8).

$$\Omega_{BA}=\frac{mgp^2}{2l\cos^3\phi}\,\theta_B \qquad \ldots (7.5)$$

Since $\theta_B=\theta_{B0}\cos\omega t$, comparison with Equation (7.1) leads to

$$\Omega_0=\frac{mgp}{2l\cos^3\phi}\,\theta_{B0}=K\theta_{B0} \qquad \ldots (7.6)$$

i.e., the amplitude of the torque on A due to B is proportional to the amplitude of B. The coupling strength K is most easily changed by changing the load m. A notable fact proved in Appendix VII B is that in the 90° geometry for mounting the lens (Fig. 7.3) the lens weight does not contribute appreciably to Ω_{BA}.

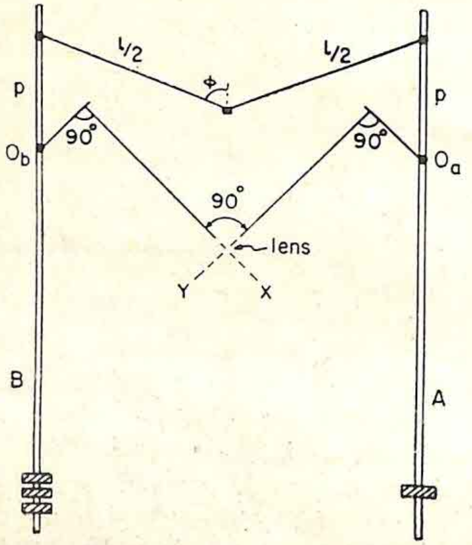

FIGURE 7.3. Arrangements for coupling between two oscillators and for producing Lissajous figures.

(*c*) Measurement of Relative Amplitudes and Phases

One of the simplest methods for measurement of relative amplitudes and phases of two oscillations of the *same frequency** is to use Lissajous figures. Contributions from the two oscillations are superposed along mutually perpendicular directions, and the resultant movement is, in general, an ellipse. We have devised an optical method for the formation of Lissajous figures. Figure 7.3 shows that a clockwise displacement of driver B would move the lens along the X-direction by an amount $p'\theta_B$ and a clockwise displacement of the driven oscillator A would move the lens along the Y-direction by an amount $p'\theta_A$.* Thus the oscillations are superposed on the lens in equal proportions. The image of the torch bulb shows these oscillations on the screen S (Fig. 7.4) with a common magnifying factor a. Thus for the x and y vibrations of the spot of light on the screen we may write

---

*In the steady state of forced oscillations this condition is satisfied.

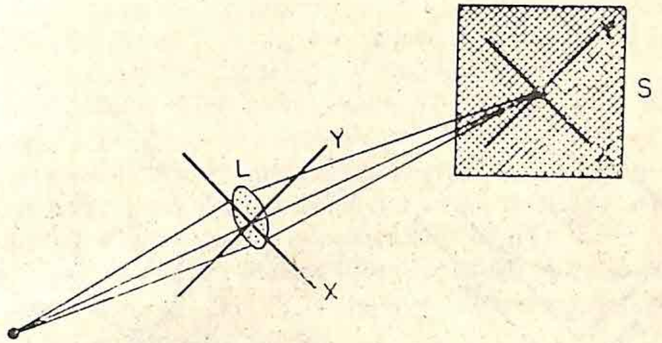

FIGURE 7.4. Formation of Lissajous figures on the screen S.

$$x = p'a\,\theta_{B0}\cos\omega t = x_0\cos\omega t \qquad \ldots (7.7a)$$

$$y = p'a\,\theta_0\cos(\omega t-\delta) = y_0\cos(\omega t-\delta) \qquad \ldots (7.7b)$$

where x_0 and y_0 are the amplitudes of oscillation of the spot of light along the x and y axes respectively. One can see that

$$\frac{y_0}{x_0} = \frac{\theta_0}{\theta_{B0}} = K\frac{\theta_0}{\Omega_0} \qquad \ldots (7.8)$$

Thus measurements of x_0 and y_0 lead to the ratio θ_0/Ω_0 *i.e.*, the *amplitude response* of the driven at the given frequency of the driver. The observing screen may be a graph paper with its lines inclined at 45° from the horizontal. Then you may observe the extreme range of displacements of the spot of light along the two axes, and obtain their ratio.

On the graph paper you may mark the rest position of the spot of light and the X and Y axes. The Lissajous figure traced by the spot of light intercepts the X-axis at two point P, Q (Fig. 7.5) and you may note the separation PQ, half of which may be called x. Since these points correspond to $y=0$, Equation 7.7(b) gives $\omega t-\delta=(n+\frac{1}{2})\pi/2$, whence Equation 7.7(a) gives $x=\pm x_0\sin\delta$.

Thus you get the phase lag δ from

$$\left|\sin\delta\right| = \frac{x}{x_0} \qquad \ldots (7.9)$$

The sign of δ is positive (*i.e.*, there is a lag of phase) if the curve is traced anticlockwise. Further δ lies between 0 and $\pi/2$ or $\pi/2$ and π according as the peak x and y values are reached in the first or the second quadrant [Figs. 7.5 (a) and (b)]. You may check these statements using Equation 7.7.

---

*The X and Y displacements are not affected (to a first approximation by the displacements of the driven and the driver respectively.

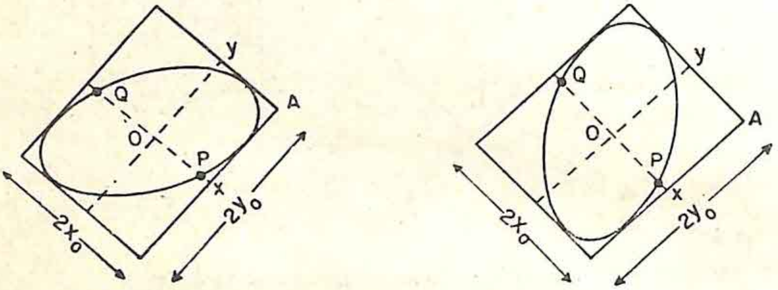

(*a*) (*b*)

FIGURE 7.5. Explaining the use of Lissajous figures.

(*d*) Measurement of Velocity Amplitude

This may be done as in the experiments of Chapter 6, using the timer and sensor. If the sensing pin diameters and their distances from the axis of oscillation are not equal for the two oscillators, this fact should be accounted for.

EXPERIMENT 7-A *To study the amplitude response in forced oscillations.*

Set up the driven oscillator A and the driver oscillator B as shown in Fig. 7.1.* First remove the coupling load and measure the period T_0 (hence frequency ν_0) of the 'driven' oscillator in free state. Then introduce the coupling load and watch the Lissajous figure on the screen to see what happens to the driven oscillator. Its amplitude shows fluctuations, but ultimately it settles down to oscillations of a constant amplitude. That

*In practice you will need to damp oscillator A by any of the arrangements used in Chapter 6. This is because the Q is ordinarily high (>100, say) and therefore the response changes rapidly with ω. In such cases a stop-watch has insufficient accuracy for measuring changes in ω. Also the transients die out very slowly, so that each observation may need tens of minutes to record.

means that the *transients* are over and a steady state has reached. Measure the period T and amplitude θ_0.*

Now change the frequency of the driver by shifting the position of the loads M_1 or M_2 or both (Fig. 7.2) in several steps. Each time allow the steady state to come and measure T and θ_0. Plot a graph showing θ_0 against either the period T or angular frequency $\omega(=2\pi/T)$ or frequency $\nu(=1/T)$. Figure 7.6 shows the results of a typical experiment.

The frequency of the driver corresponding to the maximum amplitude response $(\theta_0)_R$ of the driver is called the *resonance frequency* ν_R. A scale of ν/ν_0 is also given in Fig. 7.6 and it can be seen that $(\theta_0)_R$ corresponds to $\nu/\nu_0 \simeq 1$. It means that the resonance frequency ν_R nearly equals the natural frequency ν_0 of the driven oscillator.

From the graph of Fig. 7.6 deduce the half intensity band-width $\Delta\nu_{1/2}$ by taking points where θ_0 is $1/\sqrt{2}$ times $(\theta_0)_R$. Hence compute $\nu_0/\Delta\nu_{1/2}$, which equals Q [*see* Appendix VII-A].

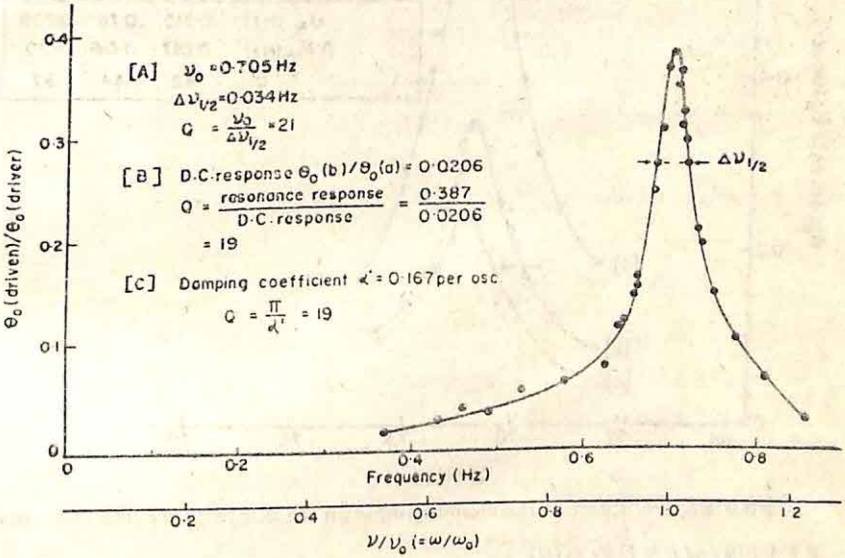

FIGURE 7.6. Displacement response of a driven oscillator.

Again, from the same graph deduce θ_0 at $\nu \to 0$. Find the ratio of $(\theta_0)_R$

---

*You will actually measure the amplitude y_0 (as shown in Fig. 7.5) which is proportional to θ_0, but we shall henceforth refer to θ_0 where we mean y_0.

to this θ_0; it gives Q [*see* Appendix VII-A]. See if the two values of Q agree*.

RELATED EXPERIMENTS

EXPERIMENT 7-A(i)

After removing the coupling, make a damping study of oscillator A, like Experiment 6-B. Deduce from it the Q value and compare it with the value obtained from the resonance half-width.

EXPERIMENT 7-A(ii)

You may change the coupling load and repeat Experiment 7-A to determine ν_R, $(\theta_0)_R$ and $\Delta\nu_{1/2}$. Figure 7.7 shows the results with three loads. Notice that ν_R and $\Delta\nu_{1/2}$ come out about the same. $(\theta_0)_R$ comes out to be proportional to the load (*see* inset, Fig. 7.7). This is in line with the theory (Equation 7.5).

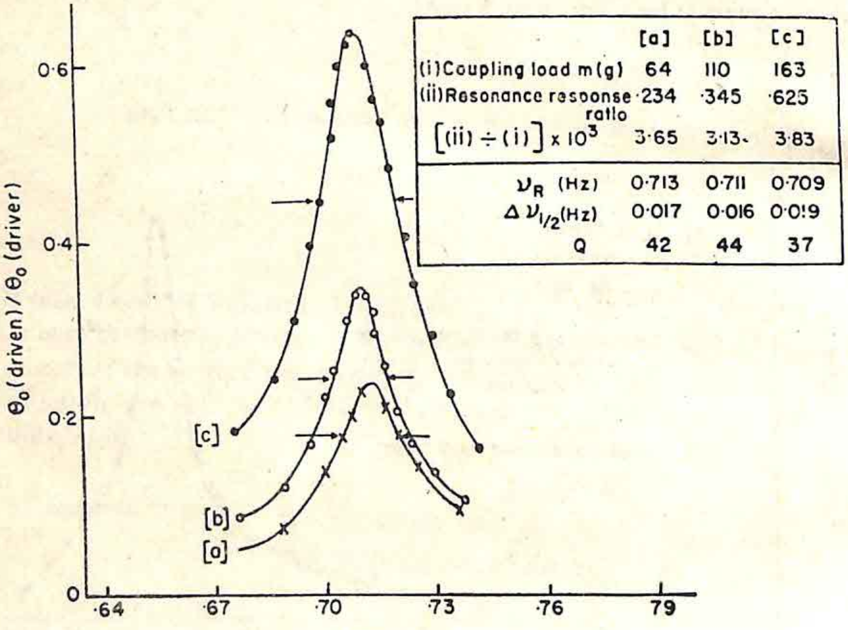

	[a]	[b]	[c]
(i) Coupling load m (g)	64	110	163
(ii) Resonance response ratio	·234	·345	·625
[(ii) ÷ (i)] × 10^3	3·65	3·13	3·83
ν_R (Hz)	0·713	0·711	0·709
$\Delta\nu_{1/2}$ (Hz)	0·017	0·016	0·019
Q	42	44	37

FIGURE 7.7. Effect of the coupling mass on the displacement response curve.

EXPERIMENT 7-A(iii)

You may introduce additional damping in the driven oscillator. For a given coupling load, see how $(\theta_0)_R$ and $\Delta\nu_{1/2}$ are affected by increase of damping. Figure 7.8 shows that $(\theta_0)_R$ measured as a falls and $\Delta\nu_{1/2}$

---

*For this purpose the experiment needs to be carried up to $\nu \ll \nu_0$. The accuracy in θ_0 measurement is rather small here; hence only order of magnitude comparison for Q values is to be expected. One alternative is to do a static experiment: Give the driver a large static deflection and note the consequent deflection of the driven. The ratio gives $\theta_0/(\theta_0)_B$ at $\nu \to 0$.

increases (*i.e.*, Q falls) as the damping is increased, (*see* inset, Fig. 7.8). The ratio a/Q remains nearly constant, showing that $(\theta_0)_R$ changes in proportion to Q of the driven oscillator.

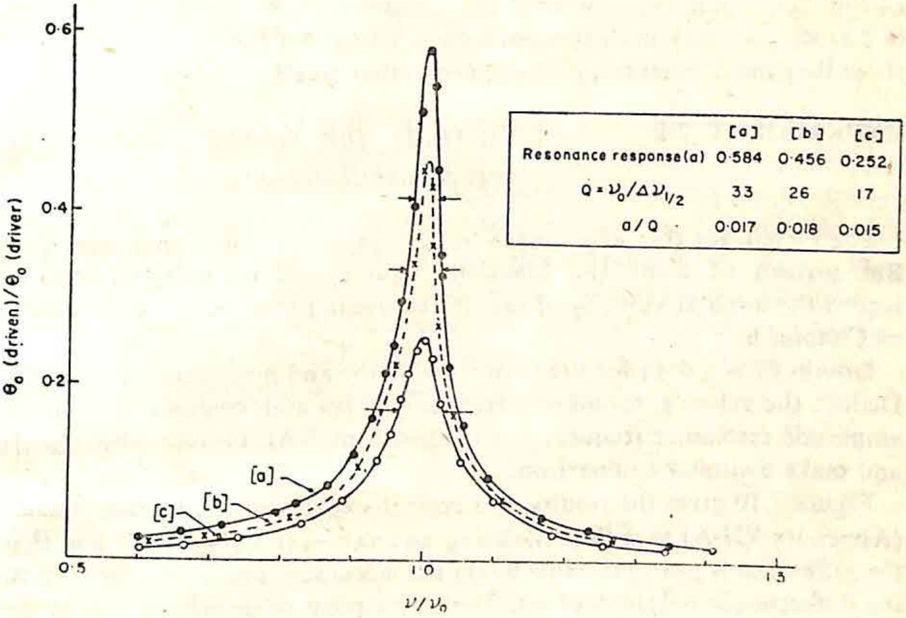

	[a]	[b]	[c]
Resonance response(a)	0·584	0·456	0·252
$Q = \nu_0/\Delta\nu_{1/2}$	33	26	17
a / Q	0·017	0·018	0·015

FIGURE 7.8. Effect of damping on the displacement response curve.

EXERCISE 7-A(*i*)

From the observed values of $(\theta_0)_R$ and $\Delta\nu_{1/2}$ (which gives γ/π vide

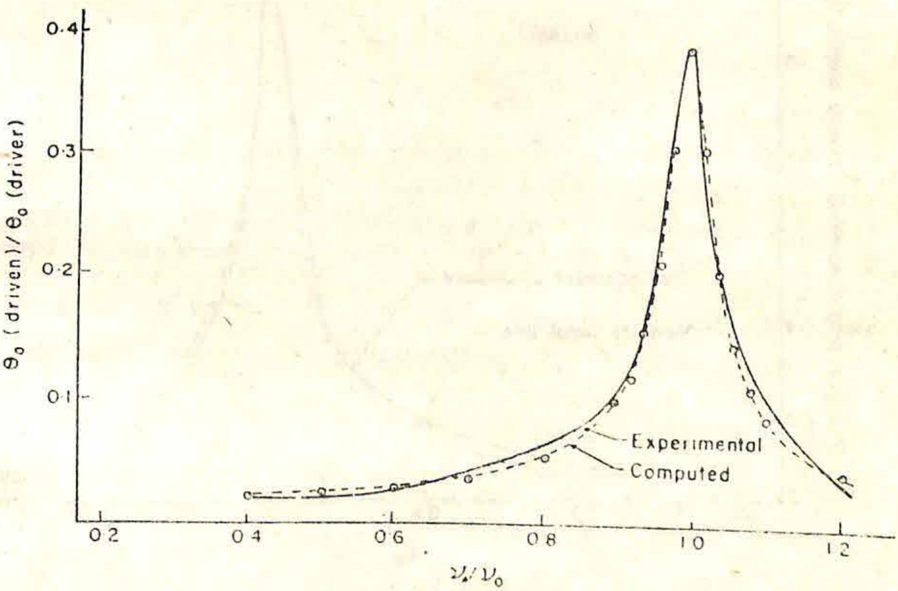

FIGURE 7.9. Comparison of the experimental and computed displacement response curves.

Appendix VII-A), compute the values of θ_0 at several ν values using Equation 7.2. Check to what extent the observed θ_0 values fit these. Figure 7.9 shows the computed data corresponding to the experimental curve of Fig. 7.6, which is reproduced for comparison. We have stated earlier (§ 7.2) why we may not expect complete fitting; but the curves of Fig. 7.9 show that the departures, if at all, are rather small.

EXPERIMENT 7-B *To study the velocity response in forced oscillations.*

The system for this experiment is the same as for Experiment 7-A. But instead of using the Lissajous figures you use a digital timer to record the angular velocity of the driven oscillator as in the experiments of Chapter 6.

Obtain $\dot{\theta}_0$ vs ν data for the driven oscillator and plot them on a graph. Deduce the velocity resonance frequency $(\nu)_{VR}$ and compare it with the amplitude resonance frequency ν_R (Experiment 7-A). Deduce also $\Delta\nu'_{1/2}$ and make a similar comparison.

Figure 7.10 gives the results of a typical experiment. Although theory (Appendix VII-A) says that $(\nu)_{VR}=\nu_0$ and $\nu_R=\nu_0\,(1-1/4Q^2)$, we find that the difference is not noticeable wihin the accuracy available (for $Q\approx 20$ the difference is $\sim 1/1600$ of ν_0). The major point of departure is that the $\dot{\theta}_0$ ratios come out lower than θ_0 ratios for $\nu<\nu_0$ and higher for $\nu>\nu_0$. The matter is of some importance because energy response is given by

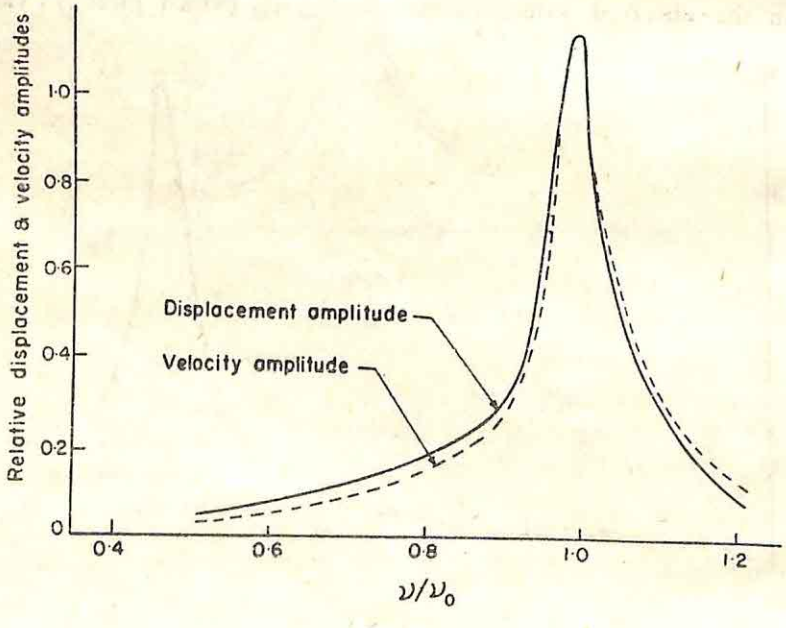

FIGURE 7.10. Comparison of the displacement and velocity response curves.

$\frac{1}{2} I \dot{\theta}_0^2$, not $\frac{1}{2} C\theta_0^{2}$*. Hence if θ_0 responses are equal for two frequencies ω_1 and ω_2 the ratio of the energy of forced oscillations in the first case will be $(\omega_1/\omega_2)^2$ times that in the second case.

RELATED EXPERIMENT

EXPERIMENT 7-B(i)

It is of some interest to study the transients, *i.e.*, the stages through which the driven oscillator passes before it attains a steady state. For this purpose choose a driven oscillator of high Q (say$>$100) and set the driver frequency ν a little (say 5 per cent) below ν_0. Observe $\dot{\theta}_0$ of the driven oscillator at every 5 or 10 oscillations and plot a graph for $\dot{\theta}_0$ against the number of oscillations n. Figure 7.11 shows the typical results of an experiment. You may note that the driven oscillator gains more energy at the start than what it has in the steady state. Also the alternate energy changes occur with larger periods near resonance.

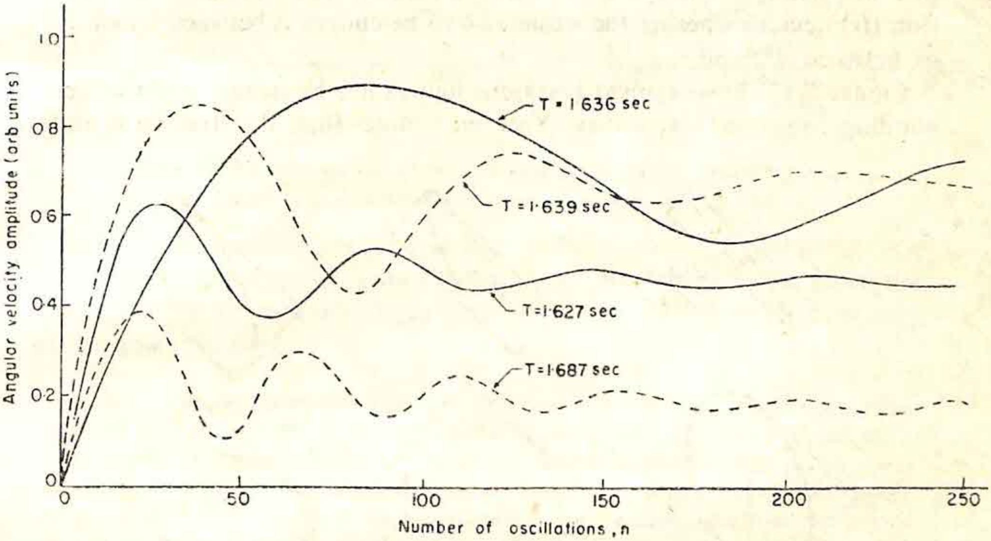

FIGURE 7.11. Variation of angular velocity amplitude with the number of oscillations during the transient states for different time periods of the driver.

EXPERIMENT 7-C** *To study how the driven oscillator lags behind the driver in phase.*

Repeat Experiment 7-A with attention on the measurement of relative phase of the driver and the driven oscillator as the frequency of the driver changes. The Lissajous figure arrangement, as described in § 7.3, useful for this purpose. Affix a graph paper on the translucent screen (Fig. 7.1) with its lines at 45° to the horizontal. Mark the image point position when both the driver and driven are at rest, and mark the X and Y axes and their positive directions corresponding to displacement of this point as the driver and the driven respectively are turned say clockwise.

---

*The expression $E=\frac{1}{2} C\theta_0^2$ is no more valid in forced oscillations. The frequency here is not ω_0 (controlled by C and I), it is ω; therefore the potential energy is not just due to work against the internal torque $C\theta$, but also has contribution from the driving torque.

**Phase difference of the driver and the driven may be measured with a timer. But Lissajous figures are more interesting for direct observation.

On this graph paper measure the following about the Lissajous figure in the steady state corresponding to each frequency of the driver: (*i*) the extreme range along x-axis ($2x_{max}$), (*ii*) the extreme range along y-axis ($2y_{max}$), (*iii*) the separation of the two points where the Lissajous figure intercepts the x-axis ($2x$), and (*iv*) whether x_{max} and y_{max} values are reached in the first quadrant or the second.

As discussed in § 7.3 (*c*), δ is given by $\sin^{-1}(x/x_{max})$. It is positive since you will find that the Lissajous figure is traced anticlockwise. Information (*iv*) decides whether the value of δ to be chosen is between 0 and $\pi/2$ or between $\pi/2$ and π.

Figure 7.12 shows typical Lissajous figures in the steady state corresponding to several ν/ν_0 values. You may note that the tracing is anticlockwise in all the cases, so that δ is positive always. The lag δ is $<\pi/2$ for $\nu<\nu_0$, and $>\pi/2$ for $\nu>\nu_0$, the major change of δ taking place

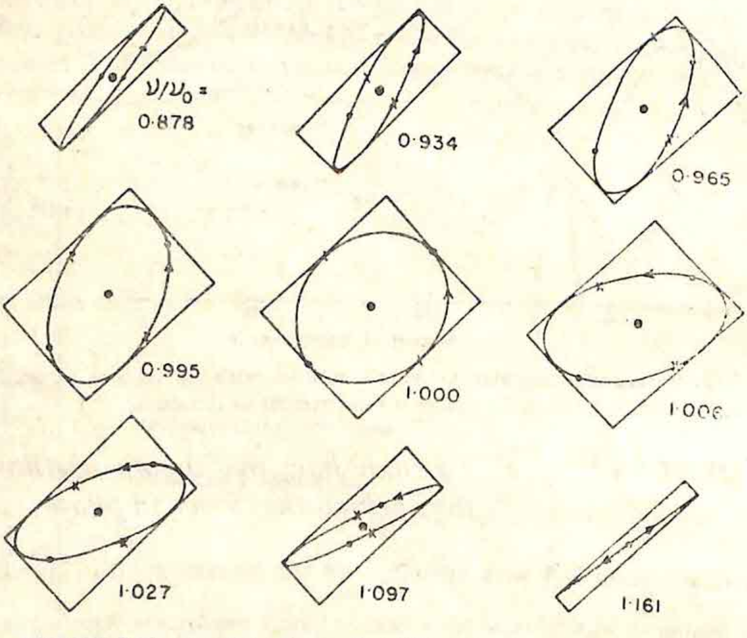

FIGURE 7.12. Lissajous figures for different ratios of the frequencies of the driver and the driven.

in a narrow range of ν around ν_0. Figure 7.13 shows the δ vs ν/ν_0 curve (along with θ_0 vs ν/ν_0 curve) for two cases of different Q. It is to be noted that at low frequencies the driver and the driven are nearly in phase ($\delta \approx 0$) but at high frequencies they move in opposite phase ($\delta \approx 180°$). At resonance ($\nu/\nu_0 \approx 1$) the phase difference is $\approx 90°$.

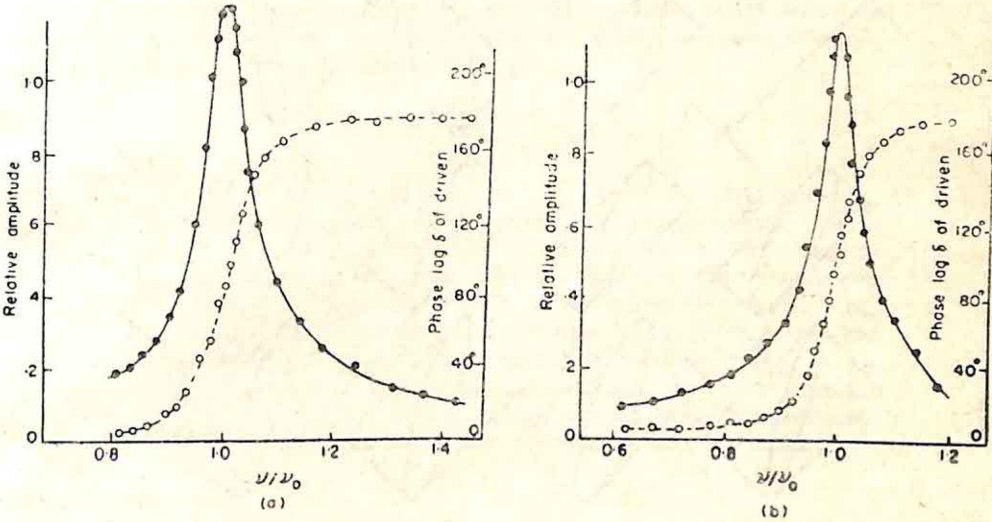

(a) (b)

FIGURE 7.13. Variation of phase lags with the driver frequency ν/ν_0 for two cases. (The amplitude response curves are also given).

Some further analysis will be of interest here. From Experiment 7-A you know $Q(=\omega_0/\triangle\omega_{1/2})$ and hence you get $\alpha(=\omega_0/2Q)$. Now use Equation (7.3) to compute δ for several values of ω and see how they fit the observed data.

Experimentally speaking, the amplitude response curve (θ_0 vs ν) and the phase lag curve (δ vs ν) are two means of studying the driven system (its ν_0 and Q). In most experiments like the sonometer, the resonance column, molecular absorption spectroscopy etc., we use the energy response method. But it is equally good to employ the phase method for studying the driven system. For example, the theory of dispersion of light (*i.e.*, variation of velocity of light with frequency) is based on the phase difference between the driver (incident light) and the driven (the molecular system in the medium). Therefore studies on dispersion serve as an equally useful tool for the study of molecules.

RELATED EXPERIMENT

EXPERIMENT 7-C(i)

Like Experiment 7-B(i) you may be interested in the driver-driven phase relation during the transient stages. Observe the Lissajous figures after (say) every 10 oscillations and make a schematic drawing of what you see. Figure 7.14 shows one such series. Two points deserve notice. The figures are traced clockwise in some stages (5, 6, 7 and 11, 12, 13), although the steady state figure is traced anticlockwise. Secondly, the driver loses amplitude in the early stages, though it regains it later. Try to understand these facts qualitatively.

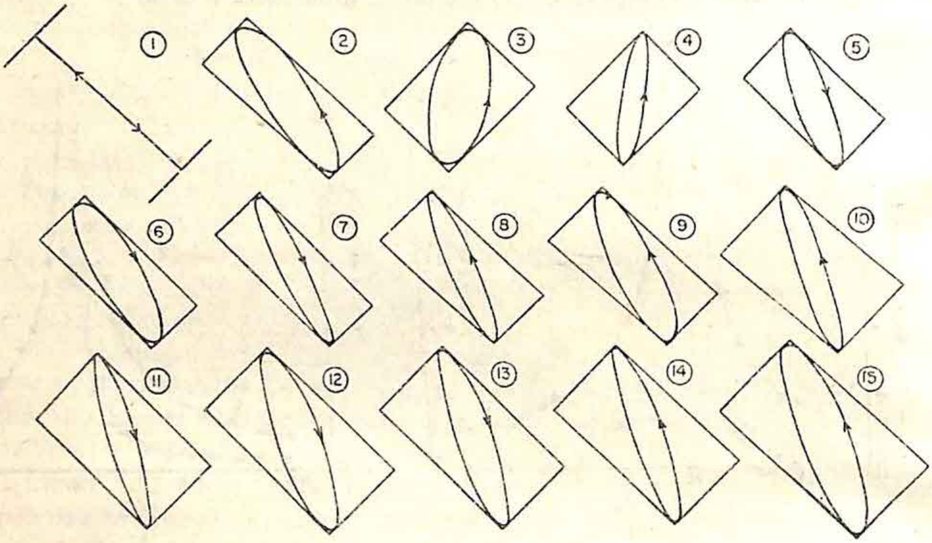

FIGURE 7.14. The stages before attainment of the steady state, shown through Lissajous figures.

A NOTE ON RESONANCE PROCESSES

Consider light passing through a gas. Light involves oscillatory electric field of different frequencies, and the molecules of the gas have some well-defined natural frequencies. Therefore light and molecules behave as the driver and driven. The energy absorption from light by the molecules is maximum when the frequency of the electric field in light coincides with one of the natural frequencies of the molecules. Using this principle we determine the vibrational frequencies of molecules of various compounds.

Consider again a crystal like NaCl, which really has Na^+ and Cl^- ions. In the crystal there are characteristic frequencies at which these ions oscillate relative to one another. If light is passed through the crystal, the energy absorption is maximum when the frequency of light coincides with the natural frequency of the lattice oscillations in NaCl.

In both the above cases the system under study has a frequency of its own. Now consider a case of another kind. Nuclei of atoms have a magnetic moment μ. When placed in a uniform magnetic field B these nuclei show a periodic motion (called precession) of angular frequency.

$$\omega_0=\mu B \qquad . (7.10)$$

If now electromagnetic radiations of angular frequency ω are passed, absorption will take place only in the neighbourhood of $\omega=\omega_0$. [In practice resonance is studied not by changing ω but by changing ω_0 through the magnetic field B.]

Thus forced oscillations and resonance phenomena are of wide applicability. The scope is widened further still. For many nuclear reactions it is found that the dependence of reaction on energy E follows the relation

$$\sigma(E)=\frac{\sigma(E_0)}{\frac{4(E-E_0)^2}{(\delta E)^2}+1} \qquad \ldots(7.11)$$

where E_0 and δE are two constants of the system and σ is called *cross section* for the occurrence of that reaction. Now, in the neighbourhood of resonance Equation VI-C(13) in Appendix VI-C can be put in the form

$$P(\omega)=\frac{P(\omega_0)}{\frac{4(\omega-\omega_0)^2}{\Delta\omega_{1/2}}+1} \qquad \ldots(7.12)$$

The similarity of the two functional relations may be noted. For this reason, the nuclear reaction which follows such a relation is called a *resonance reaction* with a *resonance energy* E and width δE. A study of such resonance nuclear reactions gives us information regarding the internal energy states of the nucleus. But you may note that while frequencies ω, ω_0 occur in the equations we have developed and used, energies E, E_0 occur in the equations in nuclear resonant reactions. It is true that E and ω are connected in quantum mechanics through the equation $E=(h/2\pi)\omega$ but that means we are applying the concepts of classical mechanics to quantum mechanics. You will have to cover a lot of ground before you appreciate the significance of the extended meaning of *resonance* without any reference to *forced oscillations*.

APPENDIX VII-A

THEORY OF FORCED OSCILLATIONS

1. General

Let an oscillator A have the parameters I, C and r as described in Appendix VI-C. If an oscillator B applies on it a torque given by

$$\Omega_{BA} = \Omega_0 \cos \omega t$$

the equation of motion becomes

$$I\ddot{\theta} = -C\theta - r\dot{\theta} + \Omega_0 \cos \omega t$$

Here A is called the *driven oscillator* and B the *driver*. For convenience the above equation may be written as

$$\ddot{\theta} + 2\alpha\dot{\theta} + \omega_0^2\theta = \frac{\Omega_0}{I} \cos \omega t \qquad \ldots \text{VII-A (1)}$$

where α and ω_0 have the same meanings as in Appendix VI-C.

The solution of Equation VII-A (1) will have one term of frequency ω_0 (that of the driven) and another of frequency ω (that of the driver). The first will have an $e^{-\alpha t}$ multiplier in the amplitude (*see* Appendix VI-C) and will therefore decay with time. In the *steady state* we are then left with only the term of frequency ω, which is the frequency of the driver. The intermediate stages are called *transients*. Since their decay depends on the $e^{-\alpha t}$ term it is clear that transients die out faster if α is large, *i.e.*, Q of the driven oscillator is small. We shall discuss only the steady state oscillations.

2. Solution for the Steady State

Let us try the solution

$$\theta = \theta_0 \cos(\omega t - \delta) \qquad \ldots \text{VII-A(2)}$$

where δ is the phase *lag* of the driven oscillator behind that of the driver. It is convenient to use complex quantities $e^{i\omega t}$ and $e^{i(\omega t-\delta)}$ in place of the corresponding cosines.* Then Equation VII-A(2) fed into VII-A(1) gives

$$\theta_0(-\omega^2 + i\omega.2\alpha + \omega_0^2) = \frac{\Omega_0}{I}(\cos\delta + i\sin\delta)$$

Equating the real and imaginary parts separately gives

$$\theta_0(\omega_0^2 - \omega^2) = \frac{\Omega_0}{I} \cos\delta$$

$$\theta_0(2\alpha\omega) = \frac{\Omega_0}{I} \sin\delta$$

---

*Wherever we write $e^{i\omega t}$ in place of cos ωt, we mean only the real part of the function. In the final solution we take the real part only.

Hence we get

$$\theta_0=\frac{\Omega_0/I}{[(\omega_0{}^2-\omega^2)^2+4\alpha^2\omega^2]^{1/2}} \qquad \ldots\text{VII-A(3)}$$

and

$$\tan\delta=\frac{2\alpha\omega}{\omega_0{}^2-\omega^2} \qquad \ldots\text{VII-A(4)}$$

We may express the results in terms of Q, instead of α. Since $Q=\omega/2\alpha$. the above equations give

$$\theta_0=\frac{\Omega_0/I}{[(\omega_0{}^2-\omega^2)^2+\omega^2\omega_0{}^2/Q^2]^{1/2}} \qquad \ldots\text{VII-A(5)}$$

$$\tan\delta=\frac{\omega\omega_0/Q}{\omega_0{}^2-\omega^2} \qquad \ldots\text{VII-A(6)}$$

3. Displacement Response

Equations VII-A(3) and (4) give the following results:

(*a*) *At low frequency*: For $\omega\to 0$,

$$(\theta_0)_{static}\to\frac{\Omega_0}{I\omega_0{}^2}=\frac{\Omega_0}{C} \qquad \ldots\text{VII-A(7)}$$

$$\delta\to 0$$

The response is thus limited by C and the phase difference is zero.

(*b*) *Amplitude resonance*. It is said to occur when θ_0 becomes maximum. It occurs at a frequency ω_R determined by $d\theta_0/d\omega=0$. From Equation VII-A(3) or (5) we get

$$\omega_R=\sqrt{\omega_0{}^2-2\alpha^2}\approx\omega_0\left(1-\frac{1}{4Q^2}\right) \qquad \ldots\text{VII-A(8)}$$

$$(\theta_0)_R=\frac{\Omega_0 Q}{I\omega_0{}^2\left(1-\frac{1}{2}\frac{\alpha^2}{2\omega_0{}^2}\right)}\approx\frac{\Omega_0 Q}{C} \qquad \ldots\text{VII-A(9)}$$

Thus $(\theta_0)_R$ comes out to be very close to $Q\times(\theta_0)_{static}$

$$(\delta)_R=\frac{1}{2}\tan^{-1}\left(\frac{\omega_R\,Q}{\omega_0}\right)\approx\frac{1}{2}\tan^{-1}Q \qquad \ldots\text{VII-A(10)}$$

(*c*) *At high frequency*: For $\omega\to\infty$,

$$\theta_0\to 0;\ \delta\to\pi$$

The driver and driven are thus in opposite phase.

4. Velocity Response

From the displacement equation

$$\theta=\theta_0\cos(\omega t-\delta)$$

the velocity equation comes out to be

$$\dot\theta=\omega\theta_0\cos(\omega t-\delta'); \qquad \delta'=\delta-\pi/2$$

Thus the velocity amplitude is given by

$$\dot\theta_0=\omega\theta_0=\frac{\omega\Omega_0/I}{[(\omega_0{}^2-\omega^2)^2+\omega^2\omega_0{}^2/Q^2]^{1/2}} \qquad \ldots\text{VII-A(11)}$$

The response at different frequencies is then as follows:

(*a*) at $\omega \rightarrow 0$ $\qquad (\dot{\theta})_{static} = 0,\ \delta' = -\pi/_2$

(*b*) *Velocity resonance*. It is said to occur when $\dot{\theta}_0$ becomes maximum. It occurs at a frequency $(\omega)_{VR}$ determined by $d\dot{\theta}_0/d\omega = 0$. Equation VII-A(11) leads to

$$(\omega)_{VR} = \omega_0 \text{ exactly} \qquad \ldots \text{VII-A(12)}$$

Correspondingly we get

$$\delta' = 0$$

It is thus to be noted that ω_0 corresponds to velocity resonance, not to the displacement resonance.*

5. Power Absorption by the driven Oscillator

In the steady state the power absorbed by the driven oscillator from the driver is equal to that dissipated by the driven oscillator. Therefore the power absorption may be deduced as follows:

$$P = \frac{1}{T}\int_0^T -\Omega'.\dot{\theta}\,dt = r.\frac{1}{T}\int_0^T \dot{\theta}^2\,dt = r\,[\dot{\theta}^2]_{av} = \frac{1}{2}\,r\,\dot{\theta}_0^2$$

since $\Omega' = -r\dot{\theta}$ and mean $\dot{\theta}^2 = \frac{1}{2}\,\dot{\theta}_0^2$ in a harmonic oscillator. Substituting for $\dot{\theta}_0$ from Equation VI-C (6) gives

$$P = \frac{r}{2}.\ \frac{\omega^2\Omega_0^2}{I^2},\ \frac{1}{(\omega_0^2-\omega^2)^2+\omega^2\omega_0^2/Q^2}$$

or

$$P = \tfrac{1}{2}\frac{\Omega_0^2\omega}{CQ}.\ \frac{1}{\left(\frac{\omega}{\omega_0}-\frac{\omega_0}{\omega}\right)^2+\left(\frac{1}{Q}\right)^2} \qquad \ldots \text{VII-A(13)}$$

since $\frac{r}{2I} = \alpha = \omega_0/2Q$ and $I\,\omega_0^2 = C$. Thus the maximum power absorption occurs at $\omega = \omega_0$ *exactly* and its value is

$$P_{max} = \tfrac{1}{2}\frac{\Omega_0^2\omega_0}{C}\ Q = \tfrac{1}{2}\ \frac{\Omega_0^2}{I\omega_0}.Q \qquad \ldots \text{VII-A(14)}$$

The power falls to half when

$$\frac{\omega}{\omega_0} - \frac{\omega_0}{\omega} = \pm\frac{1}{Q}$$

For large Q the two solutions ω_1 and ω_2 of this have a difference given by

$$\omega_1 - \omega_2 \equiv \Delta\omega_{1/2} = \frac{\omega_0}{Q} \qquad \ldots \text{VII-A(15)}$$

This is called the full width at half the maximum power.

---

*The difference $\omega_\circ - \omega_R$ may be compared with the half-width $\Delta\omega_{1/2}$ (which equals $\omega_\circ/Q$). From Equation VII-A(8) we get

$$\omega_\circ - \omega_R \approx \frac{\omega_\circ}{4Q^2} \approx \frac{\Delta\omega^{1/2}}{4Q}$$

This shows that the shift between the velocity resonance frequency and displacement resonance frequency is small compared with $\Delta\omega_{1/2}$, except when we go to low Q; but in the case of low Q resonance itself is rather flat.

APPENDIX VII-B

EFFECT OF COUPLING BY MEANS OF A LOADED THREAD TIED BETWEEN TWO RIGID PENDULUMS

Figure VII-B(1) shows the thread *APB* tied to the two rigid pendulums at distances *p* each from the axes of oscillation and carrying a load *mg* at the mid-point *P*. The thread length is *l* and angle *APB* in the equilibrium state is 2ϕ.

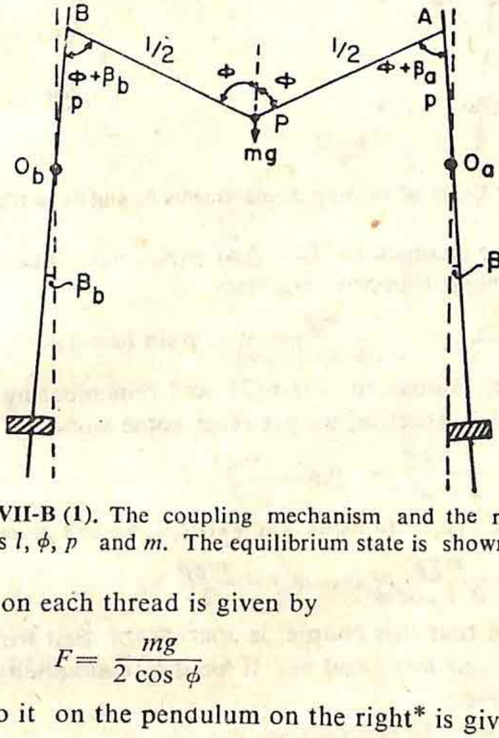

FIGURE VII-B (1). The coupling mechanism and the related parameters l, ϕ, p and m. The equilibrium state is shown here.

The tension F on each thread is given by

$$F = \frac{mg}{2\cos\phi} \qquad \ldots \text{VII-B(1)}$$

and torque due to it on the pendulum on the right* is given by

$$\Omega_{0a} = F.p \sin(\phi + \beta_a) \qquad \ldots \text{VII-B(2)}$$

where β_a is the deflection of this pendulum from the vertical in the equilibrium state. If C_a is the restoring torque factor for this pendulum, β_a is given by

$$C_a \beta_a = \Omega_{0a} \qquad \ldots \text{VII-B(3)}$$

---

* We shall write only one set of equations, for the pendulum on the right. Those for the other may be understood by symmetry.

At any instant of time let θ_a and θ_b be deflections of the two pendulums, taken positive when anticlockwise [Figure VII-B(2)]. Then distance *AB* increases by $p(\theta_b - \theta_a)$ and hence ϕ changes to $\phi + \triangle\phi$ such that

$$l \sin\ (\phi + \triangle\phi) = l \sin \phi + p(\theta_b - \theta_a)$$

$$\therefore l \cos.\ \cos\phi.\ \triangle\phi = p(\theta_b - \theta_a) \qquad \text{. . . VII-B(4)}$$

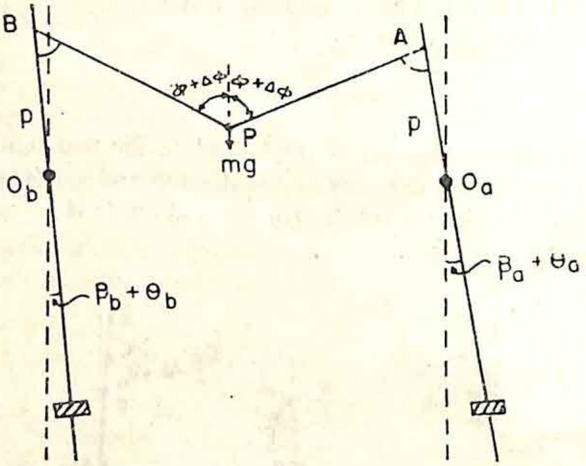

FIGURE VII-B(2). Effect of causing displacements θ_a and θ_b in the two pendulums.

The angle at *A* changes to $(\phi + \triangle\phi) + (\beta_a + \theta_a)$. The torque on the pendulum on the right therefore becomes

$$\Omega_a + \Omega_{0a} = \frac{mg}{2 \cos\ (\phi + \triangle\phi)} \cdot p \sin\ (\phi + \beta_a + \triangle\phi + \theta_a)$$

Comparing with Equation VII-B(2) and remembering that all angles except ϕ are small in practice, we get after some working

$$\Omega_a = \frac{mgp}{2 \cos^2 \phi}\ \triangle\phi + \frac{mgp}{2}\ \theta_a$$

Substitution for $\triangle\phi$ from Equation VII-B(4) finally gives

$$\Omega_a = \frac{mgp^2}{2\ l \cos^3\phi}\ (\theta_b - \theta_a) + \frac{mgp}{2}\ \theta_a \qquad \text{. . . VII-B(5)}$$

It may be noted that this couple is apart from that which changes the equilibrium positions by β_a and β_b. If we desire simplicity in form there are three alternatives:

(*i*) $p/l \cos^3 \phi \ll 1$. In this case we get

$$\Omega_a = \frac{mgp}{2}\ \theta_a \qquad \text{. . . VII-B(6)}$$

This means that C_a changes to $C'_a = C_a + mgp/2$ and in comparison the influence of θ_b on Ω_a (which is really the 'coupling') is relatively small.

(*ii*) $p/l \cos^3 \phi = 1$. In this case Equation VII-B(5) simplifies to

$$\Omega_a = \frac{mgp}{2}\ \theta_b \qquad \text{. . . VII-B(7)}$$

This means that C'_a remains the same as C_a and the coupling constant is simply $mgp/2$.

(*iii*) $p/l \cos^3 \phi \gg 1$. In this case Equation VII-B(5) gives

$$\Omega_a = \frac{mg\,p^2}{2l \cos^3 \phi}\,(\theta_b - \theta_a) \qquad \ldots \text{VII-B(8)}$$

This means that the coupling term becomes now symmetrical in θ_a and θ_b.

Since our interest is in coupling, the first alternative is of no use. The second alternative is quite attractive. It gives a driving couple to oscillator *a* in proportion to the displacement of the driver oscillator *b*, without affecting the restoring factor of *a* itself.

The arrangement represented in Figure VII-B(3) has a special interest, because a lens is mounted this way for showing Lissajous figures. The coupling may be calculated by revising the equations used earlier. Equations VII-B(2), VII-B(4) and VII-B(5) now become

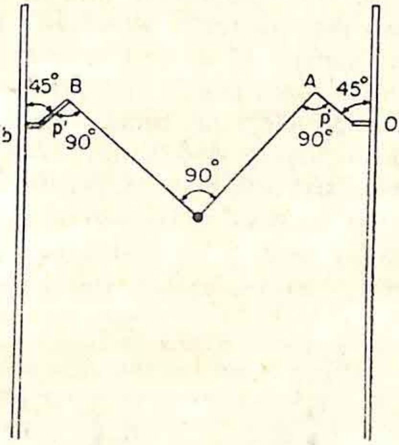

FIGURE VII-B (3). The 90° geometry for mounting the lens.

$$\Omega_{0a} = \frac{mgp^2}{2\cos\phi'}, \sin\left(\frac{\pi}{2} + \beta_a\right); \; (\phi' = 45^\circ)$$

$$l\,\triangle\phi' = p'\,(\theta_b - \theta_a).$$

and

$$\Omega_a = \frac{mgp'^2}{l\sqrt{2}}\,(\theta_b - \theta_a) \qquad \ldots \text{VII-B(9)}$$

The coupling constant $mgp'^2/l\sqrt{2}$ is thus considerably smaller than the corresponding constants in any of the situations (i), (ii), (iii), discussed before. Denoting Ω values in Equations VII-B(8) and VII-B(9) by Ω_{load} and Ω_{lens} respectively, we get

$$\frac{\Omega_{lens}}{\Omega_{load}} = \left(\frac{\sqrt{2}.\cos^3\phi}{1}\right)\left(\frac{m_{lens}}{m_{load}}\right). \; \frac{p'^2}{p^2}$$

If we consider the example of $\cos\phi = 0.3$, the first factor on the right $\sim$ 0.04, which is quite small. Thus the 90° geometry makes the lens contribute very little to the coupling.

8 COUPLED OSCILLATIONS

8.1. FREE OSCILLATIONS OF A COUPLED SYSTEM NORMAL MODES

If two oscillators *a* and *b* have an interaction between them they are said to form a coupled system, of which *a* and *b* are the components. In general neither of the two components then oscillates harmonically, except in two (and only two) particular situations. These are called the *normal modes* of the system. If we call them 1 and 2, then in mode 1 both the component oscillators vibrate with a common frequency ω_1 and in phase, the relative amplitude A_b/A_a being a specified constant r_1. In mode 2 again both the oscillators vibrate with another common frequency ω_2 and in phase,* the relative amplitude A_b/A_a having another specified value r_2. Here ω_1 and ω_2 are called the *normal mode frequencies* and r_1 and r_2 specify the *configuration* of the oscillation. Figure 8.1 shows the configurations for two normal modes in a typical case.

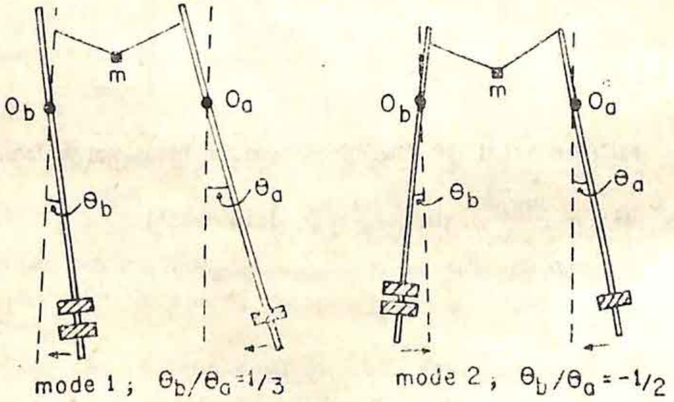

mode 1 ; $\theta_b/\theta_a = 1/3$ mode 2 ; $\theta_b/\theta_a = -1/2$

FIGURE 8.1. Configurations for the two normal modes for the system of two coupled oscillators of same frequency.

---

*'In phase means reaching the zero position simultaneously. The case of 'phase difference π' (also called *opposite phase*) is included here in the term 'in phase' because $A \cos(pt+\delta+\pi) = -A \cos(pt+\delta)$, and thus it is equivalent to amplitude becoming negative. In a system with multiple components this practice is more convenient.

The theory of coupled oscillations has been outlined in Appendix VIII-A. We shall limit our present discussion to the coupling of two identical oscillators. The equations of motion of the components a and b are written as

$$I\ddot{\theta}_a=-C\theta_a+C_{ab}(\theta_b-\theta_a)$$
$$I\ddot{\theta}_b=-C\theta_b+C_{ab}(\theta_a-\theta_b) \qquad \ldots (8.1)$$

where C_{ab} is called the *coupling constant* and we have taken $C_{ba}=C_{ab}$ by symmetry considerations. The strength of coupling is a relative term and is best measured by the ratio C_{ab}/C. Theory shows that for $C_{ab}/C\ll 1$ frequencies of the two normal modes and the configurations are

$$\left.\begin{array}{ll}\omega_1=\omega_0=\sqrt{C/I}; & r_1=+1\\ \omega_2\approx\omega_0(1+C_{ab}/C); & r_2=-1\end{array}\right\} \qquad \ldots (8.2)$$

$$\frac{\omega_2-\omega_1}{\omega_0}\approx\frac{C_{ab}}{C} \qquad \ldots (8.3)$$

We could think of a coupled system of N identical components. Then there would be N equations like (8.1) and their solution would lead to just N different modes, each with a specified frequency ω_p ($p=1$ to N) and a specified set of configuration constants $(r_i)p$, where p specifies the mode and i specifies the component. If some of the ω_p values coincide, those modes are said to be *degenerate* in frequency, but they will still correspond to different configurations. In any case the most important effect of 'coupling' is that N coincident frequencies (all ω_0) split into N distinct frequencies.

In molecular and solid state physics we so often come across coupled oscillators. For example CO molecule has one stretching frequency; in O-C-O molecule you have two CO oscillators coupled, giving two stretching frequencies*. Similarly in water two OH oscillators are coupled together to give two stretching frequencies. The case of N atoms of sodium in a crystal of sodium is also of interest. In an isolated Na atom you have energy levels described by 1*s*, 2*s*, 2*p*, 3*s* etc. (language of a spectroscopist). In a sodium crystal the N atoms are coupled, so that each level splits into N discrete levels. As Equation (8.3) shows, for a given coupling the splitting is small if the parent constant C is large. Since the binding energy in Na atom (in effect equivalent to C) is largest for the 1*s* levels and decreases as we go to 2*s*, 2*p*, 3*s*, . . . , we would expect the splitting to be the smallest in 1*s* levels and increasing as we go to 2*s*, 2*p*, 3*s*. . . states. This is what is observed; 3*s* level of Na spreads into a broad band in the crystal, while 1*s* spreads very little. You may object to applying the coupling concept to this case, because 1*s*, 2*s*, 2*p* etc. refer to energy levels, not frequencies of oscillators. The objection is right. But if concepts of classical mechanics are used to draw parallels in atomic and nuclear physics (where quantum mechanics alone gives the right description) we have to take frequency as parallel to energy!

8.2. THE EXPERIMENTAL SET-UP

The arrangement of Fig. 7.1, used for the study of forced oscillations, becomes the one for the study of coupled oscillations if the magnet is removed. Thus the two pendulums get equal status as components of a coupled system. However our experiments will be limited to the case when the frequencies ν_a and ν_b are matched to equality within half-a per cent.

---

* There is also a bending mode of oscillation in triatomic molecules. Presently we ignore that.

The coupling mechanism has been described in § 7.3(b) and the theory is given in Appendix VII-B. Referring to Fig. VII-B(1), we shall keep ϕ large enough to make $p/l \cos^3\phi \gg 1$, so that the coupling is given by Equation VII-B(8):

$$\Omega_{ab}=C_{ab}(\theta_b-\theta_a); \qquad C_{ab}=\frac{mgp^2}{2l\cos^3\phi} \qquad \ldots(8.4)$$

Typically, C of a pendulum is $\sim 3\times10^7$ dy cm/rad. With $p=10$ cm, $l=50$ cm and $\cos\phi=0.3(\phi\sim72°)$, you find that $m=10$ gm makes $C_{ab}/C\sim1$ per cent, and this factor increases in proportion to m.

The excitation of the normal modes and measurements are made with the help of Lissajous figures [*see* § 7.3(*c*)]. Figure 8.2 shows some extra features of use. O is the equilibrium position of the spot of light on the graph and OX and OY represent its motion corresponding to the clockwise rotation of oscillators a and b respectively (vide Fig. 8.1). Now, for the coupled system with identical components, Equation 8.2 shows $r=+1$ for mode 1 and -1 for mode 2. A position of the spot of light along OB_1 in Fig. 8.2 means $A_b=A_a$, *i.e.*, ratio $r=+1$, which holds for mode 1.

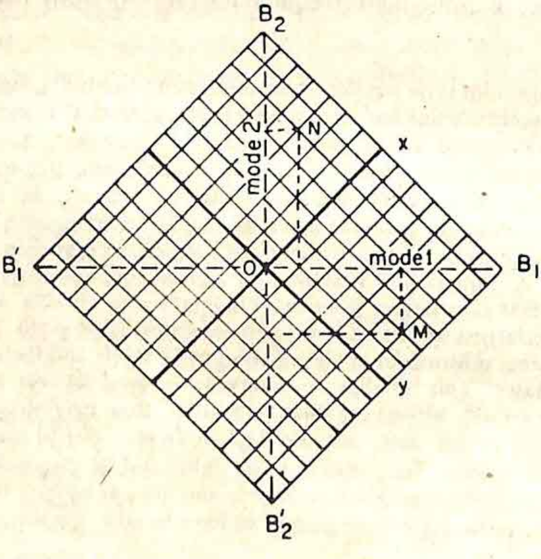

FIGURE 8.2. Displacements of the Lissajous spot corresponding to modes 1 and 2.

Similarly light spot along OB_2 corresponds to mode 2. A light spot like N represents X and Y displacements in the ratio $+5:-3$; but our interest is not in this. We take the components of ON along OB_1 and OB_2: they come in the ratio 1:4, showing that it corresponds to mixture of the modes 1 and 2 in this ratio. Thus with the help of the spot of light you can start the oscillations in any pure mode or in a desired mixture of the two modes.

EXPERIMENT 8-A* *To measure the coupling factor C_{ab} between pendulums and study its dependence on different parameters.*

Take two rigid pendulums identical in all respects including the placement of their sliding masses. By finer adjustments equalise their periods within half-a per cent. Now attach the coupling device and Lissajous figure device described in § 7.3(b) and (c).

Let the Lissajous spot be at O (Fig. 8.2) when the system is in the equilibrium state. Now deflect one pendulum *a* such that the Lissajous spot deflects along OX by an amount x_0. This corresponds to an angular deflection θ_a in pendulum *a*. Measure the resulting deflection y caused along OY, which corresponds to deflection θ_b in pendulum *b*. It means that pendulum *b* has received a torque $C\theta_b$ due to angular deflection θ_a in pendulum *a*.

We thus have

$$C\theta_b = C_{ab}\theta_a \qquad \ldots (8.5)$$

Since x_0 and y are proportional to θ_a and θ_b respectively, you get

$$\frac{C_{ab}}{C} = \frac{\theta_b}{\theta_a} = \frac{y}{x_0} \qquad \ldots (8.6)$$

You may also do the reverse. Deflect pendulum *b* by y_0 and measure the resultant deflection x caused in *a*. Then x/y_0 gives you C_{ba}/C and you may check that $C_{ba} = C_{ab}$.**

Now the theory (Appendix VII-B) shows that C_{ab} depends on the parameters p, m and ϕ of the coupling mechanism according to Equation (8.4). You may therefore vary m, p and ϕ in turns and see how the observed C_{ab}/C varies in each case. Figures 8.3(a), (b) and (c) show the results of one such study. We leave it to you to comment on them. However, it is good to measure C and then to see how far the theoretical C_{ab}/C agrees with the experimental one.

RELATED EXPERIMENT

EXPERIMENT 8-A (1)

Couple two pendulums of unequal C values but equal periods. Equation (8.6) now gives $C_{ab}/C_a = y/x_0$; the corresponding equation for

---

*This is a preliminary static experiment to enable you to appreciate the role of different parameters in determining the coupling. *See* Appendix VII-C for the theoretical approach. In practice the coupling ratio C_{ab}/C has to be kept small (0.1 or less). Hence the measurements are not accurate. Yet they give useful insight.

**Here this is to be expected from symmetry since the two component pendulums are identical.

the reverse exercise being $C_{ba}/C_b = x/y_0$. Repeat Experiment 8-A to measure y/x_0, and x/y_0, and then deduce C_{ab} and C_{ba}. See if they come out equal.

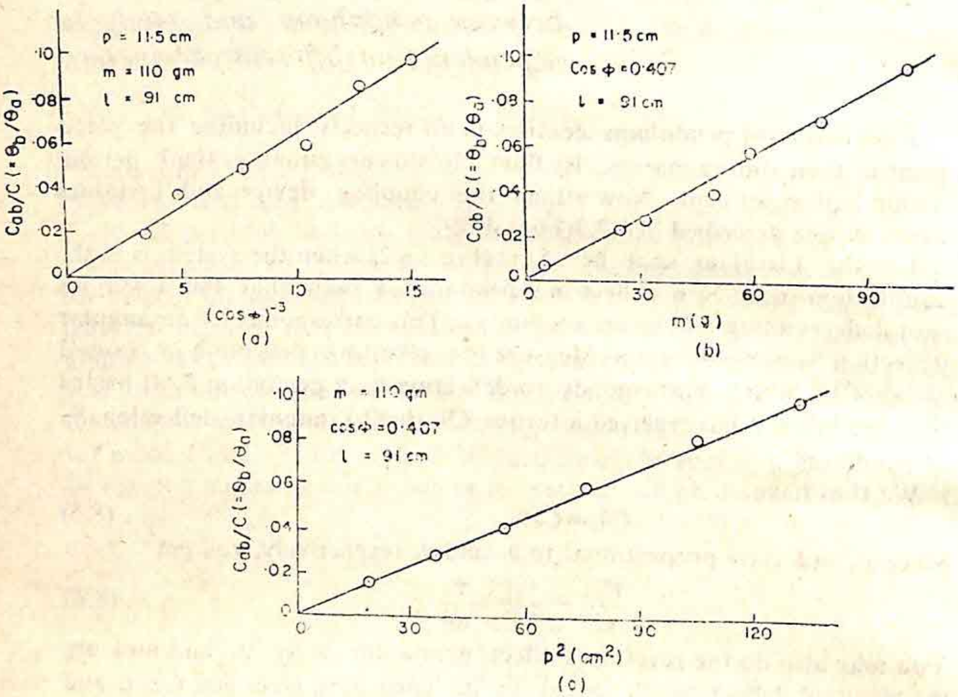

FIGURE 8.3. Variation of the coupling with (a) $(\cos\phi)^{-3}$, (b) m, and (c) p^2.

EXPERIMENT 8-B *To study the frequency of normal modes in a coupled oscillator.*

With the arrangement of Experiment 8-A, turn both the pendulums clockwise or both anticlockwise in such a way that the Lissajous spot (Fig. 8.2) is along the horizontal line B_1OB_1' (anywhere). Release both the pendulums simultaneously.* The spot will move along line B_1OB_1' back and forth steadily for quite a long time.** This means that the two component pendulums maintain the same frequency and amplitude ratio. Such a mode is called a *normal mode* of the coupled system. Measure its period T_1, hence frequency ν_1. An initial spot displacement along the line B_2OB_2' and simultaneous release of the pendulums results in oscillations in another *normal mode* of the system. Measure its period

---

*The periods are ~1 sec; hence 1/10 sec difference in release time amounts to a phase error $\sim 2\pi/10$, which is not negligible. Hence care is needed in this.

**The amplitude will decrease with time (due to damping) but the line of oscillation will not change.

T_2, hence frequency ν_2. Repeat the measurements with different coupling masses m, and plot ν_1 vs m and ν_2 vs m on the same graph.

Figure 8.4 (a) shows the results of a typical experiment with parameters given in the inset. Unlike the expectation from Equation (8.2),

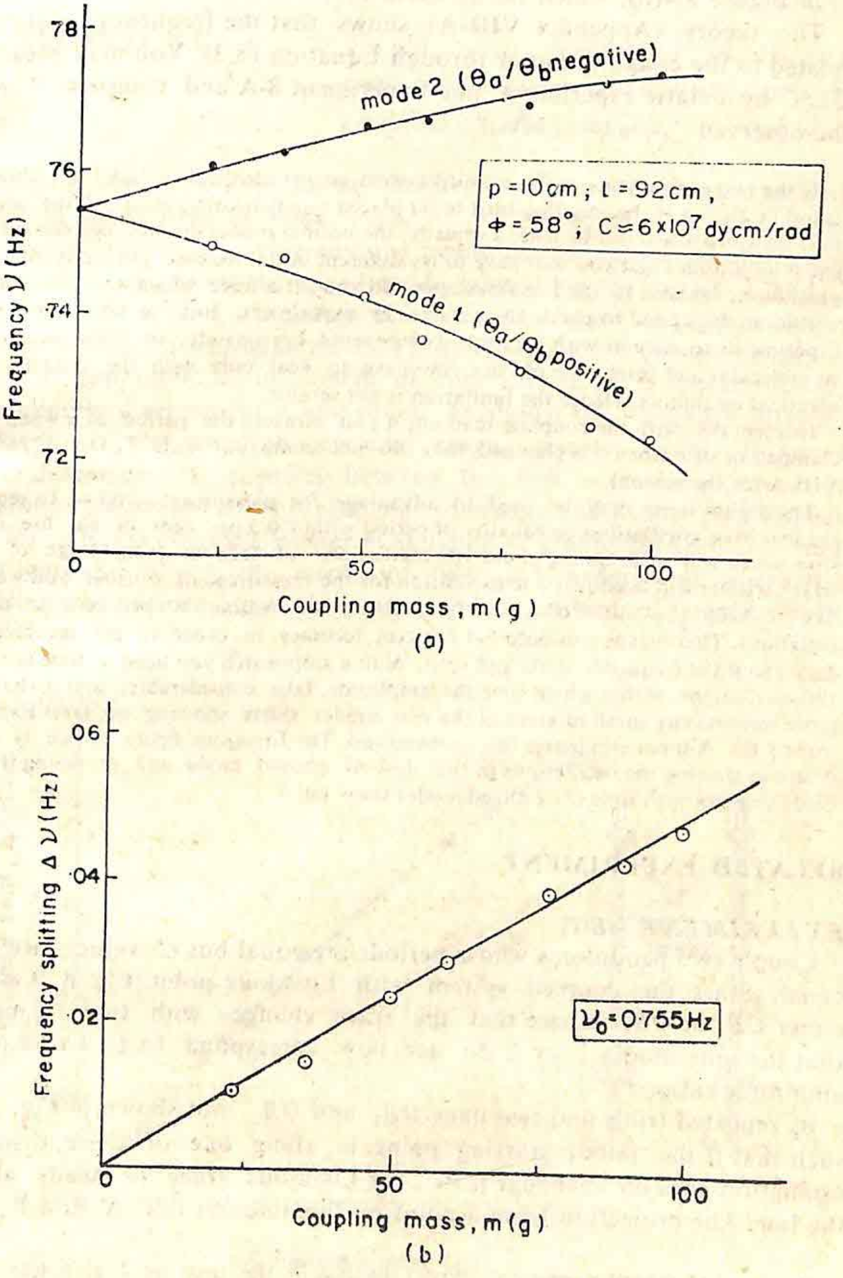

FIGURE 8.4. (*a*) Variation of frequencies of the two modes with the coupling mass, (*b*) Frequency splitting vs coupling mass m for the data of (*a*).

the mode 1 frequency does not remain constant; it decreases as the coupling increases. (You may look into Appendix VII-C and Appendix VIII-A to search for the reason.) In any case the splitting $\nu_2 - \nu_1$ increases with increasing m. The frequency splitting $\triangle\nu = \nu_2 - \nu_1$ is plotted against m in Figure 8.4(b), which shows linear relation.

The theory (Appendix VIII-A) shows that the frequency splitting is related to the coupling factor through Equation (8.3). You may measure C_{ab}/C by a static experiment* like Experiment 8-A and compare it with the observed $\triangle\nu/\nu_0$ $(=\triangle\omega/\omega_0)$.

If the two components in the coupled system are *not* identical in I and C (though equal in T_0), or if the coupling load is *not* placed symmetrically, most of the aforesaid statements will not be true. Typically, the normal modes do not correspond to equal amplitudes and you will have to try different initial release positions for the pendulums (as seen by the Lissajous spot) till you get a trace which does not change with time. It is good to check these facts by experiment. But we shall limit our experiments to systems with identical components. Fortunately, in most situations in molecular and solid state physics you have to deal only with the coupling of identical oscillators. Hence the limitation is not serious.

Incidentally, with the coupling load on, if you measure the period of a when b is clamped or of b when a is clamped, they do not come out to be T_0 (*see* Appendix VIII-A for the reason).

The digital timer may be used to advantage for measuring ν_1 and ν_2. In setting the two 'free' oscillations to equality of period within 0.5 per cent or so, use of a stop-watch will mean timing about 100 oscillations of each at every stage of the trial. A timer will need just one oscillation for the measurement. Further, you would like to keep the shifts of ν_1 and ν_2 from ν_0 small—within 10 per cent in most situations. That means you need ~1 per cent accuracy in order to get meaningful data about the frequency shifts and split. With a stop-watch you need to time around 100 oscillations, within which time the amplitude falls considerably, and (what is more serious) any small mixture of the two modes starts showing up (*see* Experiment 8-C). A timer eliminates this problem too. The Lissajous figure device is still of use in starting the oscillations in the desired normal mode and in seeing if the mode changes with time (*i.e.*, mixed modes show up).

RELATED EXPERIMENT

EXPERIMENT 8-B(i)

Couple two pendulums whose periods are equal but C values are *not* equal. Start the coupled system with Lissajous point (Fig. 8.2) along either OB_1 or OB_2 and see that the trace changes with time. It means that the pure modes 1 or 2 do *not* now correspond to 1 : 1 or 1 : −1 amplitude ratio.

By repeated trials find two lines OB_1' and OB_2' (not shown in Fig. 8.2) such that if the initial starting point is along one of these, then the oscillation goes on unchanged, *i.e.*, the Lissajous trace is steady along the line. The projection from a point on this line on the X and Y axes of Fig. 8.2 give the configuration (amplitude ratio) for the corresponding normal mode.

---

*You could as well compute C_{ab} from the data in the inset of Fig. 8.4(a) and Equation 8.4. But C will have to be determined then.

Estimate C_a and C_b and compute the configurations of normal modes from the theory given in Appendix VIII-A. Compare them with the experimental values.

EXPERIMENT 8-C *To study the frequency of energy transfer between the components in coupled oscillations.*

Give the system of Experiment 8-B an initial displacement which is neither in mode 1 nor in mode 2. (*see* § 8.2). Typically, you may excite the coupled system by giving any one pendulum an initial displacement which would mean that the mixed mode excited has the modes 1 and 2 in the ratio 1 : 1. Now watch how the Lissajous figure changes with the passage of time. It will be noted that if initially the excitation energy is given to pendulum *a*, in course of time whole of it passes to *b*, subsequently it returns to *a*, and so on. As shown in Appendix VIII-A, the frequency with which this cycle of energy transfer occurs is equal to the difference of frequencies between the two normal modes ($\triangle\nu$). Determine the period for this exchange of energy and hence $\triangle\nu$. Repeat this for different coupling masses *m* and plot a graph between $\triangle\nu$ and *m*. Figure 8.5 shows the results of one such experiment where the coupling was kept weaker by keeping ϕ and p smaller (*see* Equation 8.4).

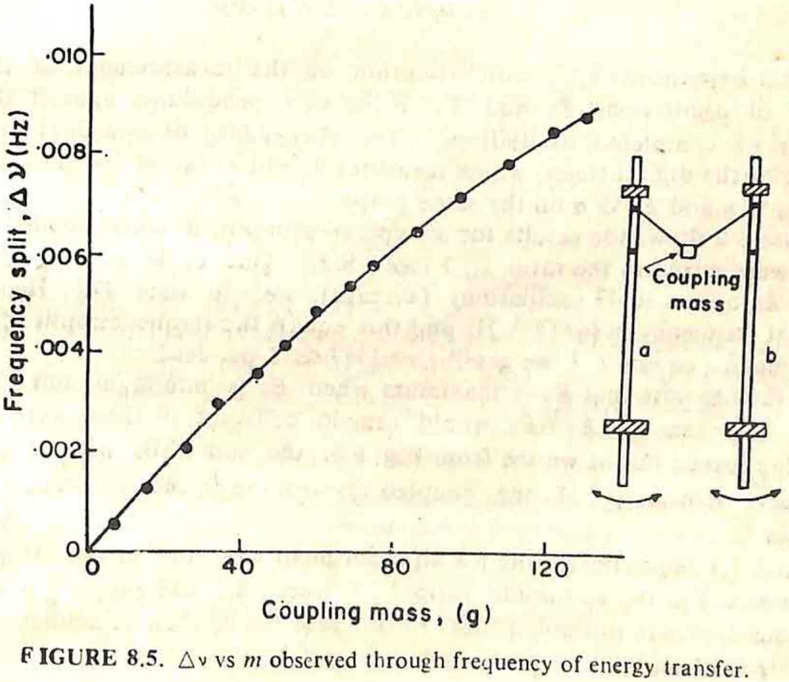

FIGURE 8.5. $\triangle\nu$ vs m observed through frequency of energy transfer.

You may note that while Experiment 8-B measures ν_1 and ν_2 from which their difference $\triangle\nu$ is to be computed, this experiment measures $\triangle\nu$ directly. In keeping with the general principle that small differences of large quantities are best measured directly, this Experiment 8-C is better for determining $\triangle\nu$. That is why this experiment enabled us to get $\triangle\nu$ vs m data for much smaller coupling than that used in Experiment 8-B, although the information given by Fig. 8.4 (a) is now missed.

RELATED EXPERIMENT

EXPERIMENT 8-C (i)

Couple two pendulums whose frequencies ν_a and ν_b differ by (say) 10 per cent. Start the coupled system with the Lissajous point in various orientations in Fig. 8.2, and in each case see if the trace would remain a straight line passing through 0. Thus search for the two lines OB'_1 and OB'_2 [as in Experiment 8-B (*i*)] which would correspond to the two normal modes. Hence deduce the configurations for these modes. Also measure the normal mode frequencies.

EXPERIMENT 8-C (ii)

Extend the above experiment to see the result of increasing the coupling strength on (*i*) the configuration of the normal modes (*ii*) the frequency separation.

EXPERIMENT 8-D *To study the details of energy transfer between the components in coupled oscillations.*

Repeat Experiment 8-C, with attention on the measurement of the energy of oscillations E_a and E_b of the two pendulums against the number of completed oscillations. The energy may be measured with the use of the digital timer, which measures $\dot{\theta}_a$ and $\dot{\theta}_b$ (as in Chapter 6). Plot E_a vs n and E_b vs n on the same graph.

Figure 8.6 shows the results for a typical experiment when modes 1 and 2 were mixed in the ratio 1 : 1 (*see* § 8.2). One cycle of rise and fall of E_a occurs in 47 oscillations (average), *i.e.*, in time $47T$. Hence the beat frequency is $(47T)^{-1}$ Hz and this equals the frequency split $\triangle\nu$. Since mean ν equals T^{-1}, we get $\triangle\nu/\nu = 1/47 \approx 2$ per cent.

We further note that E_a is maximum when E_b is minimum and *vice versa*. The sum of $E_a + E_b$ would remain constant if there were no damping losses; but as we see from Fig 8.6, the sum falls with n and we may deduce Q of the coupled system as in the experiments in Chapter 6.

Figure 8.7 shows the results for an experiment when the modes 1 and 2 were mixed in the amplitude ratio 2 : 1 (*see* § 8.2 and Figure 8.8; the Lissajous spot was initially at M). In this case the minima of neither E_a nor E_b fall to zero.

A mixed mode oscillation in the present case may be represented by the equations

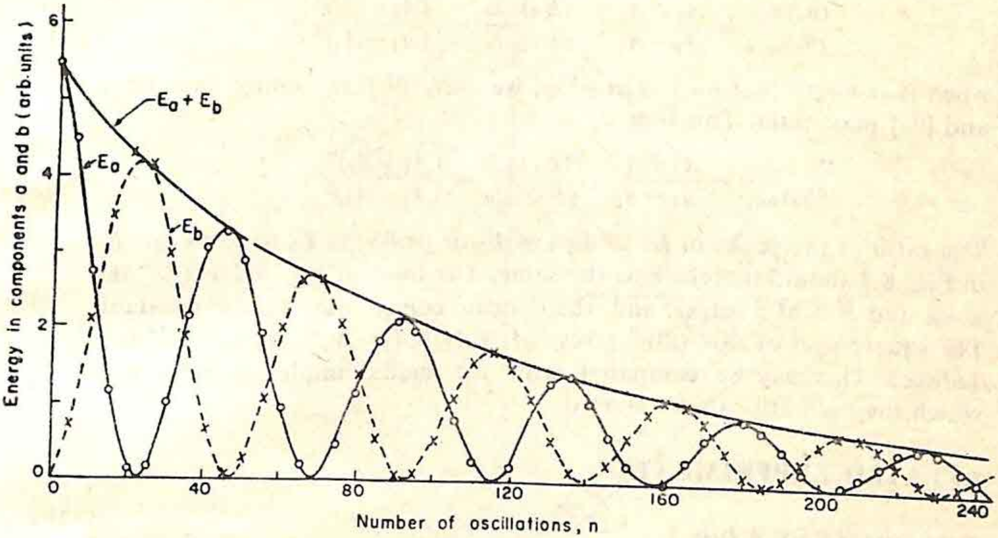

FIGURE 8.6. Energy in individual component pendulums *vs* the number of oscillations, when the two modes are mixed in equal proportions.

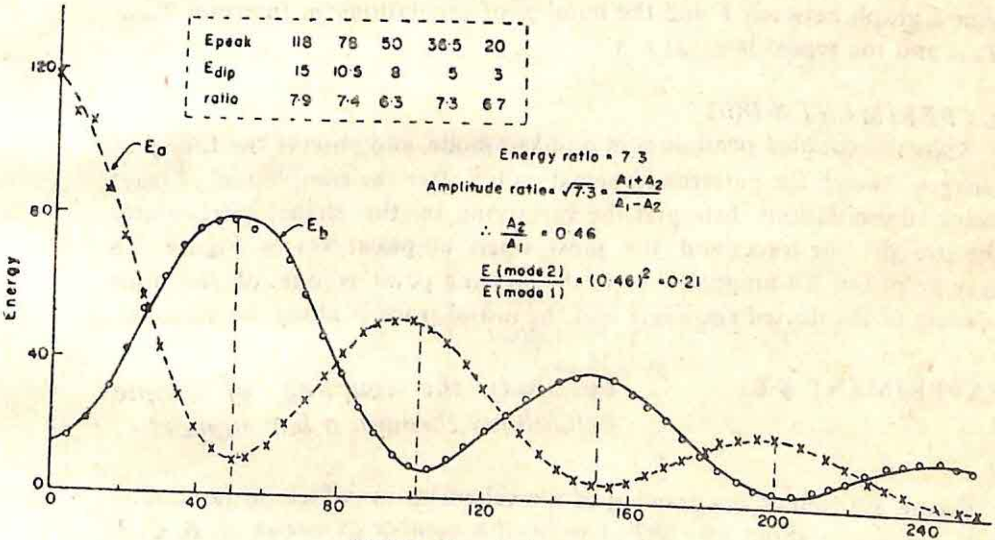

FIGURE 8.7. Variation of the energy of individual component pendulums with the number of oscillation when the two modes are mixed in unequal proportions.

$$\theta_a = A_1 \cos(\omega_1 t + \delta_1) + A_2 \cos(\omega_2 t + \delta_2)$$
$$\theta_b = A_1 \cos(\omega_1 t + \delta_1) - A_2 \cos(\omega_2 t + \delta_2)$$

When $(\omega_1 t + \delta_1) - (\omega_2 t + \delta_2) = 2n\pi$, the amplitude of θ_a becomes maximum (A_1+A_2) and that of θ_b becomes minimum (A_1-A_2). Hence, expressing amplitudes by (θ_a) and (θ_b),

$$\frac{(\theta_a)_{max}}{(\theta_b)_{min}}=\frac{A_1+A_2}{A_1-A_2};\quad \frac{(E_a)_{max}}{(E_b)_{min}}=\frac{(A_1+A_2)^2}{(A_1-A_2)^2}$$

when $(\omega_1 t+\delta_1)-(\omega_2 t+\delta_2)=(2n+1)\pi$, we find (θ_a) becoming minimum, and (θ_b) maximum. This time

$$\frac{(\theta_b)_{max}}{(\theta_a)_{min}}=\frac{A_1+A_2}{A_1-A_2};\quad \frac{(E_b)_{max}}{(E_a)_{min}}=\frac{(A_1+A_2)^2}{(A_1-A_2)^2}$$

The ratio of the peaks in E_a to dips in E_b or peaks in E_b to dips in E_a in Fig. 8.7 should therefore be the same. The inset in Fig. 8.7 marks the E_{peak} and E_{dip} at 5 stages, and their ratio comes out nearly constant. The square root of this ratio gives $(A_1+A_2)/(A_1-A_2)$, whence A_2/A_1 is deduced. This may be compared with the mode amplitude ratio with which the oscillations were started.

RELATED EXPERIMENTS

EXPERIMENT 8-D(i)

Start the coupled pendulum in a mixed mode and measure the period T of any one component (*a* or *b*) at intervals of (say) every 5 oscillations. Plot a graph between T and the number of oscillations n. Interpret T_{max}, T_{min} and the repeat interval $\triangle n$.

EXPERIMENT 8-D(ii)

Start the coupled pendulum in a mixed mode, and observe the Lissajous pattern. Sketch the patterns (schematically) after the completion of (say) every 10 oscillations. Interpret the variations in the shape, particularly the straight line traces and the most open elliptical traces. Figure 8.8 may help. For 2:1 amplitude ratio the starting point is one of the four corners of the dotted rectangle and the initial trace is along the diagonal.

EXPERIMENT 8-E

To study the coupling of simple pendulums through a bar support.

Figure 8.9 shows the drawing of a mechanism in which a horizontal bar, oscillating about axis *OO'*, has in it a number of screws *A*, *B*, *C*, *D* which support simple pendulums of varying lengths (lower parts not shown). As the bar makes angular oscillations about *OO'*, the suspension point of each pendulum makes oscillations—and the amplitude of this is proportional to the separation(s) of the suspension point from the line *OO'*. This separation can be varied by turning the screws *A*, *B*, *C*, *D*. One can have s positive or negative too; in Fig. 8.9 the tip of *A* is below the *OO'* line while that of *B* is above. The pendulum lengths—and hence the

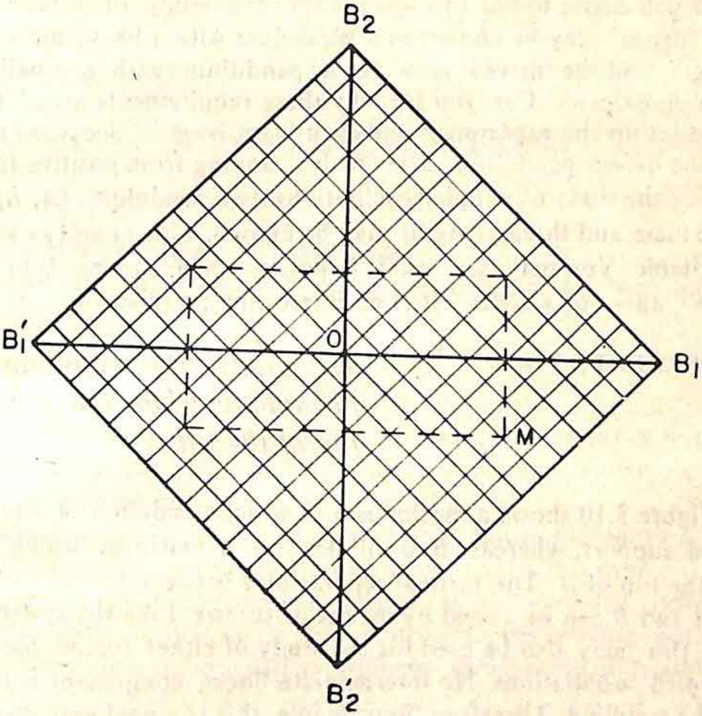

FIGURE 8.8. Light spot in the Lissajous figure arrangement in relation to modes 1 and 2.

ν_0 values—are unaffected by the coupling, which is a significant point about this system.

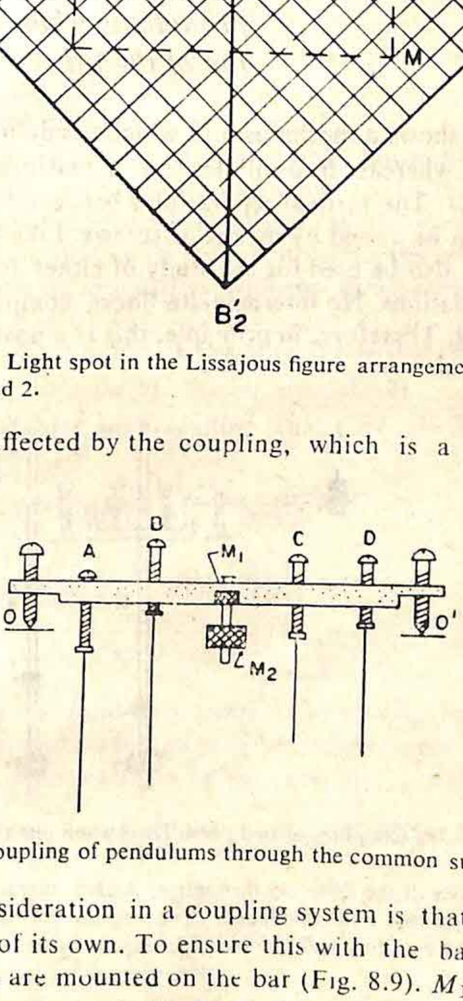

FIGURE 8.9. Coupling of pendulums through the common suspension bar.

An essential consideration in a coupling system is that it should not have a frequency of its own. To ensure this with the bar coupling two masses M_1 and M_2 are mounted on the bar (Fig. 8.9). M_1 can be moved horizontally and transverse to the bar to keep the screws vertical in the equilibrium state, and M_2 can be moved vertically till the bar (without the pendulum loads) shows an oscillation period $T \rightarrow \infty$.

If you desire to use this system for the study of forced oscillations, the 'driver' may be chosen as a pendulum with a heavy mass and variable length, and the 'driven' may be a pendulum with a small mass and a damping device. Can you see why these requirements arise? The best way is to set up the experiment and then learn from it. See how the response of the driven pendulum varies with s ranging from positive to negative.

For the study of coupled oscillations, two pendulums (A, B) of identical bob mass and thread lengths may be chosen, with s_A and s_B as the variants available. You may see what happens when $s_A=s_B=0$ or $s_A=s_B=s$ or $s_A=-s_B=s$ or $s_A \neq |s_B|$: It is an interesting exercise.

EXPERIMENT 8-F *To study the coupling of rigid pendulums when one rides over the top of the other.*

Figure 8.10 shows a mechanism in which pendulum A oscillates on a fixed support, whereas B oscillates on a platform which is mounted on the top of A. The vertical separation s between the axes of oscillations of A and B can be varied by means of screws. Like the system of Figure 8.9 this may also be used for the study of either forced oscillations or coupled oscillations. No intermediate 'loose' component is involved here in the coupling. Therefore, in principle, this is a neat system—nearest the theoretical ideal.

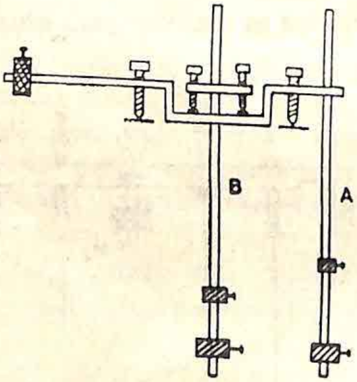

FIGURE 8.10. Coupling of two pendulums when one rides over the other.

Thus our choice of the coupling through a loaded thread was the poorest of the three alternatives we had developed! The reason for that choice was the easy variability of the coupling and the use of Lissajous figures device.

APPENDIX VIII-A

THEORY OF COUPLED OSCILLATIONS

1. System with Two Degrees of Freedom

When two oscillators a and b are coupled together, their equations of motion become

$$I_a\ddot{\theta}_a = -C_a\theta_a + C_{ab}\theta_b \qquad \ldots\text{VIII-A(1)}$$
$$I_b\ddot{\theta}_b = -C_b\theta_b + C_{ab}\theta_a$$

where C_{ab} represents the coupling constant and the other terms have their usual meanings. The oscillators are said to form one system, comprising two moving parts.

In general neither a nor b shows simple harmonic motion. But all possible motions of the system can be shown to be the superposition of just two *modes*, called the *normal modes* of the coupled system. The characteristic of a normal mode is that in it all the moving parts (here two) oscillate simple harmonically, with the same frequency, and in the same phase.*

Let a normal mode solution of Equation VIII-A(2) be

$$\theta_a = A_a \cos(\omega t+\delta)\ ;\ \theta_b = A_b \cos(\omega t+\delta)$$

Substitution in VIII-A(1), and recalling that $C_a/I_a=\omega_a^2$ and $C_b/I_b=\omega_b^2$, we get

$$(\omega_a^2-\omega^2)\theta_a - \frac{C_{ab}}{I_a}\theta_b = 0 \qquad \ldots\text{VIII-A(2)}$$

$$-\frac{C_{ab}}{I_b}\theta_a + (\omega_b^2-\omega^2)\theta_b = 0$$

whence $$(\omega_a^2-\omega^2)(\omega_b^2-\omega^2) - \frac{C_{ab}^2}{I_a I_b} = 0 \qquad \ldots\text{VIII-A(3)}$$

This equation gives two (and only two) values of ω^2, which we call ω_1^2 and ω_2^2. The corresponding modes may be called mode 1 and mode 2, and their *configurations* are given by the ratio $\theta_b/\theta_a = A_b/A_a$. We get

$$\left(\frac{\theta_b}{\theta_a}\right)_{\text{mode 1}} = \left(\frac{A_b}{A_a}\right)_{\text{mode 1}} = \frac{\omega_a^2-\omega_1^2}{C_{ab}/I_a} \qquad \ldots\text{VIII-A(4)}$$

$$\left(\frac{\theta_b}{\theta_a}\right)_{\text{mode 2}} = \left(\frac{A_b}{A_a}\right)_{\text{mode 2}} = \frac{\omega_a^2-\omega_2^2}{C_{ab}/I_a}$$

As an example consider a case when

$$\omega_a=\omega_b,\ I_a=4\,I_b,\ C_{ab}/I_a=0.1\,\omega_a^2$$

---

* See footnote on page 154.

The equations give the following normal mode frequencies and configurations

$$\omega_1 = 0.894\ \omega_a\ ;\ \ \omega_2 = 1.096\ \omega_a$$

$$\left(\frac{A_b}{A_a}\right)_{\text{mode 1}} = +2\ ;\ \left(\frac{A_b}{A_a}\right)_{\text{mode 2}} = -2$$

As another example consider the case

$$\omega_a = 2\omega_b,\ I_a = I_b,\ C_{ab}/I_a = 0.2\ \omega_a^2$$

The results for this case are

$$\omega_1 = 0.447\ \omega_a\ ;\ \omega_2 = 1.025\ \omega_a$$

$$\left(\frac{A_b}{A_a}\right)_{\text{mode 1}} = +4,\ \ \left(\frac{A_b}{A_a}\right)_{\text{mode 2}} = -\frac{1}{4}$$

Thus the two normal mode frequencies and relative amplitudes in them follow no simple rules; they depend so much on the parameters of the two component oscillators. For C_{ab} positive (*i.e.*, clockwise θ_b causing clockwise torque on oscillator *a*) the mode of higher frequency has *a* and *b* oscillating oppositely (*i.e.*, amplitude ratio negative). The general oscillation is a superposition of the two modes and may be written as

$$\theta_a = A_{a1}\cos(\omega_1 t + \delta_1) + A_{a2}\cos(\omega_2 t + \delta_2)$$
$$\theta_b = A_{b1}\cos(\omega_1 t + \delta) + A_{b2}\cos(\omega_2 t + \delta)$$

where the ratios A_{b1}/A_{a1} and A_{b2}/A_{a2} are given by Equation VIII-A(3). The boundary conditions decide A_{a1}, A_{b2}, δ_1, and δ_2.

2. System with Three Degrees of Freedom

The equations of motion for a system with three degrees of freedom will be

$$\begin{aligned} I_a\ddot{\theta}_a &= -C_a\theta_a + C_{ab}\theta_b + C_{ca}\theta_c \\ I_b\ddot{\theta}_b &= +C_{ab}\theta_a - C_b\theta_b + C_{bc}\theta_c \\ I_c\ddot{\theta}_c &= +C_{ca}\theta_a + C_{bc}\theta_b - C_c\theta_c \end{aligned} \qquad \ldots\text{VIII-A(5)}$$

where C_{ab}, C_{bc} and C_{ca} are the three coupling constants. The equations leading to the normal mode frequency ω are, like Equation VIII-A(2),

$$\begin{aligned} (\omega_a^2-\omega^2)\theta_a - \frac{C_{ab}}{I_a}\ \theta_b - \frac{C_{ca}}{I_a}\ \theta_c &= 0 \\ -\frac{C_b}{I_b}\ \theta_a + (\omega_b^2-\omega^2)\theta_b - \frac{C_{bc}}{I_b}\ \theta_c &= 0 \\ -\frac{C_{ca}}{I_c}\ \theta_a - \frac{C_{bc}}{I_c}\ \theta_b + (\omega_c^2-\omega^2)\theta_c &= 0 \end{aligned} \qquad \ldots\text{VIII-A(6)}$$

Therefore ω^2 is given by the determinant equation

$$\begin{vmatrix} \omega_a^2-\omega^2 & -\dfrac{C_{ab}}{I_a} & -\dfrac{C_{ca}}{I_a} \\ -\dfrac{C_{ab}}{I_b} & \omega_b^2-\omega^2 & -\dfrac{C_{bc}}{I_b} \\ -\dfrac{C_{ca}}{I_c} & -\dfrac{C_{bc}}{I_c} & \omega_c^2-\omega^2 \end{vmatrix} = 0 \qquad \ldots\text{VIII-A(7)}$$

This would give three (and only three) solutions for ω^2. You may extend the idea to state that for N oscillators, which are coupled together to form a system, there will be N equations like

$$I_i\ddot{\theta}_i = -C_i\theta_i + \Sigma' C_{ij}\theta_j \qquad \text{...VIII-A(8)}$$

and these will give exactly N solutions for ω^2. Each normal mode will have a distinct configuration (*i.e.*, relative amplitudes of the component oscillators). Two or more normal modes may coincide in frequency, yet they are distinguished by the configuration of the oscillation. Such modes are said to be degenerate.

3. Coupling of Identical Oscillators

If we consider two identical oscillators ($I_a = I_b = I$, $C_a = C_b$), the coupling is expressed more conveniently as*

$$\begin{aligned} I\ddot{\theta}_a &= -C\theta_a + C_{ab}(\theta_b - \theta_a) \\ I\ddot{\theta}_b &= -C\theta_b + C_{ab}(\theta_a - \theta_b) \end{aligned} \qquad \text{...VIII-A(9)}$$

In the absence of coupling the frequency ω_0 is given by

$$\omega_0^2 = \frac{C}{I}$$

The coupling adds for oscillator a one torque $-C_{ab}\,\theta_a$ and another torque $C_{ab}\theta_b$. The first may be considered as responsible for changing ω_0 to ω_0' given by

$$\omega_0'^2 = \frac{C + C_{ab}}{I}$$

and the second is the coupling (torque on a due to b).

We shall use a different procedure for solving Equation VIII-A(9) than that given in § 1 above. Adding and subtracting the two equations in turns we get

$$I.\frac{d^2(\theta_a + \theta_b)}{dt^2} = -C(\theta_a + \theta_b)$$

and

$$I\,\frac{d^2(\theta_a - \theta_b)}{dt^2} = -(C + 2C_{ab})\,(\theta_a - \theta_b) \qquad \text{...VIII-A(10)}$$

Thus the first equation involves only $\theta_a + \theta_b$, the second only $\theta_a - \theta_b$. These are called *normal coordinates* and for them the equations become uncoupled. The solutions of these equations give the two *normal modes*

mode 1 $\quad \theta_a + \theta_b = A_1 \cos(\omega_1 t + \delta_1)$;

with

$$\omega_1^2 = \frac{C}{I} = \omega_0^2 \qquad \text{...VIII-A(11)}$$

mode 2 $\quad \theta_a - \theta_b = A_2 \cos(\omega_2 t + \delta_2)$;

with

$$\omega_2^2 = \frac{C + 2C_{ab}}{I}$$

---

* $C = C_a + C_{ab} = C_a + C_{ab}$.

Now pure mode 1 means $A_2=0$, which leads to

$$\frac{\theta_b}{\theta_a}=+1$$

Similarly, pure mode 2 means

$$\frac{\theta_b}{\theta_a}=-1$$

Thus the two oscillators move with equal amplitudes in both modes, but the phase difference is zero in mode 1 and π in mode 2.

Consider a typical case of weak coupling, $C_{ab}=0.04C$. Then the equations give

$\omega_0'=1.02\ \omega_0$; $\omega_1=\omega_0$; $\omega_2=1.04\ \omega_0$. You may see that

$$\frac{\omega_2-\omega_1}{\omega_0}=0.04=\frac{C_{ab}}{C} \qquad \text{. . . VIII-A(12)}$$

which means that for weak coupling the fractional frequency split is equal to the ratio of the coupling constant to the restoring constant of each component oscillator.

One could have strong coupling too, like $C_{ab}=2C$. Then one gets

$$\omega_0'=1.73\ \omega_0;\ \omega_1=\omega_0;\ \omega_2=2.24\ \omega_0$$

Equation VIII-A(12) is not applicable for cases of strong coupling.

4. Superposition of Modes and Beats

A general oscillation of the coupled oscillator involves superposition of both the normal modes. Equations VIII-A(11) lead to

$$\theta_a=\tfrac{1}{2}[A_1\cos(\omega_1 t+\delta_1)+A_2\cos(\omega_2 t+\delta_2)]$$
$$\theta_b=\tfrac{1}{2}[A_1\cos(\omega_1 t+\delta_1)-A_2\cos(\omega_2 t+\delta_2)] \qquad \text{. . . VIII-A(13)}$$

Both these equations show that the motion of the pendulums would not be harmonic, but would show beats of angular frequency $\omega_2-\omega_1$. If A_a and A_b are the amplitudes of a and b respectively, we have

$$\left.\begin{aligned}A_a&=A_1+A_2\\ A_b&=A_1-A_2\end{aligned}\right]\ \text{when } (\omega_1 t+\delta_1)=(\omega_2 t+\delta_2)$$

and

$$\left.\begin{aligned}A_a&=A_1-A_2\\ A_b&=A_1+A_2\end{aligned}\right]\ \text{when } (\omega_1 t+\delta_1)=(\omega_2 t+\delta_2)+\pi$$

Thus the amplitude A_a becomes maximum when A_b is minimum and *vice versa*. For any *mixed mode* the proportion of the normal modes present may be deduced from $(A_a)_{max}$ and $(A_a)_{min}$. Thus

$$A_1=\tfrac{1}{2}[(A_a)_{max}+(A_a)_{min}]$$
$$A_2=\tfrac{1}{2}[(A_a)_{max}-(A_a)_{min}] \qquad \text{. . . VIII-A(14)}$$

The fact that the beat frequency is equal to the difference of the frequencies of the two normal modes is useful in determining the frequency difference.

9

STUDIES WITH THE TORSIONAL TRANSMISSION LINE

9.1. INTRODUCTION

The propagation of waves is perhaps best understood in terms of transfer of energy through a system of coupled mechanical oscillators arranged as a transmission line in one dimension. One can visually observe how the velocity, wavelength, reflection etc. are dependent on various parameters of the line and are mutually related. One can also study reflection, transmission and scattering at a discontinuity.

Some additional features also come out because the transmission line is a lumped medium with a finite number of units, as distinct from a continuous medium. Firstly, the number of normal modes of oscillation is finite (equal to the number of lumped units), each mode having a specific configuration of its own. Secondly, ω/k is not constant, *i.e.*, the line shows dispersive character. In fact, ω attains a limiting upper value ω_c, which is the cut-off frequency for the system.

9.2. DESCRIPTION OF THE TORSIONAL TRANSMISSION LINE

A flat steel measuring tape, 6 mm wide and $\sim$2 m long, is suspended vertically on a stand and loaded with several dumb-bells, clamped at equal spacing. Each dumb-bell comprises of a horizontal rod, about 25 cm in length, carrying loads of $\sim$50 gm each on either side. The clamping is achieved with a flat contact of 6 mm width, so that no discontinuity is produced, which otherwise may result in a frictional loss. The loads on the dumb-bell can be slided in and out so that the moment of inertia may be varied from $\sim$ 500 to $\sim$ 12000 gm cm^2. The dumb-bell spacing along the tape can be varied from about 3 cm to 30 cm. Figure 9.1 gives a photograph of the apparatus.

A circular scale is mounted on the stand to measure the angular displacement of any dumb-bell. There is also a provision for clamping one or more of the dumb-bells to the stand. At the bottom end of the tape a heavy load is suspended to minimise the variation of tension along the tape; but the moment of inertia of this section may be matched with that of the other dumb bells in the line. The bottom section may be replaced by a wire-net, which may be dipped in water up to different depths (see Figure 9.1). This provides a variable (and measurable) termination at the lower end.

Two straight aluminium rods, ~ 2 m long and 1 cm × 1 cm cross-section, are provided to make all the dumb-bells come to equilibrium state at the start of an experiment.

9.3. CONSTANTS OF THE LINE

The torsional line may be treated as a chain of coupled oscillators, as shown in Figure 9.2. The behaviour of each oscillator depends on the parameters : (*i*) moment of inertia I, and (*ii*) restoring torque factor C, which depends on the tape length (spacing) a. Since C is proportional to $1/a$ for a given tape, it is useful to define

$$C' = Ca \qquad \ldots (9.1)$$

where C' is restoring factor for unit length and hence is a constant for the given tape (units: dy. cm^2/rad).

For purposes of comparison it is useful to define a *uniform* line equivalent to the *lumped* line. If dumb-bells of moment of inertia I each and spacing a are replaced by those of moment of inertia I/n each and spacing a/n, then with $n \to \infty$ we get a uniform equivalent line. It is equivalent in so far as the moment of inertia per unit length of the line (I') remains the same. We thus define I' through

$$I' = I/a \qquad \ldots (9.2)$$

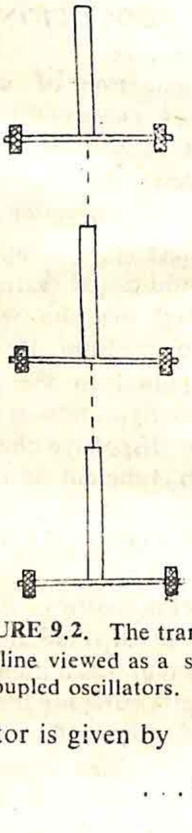

FIGURE 9.2. The transmission line viewed as a system of coupled oscillators.

The period of oscillation of the individual oscillator is given by

$$T_0 = 2\pi \sqrt{\frac{I}{C}} = 2\pi a \sqrt{\frac{I'}{C'}} \qquad \ldots (9.3)$$

The quantity

$$r_c = \sqrt{C'I'} = \sqrt{CI} \qquad \ldots (9.4)$$

is called the *characteristic impedance* of the line. It governs the reflection and absorption of waves. If I' is kept constant, then r_c will be constant for different 'lines' on the same tape.

Appendix IX-A gives the theory of oscillations on the transmission line. The main results are the following. For $\lambda \gg a$ the wave velocity is given by*

$$v = \frac{\omega}{k} = \sqrt{\frac{C'}{I'}} = \sqrt{\frac{C}{I}} \qquad \ldots (9.5)$$

---

*$\omega = 2\pi/T$ and $k = 2\pi/\lambda$. Hence $\omega/k = \lambda/T =$ velocity.

and for low λ values (high k) ω tends to a maximum value ω_{max} given by

$$\omega_{max} \approx \frac{2}{a}\sqrt{\frac{C'}{I'}} = 2\sqrt{\frac{C'}{Ia}} \qquad \ldots(9.6)$$

The traversal time per section (T_S) is given, using Equation (9.5), by

$$T_S = \frac{a}{v} = \sqrt{\frac{I}{C}} = \frac{T_0}{2\pi} \qquad \ldots(9.7)$$

9.4. EXCITING THE TORSIONAL TRANSMISSION LINE

Modes in a bounded transmission line may be excited by the resonance

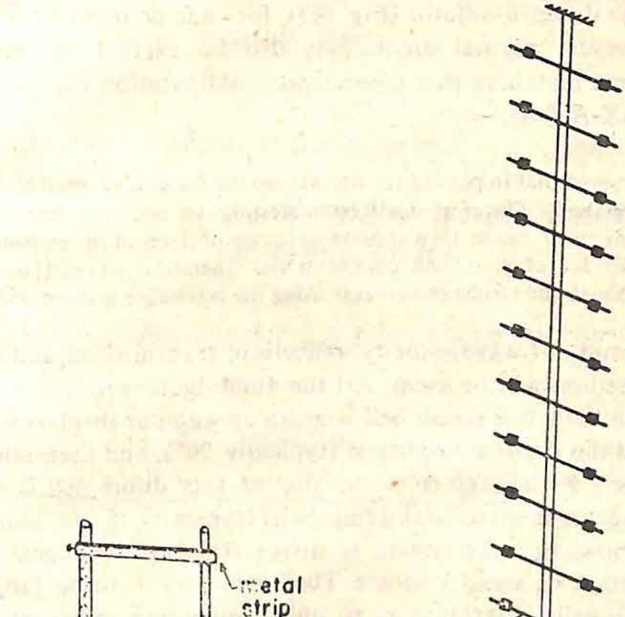

FIGURE 9.3. The mechanical driving oscillator coupled to the transmission line.*

*This is similar to the one shown in Fig. 5.2(b) and described in § 5.3, except that no magnet is needed here.

technique. As shown in Figure 9.3 a mechanical oscillator is coupled to one dumb-bell unit of the line (by two loaded threads), providing a harmonic driving torque of variable frequency ω. The normal modes (also called the standing wave modes) are excited whenever ω of this driver coincides with the frequency of one of the normal modes of the line. A normal mode is judged by the criterion that in it all the dumb-bells oscillate in phase, *i.e.*, they come to rest simultaneously during the oscillations. Absence of this condition means oscillations in a mixed mode.

However, two problems arise because of high Q of the system: (*i*) The transients die out very slowly, so that each trial needs several minutes; and (*ii*) fine frequency changes have to be tried out to locate the resonant frequencies. For the latter reason two smaller sliding masses are provided on the driver-oscillator (Fig. 9.3) for fine changes in I and hence in ω. However, normal modes may also be excited by giving initial displacements matching the theoretical configuration for each mode (*see* Appendix IX-A, § 4).

It may be noted that in physics the normal modes are always excited through the resonance method. Therefore it will be interesting to use that method. The configuration for each mode then appears as the natural result of excitation. But the process needs lot of time and careful trials. Therefore we will use the second method, although the results of two case using the resonance method will be cited.

For the study of wave velocity, reflection, transmission and absorption, the pulse method will be used. All the dumb-bells are initially brought to rest, and then one dumb-bell is given an angular displacement slowly, going up to the desired amplitude (typically 90°), and then released. The rate is to be slow enough to ensure that as this dumb-bell is turned, the pulse spreads over to several dumb-bells (typically 5 or more). Appendix IX-A shows that the system is dispersive (ω/k changes with k) at high k values, *i.e.*, small λ values. The 'smallness' is to be judged relative to the dumb-bells separation a. A pulse spreading over several dumb-bells means that we are working in the larger λ (smaller k) range, where ω/k is almost constant, *i.e.*, the medium behaves as a non-dispersive one. The timing of the whole process determines the 'shape' of the pulse; however, for a slow enough pulse (as described above) most results do

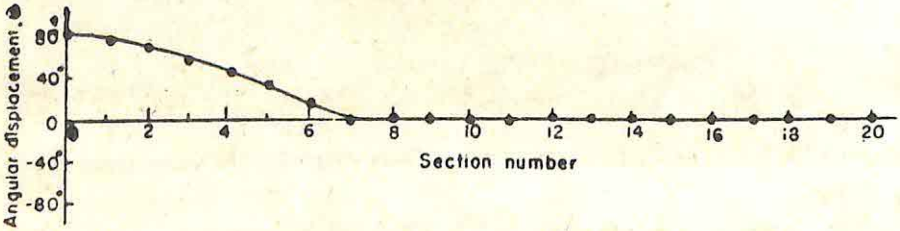

FIGURE 9.4(a). One typica lpulse shape.

not depend sharply on the pulse shape. For this reason a mechanical device to ensure the generation of a reproducible pulse is not necessary.

Figure 9.4 (a) shows the pulse described above. You may note that dumb-bell 0, from which the pulse is generated, is released at some angle (here 80°) and not brought to $\theta=0$. But you could as well bring the dumb-bell back (slowly, of course) to $\theta=0$ before release. The pulse generated then will have a shape shown in Fig. 9.4(b).

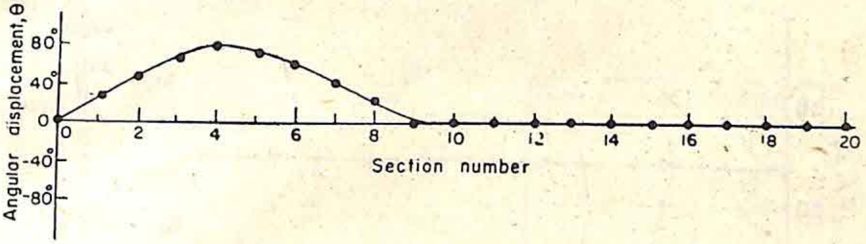

FIGURE 9.4(b). Another typical pulse shapes.

EXPERIMENT 9-A *To determine the constant C′ of the transmission line.*

Mount a single dumb-bell (inset Fig. 9.5) on a sample of the same tape

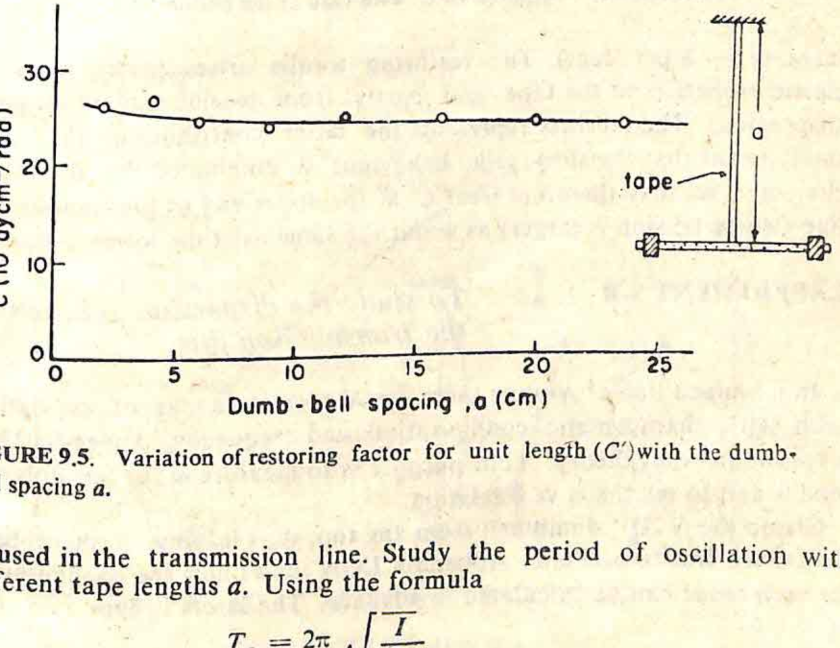

FIGURE 9.5. Variation of restoring factor for unit length (C') with the dumb-bell spacing a.

as used in the transmission line. Study the period of oscillation with different tape lengths a. Using the formula

$$T_\circ = 2\pi\sqrt{\frac{I}{C}}$$

deduce C and hence $C'=C.a$. Plot a graph between C' and a.

Figure 9.5 shows the results of a typical experiment. We expect C' to be independent of a, but in practice it falls off a little as a increases from a low value. (For practical purposes we may take $C'=24\times10^4$ dy cm^2/rad for all the experiments discussed hereafter).

Next, with a fixed, suspend various loads on the section with the help of a thin and long* thread (*see* inset, Fig. 9.5), and measure C'. Plot a graph for C' vs the load. Figure 9.6 shows the results of a typical experiment. For a load equivalent to 30 dumb-bells C' shows a small increase ($\sim$ 8 per cent). The restoring torque arises partly from the elastic properties of the tape and partly from tension (as in a bifilar suspension). The increase represents the latter contribution; that it is small means that the steel tape behaviour is dominated by the elastic character. We may therefore treat C' at the upper end of the transmission line (where tension is larger) as about the same as at the lower end.

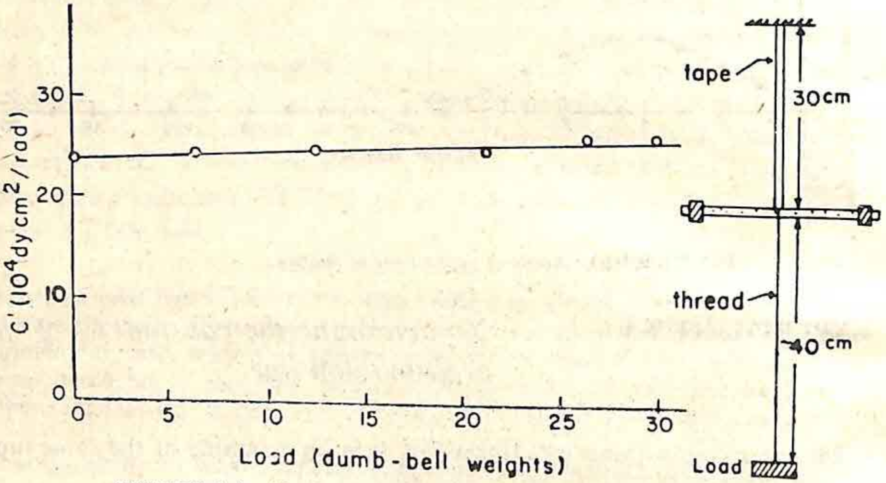

FIGURE 9.6. Variation of C' with load at the bottom end.

EXPERIMENT 9-B *To study the dispersion relation in the transmission line.*

In a lumped line of N units there are N normal modes of oscillation, each with characteristic configuration and frequency. Appendix IX-A gives the relevant theory. Your purpose is to measure ω for the different modes and to see the ω vs k relation.

Clamp the $N+1^{th}$ dumb-bell from the top, thus leaving N dumb-bells in between free to oscillate. Appendix IX-A shows how the configuration for each mode can be calculated in advance. The insets in Figs. 9.7 (a),

---

*This will keep the contribution to restoring torque due to the thread negligibly small.

(b) and (c) show the configurations thus deduced for all the modes with $N=3$, 4 and 5 respectively.

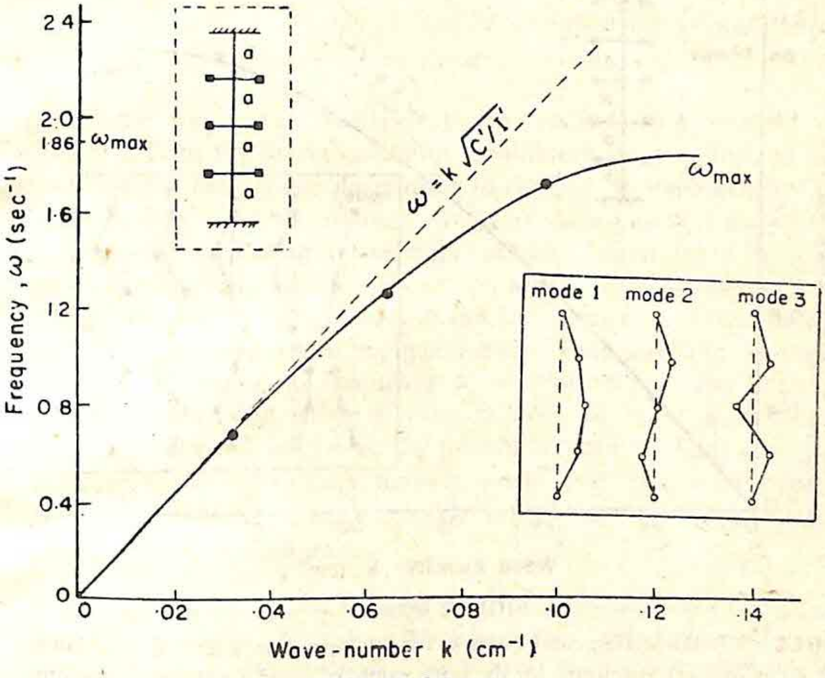

FIGURE 9.7. (a)

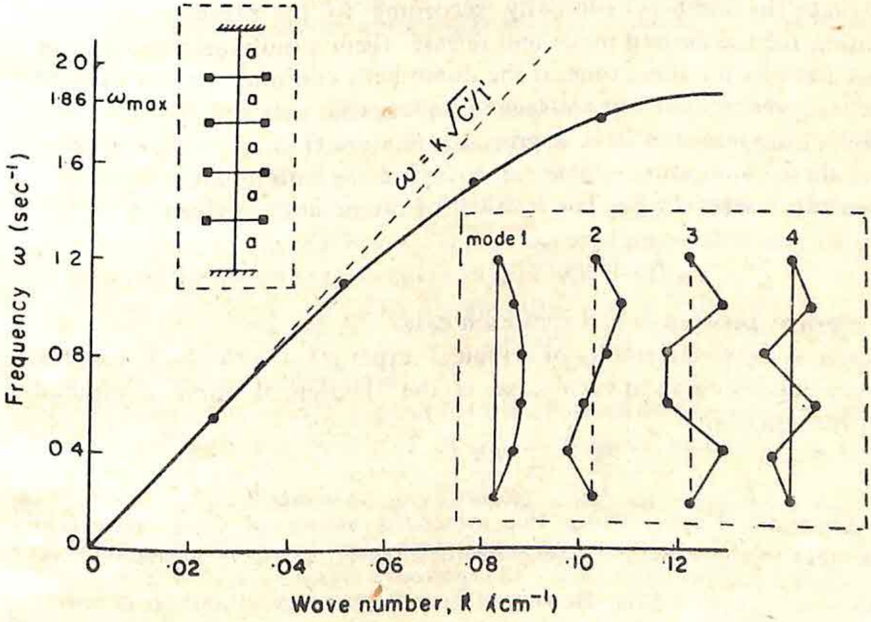

FIGURE 9.7 (b)

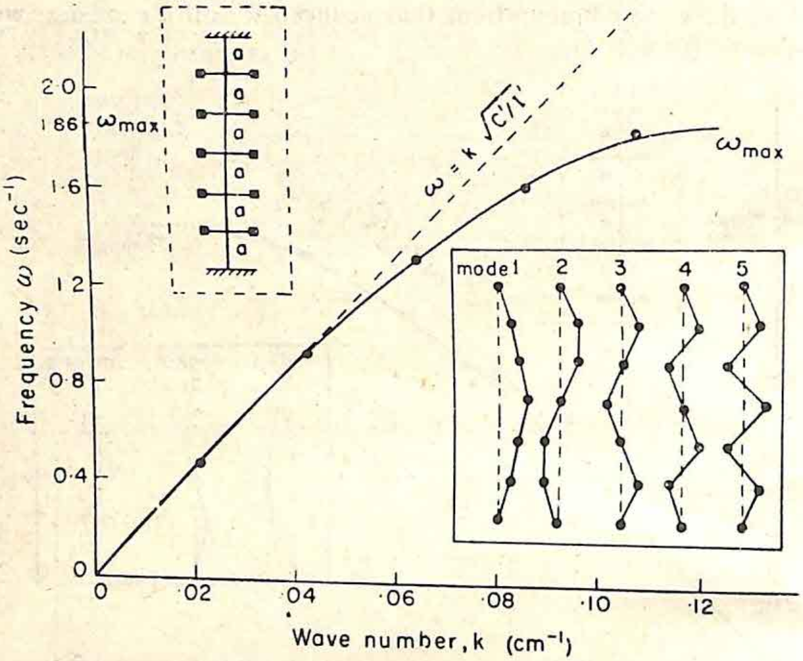

FIGURE 9.7.(c)

FIGURE 9.7. Dispersion curve (ω vs k) for a lumped line with (*a*) 3 sections. (*b*) 4 sections, (*c*) 5 sections, for the same values of a and I (The corresponding normal mode configurations are also shown in each figure).

Displace the dumb-bells initially according to the precalculated configuration for the desired mode and release them simultaneously. Watch the oscillations for some time; if the dumb-bells continue to oscillate in phase (*i.e.*, reach their rest states simultaneously), you are assured that the oscillation does not have appreciable mixture from the other modes. Under these conditions, measure the period T with a stop-watch and hence deduce ω ($= 2\pi/T$). The k value for the modes are given by*

$$k_p = p.\frac{\pi}{(N+1)a}$$

Plot a graph between ω and k in each case.

Figure 9.7 give the results of a typical experiment with N=3, 4 and 5. The continuous curve in each case is the theoretical curve computed from the equation

$$\omega^2 = \frac{4C'}{Ia}\sin^2\frac{ka}{2}, \qquad k = p.\frac{\pi}{(N+1)a} \qquad \ldots(9.8)$$

(*see* Appendix IX-A), using the measured values of C', I and a. The agreement of the observed data with the theoretical curve is remarkable.

---

*Largest $\lambda = 2L = 2(N+1)a$. Hence smallest $k = 2\pi/2L = \pi/(N+1)a$. Other k values are integral multiples of this.

EXPERIMENT 9-C *To study the normal mode configurations and dispersion relation in the transmission line using the resonance method.*

Couple the driver oscillator to the transmission line as shown in Fig. 9.3. Start the driver oscillator at different frequencies and each time look for the oscillations developing in the line. In each attempt you may have to wait for 5-10 minutes.* In most cases you will find the different dumb-bells oscillating in different phases; but in some cases a normal mode is excited, which means that all the dumb-bells oscillate in one phase. The relative amplitudes of the dumb-bells now remain fixed, this set of relative amplitudes being called the configuration. In these cases you may determine the frequency of oscillations, ω. The corresponding k is given by $(\pi/L)p$, where p is the number of segments into which the total line length L is divided by the configuration. Thus you get ω vs k data for the line. For each normal mode you may also estimate the ratio of amplitudes of the successive dumb-bells so as to represent the configuration in a diagram.

It is useful to calculate the lowest $k (k_1=\pi/L)$ and hence $\omega_1=k_1\sqrt{C'/I'}$. The driver frequency may be set a little above this value and gradually decreased** to search for resonance. For the next mode, the frequency may be set a little above $2\omega_1$ and gradually decreased in search for resonance. It is useful to remember that if p^{th} mode frequency is ω_p, the frequency of the $p+1^{th}$ mode is a little below ω_p, $(p+1)/p$.

When the driver frequency matches that of a normal mode, the 'line' picks up oscillations with a specific configuration and it is interesting to see the configuration develop by itself.

Figure 9.8 shows schematically the configurations obtained experimentally using the resonance method for a line with $N=8$ with both ends clamped. The frequencies of the 8 modes have also been stated there. You may draw a graph of ω or ν versus p, which corresponds to the dispersion curve.† Below Fig. 9.8 the experimental values of ν_p/ν_8 are given along with the theoretical values deduced from

$$\frac{\nu_p}{\nu_8}=\frac{\omega_p}{\omega_8}=\frac{\sin (10p)^\circ}{\sin 80^\circ} \qquad (p=1 \text{ to } 8)$$

The agreement is very good.

Figure 9.9 shows the typical results obtained by the resonance method for a line with $N=15$. A plot of ω against mode number p is shown. It

---

* The driver will have to be supplied energy every few minutes and this may be done by just an appropriate push.

**Decrease of ω may be achieved by adding loads on the oscillator arms even as it is in motion. This is a useful procedure in finer adjustments, though for major changes in ω the masses have to be slided.

†$\omega_p=2\pi\nu_p$ and $k_p=p(\pi/L)$.

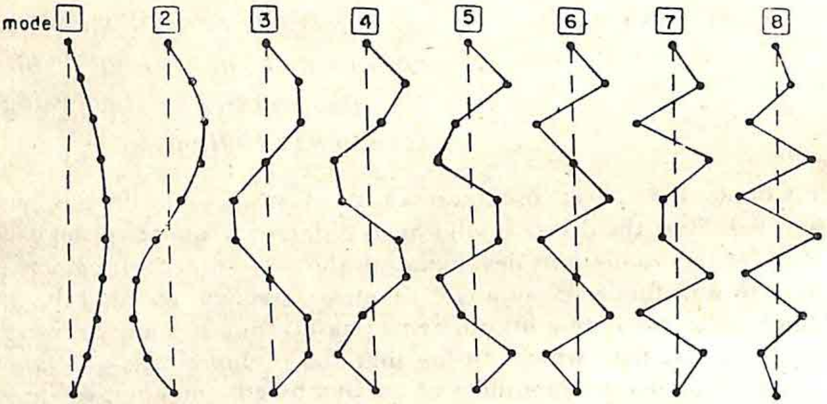

mode	1	2	3	4	5	6	7	8
ν_p =	0·080	0·160	0·236	0·307	0·357	0·400	0·444	0·463 (Hz)
$(\frac{\nu_p}{\nu_8})_{cal}$ =	0·173	0·346	0·510	0·663	0·771	0·864	0·959	1·00
$\frac{\nu_p}{\nu_8})_{theo}$ =	0·176	0·348	0·515	0·653	0·776	0·880	0·955	1·00

FIGURE 9.8. Configurations and frequencies for the 8 modes excited in a line with $N=8$ by the resonance method. $(\nu_p/\nu_s)_{exp}$ compared with the corresponding theoretical values.

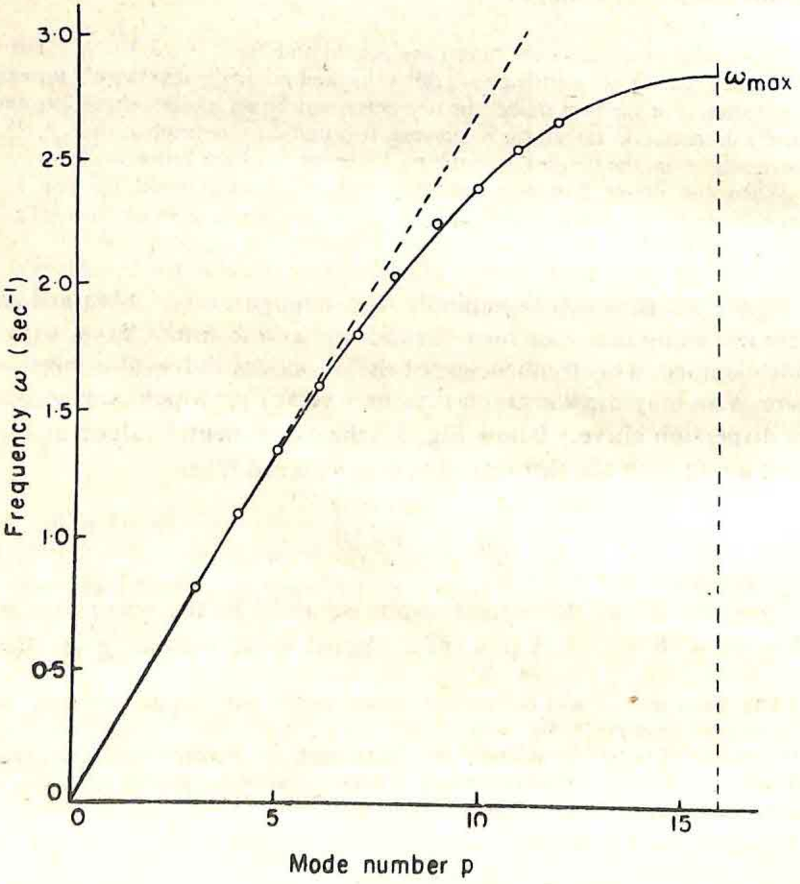

FIGURE 9.9. Dispersion curve for a line with $N=15$ studied by the resonance method. Modes $p=1$, 2, 13, 14, 15 could not be studied (*see* text).

will be noted that modes 1 and 2 could not be excited since they needed a driver frequency below the minimum available with the given driver. Modes 13, 14 and 15 also could not be excited, apparently because the frequencies in this region are too much crowded together. Possibly small differences of I and a in the line cause more noticeable departures from the theoretical ideal in these higher modes than in the lower modes. The higher modes thus "see" such departures more seriously.

In Fig. 9.9 the theoretical curve is obtained from Equation (9.8) using ω_3 (ω for $p=3$) to eliminate the constant $4C'/Ia$. It will be noted that the experimental points fit the curve quite well.

EXPERIMENT 9-D *To study the propagation velocity along the line.*

Set up the propagation line with a larger number of identical dumb-bells (say$>$20) with equal spacing a. Bring the system to the state of rest and generate a pulse at the bottom end. See how the pulse travels up and down. See also if the reflections at the top and the bottom ends are different.

With a stop-watch determine the time t for transmission of the pulse across different lengths l on the line, and plot a graph between t and l.* Also count the number of sections n corresponding to each l and plot t vs n graph.

Figure 9.10 shows the typical results of one such experiment. The t vs l plot is a straight line. Since the data extend to as many as 10 back-and-forth journeys, in which the pulse becomes quite weak, the straight line character of the curve shows that the pulse velocity does not depend on the amplitude in the range used (initial $\theta_0=90°$). The slope $\Delta l/\Delta t$ gives the velocity v in terms of cm/sec, while the slope $\Delta n/\Delta t$ gives the velocity v_s in terms of sections/sec.

The constants given in the inset, when used in Equation IX-A(15) of Appendix IX-A, give the velocity as

$$v=\frac{\omega}{k}=\sqrt{\frac{24\times 10^4}{(1.32/6.2)10^4}}=10.8 \text{ cm/sec.}$$

which compares well with the experimental value 11.1 cm/sec

The *traversal time* per section (T_s) comes out to be 0.59 sec. Although T_0 could be computed from C', I and a it was measured directly and it came to 3.75 sec., which gave $T_0/2\pi=0.594$ sec.$=T_s$. This is in agreement with Equation (9.7).

In about 15 to 20 passages up and down the line, the pulse starts degenerating into 'noise'—which means random disturbance. How would you explain such occurrence?

---

*In each unit there is a deed length of 0.6 cm corresponding to clamping of the unit with the tape. In the measurement of l this length must be accounted for.

You may try to generate 'sharper' pulses (less spread in Figure 9.4) and see if the pulse degenerated faster or slower. In fact, you may try to measure the velocity with a pulse generated by an angular 'kick' to one dumb-bell and see the difficulties.

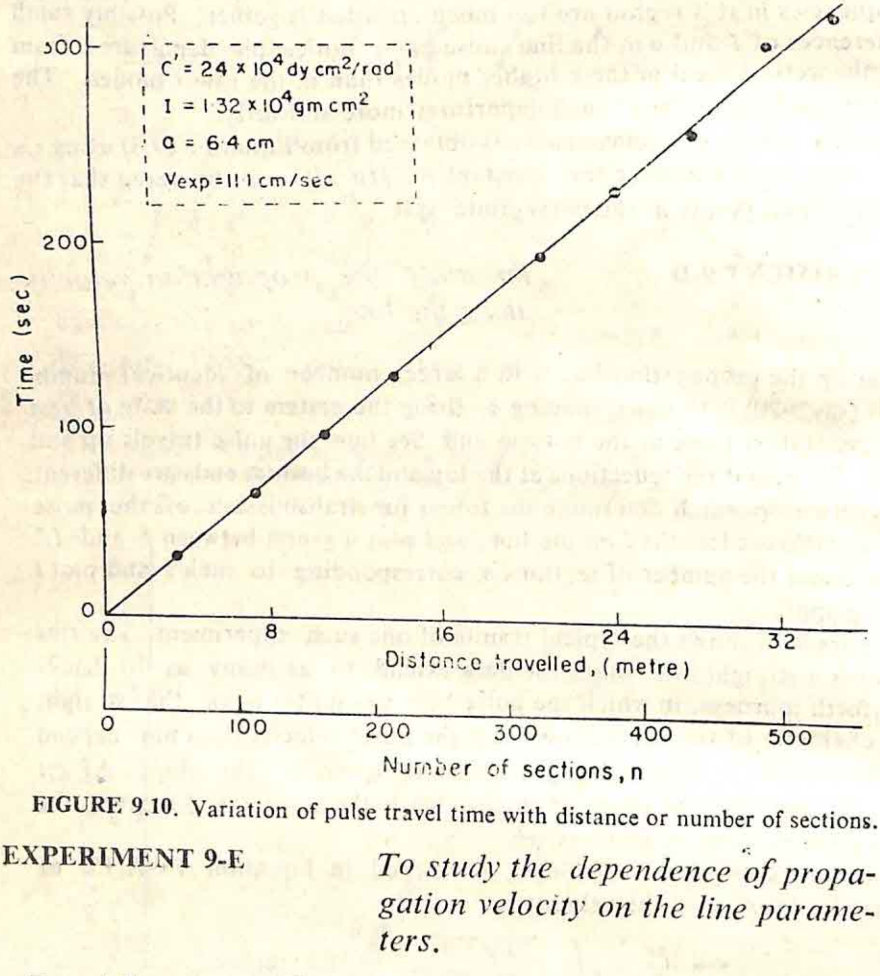

FIGURE 9.10. Variation of pulse travel time with distance or number of sections.

EXPERIMENT 9-E *To study the dependence of propagation velocity on the line parameters.*

Repeat Experiment 9-D varying I of each dumb-bell in one series and varying the spacing a between the dumb-bells in another series. Show the results in two graphs (*a*) T_s vs I and (*b*) T_s vs a.

Figure 9.11 (*a*) and (*b*) represent the typical results of an experiment. The curves do not come out as straight lines; the curvatures show T_s increasing with both I and a. Nature of the curves appears parabolic. Therefore in Fig. 9.12 (*a*) and (*b*) we show plots of

$$T_s \text{ vs } \sqrt{I} \text{ and } T_s \text{ vs } \sqrt{a}$$

respectively. You may see that the experimental points fall smoothly on a straight line in each case, showing that

$$T_s \propto \sqrt{I} \quad \ldots (9.9)$$

and

$$T_s \propto \sqrt{a} \quad \ldots (9.10)$$

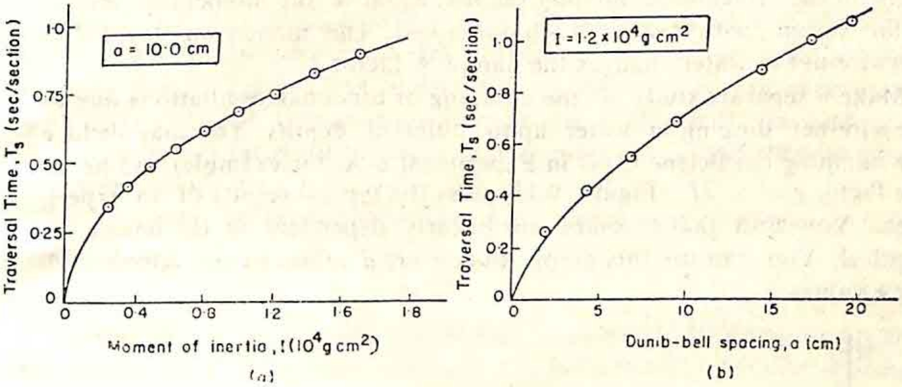

FIGURE 9.11. Traversal time per section as a function of (*a*) the moment of inertia *I* of each dumb-bell, (*b*) the spacing *a*.

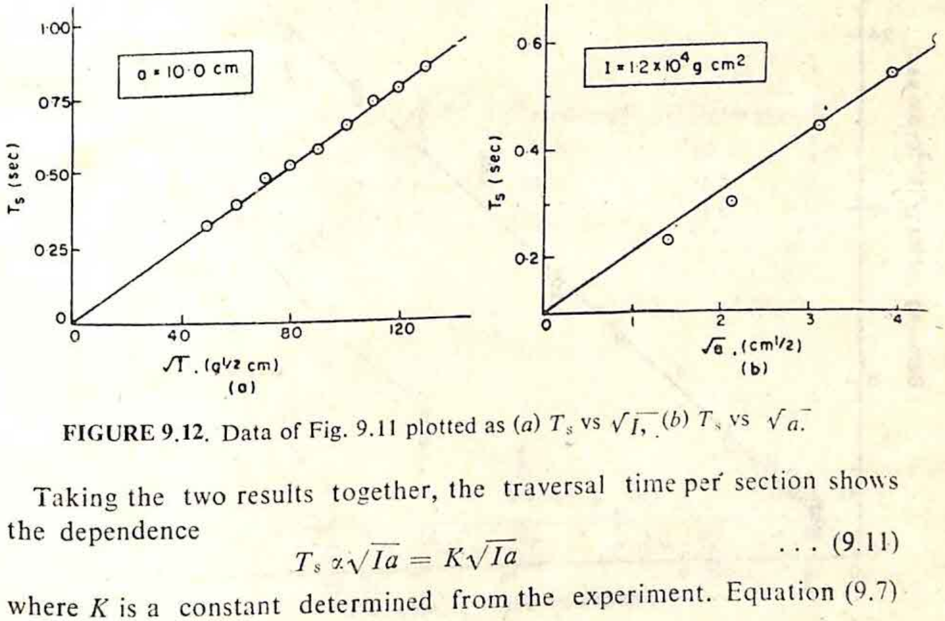

FIGURE 9.12. Data of Fig. 9.11 plotted as (*a*) T_s vs $\sqrt{I}$, (*b*) T_s vs $\sqrt{a}$.

Taking the two results together, the traversal time per section shows the dependence

$$T_s \propto \sqrt{Ia} = K\sqrt{Ia} \qquad \ldots (9.11)$$

where K is a constant determined from the experiment. Equation (9.7) would suggest

$$T_s = \sqrt{\frac{I}{C}} = \frac{I}{\sqrt{C'}}\sqrt{Ia} \qquad \ldots (9.12)$$

Hence you may check if the experimental K is equal to $1/\sqrt{C'}$

EXPERIMENT 9-F *To study the variation of reflection coefficient with termination.*

Terminate the open end (the bottom) of the line by attaching a wire-net dipping into water in a bucket placed under it. Using the adjustable loads on the attachment holding the net, equalise the moment of inertia of this system with that of each dumb-bell. The immersion depth d of the wire-net in water changes the damping factor r.

Make a separate study of the damping of torsional oscillations due to the wire-net dipping in water up to different depths. You may deduce the damping coefficient α (as in Experiment 6-A, for example) and hence the factor $r = \alpha . 2I$. Figure 9.13 gives the typical results of an experiment. You find that r comes out linearly dependent on the immersion depth d. You can use this graph to convert d values to the corresponding r values.

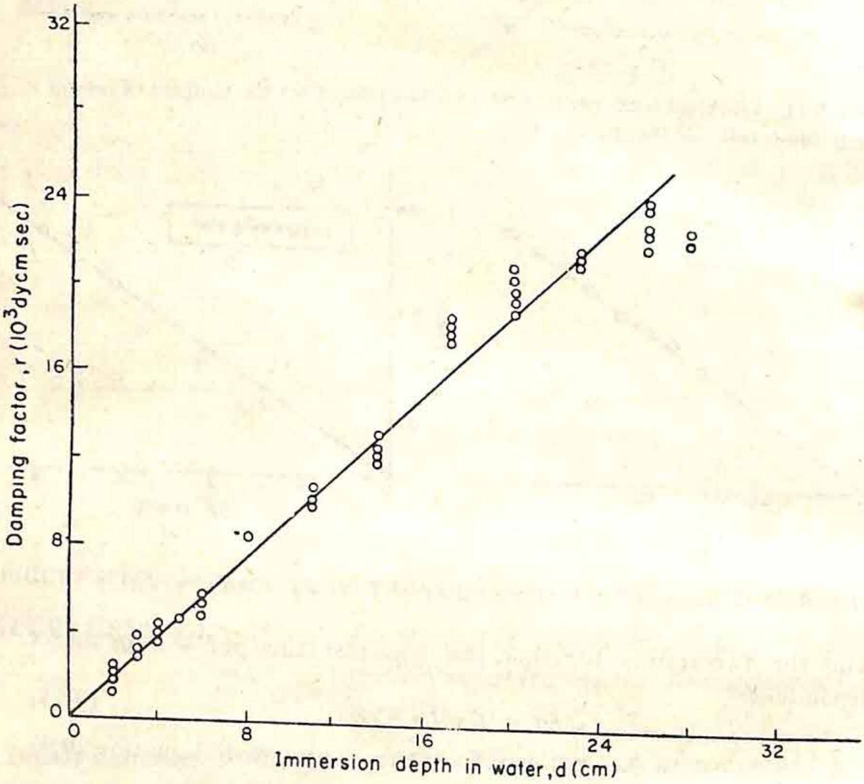

FIGURE 9.13. Variation of damping factor r due to the wire net with its immersion depth d.

Now set the circular scale at the level of a particular dumb-bell A in the line. Start a pulse from anywhere above this dumb-bell and measure the amplitude θ_0 of the dumb-bell A as the pulse passes down and the amplitude θ_0' of the reflected pulse from the bottom when it passes through the dumb-bell A. The ratio θ_0'/θ_0' gives you the reflection coefficient R for amplitude, and you may take note of the signs of θ_0 and θ_0' in deducing its value. (To check that R is not dependent on θ_0 you may make several sets of observations with different θ_0).

Now study the variation of *R* with the immersion depth *d* of the wire-net in water. Converting *d* into the corresponding *r* values, plot a graph showing *R* vs *r*. Figure 9.14 shows the results of a typical experiment with three different transmission lines (*I* and *a* changed). In each case *R* falls from +1 (at $r=0$) to zero at a particular $r=r_c$, and then becomes negative.

In the theory of transmission line the *characteristic impedance* r_c is definded as

$$r_c=\sqrt{I'C'} \qquad \ldots (9.13)$$

Now, if an end section has a damping, represented by damping factor *r*, then the wave is partially reflected, the coefficient of reflection *R* being given by

$$R=\frac{r_c-r}{r_c+r} \qquad \ldots (9.14)$$

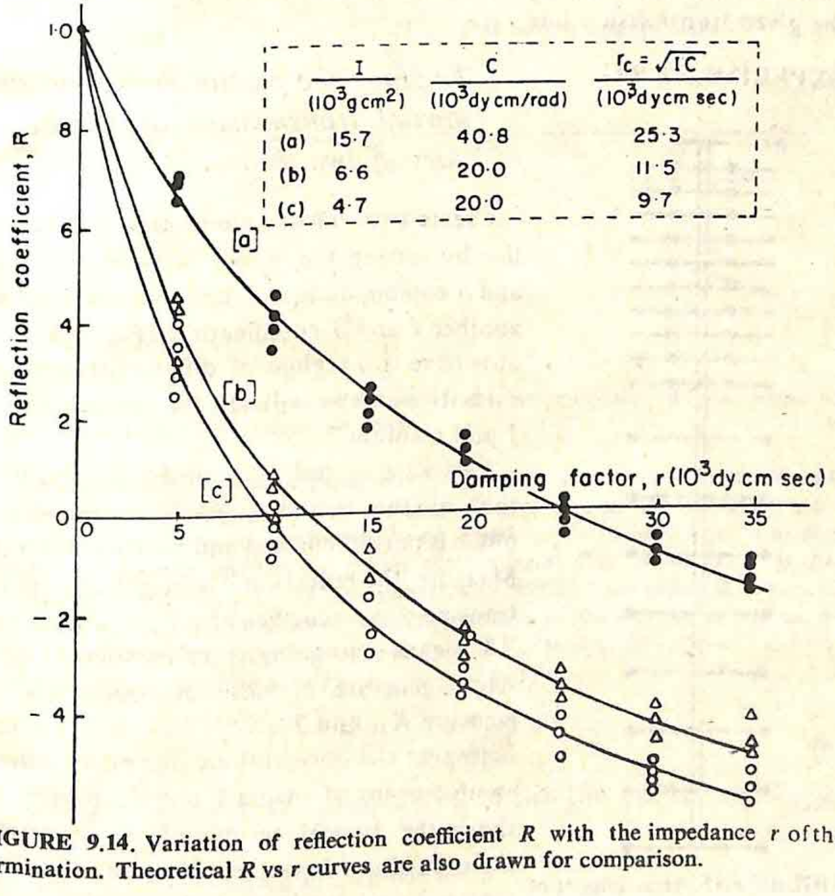

	I (10³g cm²)	C (10³dy cm/rad)	$r_c=\sqrt{IC}$ (10³dy cm sec)
(a)	15·7	40·8	25·3
(b)	6·6	20·0	11·5
(c)	4·7	20·0	9·7

FIGURE 9.14. Variation of reflection coefficient *R* with the impedance *r* of the termination. Theoretical *R* vs *r* curves are also drawn for comparison.

It means that if $r = r_c$ there is no reflection at all and the entire energy of the incident wave is absorbed by the damping system. For $r>r_c$ the wave is partially reflected with reversal of phase (*R* negative) and for $r<r_c$ the wave is again partially reflected, but without phase reversal (R positive). r_c is called the *characteristic termination impedance.*

It may be noted that absorption of the incident wave energy does not increase monotonously as r increases. It reaches a maximum (100% absorption) at $r=r_c$ and decreases for larger as well as smaller r.

Now from the data in the inset of Fig. 9.14 one may compute r_c and then plot R vs r curves for the three r_c values. These curves are shown in the figure, and it may be noted that the experimental points fit the curves well.

RELATED EXPERIMENT

EXPERIMENT 9-F (i)

You may change the termination by changing either the wire-net or the liquid or both and repeat Experiment 9-E. The R vs d and d vs r data will, of course, change. Check if R vs r data come out the same for the given transmission line.

EXPERIMENT 9-G

To study the partial reflection and partial transmission at the boundary of two media.

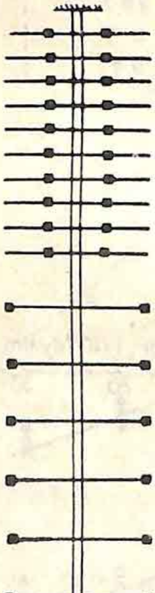

FIGURE 9.15. Arrangement of the transmission line behaving as two media.

Create two 'media' along the transmission line by setting the upper sections with one I and a combination and the lower sections with another I and a combination (Fig. 9.15). You now have two regions of different transmission velocities and we will call the regions medium 1 and medium 2.

Generate a pulse in medium 1 and notice that at the boundary of the two media the pulse is partly reflected and partly transmitted. Measure the reflection coefficient R_{12} and the, transmission coefficient T_{12}, where suffix '12' means "in going from medium 1 to 2." Also generate a pulse in medium 2 and measure R_{21} and T_{21}.

Repeat the observations for many different combinations of media 1 and 2. Figure 9.16 shows the typical results of an experiment where medium 1 was kept the same ($v_1 = 9.2$ cm/sec.) and medium 2 was varied so as to change v_2 from ~ 3 to 18 cm/sec. It was found that

$$R_{21} = -R_{12} \text{ and } T_{21} = +T_{12} \qquad \ldots(9.15)$$

within the range of experimental errors. For this reasons only T_{12} and R_{12} are plotted against v_2 in Fig. 9.16.

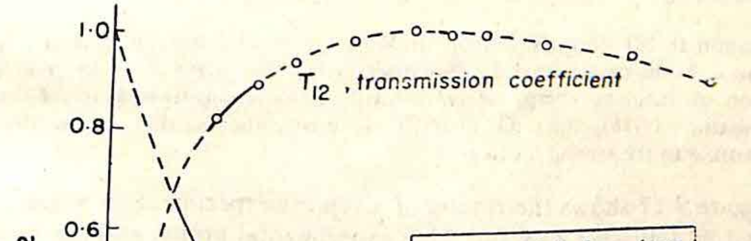

FIGURE 9.16. Reflection and transmission at the boundary of two media as a function of v_2 when v_1 is kept constant.

The results stated through Equation (9.15) are in themselves quite significant; the transmitted pulse always goes without change of sign, whereas the reflected pulse goes with the same or reversed sign depending on whether it is incident from a medium of smaller v or larger v respectively. From the curves of Fig. (9.16) check if R^2+T^2 comes out to be constant (= 1) throughout. Why would you expect it? What would $v_2 \to 0$ and $v_2 \to \infty$ imply in terms of (say) the spacing a of the sections or I of the dumb-bells? In view of this what values would R_{12} and T_{12} tend to as $v_2 \to 0$ and $v_1 \to \infty$?

In transmission line theory, R_{12} is given by

$$R_{12} = \frac{r_{c1}-r_{c2}}{r_{c1}+r_{c2}} \qquad \ldots(9.16)$$

where r_{c1} and r_{c2} are the impedances of the two media (*see* Appendix IX-A).

This may be expressed also in the form

$$R_{12} = \frac{\mu_{12}-1}{\mu_{12}+1} \qquad \ldots(9.17)$$

where μ_{12} is defined as the ratio of the wave velocities in the two media and may be called the refractive index. To see whether Equation (9.12) holds in the case of the one-dimensional mechanical wave, you may compute μ_{12} from your data and plot R_{12} against μ_{12}.

Equation (9.16) appears similar to Equation (9.14). But there is one important difference. In the case related to Equation (9.14), the quantity $(1-R^2)$ represents the fraction of incident energy *absorbed* at the termination, whereas in the case related to Equatio (9.16), the same quantity represents the fraction of incident energy *transmitted* to the second medium.

Figure 9.17 shows the results of a typical experiment in which μ_{12} was varied in a number of ways. The experimental points and the theoretical curve for R_{12} vs μ_{12} are shown and you may note that the agreement is satisfactory.

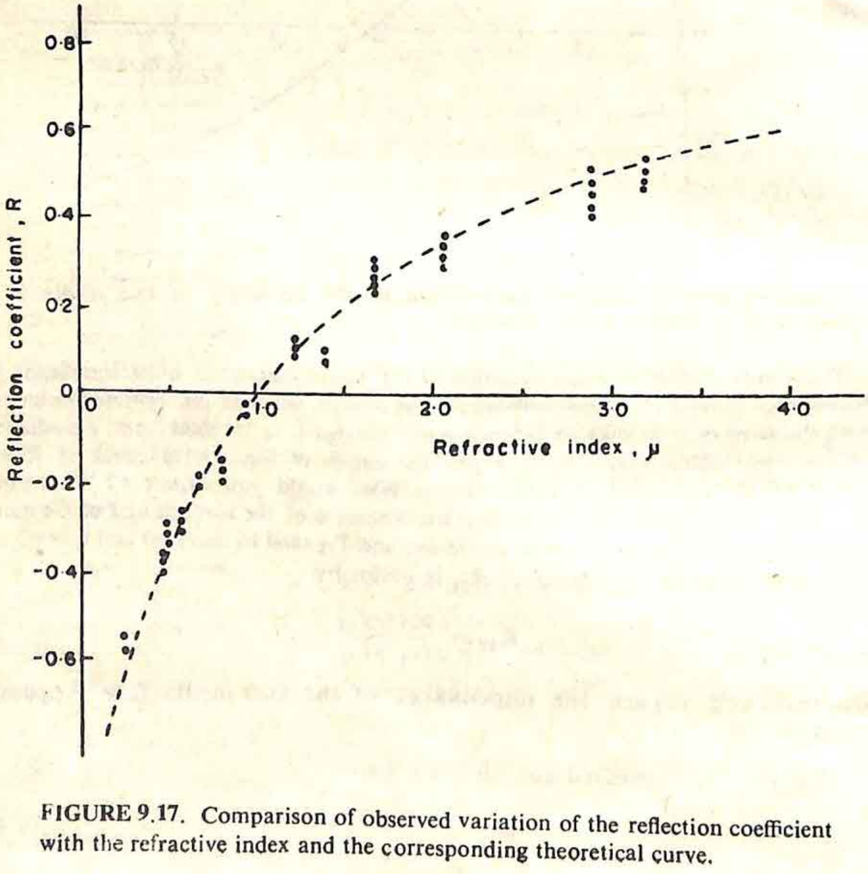

FIGURE 9.17. Comparison of observed variation of the reflection coefficient with the refractive index and the corresponding theoretical curve.

APPENDIX IX-A

THEORY OF THE MECHANICAL TRANSMISSION LINE

1. The Uniformly Distributed Line

For a uniformly distributed line we shall follow the analogy of a string under tension. For a string under tension F and mass m' per unit length, the wave velocity is $\sqrt{\frac{F}{m'}}$. If a length L is clamped at both the ends, the standing wave modes have wavelengths given by $2L/p$, where p is an integer. Thus the frequency of the p^{th} modes is:

$$\omega_p = \frac{\pi p}{L}\sqrt{\frac{F}{m'}} = k_p\sqrt{\frac{F}{m'}} \qquad \text{. . .IX-A(1)}$$

where k_p is the wave number of the p^{th} mode. For torsional oscillations of a strip we write by comparison

$$\omega_p = k_p\sqrt{\frac{C'}{I'}} \qquad \text{. . .IX-A(2)}$$

where C' is restoring factor for unit length, and I' is the moment of inertia per unit length in the distributed line. The available k_p values are:

$$k_p = \frac{\pi p}{L}\ (p=1 \text{ to } \infty) \qquad \text{. . .IX-A(3)}$$

there being no upper limit for p since the line is supposed to be continuous.

In case the ratio ω/k, which equals the velocity v of the waves on the line, is independent of k, the system (or medium) is called *non-dispersive.* As we shall see, a lumped transmission line is dispersive.

2. The Lumped Transmission Line

Figure IX-A(1) shows a line comprising of dumb-bells of moment of inertia I each mounted on a steel tape with equal spacing a. Dumb-bells 0 and $N+1$ are clamped, so that there are N free dumb-bells and total length of the strip is

$$L=(N+1)\,a \qquad \ldots \text{IX-A(4)}$$

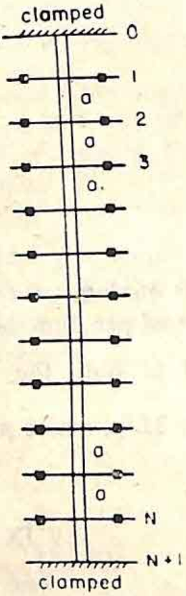

FIGURE IX-A(1). *N* lumped units in a transmission line closed at both ends.

The equation of motion for each dumb-bell in the line, assuming nearest neighbour coupling, can be written as:

$$I\ddot{\theta}_n=C'\,\frac{\theta_{n+1}-\theta_n}{a}-C'\,\frac{\theta_n-\theta_{n-1}}{a}. \quad \ldots \text{IX-A(5)}$$

There are N equations like this, and their simultaneous solution leads to N *normal modes*. As discussed in Chapter 8, all the members oscillators with the same frequency and phase in a given mode, although with different amplitudes. Any general oscillation is a superposition of the normal modes.

3. The Normal Modes

Consider the p^{th} normal mode. For the n^{th} dumb-bell in this mode the oscillation may be written

$$(\theta_n)_p=(A_n)_p\cos(\omega_p t+\delta_p) \qquad \ldots \text{IX-A(6)}$$

where ω_p and δ_p are the same for all the dumb-bells in a given mode (here p^{th}). Substitution of this and similar equations in Equation IX-A(5) leads to

$$(A_{n+1})_p+(A_{n-1})_p=(A_n)_p\left[2-\frac{Ia}{C'}\,\omega_p{}^2\right] \qquad \ldots \text{IX-A(7)}$$

The configuration *i.e.*, the relative values of A_{n+1}, A_n and A_{n-1} must satisfy this relation. Let us try the solution—

$$(A_n)_p=A_p\sin k_p na \qquad \ldots \text{IX-A(8)}$$

This will satisfy Equation IX-A(7) if

$$\omega_p{}^2=\frac{4C'}{Ia}\sin^2\frac{k_p a}{2} \qquad \ldots \text{IX-A(9)}$$

Thus the solution for the normal mode oscillations is

$$(\theta_n)_p=A_p\sin k_p na\cos(\omega_p t+\delta_p) \qquad \ldots \text{IX-A(10)}$$

where ω_p is related to k_p through Equation IX-A(9). This is called the *dispersion relation*. The allowed k_p values are given by the boundary conditions.

4. Boundary Conditions: Available Normal Modes

The boundary conditions are $\theta_0=0$ and $\theta_{N+1}=0$ for all p values. Equation IX-A(8) satisfies the first anyway. The second boundary condition leads to

$$[\sin k_p na]_{n=N+1}=0 \quad \Rightarrow \quad \sin k_p L=0$$

Thus the k values of the available normal modes are

$$k_p = p\frac{\pi}{(N+1)a} = p\frac{\pi}{L},\ (p=1 \text{ to } N) \qquad \ldots \text{IX-A(11)}$$

Equation IX-A(9) may now be written as

$$\omega_p = 2\sqrt{\frac{C'}{Ia}}\ \sin\ \frac{p\pi}{2(N+1)},\ (p=1 \text{ to } N) \qquad \ldots \text{IX-A(12)}$$

and Equation IX-A(8) as

$$(A_n)_p = A_p \sin \frac{pn\pi}{N+1} \qquad \ldots \text{IX-A(13)}$$

The values of A_p and δ_p are arbitrary, which means that the different modes may mix in any proportion of amplitudes and any relative phases. A pure mode, say $p_1{}^{th}$, would mean that $A_p=0$ for all values of p other than p_1.

5. Discussion

(*a*) *Long wavelength approximation.* Let $p\pi/2(N+1) \ll 1$. In that case using Equation IX-A(12) and IX-A(11) leads to

$$\omega_p = 2\sqrt{\frac{C'}{Ia}} \cdot \frac{p\pi}{2(N+1)} = \sqrt{\frac{C'}{I'}} \cdot k_p \qquad \ldots \text{IX-A-(14)}$$

where $I'=I/a$. This holds when p (the mode number) is small, which means λ is large (compared with a). In this range ω/k is constant, so that the medium is non-dispersive. We get

$$\Big[V\Big]_{\lambda \gg a} = \sqrt{\frac{C'}{I'}} \qquad \ldots \text{IX-A(15)}$$

Sometimes the velocity is put in terms of *sections* per second. Calling it $v_s = v/Q_a$, we get

$$\Big[V_s\Big]_{\lambda \gg a} = \sqrt{\frac{C'}{I'a}} = \sqrt{\frac{C}{I}} \qquad \ldots \text{IX-A(16)}$$

The *traversal time per section* T_s is reciprocal of V_s.

$$T_s = \sqrt{\frac{I'a}{C'}} = \sqrt{\frac{I}{C}} \qquad \ldots \text{IX-A(17)}$$

(*b*) *Short wavelength approximation.* High k corresponds to low λ. Equation IX-A(11) shows that in the upper range of modes p

$$k \rightarrow \frac{N\pi}{(N+1)a} \approx \frac{\pi}{a};\ \lambda \approx 2a$$

thus λ comparable with $2a$ is the short wavelength range for the transmission line.

Equation IX-A(12) shows that the maximum value ω can have is

$$\omega_{max} = 2\sqrt{\frac{C'}{Ia}}\ \sin\ \frac{N}{N+1}\ \frac{\pi}{2}$$

and it corresponds to the k and λ values cited above. The quantity $2\sqrt{C'I/a}$ is called the *cut-off frequency* ω_c because waves of frequency higher than ω_c cannot propagate on this line. For large N we have $\omega_{max} \approx \omega_c$, where

$$\omega_c = 2\sqrt{\frac{C'}{Ia}} \qquad \ldots \text{IX-A(18)}$$

(*c*) *An example.* Figure IX-A(2) shows a line which has (a) 5, (b) 8 and (c) 17 sections in the same length L. Thus the values of a in the three cases are $L/6$, $L/9$ and $L/18$, which means a ratio 3:2:1. The total moment of inertia is kept constant *i.e.* I is unchanged, this means

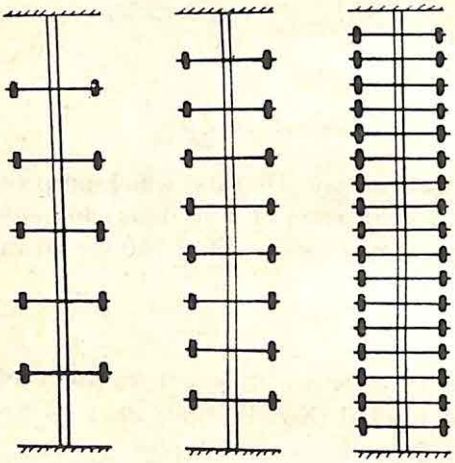

FIGURE IX-A(2). Three different 'lines' with same C' and I' and same total length L, but having different number of sections.

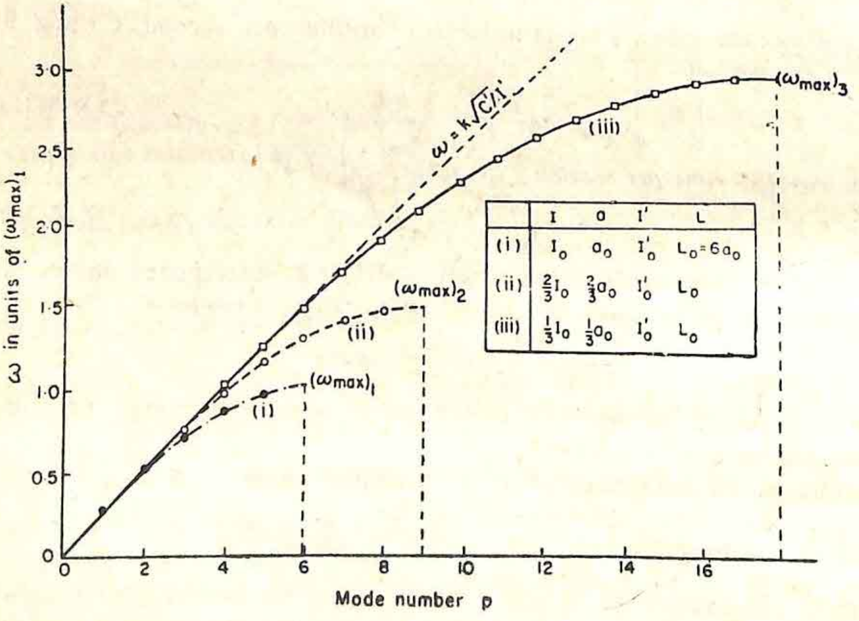

FIGURE IX-A(3). Theoretical dispersion curves for the three 'lines' of Fig. IX-A-(2).

that the I values of individual dumb-bells are also changed in the ratio 3:2:1.

The ω vs k curve (dispersion curve) for the first case is given in Fig. IX-A(3), and the configurations for the five modes are shown in Fig. IX-A(4). These are deduced from Equation IX-A(12) and IX-A(13) respectively.

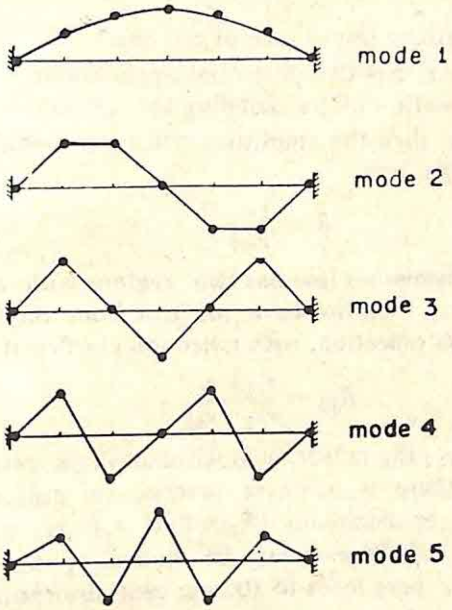

FIGURE IX-A (4). Theoretical configurations for the five normal modes in a 'line' with $N=5$.

The effect of changing a and I (as described) is also shown in Fig. IX-A(3). Firstly, ω_{max} increases in the ratio 2:3:6. Secondly, the number of observed modes increases from 5 to 8 to 17. Thirdly, ω for modes 4 and 5 (for example) is much below the 'non-dispersion' curve (the dotted line) in case (*i*) whereas the same modes are nearer that curve in case (*ii*), and almost on the curve in case (*iii*).

6. Transmission of a Pulse

A pulse, according to Fourier's theorem, is the superposition of harmonic waves of several k values. We have seen that non-dispersive character (ω/k=constant) holds if $k\ a/2 \ll L$. The pulse will travel without appreciable dispersion if (*i*) the contribution of high k components is relatively small, and (*ii*) a value of the transmission line is small. In that limit the pulse travels with a velocity given by

$$v = \frac{\omega}{k} = \sqrt{\frac{C'a}{I}} = \sqrt{\frac{C'}{I'}} \qquad \text{.. IX-A(19)}$$

7. Termination and Reflection of a Wave

The product $I'C'$ is characteristic of a transmission line in the sense that if a lumped line of constants I and a is changed to one of constants I/q and a/q the product $I'C'$ remains unchanged; in the limit $q \rightarrow \infty$ we go over to the equivalent continuous line of the same $I'C'$ the dimension of $\sqrt{I'C'}$ are those of the damping factor r (*see* Chapter 6). The quantity

$$r_c = \sqrt{I'C'} \qquad \ldots \text{ IX-A(20)}$$

is called characteristic impedance of the line.*

The impedance r_c has two particular applications:

(1) If an end section offers damping for torsional oscillations with a damping factor r, then the amplitude reflection coefficient R for the wave at this end is given by

$$R = \frac{r_c - r}{r_c + r} \qquad \ldots \text{ IX-A(21)}$$

(2) If the transmission line has two regions with characteristic impedances r_{c1} and r_{c2}, then the wave incident from the first region towards the second suffers reflection, with reflection coefficient R_{12} given by

$$R_{12} = \frac{r_{c1} - r_{c2}}{r_{c1} - r_{c2}} \qquad \ldots \text{ IX-A(22)}$$

Thus, if $r_{c1} > r_{c2}$ the reflection is without phase reversal (R_{12} positive), and if $r_{c1} < r_{c2}$ there is a phase reversal on reflection (R_{12} negative). There is 100% transmission ($R_{12} = 0$) if $r_{c1} = r_{c2}$, which means $I_1'C_1' = I_2'C_2'$. Similar inferences may be drawn from Equation IX-A(21), except that $r = r_c$ there leads to 100 per cent absorption.

If the two regions are on the same tape (C' equal, as in our experiments), we have

$$\frac{r_{c1}}{r_{c2}} = \frac{\sqrt{C'I'_1}}{\sqrt{C'I_2'}} = \frac{\sqrt{I_2'/C'}}{\sqrt{I_1'/C'}} = \frac{v_2}{v_1} = \mu_{12} \text{ (say)}$$

Equation IX-A(22) can then be also written as

$$R_{12} = \frac{\mu_{12} - 1}{\mu_{12} + 1} \qquad \ldots \text{ IX-A(23)}$$

REFERÉNCE

An excellant treatment of the subject of this Chapter may be found in F.S. Crawford, *Waves, Berkeley Physics Course*, Vol. III, McGraw-Hill, New York, 1968.

---

* Dimensionally, we have -

$$[r_c] = [CI] = [ML^2T^{-1}] = [ML^2T^{-2}/T^{-1}]$$

= (torque/angular velocity) = (impedance in rotational motion

This justifies the name 'characteristic impedance for r_c. Exact calculation shows the proportionality constant between them to be unity.

Physics Through Experiment 1

"I have no doubt that this course in experimental Physics, would go a long way not only in improving the experimental aptitude of the student but also in inculcating in him the attitude of enquiry so essential for scientific thinking."

H.G. Devare
Tata Institute of Fundamental Research, Bombay

PHYSICS NEWS, December 1976.

Physics Through Experiment 2

"I feel that this book will be a valuable reference for any one interested in improving the physics laboratory. I expect that many of the experiments will find general acceptance. I also hope that the mode of presentation will be used as a model for laboratory instructions in this country."

Leonard Dart
Claremont College, Claremont, CA, USA

American Journal of Physics, March 1981.

Rs 60 1V2SJ439 ISBN 0-7069-4540-9

VIKAS PUBLISHING HOUSE PVT LTD